



NTNU – Trondheim
Norwegian University of
Science and Technology

Evaluation on the Squeezing Phenomenon at the Headrace Tunnel of Chameliya Hydroelectric Project, Nepal

Chhatra Bahadur Basnet

Hydropower Development

Submission date: June 2013

Supervisor: Krishna Kanta Panthi, IGB

Co-supervisor: Pawan Kumar Shrestha, IGB

Norwegian University of Science and Technology
Department of Geology and Mineral Resources Engineering



Your ref.: MS/I08T18/IGB/CBBKP

Date: 04.01.2013

**TGB4910 Rock Engineering - MSc thesis
for
Chhatra Bahadur Basnet**

**EVALUATION ON THE SQUEEZING PHENOMENON AT THE HEADRACE TUNNEL OF
CHAMELIYA HYDROELECTRIC PROJECT**

Background

Tunnel squeezing is a phenomenon, which is frequently confronted while tunnelling through Himalayan rock mass. Weak and schistose rocks like mudstone, shale, slate, phyllite, schist, highly schistose and sheared rocks and the rock mass of the tectonic fault zones are incapable of sustaining high stresses. Excessive tunnel squeezing occurred along the headrace tunnel of the Chamelia Hydroelectric Project during tunnel excavation. Even though, considerable amount of rock support measures were used in controlling deformation, the tunnel has lost almost 30 percentage of its theoretical dimension.

In this respect, documentation of the squeezing phenomenon at this tunnel project would be an important issue for the engineers, project developers and as a whole to the scientific community involved in engineering geology, tunnelling and rock mechanics.

MSc thesis task

Hence, this MSc thesis is to focus on the documentation and evaluation of squeezing phenomenon at the headrace tunnel of Chamelia Hydroelectric Project, with a main focus on the following issues:

- Review existing theory on the stability issues in tunnelling with particular focus on tunnel squeezing.
- Briefly describe about Chamelia Hydroelectric Project including the extent of engineering geological investigations carried out during planning.

- Document on the rock support principle used while tunnelling. Document on the measured deformation along tunnel alignment.
- Back analyse on the squeezing phenomenon using existing empirical and analytical approaches.
- Attempt to produce a support characteristic curve based on applied support, measured final deformation and reviewed theory.
- Carry out stability analysis using Numerical Modeling.
- Compare and discuss the analysis results from empirical, analytical and numerical approaches.

Relevant computer software packages

Candidate shall use *roc-science package* and other relevant computer software for the master study.

Background information for the study

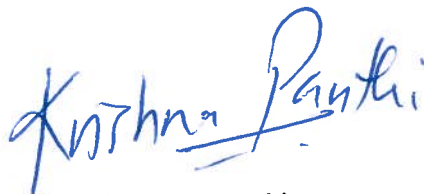
- Relevant information about the project such as reports, maps, information and data collected by the candidate.
- The information provided by the professor about the project.
- Scientific papers, reports and books related to the Himalayan geology and tunnelling.
- Scientific papers and books related to international tunnelling cases.
- Literatures in rock engineering, rock support principles, rock mechanics and tunnelling.

Mr. Pawan Kumar Shrestha will be the co-supervisor of this MSc thesis.

The project work is to start on January 14, 2013 and to be completed by June 8, 2013.

The Norwegian University of Science and Technology (NTNU)
Department of Geology and Mineral Resources Engineering

January 04, 2013



Dr. Krishna K. Panthi

Associate Professor of geological engineering, main supervisor

FOREWORD

This master thesis titled “**Evaluation on the Squeezing Phenomenon at the Headrace Tunnel of Chameliya Hydroelectric Project, Nepal**” is submitted to the Department of Geology and Mineral Resources Engineering for the requirement to partial fulfillment of Master of Science in Hydropower Development Program (2011-2013) conducted by Department of Hydraulic and Environmental Engineering, Norwegian University of Science and Technology (NTNU), Trondheim, Norway.

The thesis work mainly focuses on the squeezing analysis of headrace tunnel of Chameliya Hydroelectric Project in Nepal using different methods such as empirical, semi-analytical and analytical methods. The result obtained from these methods has been verified using numerical program, phase2. The thesis work started in January 2013 and completed in June 2013. The study during this period was mainly based on the data collected in June 2012 to August 2012 from Chameliya Hydroelectric Project, Nepal. This thesis is purely an academic exercise carried out by the candidate and significant outside contributions have been highly acknowledged.

Chhatra Bahadur Basnet
NTNU, Norway
June, 2013

ACKNOWLEDGEMENTS

For this thesis work, Associate Prof. Dr. Krishna Kanta Panthi has been my main supervisor. I would like to express my gratitude towards him for his valuable guidance, suggestions and discussions from the very beginning of work to the very end of the work i.e. from topic selection to thesis submission. Without his continuous help and support, the thesis work would not have been in this level. Also, I would like to extend my acknowledgement to co-supervisor Mr. Pawan Shrestha, Phd Candidate in Department of Geology and Mineral Resources Engineering, for his valuable guidance to the subject matter and to go deep into the squeezing phenomenon and stability analysis of tunnel.

I would like to express my gratitude to Prof. Ånund Killingtveit, Professor-in-charge of Hydropower Development Program, for his continuous support. My Sincere gratitude also goes to Mrs. Hilbjørg Sandvik, course coordinator of Hydropower Development Program, for her generous support and help, and continuous information during two years of stay in Norway. Likewise, I would like to thank all department staffs, faculties, professors and students for creating homely environment in the department.

Again, I would like to express my gratitude to the State Educational loan fund of Norway, Lånekassen, for supporting living expenses during my stay in Trondheim. I am also grateful to Office of International Relations, NTNU for administrative arrangements for loan and residence permit.

I am grateful to Mr. Gopal Babu Bhattraï, Project Director, Chameliya Hydroelectric Project (CHEP), for his help and legal support for the data collection from project site in Darchula, Nepal as well as from main office in Kathmandu, Nepal. Also, I am thankful to Mr. Mohan Raj Pant, Executive Member of Nepal Electricity Authority (NEA) for his intensive help in the data collection. Again, I would like to express my thanks to Mr. Ajab Singh Mahara, Geologist, CHEP and Er. Lok Raj Joshi, Project engineer, CHEP for their support in the data collection from project site. Likewise, I would like to extend my thanks to Er. Surya Poudel, Shah Consult International (P.) Ltd. for providing the CHEP related documents. I am also grateful to Er. Mani Raj Dahal, Chief Executive Officer, Clean Energy Consultant Pvt. Ltd., for his continuous encourages and assistance for the master study in Norway.

Further, I would like to extent my gratitude to my parents, other family members and relatives for their blessings and encouragements. I would like to thank my wife for her continuous love towards me that always encourages me to the blissfulness and happiness. Last but not least, I would like to thank all my friends for their continuous encourages and help in conducting the thesis work.

“Gratitude to the existence”

ABSTRACT

Growing demand of electricity in Nepal can be fulfilled by hydropower generation. The huge potentiality of hydropower generation in Nepal is mainly due to abundant water resources and available geographical head due to steep Rivers. In medium and large hydropower projects, huge amount of water discharge has to be handled from intake to power station and ultimately back to river again. Also, because of steep topography, the construction of pipe and canal on the surface of terrain could be very difficult and expensive for larger discharges. Hence, underground construction such as tunnels or shafts could only be the feasible options of water conveyance system for large discharges and in case of steep terrains. But, at the same time, there are higher risks and uncertainties associated with the underground works like tunnels and shafts or caverns.

The main risks and uncertainties associated with the underground works are stress induced instability, water leakage, mud flows and finally the cost overrun during construction. When there is overstressing of rock mass that means rock stresses exceed the strength of rock mass, there will be stress induced instability in the tunnel. If the rock mass is very weak, schistose and deformable, squeezing phenomenon will occur with the development of plastic zone around the tunnel which causes excessive deformation of tunnel. In the Himalayan region, due to the high degree of schistosity, fracturing and shearing, weak rocks such as mudstone, shale, slate, phyllite, schist, highly schistose gneiss and the rock mass of the tectonic fault zones are not capable to withstand the high stresses. Basically, squeezing has been common phenomenon in the tunnels in these weak and deformable rock masses.

In this thesis, Chameliya Hydroelectric Project (CHEP), located in far western region of Nepal, has been taken as the case study. In this project, huge squeezing problem occurred in about 800m stretch of headrace tunnel from chainage 3+100m to 3+900m. The most affected section is about 550m in between these chainages. At several locations in squeezing section, the tunnel wall closure (deformation) has been recorded well over 1.0 m in an average and the maximum above 2.0 m where the original tunnel diameter is 5.2m. Hence, the thesis basically deals with squeezing analysis of the case using different approaches. Rock types along the headrace tunnel alignment are dolomite, slate, talcosic phyllite and dolomite intercalated with phyllite. Mostly, talcosic phyllite has been found in the squeezed section. The rock mass quality in the squeezed section is extremely poor to exceptionally poor.

The main objectives of this thesis are the assessment of squeezing phenomenon, evaluation of stability of the tunnel and support pressure estimation. In this thesis, four main methods have been used to evaluate the squeezing phenomenon viz.; empirical methods such as Singh et al (1992) and Q-system (Grimstad and Barton, 1993), semi-analytical method such as Hoek and Marinos (2000), analytical method such as Convergence Confinement Method (Carranza-Torres and Fairhurst, 2000) and numerical program Phase². Initially, seventeen tunnel sections at different chainages have been taken into consideration. The squeezing prediction criteria, such as Singh et al (1992), Q-system and Hoek and Marinos (2000) approach, show that there is severe squeezing in last ten sections. Hence more detail squeezing analysis has

been done for these ten sections using Hoek and Marinos (2000) and Convergence Confinement Method, and support pressure has also been estimated using these two approaches and Barton et al. (1974) approach. Hoek and Marinos (2000) and Convergence Confinement Method analysis show that there is significant amount of tunnel deformation to cause squeezing problems.

The main factors that control the squeezing phenomenon are the rock mass parameters and rock stresses. Therefore, quality of squeezing analysis largely depends upon the correct estimation of these input parameters. The main components of rock stresses are gravity and tectonic stresses. The rock stresses in the project area were not measured, so Phase² program has been used to estimate the tectonic stress value from measured deformation. The tectonic stress value has been found to be equal to 3.5MPa in this area, but stress measurement will be necessary to verify this value. Uniaxial unconfined strength of intact rock in four tunnel sections has been back calculated from measured deformations using Phase² program and found to be in the range of 10 to 15Mpa in the squeezed section. Later, the deformation has been calculated using Hoek and Marinos (2000) and Convergence Confinement Method for improved intact rock strength and compared with Phase² result. All analyses show that there is significant deformation to cause squeezing problem.

In CHEP, tunnel cross section has reduced considerably in several stretches of tunnel. Due to the excessive deformation, temporary supports were provided at several locations, steel ribs and lattice girders are buckled at several locations and shotcrete lining is also cracked. All these have to be removed before application of final lining. Finally, two different possible solutions have been studied using Phase² program to address the existing problems in squeezed section of the headrace tunnel.

TABLE OF CONTENTS

FOREWORD.....	I
ACKNOWLEDGEMENTS	II
ABSTRACT.....	III
LIST OF TABLES	IX
LIST OF FIGURES	X
LIST OF ABBREVIATIONS	XV
1 INTRODUCTION	1-1
1.1 BACKGROUND	1-1
1.2 OBJECTIVE AND SCOPE OF THE STUDY	1-1
1.3 METHODOLOGY OF THE STUDY	1-2
1.4 ORGANIZATION OF THE THESIS	1-2
1.5 LIMITATION OF THE STUDY.....	1-3
2 ROCK AND ROCK MASS PROPERTIES.....	2-1
2.1 INTRODUCTION.....	2-1
2.2 ROCK MASS STRUCTURES.....	2-2
2.2.1 <i>Bedding plane</i>	2-2
2.2.2 <i>Jointing of rock mass</i>	2-2
2.2.3 <i>Weakness Zones and faults</i>	2-3
2.3 ROCK MASS STRENGTH AND DEFORMABILITY	2-4
2.3.1 <i>Uniaxial Compressive strength test</i>	2-4
2.3.2 <i>Factor influencing the rock strength</i>	2-4
2.3.3 <i>The point load test</i>	2-8
2.3.4 <i>Field estimates of σ_{ci}</i>	2-9
2.3.5 <i>Failure criteria</i>	2-9
2.3.6 <i>Rock mass strength estimation</i>	2-12
2.3.7 <i>Rock mass deformability estimation</i>	2-13
3 STRESS INDUCED INSTABILITY IN TUNNELING.....	3-1
3.1 INTRODUCTION.....	3-1
3.2 ROCK STRESSES.....	3-1
3.2.1 <i>In situ rock stresses</i>	3-1
3.2.2 <i>Stresses surrounding underground openings</i>	3-3
3.2.3 <i>Rock stress estimation</i>	3-5
3.2.4 <i>In situ stress measurements</i>	3-5
3.3 TUNNEL STABILITY PROBLEMS	3-5
3.3.1 <i>Problems due to tensile stress</i>	3-5
3.3.2 <i>Problems due to high compressive stress</i>	3-6

3.4	REVIEW ON SQUEEZING PHENOMENON	3-6
3.4.1	<i>Instantaneous Squeezing</i>	3-7
3.4.2	<i>Squeezing by creep</i>	3-8
3.4.3	<i>Factor influencing the squeezing phenomenon</i>	3-9
3.5	CONCLUDING REMARKS.....	3-10
4	THE CASE: CHAMELIYA HYDROELECTRIC PROJECT (CHEP)	4-1
4.1	PROJECT DESCRIPTION	4-1
4.1.1	<i>General</i>	4-1
4.1.2	<i>Project Location</i>	4-1
4.1.3	<i>Project layout features</i>	4-2
4.2	REGIONAL GEOLOGY	4-3
4.3	GEOLOGY AND ENGINEERING GEOLOGY OF THE PROJECT AREA.....	4-6
4.3.1	<i>Geological investigations</i>	4-6
4.3.2	<i>Headworks area</i>	4-7
4.3.3	<i>Headrace tunnel alignment</i>	4-8
4.3.4	<i>Surge shaft and vertical shaft area</i>	4-8
4.3.5	<i>Powerhouse area</i>	4-8
4.4	ROCK MASS CONDITION ALONG HEADRACE TUNNEL	4-10
4.5	INSTABILITY ALONG HEADRACE TUNNEL	4-12
4.6	TUNNEL EXCAVATION AND SUPPORT MEASURE.....	4-13
5	REVIEW OF PROJECTS WITH SIMILAR INSTABILITY PROBLEMS	5-1
5.1	KALIGANDAKI “A” HYDROELECTRIC PROJECT, NEPAL.....	5-1
5.1.1	<i>Project Geology</i>	5-3
5.1.2	<i>Rock mass conditions</i>	5-3
5.1.3	<i>Tunnel stability problems</i>	5-4
5.2	YACAMBÚ-QUIBOR TUNNEL, VENEZUELA	5-6
5.2.1	<i>Project Location and Geology</i>	5-6
5.2.2	<i>Rock mass properties</i>	5-8
5.2.3	<i>Tunnel stability problems</i>	5-9
5.2.4	<i>Design of support and final lining</i>	5-12
6	SQUEEZING ANALYSIS METHODS AND SUPPORT DESIGN	6-1
6.1	GENERAL	6-1
6.2	EMPIRICAL METHOD	6-1
6.2.1	<i>Singh et al approach</i>	6-1
6.2.2	<i>Q-system</i>	6-2
6.3	SEMI-ANALYTICAL METHOD	6-4
6.3.1	<i>Hoek and Marinos approach</i>	6-4
6.4	ANALYTICAL METHOD	6-7
6.4.1	<i>Convergence-Confinement Method (CCM)</i>	6-7
6.4.2	<i>Limitations of CCM</i>	6-17
6.5	NUMERICAL ANALYSIS	6-18

6.5.1	<i>General</i>	6-18
6.5.2	<i>Selection of the computer program</i>	6-19
6.5.3	<i>The Phase² Program</i>	6-20
6.5.4	<i>Input parameters for Phase²</i>	6-20
6.5.5	<i>Interpretation of the results</i>	6-21
6.5.6	<i>3D tunnel simulation using the core replacement technique in Phase2</i>	6-21
6.6	CONCLUDING REMARKS ON THE SQUEEZING ANALYSIS TECHNIQUES	6-22
7	SQUEEZING ANALYSIS	7-1
7.1	GENERAL	7-1
7.2	INPUT DATA COLLECTION	7-3
7.2.1	<i>Data collection from field</i>	7-3
7.2.2	<i>Rock mass parameters estimation</i>	7-5
7.2.3	<i>Selection of representative sections for analysis</i>	7-7
7.2.4	<i>Summary of input data for selected tunnel sections</i>	7-7
7.2.5	<i>Rock mass strength calculation</i>	7-9
7.2.6	<i>Rock mass modulus calculation</i>	7-9
7.3	ROCK MASS CLASSES AND SUPPORT TYPE.....	7-10
7.4	SQUEEZING ANALYSIS	7-11
7.4.1	<i>Squeezing prediction criteria</i>	7-12
7.4.2	<i>Rock support interaction using CCM</i>	7-13
7.4.3	<i>Estimation of support pressure and capacity of support</i>	7-17
7.4.4	<i>Deformation due to squeezing</i>	7-21
7.5	NUMERICAL ANALYSIS	7-23
7.5.1.1	<i>Back calculation of intact rock strength</i>	7-23
7.5.2	<i>Input data in Phase2 program</i>	7-23
7.5.3	<i>Phase2 model generation</i>	7-25
7.5.4	<i>Elastic Analysis</i>	7-26
7.5.5	<i>Plastic analysis</i>	7-28
7.6	COMPARISON OF THE RESULTS	7-34
8	EXISTING CHALLENGES AND POSSIBLE SOLUTIONS	8-1
8.1	RE-EXCAVATION OF SQUEEZED SECTION	8-1
8.2	FINAL LININGS.....	8-1
8.2.1	<i>Concrete lining in horse shoe shape</i>	8-1
8.2.2	<i>Steel ribs and shotcrete lining in circular shape</i>	8-3
8.3	COMPARISON BETWEEN THE POSSIBLE SOLUTIONS.....	8-5
9	CONCLUSIONS AND RECOMMENDATIONS	9-1
9.1	CONCLUSIONS	9-1
9.2	RECOMMENDATIONS	9-3
	REFERENCES	A

APPENDICES

APPENDIX A: PROJECT RELATED DOCUMENTS AND DRAWINGS

APPENDIX B: STANDARD CHARTS AND FIGURES

APPENDIX C: DETAIL OF CALCULATIONS AND RESULTS

APPENDIX D: PHASE2 MODELING AND RESULTS

APPENDIX E: FORMAL LETTERS

LIST OF TABLES

Table 2-1: Typical value of density and effective porosity of different types of rock (Panthi, Spring 2012).....	2-1
Table 2-2: Weathering classification according to ISRM, 1978 (Panthi, 2006)	2-6
Table 2-3: Empirical formula for estimation of rock mass strength (Panthi, 2006).....	2-13
Table 2-4: Empirical formula for rock mass deformation modulus in GPa (Panthi, 2006) .	2-14
Table 4-1: Regional Stratigraphy (NEA, 1997)	4-5
Table 4-2: Types of Himalayan rocks and their geomorphic units (Panthi, 2006)	4-5
Table 4-3: Summary of core drilling (NEA, 1998)	4-6
Table 4-4: Summary of seismic refraction survey (NEA, 1998).....	4-7
Table 4-5: Geology of tunnel and rock support class (NEA, 1997).....	4-10
Table 4-6: Predicted support type based on rock mass quality (Q-value).....	4-13
Table 5-1: Classification of Yacambú-Quibor rock units (Hoek and Guevara, 2009a).....	5-9
Table 6-1: Squeezing condition according to Q-system (Barton 2002).....	6-3
Table 6-2: Geotechnical issues associated with the squeezing severity classes and appropriate support types (Hoek and Marinos, 2000).....	6-6
Table 7-1: Input parameters for squeezing analysis of selected tunnel sections.....	7-8
Table 7-2: Rock mass quality class and required support type based on Q-system and applied support type in actual field.....	7-11
Table 7-3: Squeezing prediction according to Singh et al (1992), Q-system (Grimstad and Barton, 1993) and Hoek and Marinos (2000)	7-12
Table 7-4: Properties of rock bolts and shotcrete in R5 and R6 support types	7-14
Table 7-5: Detail composition of support type for selected tunnel sections	7-15
Table 7-6: Maximum support pressure provided by the support system and maximum allowable displacement of support.....	7-15
Table 7-7: Calculation of normal and limiting stress ratio in selected tunnel sections.....	7-17
Table 7-8: Estimation of support pressure using three different approaches	7-18
Table 7-9: Estimated residual support pressure using HM and CCM and assumed residual support pressure at different tunnel sections.....	7-19
Table 7-10:Support capacity estimation in case of Barton et al. (1974) and CCM with 1.5 factor of safety	7-20
Table 7-11:Tunnel strain percentage (tunnel wall closure/tunnel diameter x 100) calculation using Hoek and Marinos (2000) and CCM approaches with and without support....	7-22
Table 7-12:Back calculation of intact rock strength using Hoek and Marinos (2000) approach	7-23
Table 7-13:Input parameters for Phase2 analysis in each tunnel sections for both elastic and plastic analysis	7-24
Table 7-14:Deformation of tunnel from Phase ² program with back calculated intact rock strength from Hoek and Marinos (2000)	7-32
Table 7-15:Improved rock mass properties and corresponding deformation values from Phase ² program	7-32

LIST OF FIGURES

Figure 2-1:	Characteristics of jointing of rock mass after mapping (Panthi, 2006)	2-2
Figure 2-2:	Types of faults and weakness zones (Panthi, Spring 2012).....	2-3
Figure 2-3:	Swelling pressure as a function of expansion measured in NTH Rock Engineering Laboratory, Norway (Nilsen and Thidemann, 1993).....	2-3
Figure 2-4:	Influence of specimen size on the strength of intact rock (Panthi, 2006).....	2-5
Figure 2-5:	Uniaxial compressive strength of rock (left) and strength reduction in percentage (right) as the function of weathering grade (Panthi, 2006)	2-6
Figure 2-6:	Drained and undrained triaxial compression test results for a shale of Pennsylvanian age; w_i is the initial water content, p_w is the pore water pressure (Goodman, 1989).....	2-7
Figure 2-7:	Uniaxial compressive strength at different angle of schistosity plane (Panthi, 2006).....	2-8
Figure 2-8:	Axial and lateral normal strain with increasing deviatoric axial stress (Hypothetical curves) (Goodman, 1989).....	2-9
Figure 2-9:	The Mohr-Coulomb failure criterion with a tension cutoff (Goodman, 1989).....	2-11
Figure 2-10:	Selection of failure criteria according to rock mass condition (Panthi, Spring 2012).....	2-12
Figure 2-11:	Relationship between major and minor principle stresses for Hoek-Brown and equivalent Mohr-Coulomb criteria (Hoek et al., 2002).....	2-12
Figure 3-1:	Plot of vertical stresses against depth below surface (left) and variation of ratio of average horizontal stress to vertical stress with depth below surface (right) (Hoek and Brown, 1980).....	3-2
Figure 3-2:	Stress map of the Himalaya and adjacent region (World Stress Map, 2008) ...	3-3
Figure 3-3:	Stress trajectories in rock mass surrounding a circular opening (left) and tangential and radial stress distribution in elastic and non elastic conditions (right) (Panthi, 2006).....	3-4
Figure 3-4:	An illustration of squeezing in a circular tunnel (Panthi, 2006).....	3-7
Figure 3-5:	Creep in relation to the complete stress-strain curve(Goodman, 1989).....	3-8
Figure 3-6:	Regions of behavior in creep (Goodman, 1989).....	3-9
Figure 4-1:	Project area location map (NEA, 1997).....	4-2
Figure 4-2:	Layout of project components	4-3
Figure 4-3:	Geological map of Nepal (Dahal and Hasegawa, 2008).....	4-4
Figure 4-4:	Block Diagram of the Himalaya giving different litho-tectonic units (Deoja, 1991).....	4-4
Figure 4-5:	Geological Plan and Profile along headrace tunnel alignment of CHEP (Source: Latest information from CHEP site office, 2012)	4-9
Figure 4-6:	Predicted rock classes along headrace tunnel (NEA, 1997)	4-10
Figure 4-7:	Orientation of main joint sets and headrace tunnel alignment of CHEP ((NEA, 1997).....	4-11
Figure 4-8:	Rock mass condition at different chainage along headrace tunnel of CHEP	4-11

Figure 4-9:	Tunnel squeezing in headrace tunnel of CHEP: Significant floor heave (left) and wall closure in hill side (right).....	4-12
Figure 4-10:	Several instances of tunnel excavation in CHEP at squeezing part	4-14
Figure 5-1:	Location map of Kaligandaki “A” Hydroelectric Project, Nepal	5-2
Figure 5-2:	Project topography and longitudinal profile with geological description of Kaligandaki “A” hydroelectric project (Panthi, 2006).....	5-2
Figure 5-3:	Geological environment of Kaligandaki “A” Hydroelectric Project (Panthi, 2006).....	5-3
Figure 5-4:	Orientation of main joint sets and Kaligandaki “A” headrace tunnel (Panthi, 2006).....	5-4
Figure 5-5:	Collapse due to strength and stress anisotropy (left) and cracks formed by high squeezing pressure (right) (Panthi, 2006).....	5-5
Figure 5-6:	Horizontal strain (%) between chainage 1964 and 4032 in Kaligandaki headrace tunnel (left), typical tunnel section indicating tape extensometer measuring point (right) (Panthi, 2006).....	5-5
Figure 5-7:	Location map of Yacambú-Quibor tunnel project, Venezuela (Hoek and Guevara, 2009a)	5-7
Figure 5-8:	Plan and cross section along tunnel alignment of Yacambú-Quibor project, Venezuela (Hoek and Guevara, 2009a).....	5-7
Figure 5-9:	Tectonic plates in the south-western region of South America and Panama (Hoek and Guevara, 2009a).....	5-8
Figure 5-10:	Floor heave about 100m behind the Intake drive TBM in 1979 at a depth of 400 to 425 m below surface (Hoek and Guevara, 2009a) (left) and Mining out the remains of a tunnel boring machine trapped by squeezing of the tunnel during a stoppage of the drive (Hoek, 2001) (right).....	5-10
Figure 5-11:	Geometry of lining used between Chainage 12750 and 12850 (Hoek and Guevara, 2009a)	5-10
Figure 5-12:	Evolution of the damage caused by squeezing between Chainage 12+750 and 12+850 (Hoek and Guevara, 2009a)	5-11
Figure 5-13:	Design details of yielding support (left) and installation of circular lining such as that illustrated in figure 5-15 (right) (Hoek and Guevara, 2009a)	5-12
Figure 5-14:	Details of one of the two sliding joints in the steel sets (left) and assembled steel set with two sliding joints (right) (Hoek and Guevara, 2009a).....	5-13
Figure 5-15:	Completed tunnel lining in one of the deepest sections between Chainages 10000 and 12000 in Yacambú-Quibor tunnel (Hoek and Guevara, 2009a).....	5-13
Figure 6-1:	Criteria for predicting squeezing ground (Singh et al., 1992)	6-2
Figure 6-2:	Plot of tunnel convergence against the ratio of rock mass strength to in situ stress in case of unsupported tunnel (Hoek and Marinos, 2000).....	6-4
Figure 6-3:	Approximate relationship between strain and the degree of difficulty associated with tunneling through squeezing rock in case of unsupported tunnel (Hoek and Marinos, 2000).	6-5
Figure 6-4:	a) Cylindrical tunnel of radius R driven in the rock mass. b) Cross-section of the rock mass at the section A-A'. c) Cross-Section of the circular support installed at section A-A' (Carranza-Torres and Fairhurst, 2000).....	6-8

Figure 6-5:	Loading of the support at section A-A' due to progressive advance of the tunnel face (Carranza-Torres and Fairhurst, 2000).	6-9
Figure 6-6:	Schematic representation of Longitudinal Displacement Profile (LDP), Ground Reaction Curve (GRC) and Support Characteristics Curve (Carranza-Torres and Fairhurst, 2000)	6-10
Figure 6-7:	Representation of an ungrouted mechanical-anchored bolt (Carranza-Torres and Fairhurst, 2000)	6-14
Figure 6-8:	Maximum Support pressure versus tunnel radius for the different types of support (Hoek, Corner).....	6-15
Figure 6-9:	Loading test on lattice girder (Baumann and Betzle, 1984)	6-16
Figure 6-10:	Measured and computed load-deformation deformation for the test girder (Baumann and Betzle, 1984).....	6-16
Figure 6-11:	a) circular cavity in a Mohr-coulomb material subject to uniform internal pressure and unequal far field stress. b) limiting values of stress ratio k_{lim} as a function of scaled mean stress σ_o/σ_{ci} and friction angle ϕ (Carranza-Torres and Fairhurst, 2000).	6-18
Figure 6-12:	LDP templates to be used as an alternative to equations 6-8, 6-9, 6-10 (Vlachopoulos and Diederichs, 2009).....	6-21
Figure 7-1:	Flowchart of the methodology applied for the estimation of more accurate rock mass parameters. (Note: HM is Hoek and Marinos (2000) and CCM is Convergence Confinement Method)	7-2
Figure 7-2:	A typical tunnel log of CHEP headrace tunnel at chainage 3+404.....	7-3
Figure 7-3:	Convergence measurement data in headrace tunnel of CHEP at different time and typical tunnel section for the extraction of convergence data (right top corner of figure).....	7-4
Figure 7-4:	Matching the tunnel wall closure with measured value for different value of tectonic stress and intact rock strength combinations in Phase ² program (Tunnel section at chainage 3+404)	7-6
Figure 7-5:	Matching the crown displacement with measured value for different value of tectonic stress and intact rock strength combinations in Phase ² program (Tunnel section at chainage 3+404m).....	7-6
Figure 7-6:	Verification of tunnel wall closure with measured value for 3.5 MPa tectonic stress in Phase ² program (Tunnel section at chainage 3+420m).....	7-7
Figure 7-7:	Rock mass strength estimation using five different methods for the selected tunnel sections	7-9
Figure 7-8:	Rockmass Modulus estimation using five different methods for selected tunnel sections	7-10
Figure 7-9:	Squeezing and non-squeezing sections of tunnel according to Singh et al (1992) (left) and Squeezing classes for different sections of tunnel with respect to calculated strain % according to Hoek and Marinos (2000) for unsupported tunnel and measured strain % (right)	7-13
Figure 7-10:	GRC and LDC of ten tunnel sections at different chainages	7-14
Figure 7-11:	Interaction of GRC, LDP and SCC in tunnel section 3+404m	7-16

Figure 7-12: Comparison chart of estimated support pressure by three different approaches and applied support capacity	7-18
Figure 7-13: Comparison of residual support pressure estimated by HM and CCM with assumed pressure at CHEP site for different tunnel sections	7-19
Figure 7-14: Comparison of estimated support capacity (1.5 FOS) with provided support capacity.....	7-20
Figure 7-15: Plastic zone radius around the tunnel after excavation (with and without support) using HM and CCM approaches	7-21
Figure 7-16: Comparison of strain percentage (with and without support) calculated using HM and CCM approaches with measured strain percentage	7-22
Figure 7-17: Typical output from rock lab software for tunnel section 3+404	7-24
Figure 7-18: Finished model in Phase2 for tunnel section at chainage 3+404m	7-25
Figure 7-19: Closure view of tunnel excavation and support application for tunnel section at chainage 3+404m	7-25
Figure 7-20: Major Principal Stress before excavation (top), after excavation (bottom left) and after excavation with support (bottom right) for section 3+404m (Elastic Analysis).....	7-26
Figure 7-21: Strength factor before and after support application for section 3+404m (Elastic Analysis).....	7-27
Figure 7-22: Total displacement before and after support application for section 3+404m (Elastic Analysis)	7-27
Figure 7-23: Tunnel wall closure at different tunnel sections from Phase ² analysis (Elastic) and measured convergence.....	7-28
Figure 7-24: Sheared rock mass condition before tunnel excavation i.e. stage 1 (left) and after tunnel excavation i.e. stage 2 (right) in section at chainage 3+404m. ...	7-29
Figure 7-25: Closure view of sheared rock mass condition before (left) and after (right) tunnel excavation in section at chainage 3+404m.....	7-29
Figure 7-26: Major Principal Stress before excavation (top), after excavation without support (bottom left) and after excavation with support (bottom right) for section 3+404m (Plastic Analysis)	7-30
Figure 7-27: Strength factor before and after support application for section 3+404m (Plastic Analysis).....	7-31
Figure 7-28: Total displacement before and after support application for section 3+404m (Plastic Analysis).....	7-31
Figure 7-29: Total tunnel wall closure from Phase2 analysis and measured value for different tunnel sections	7-33
Figure 7-30: Crown displacement from Phase2 analysis and measured value for different tunnel sections	7-33
Figure 7-31: Comparison of intact rock strength back calculated from Hoek and Marinos (2000) with improved strength using Phase ²	7-34
Figure 7-32: Tunnel wall closure in percentage without support from different methods using improved input intact rock strength.....	7-34
Figure 7-33: Tunnel wall closure in percentage with support from different methods using improved input intact rock strength.....	7-35

Figure 7-34: Discrepancies of results i.e. from HM and CCM with respect to Phase2 results for both cases; with support and without support.....7-35

Figure 7-35: Comparison of Phase2 result with the deformation from HM analysis in case of isostatic stress condition and circular tunnel section in Phase2 model7-36

Figure 8-1: Deformation after concrete lining in tunnel sections at chainage 3+190m (top left), 3+404m (top right), 3+420m (bottom left) and 3+733m (bottom right) .8-2

Figure 8-2: Tunnel strain (%) in different location of tunnel contour (with concrete lining)8-3

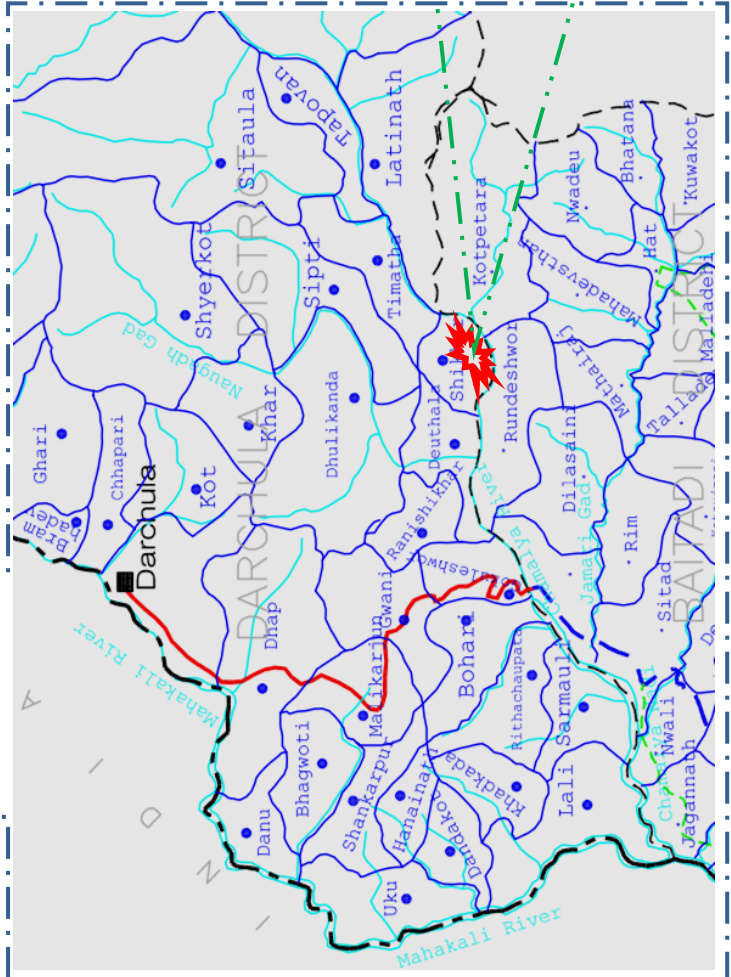
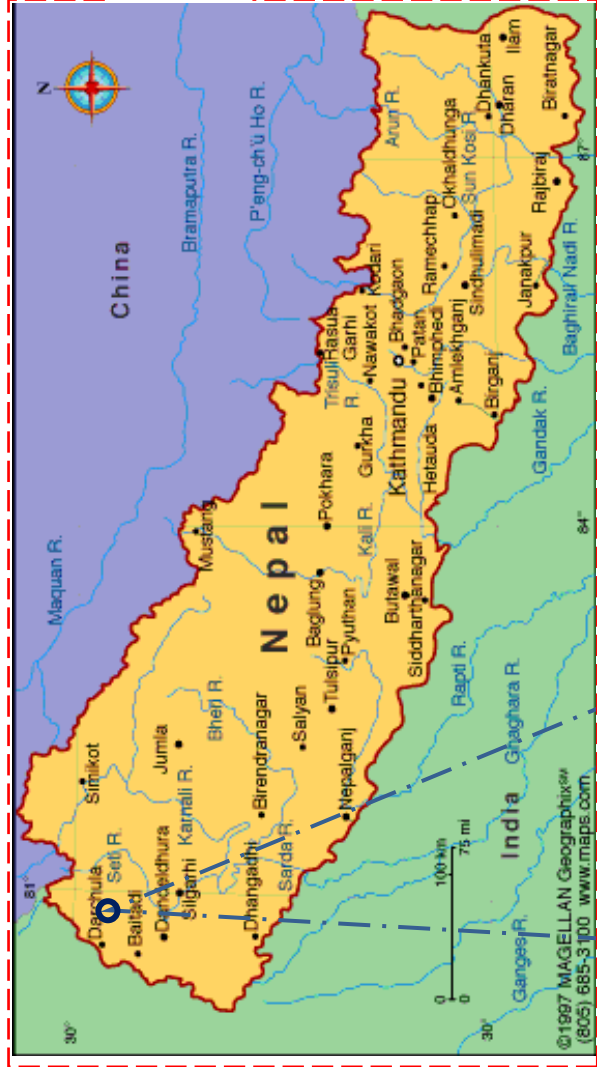
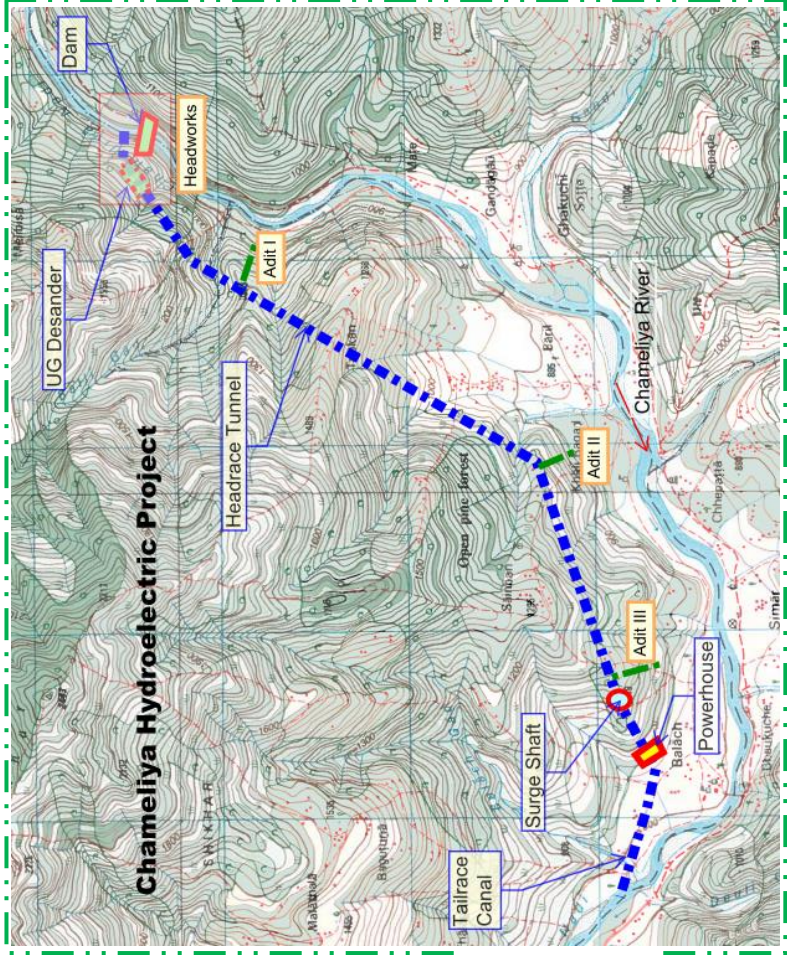
Figure 8-3: Support capacity plots of concrete lining in tunnel sections at chainage 3+190m (top left), 3+404m (top right), 3+420m (bottom left) and 3+733m (bottom right)8-3

Figure 8-4: Deformation after final lining in tunnel sections at chainage 3+190m (top left), 3+404m (top right), 3+420m (bottom left) and 3+733m (bottom right).....8-4

Figure 8-5: Tunnel strain (%) in different location of tunnel in circular shape (With steel ribs and shotcrete)8-4

LIST OF ABBREVIATIONS

CCM	Convergence Confinement Method
CHEP	Chameliya Hydroelectric Project
ESR	Excavation Support Ratio
FOS	Factor of Safety
GRC	Ground Reaction Curve
GSI	Geological Strength Index
GWh	Giga Watt Hour
HM	Hoek and Marinos (2000)
ISRM	International Society for Rock Mechanics
LDP	Load Displacement Curve
MBT	Main Boundary Thrust
MCT	Main Central Thrust
MPa	Mega Pascal
MW	Mega Watt
NEA	Nepal Electricity Authority
NGI	Norges Geotekniske Institutt
NTH	Norges Tekniske Høgskole
NTNU	Norwegian University of Science and Technology
RMR	Rock Mass Rating
RQD	Rock Quality Desination
SCC	Support Characteristics Curve
SRF	Strength Reduction Factor
TBM	Tunnel Boring Machine
UCS	Uniaxial Compressive Strength
VDC	Village Development Committee



1 INTRODUCTION

1.1 BACKGROUND

At present condition, the development of Nepal is directly related to energy production. One of the main sources of energy production is water resource and available topography of Nepalese hills. Most of the proposed projects are medium to large in capacity. For larger projects, the discharge will be higher that means huge amount of water has to be handled in water conveyance system. Also, the steep topography has been helping to produce more energy within a short stretch of steeper rivers. Because of the steep topography, it is proved to be very difficult to build canal or pipe as water conveyance system on the surface. Hence, tunnel has been only the remaining feasible alternative to be used as water conveyance system. But, at the same time, there are higher risks and uncertainties in underground works like tunnels and shafts or caverns.

The very young and fragile geological formation of Nepal Himalayas has been challenging the underground works in this area. Mainly, there are two types of stability problems viz. squeezing in weak and deformable rocks and rock burst and spalling in very strong and brittle rocks. According to Panthi (Autumn 2012), tunnel squeezing is a common phenomenon in the Himalayan rock mass with high degree of schistosity. Weak rocks like mudstone, shale, slate, phyllite, schist, highly schistose gneiss and the rock mass of the tectonic fault zones are incapable of sustaining high stresses. A reliable prediction on the extent of squeezing is therefore essential to make strategy regarding stabilizing measures and optimization of tunnel rock support well in advance. With this background, one of the projects in Nepal, Chameliya hydroelectric Project (CHEP), has been decided to consider as a case study. The Chameliya Hydroelectric Project site is located on the Chameliya River in Darchula district of the far western region of Nepal and has installed capacity of 30 MW. The headrace tunnel is horseshoe type and has diameter of 5.2-4.2m, where 4.2m is on the concrete lined part. On the headrace tunnel of CHEP, there is high degree of squeezing problem that is faced in about 800m long stretch of tunnel. Hence, the title of thesis has been chosen as “Evaluation on the Squeezing Phenomenon at the Headrace Tunnel of Chameliya Hydroelectric Project, Nepal”.

1.2 OBJECTIVE AND SCOPE OF THE STUDY

The main objectives of the study are;

- Assessment of squeezing and evaluation of stability of the tunnel
- Assessment of rock support interaction and optimization of rock support
- Solution of existing problem due to squeezing based on the experience from other similar projects with same stability problems

The scope of this thesis covers the following extent;

- Review existing theory on the stability issues in tunnelling with particular focus on tunnel squeezing.
- Briefly describe about the Chameliya Hydroelectric Project including the extent of engineering geological investigations carried out during planning.

- Document on the rock support principle used while tunnelling. Document on the measured deformation along the tunnel alignment.
- Back analyse on the squeezing phenomenon using existing empirical, semi-analytical and analytical approaches.
- Attempt to produce a support characteristic curve based on applied support, measured final deformation and reviewed theory.
- Carry out stability analysis using Numerical Modeling.
- Compare and discuss the analysis results from empirical, semi-analytical, analytical and numerical approaches.

1.3 METHODOLOGY OF THE STUDY

The case, Chameliya Hydroelectric Project, has been chosen for the evaluation of squeezing phenomenon. Two more cases histories i.e. Kaligandaki “A” Hydroelectric Project, Nepal and Yacambú-Quibor tunnel, Venezuela, with similar stability problems have been chosen to understand more about squeezing phenomenon and to propose the solution to the problem caused by squeezing. The following methodology has been applied during the study;

1. Literature review

- Background theories on rock mass properties and stress induced instability in tunneling such as squeezing phenomenon
- Review of cases histories
- Background theories on stability analysis and deformation calculation

2. Data collection

The data consisted of deformation measurements, feasibility reports and other project related reports, photographs, lab test results etc. These data has been collected from CHEP project site and main office located in Kathmandu, the capital city of Nepal. The remaining data have been assumed based on the different literatures available.

3. Squeezing analysis and support measure

Based on these data, the analysis of squeezing phenomenon has been done using different approaches. The empirical methods; Singh et al. (1992), Q-system, semi-analytical method; Hoek and Marinos (2000), Analytical method; Convergence Confinement Method (Carranza-Torres and Fairhurst, 2000) and numerical method; Phase² have been used for the squeezing analysis. The rock mass parameters are back calculated from measured deformation using Hoek and Marinos (2000) approach and refined using Phase² program. More detail study has been done further using improved rock mass parameters and compare the results obtained from different methods.

4. Solution to the existing problems caused by squeezing

Based on the available support types and experience form different cases histories, different solutions have been proposed and analyzed using Phase² program.

1.4 ORGANIZATION OF THE THESIS

There are altogether 9 chapters in this thesis report. Each chapter has its own importance. Chapter 1 covers the introduction of thesis, its objective and scope. From chapter 2 literature review starts. Chapter 2 covers rock and rock mass properties, which is the basic foundation

in any rock engineering study. Likewise, chapter 3 illustrates the tunnel stability problems caused due to overstressing of rock mass with main focus on squeezing phenomenon. Chapter 4 explains about the case, its location, geology, rock mass quality, stability problems in headrace tunnel etc. Similarly, chapter 5 covers two cases histories; one is from Nepal and another is from Venezuela. The main focus of this thesis starts from chapter 6. It covers existing methods of squeezing analysis, use of stability analysis techniques in squeezing analysis etc. Likewise, chapter 7 focuses on the squeezing analysis, comparison of results from different approaches where as chapter 8 explains about possible solutions to the existing squeezing problem. In the end, chapter 9 covers discussion, conclusions of the thesis and recommendation for further study.

1.5 LIMITATION OF THE STUDY

The main problem faced during the study is the input parameter estimation. The main source of input data is information gathered from CHEP officials and field. The information from field was lacking testing data. So, this information was not sufficient to estimate all the required data. Hence many literatures such as books, journals, thesis reports and discussions with supervisor and co-supervisor have been used to estimate the remaining parameters that were not found from project documents. The parameters estimated from literatures or similar reference project may not represent the reality of study case. In addition to input parameter estimation, the difficulty is also with availability of time for the analysis and verification. It would be far better to have at least one field visit to the project site in the middle of study period in order to test the rock strength and rock stresses. But because of the time and money constraints, it was impossible to go far western region of Nepal from Norway and conduct the testing in project site.

2 ROCK AND ROCK MASS PROPERTIES

2.1 INTRODUCTION

Rock is a naturally occurring and composed aggregate of one or more minerals. Some of the rocks have only one mineral whereas most rocks contain two, three or four main minerals and other few accessory minerals. Different minerals have different physical properties. Hence the physical properties of the rock will clearly depend upon the type and amount of different minerals present in it. On the other hand, shape, size, orientation of the minerals and also the binding forces between the minerals largely influence the physical as well as mechanical properties of rocks (Nilsen and Thidemann, 1993). The main physical properties of the rocks are density, porosity, wave velocity and heat transfer and expansion. The density and porosity of most typical rock types are given in Table 2-1.

Table 2-1: Typical value of density and effective porosity of different types of rock (Panthi, Spring 2012)

Rock type	Dry (t/m ³)	Effective porosity (%)	
	mean	Typical values	St. dev.
Banded gneiss	2.68	0.87	0.1
Micagneiss	2.73	0.76	0.1
Limestone, dolomite and marble	2.82	0.50	0.1
Phyllite	2.78	0.45	0.05
Trondemite	2.70	0.84	0.05
Granite and quartzite	2.65	0.22	0.05
Gabbro and amphibolite	3.15		
Metasandstone	2.65	0.81	0.2
Yong sandstone	2.50	30%	

The density of different rock types is in the range of 2.5 to 3.2 t/m³ and effective porosity is less than 1% for nonporous crystalline rocks and exceeding 30% in case of young sedimentary rocks. Basically, rocks are inhomogeneous due to the different mineral composition. Anisotropy¹ is a distinctive feature of many types of rock. Mainly mica-content is the governing factor for degree of anisotropy. While considering the mechanical and physical properties, two terms should be considered i.e. rock and rock mass. Rock mass is the total in-situ material containing intact rock, all joints and other discontinuities and structural features. The properties of rock mass may be quite different from that of intact rock and has more concern in practical life (Nilsen and Thidemann, 1993). The properties of intact rock can be found by testing it in laboratory while the properties of rock mass will depend upon the field testing and measurements.

¹ Anisotropy means the properties of rocks that are different in different directions.

2.2 ROCK MASS STRUCTURES

Rock mass structure is the nature and distribution of structural features within the rock mass. The main types of structural features of the rock mass are bedding plane, joints, folds, faults, shear zones and dykes (Brady and Brown, 2007). The term discontinuity is used as a collective term for all fractures and structural features. The presence of structural features largely influences the properties of rock mass which could be different from intact rock. Some of the structural features are described below.

2.2.1 Bedding plane

Bedding planes divide the rock into bed or strata basically in sedimentary rocks and are highly persistent features. It may contain parting material of different grain size from sediment forming the rock mass, or may have been partly healed by low-order metamorphism. In either of these two cases, there would be cohesion between the beds; otherwise, shear resistance on bedding planes would be purely frictional. Arising from the depositional process, there may be a preferred orientation of particles in the rock, giving rise to planes of weakness parallel to bedding (Brady and Brown, 2007).

2.2.2 Jointing of rock mass

Joints are the most common structural features present in the rock mass. A group of parallel joints is called a joint set and joint sets intersect to form a joint system. Joints may be open, filled or healed. They frequently form parallel to bedding planes, foliations or slaty cleavage, where they may be termed bedding joints, foliation joints or cleavage joints. Sedimentary rocks often contain two sets of joints approximately orthogonal to each other and to the bedding planes (Brady and Brown, 2007).

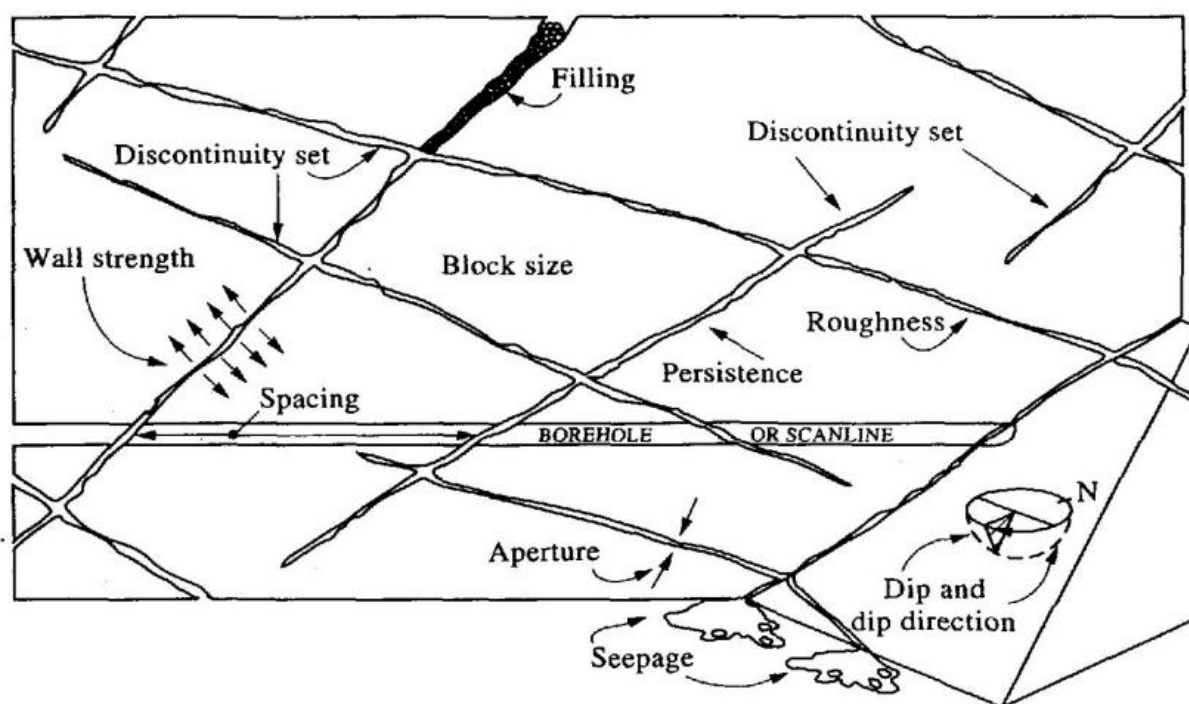


Figure 2-1: Characteristics of jointing of rock mass after mapping (Panthi, 2006)

Figure 2-1 shows the different characteristics of the joints that can be identified during the field mapping. After field mapping, joint orientation can be presented with the help of joint rosette and stereographic projection.

2.2.3 Weakness Zones and faults

The number of lineaments can be observed in the bed rock from a far distance, for instance from an aeroplane. These lineaments can make a joint patterns but on a much larger scale. The distance between parallel lineaments can be in the order of hundreds and thousands of meters. These lineaments are the weakness zones present in bed rock. There are mainly two types of weakness zones (Nilsen and Thidemann, 1993);

- beds or layers of particularly weak rock in a series of sedimentary or metamorphic rocks,
- a zone of crushed and/or altered rock formed by faulting or other tectonic movements

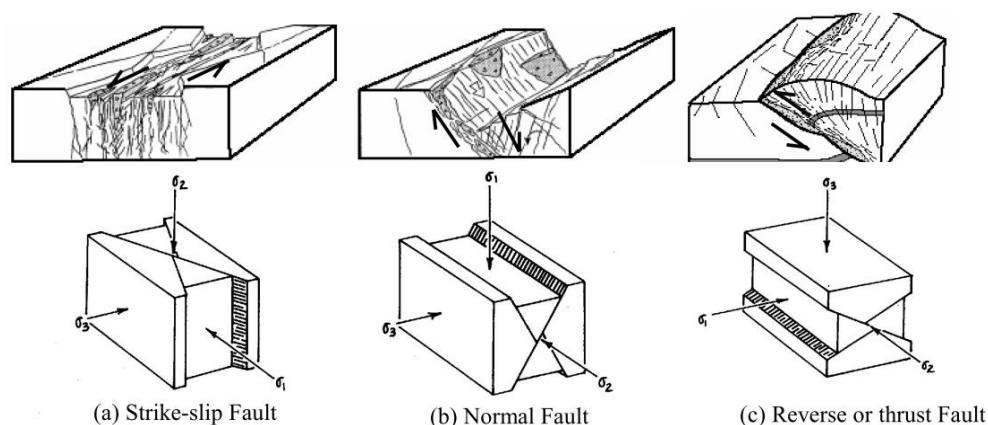


Figure 2-2: Types of faults and weakness zones (Panthi, Spring 2012)

Fault is also a weakness zone where identifiable shear displacement has taken place. They may be recognized by the relative displacement of the rock on opposite side of the fault plane. The sense of these displacements is often used to classify faults.

The filling materials within weakness zones are called **gouge materials**. The main gouge materials are often coarse rock fragments. But some minerals may be altered or changed into new minerals and form clay minerals. Some clay minerals, e.g. smectites, have a swelling capacity when exposed to water. The swelling pressure can be measured by using oedometer test. It can clearly be seen in figure 2-3 that the swelling pressure drops dramatically if the smectite is given a few percent pre-expansion. This condition should be kept in mind when rock support is

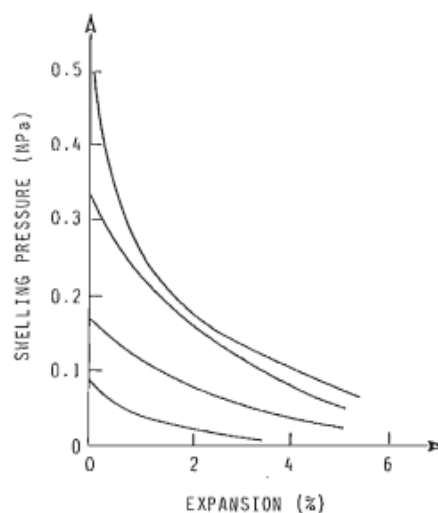


Figure 2-3: Swelling pressure as a function of expansion measured in NTH Rock Engineering Laboratory, Norway (Nilsen and Thidemann, 1993)

to be designed in the areas with weakness zones containing smectite.

2.3 ROCK MASS STRENGTH AND DEFORMABILITY

Strength and other mechanical properties of the rock such as elasticity, is very important in all aspects of rock engineering. The most commonly used methods for strength testing are uniaxial compressive strength test, triaxial strength test and point load strength test. The failure criterion of the rock depends upon these laboratory testing. The different failure criteria will be discussed further in this chapter.

2.3.1 Uniaxial Compressive strength test

Uniaxial compression of cylindrical intact rock specimens prepared from drill core is probably the most widely used test on rock. It is basically used to determine the uniaxial or unconfined compressive strength, σ_{ci} , and the elastic constants, Young's modulus, E , and Poisson's ratio, ν , of the rock materials. The uniaxial compressive strength of the intact rock is used in rock mass classification systems and as a basic parameter in the rock mass strength criteria.

The test is very simple but the great care should be taken in interpreting the results from it. The observed response will depend on the nature and composition of rock and the condition of the test specimens. Brady and Brown (2007) explained that for similar mineralogy, σ_{ci} will decrease with increasing porosity, increasing degree of weathering, increasing degree of micro fissuring and increasing water content. Thus the uniaxial compressive strength of rock will vary with the grain size, packing density, the nature and extent of cementing between the grains and the level of pressure and temperature that the rock has been subjected to throughout its history (Brady and Brown, 2007). The detail of standard test procedure and interpretation is described in the book by Brady and Brown (2007).

2.3.2 Factor influencing the rock strength

The rock mass strength depends upon the uniaxial compressive strength of the intact rock. Hence the factors that influence the intact rock strength also influence the rock mass strength. There are many factors that affect the intact rock strength and some of them are explained in the following text.

Scale Effect

The size dependency of rock strength is influenced by the degree of metamorphism or gneissosity in the rock mass. Crystalline unweathered rocks have relatively small size effect, while highly schistose, foliated and deformed rocks of sedimentary and metamorphic origin such as shale, slate, phyllite and schist have considerable size as well as directional effect on their strength which is shown in Figure 2-4 (Panthi, 2006).

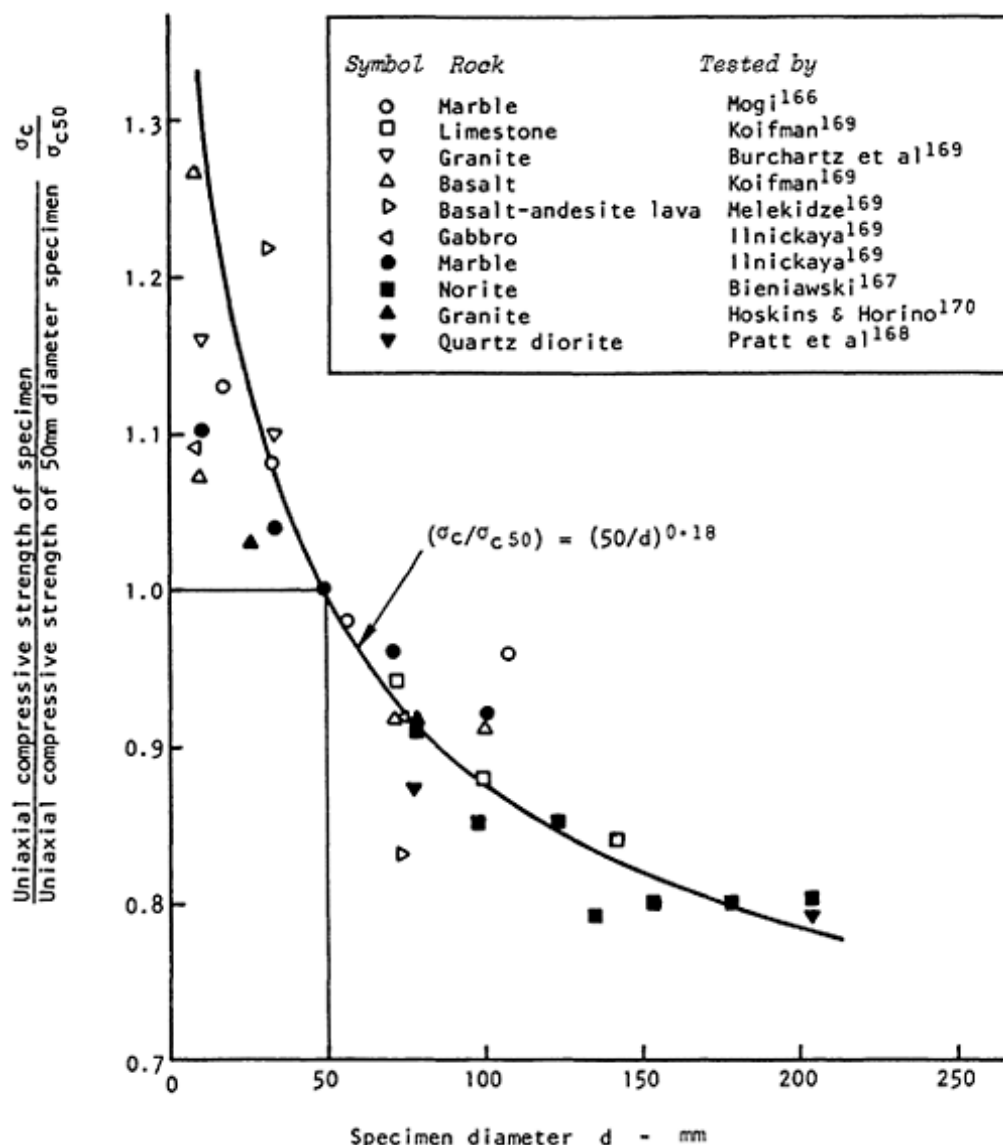


Figure 2-4: Influence of specimen size on the strength of intact rock (Panthi, 2006)

The figure is an example of great significance that demonstrates considerable reduction on rock strength by the increase in sample size. For example, from figure we can say that by increasing the specimen diameter from 50 mm to 200 mm, the rock strength is reduced by almost 25 percent (Panthi, 2006).

Weathering effect

Generally, weathering process in the rock mass starts from its discontinuities and migrates to the rock minerals. Weathering reduces properties such as rock mass strength, deformability, slaking durability and frictional resistance. At the same time it may increase permeability considerably. There could be variation in degree of weathering in the rock masses. Panthi (2006) explained that there are six categories of weathering grades that are defined by ISRM (1978) which are given in Table 2-2.

Table 2-2: Weathering classification according to ISRM, 1978 (Panthi, 2006)

Term	Description of rock mass conditions	Weathering grade
Fresh rock	No visible sign of rock material weathering; perhaps slight discolouration on major discontinuity surfaces.	I
Slightly weathered	Discolouration indicates weathering of rock material and discontinuity surfaces. All the rock material may be discoloured by weathering and may be some what weaker externally than in its fresh condition.	II
Moderately weathered	Less than half of the material is decomposed and/or disintegrated to a soil. Fresh or discoloured rock is present either as a continuous framework or as corestones.	III
Highly weathered	More than half of the rock material is decomposed and/or disintegrated to a soil. Fresh or discoloured rock is present either as a discontinuous framework or as corestones.	IV
Completely weathered	All rock material is decomposed and/or disintegrated to soil. The original mass structure is still largely intact.	V
Residual soil	All rock material is converted to soil. The mass structure and material fabric are destroyed. There is a large change in volume, but the soil has not been significantly transported.	VI

According to Panthi (2006), Beavis (1985) and Gupta and Seshagiri Rao (2000) evaluated the weathering effect on the rock mass properties such as porosity, density, tensile strength, uniaxial compressive strength and elasticity modulus and concluded that there is a considerable reducing effect, as illustrated in Figure 2-5.

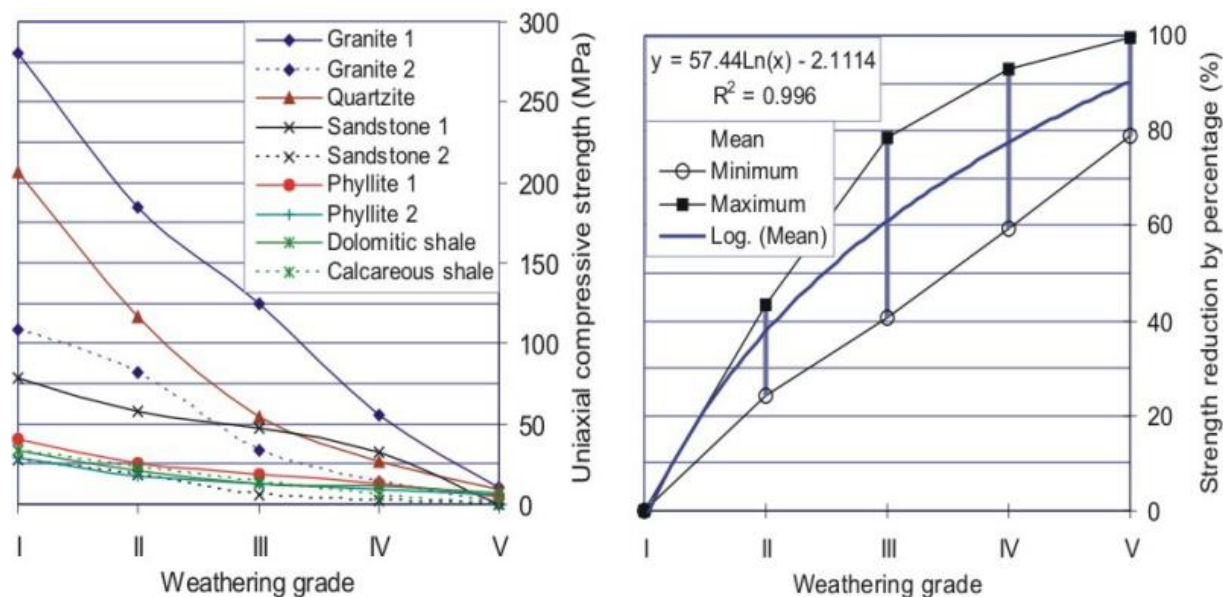


Figure 2-5: Uniaxial compressive strength of rock (left) and strength reduction in percentage (right) as the function of weathering grade (Panthi, 2006)

In actual field, based on the information given in the Table 2-2, the weathering grade can be defined and intact rock strength can be reduced by the percentage according to the information shown in the Figure 2-5.

Effect of water

According to Goodman (1989), some rocks are weakened by the addition of water, the effect being a chemical deterioration of the cement or clay binder. A friable sandstone may, typically, lose 15% of its strength by mere saturation. In extreme cases, such as montmorillonitic clay shale, saturation is totally destructive. In most cases, however, it is the effect of pore and fissure water pressure that exerts the greatest influence on rock strength. If drainage is impeded during loading, the pores or fissures will compress the contained water, raising its pressure.

Figure 2-6 shows the development of pore pressure and consequent loss in strength of a Pennsylvanian shale tested in triaxial compression. Two separate test results are presented in this diagram: the circles represent triaxial compression of a saturated specimen under conditions such that excess pore pressures could drain away rather than accumulate (“drained conditions”); the triangles represent a saturated shale specimen tested without drainage, so that excess pore pressures that develop must accumulate (“undrained conditions”). In the undrained test, the tendency for volume change cannot be fully realized because the water filling the voids undergoes compression rather than drainage. As a result, the water pressure p_w inside the pores begins to increase. This dramatically lowers the peak stress and flattens the post peak curve.

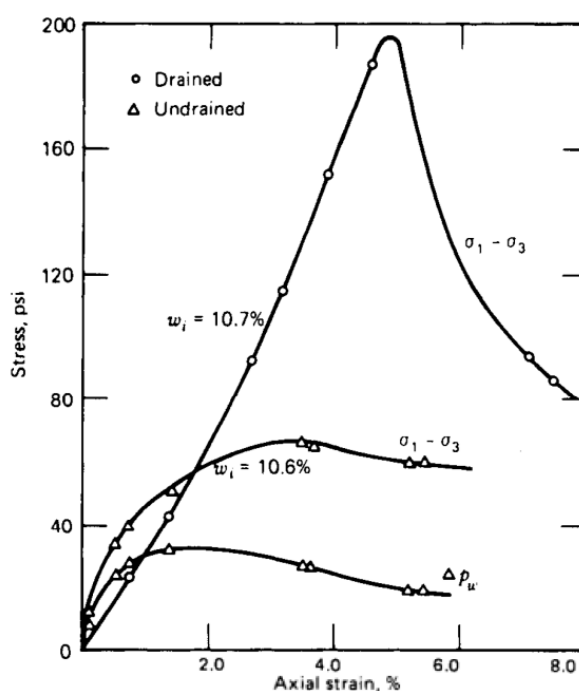


Figure 2-6: Drained and undrained triaxial compression test results for a shale of Pennsylvanian age; w_i is the initial water content, p_w is the pore water pressure (Goodman, 1989)

Many investigators have confirmed the validity of Terzaghi’s effective stress law for rocks, which states that a pressure of p_w in the pore water of a rock will cause the same reduction in peak normal stress as caused by a reduction of the confining pressure by an amount equal to p_w (Goodman, 1989).

Schistosity effect

According to Panthi (2006), the rocks of Himalaya are highly directional in strength and deformability. In most of the cases, thin bands of very weak, highly sheared and thinly foliated rocks such as slate, phyllite and schist are intercalated within the bands of relatively strong and brittle rocks such as gneiss, quartzite and dolomite. Goodman (1989) explained

that sedimentary and metamorphic rocks commonly have strength anisotropy as a result of bedding, foliation and schistosity.

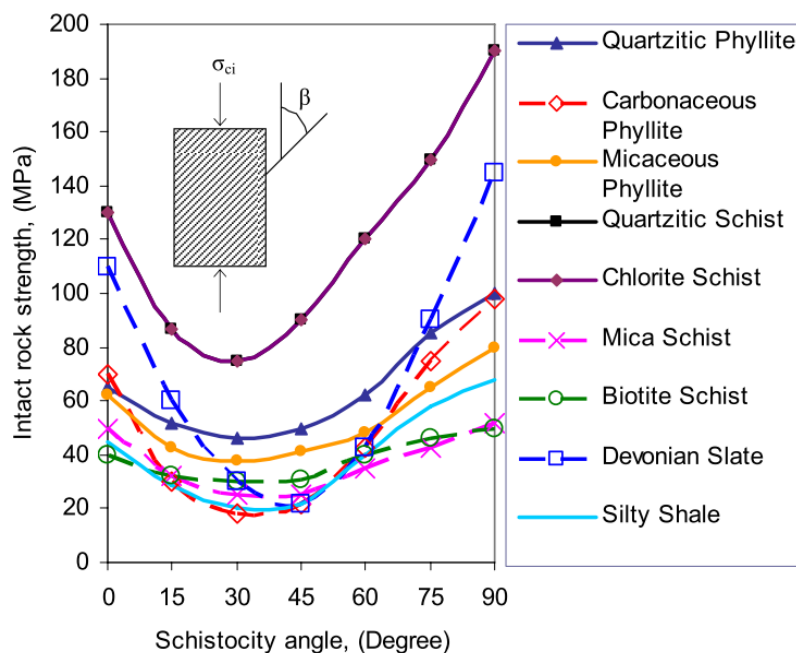


Figure 2-7: Uniaxial compressive strength at different angle of schistosity plane (Panthi, 2006)

Based on the research for different rocks of Himalaya and other part of the world, the effect of schistosity angle on intact rock strength of different rock types has been studied. Figure 2-7 shows that the strength is smallest when the schistosity plane is inclined at around 30 degrees from the direction of loading and is highest when the plane is perpendicular to direction of loading. Hence compressive strength measured on core drilled parallel and normal to the schistosity may give false impression of an isotropic material (Panthi, 2006).

2.3.3 The point load test

Sometimes the facilities required to prepare the specimens and carry out the uniaxial compression tests are not available. In some situations, the detail of uniaxial compressive strength and associated stress-strain behavior need not be required; the point load test can be used for the indirect estimate of uniaxial compressive strength. From the test, a point load index can be calculated as (Brady and Brown, 2007)(Brown and Brady, 1985):

$$I_s = \frac{P}{D^2} \tag{2-1}$$

Where, P is the breaking load and D is diameter of the core

For D = 50mm, it was found that (Broch and Franklin, 1972),

$$\sigma_{ci} \cong 24 I_s \tag{2-2}$$

For other values of D, the following relations can be used (Bieniawski, 1975);

$$\sigma_{ci} = (14 + 0.175D) I_s \tag{2-3}$$

In the case of very weak and/or fissile rocks such as clayey shales or sheared siltstones, the indication of the loading points may cause plastic deformation rather than fracture of the specimen. In such cases the Point Load Test does not give reliable results (Hoek and Marinos, 2000).

2.3.4 Field estimates of σ_{ci}

In case of very weak, highly fractured and schistose rocks, the extraction of test specimen from field is very difficult. The sample will contain discontinuities in the form of bedding and schistosity planes or joints. In such special cases, if it is not possible to obtain the samples for uniaxial compressive strength testing and point load testing, the only way to estimate the uniaxial compressive strength of intact rock is to use the qualitative description of rock materials. The listing of such estimates for different rock types is given in Appendix B0.

2.3.5 Failure criteria

The term “failure” means an almost complete loss of integrity in a sample of rock but in an engineering context, it usually implies loss of ability to perform the intended function. For the purpose of engineering design, it is usual to measure the peak stress value which is point D and can be seen in the Figure 2-8. The failure criteria are related to these peak stresses and the different failure criterion are discussed later in this chapter. But the test may proceed all the way to point E or beyond if the loading system is very stiff. The rock will exhibit a complete stress-strain curve if tested in a stiff system because the system responds to gradual deterioration in load carrying capacity through automatic reduction in the applied load (Goodman, 1989).

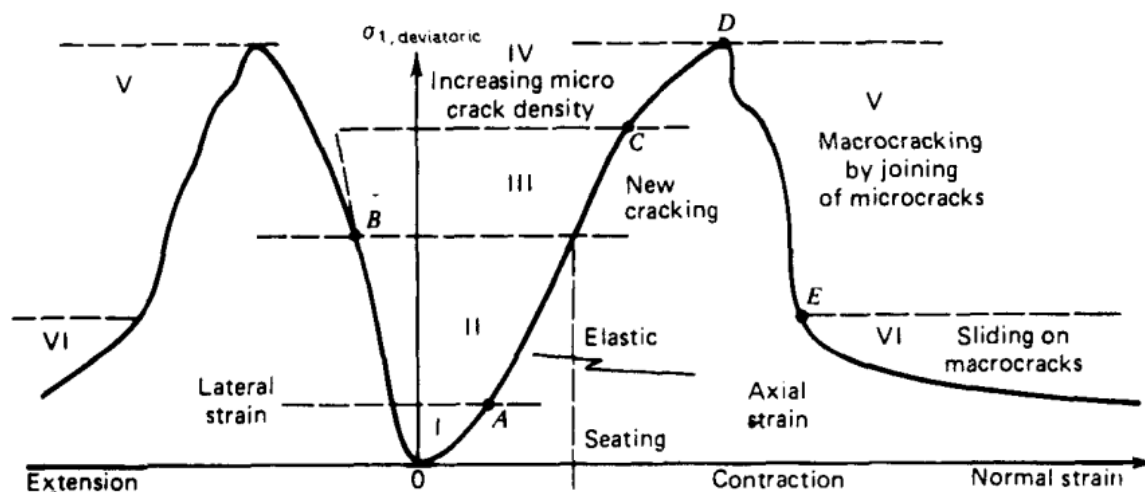


Figure 2-8: Axial and lateral normal strain with increasing deviatoric² axial stress (Hypothetical curves) (Goodman, 1989)

However, the failure criteria are valid only for intact rock materials. As stability problems in tunnels and other underground openings are related to natural joints or cracks created by blasting, such criteria are of less importance for practical tunneling (Nilsen and Thidemann, 1993, p20).

² Deviatoric stresses are the normal and shear stresses that remain after subtracting a hydrostatic stress, equal to the mean normal stress, from each normal stress component.

Hoek-Brown Failure Criteria

The original Hoek-Brown failure criterion in terms of principle stress relationship is defined by the following equation (Hoek and Brown, 1980);

$$\sigma_1' = \sigma_3' + \sigma_{ci} \left(m \frac{\sigma_3'}{\sigma_{ci}} + s \right)^{0.5} \quad 2-4$$

Where,

σ_1' and σ_3' are the major and minor effective principle stresses at failure, σ_{ci} is the uniaxial compressive strength of intact rock material which is discussed in section 2.3.1 and m and s are material constants, where $s=1$ for intact rock.

The derivation angles and cohesive strengths for various practical situations were discussed by Hoek (1990). These derivation were based upon tangents to the Mohr envelop. The shape of principle stress plot or the Mohr envelop could be adjusted by means of a variable coefficient a in place of the square root term in equation . The generalized Hoek-Brown criterion is expressed as (Hoek et al., 2002);

$$\sigma_1' = \sigma_3' + \sigma_{ci} \left(m_b \frac{\sigma_3'}{\sigma_{ci}} + s \right)^a \quad 2-5$$

Where m_b is a reduced value of the material constant m_i and is given by,

$$m_b = m_i \exp \left(\frac{GSI-100}{28-14D} \right) \quad 2-6$$

The basis of values for the material constant m_i and Geological Strength Index, GSI, are given in Appendix B1 and B2 respectively.

s and a are constants for the rock mass given by the following relationships;

$$s = \exp \left(\frac{GSI-100}{9-3D} \right) \quad 2-7$$

$$a = \frac{1}{2} + \frac{1}{6} (e^{-GSI/15} - e^{-20/3}) \quad 2-8$$

D is the factor which depends upon the degree of disturbance to which the rock mass has been subjected by blast damage and stress relaxation. It varies from zero for undisturbed in situ rock masses to 1 for very disturbed rock masses. The guidelines for the selection of D are given in Appendix B3.

Mohr-Coulomb Failure Criteria

According to Goodman (1989), the variation peak stress σ_1 with confining pressure σ_3 is the failure criteria. The simplest and best known criterion of failure for rocks is the Mohr-Coulomb criterion. Figure 2-9 shows the Mohr-Coulomb failure criterion which consists of a linear envelops touching all Mohr's circles representing critical combinations of principle stresses. It is stated in terms of normal and shear stresses on the plane represented by the point of tangency of a Mohr circle with the envelop in equation 2-9.

$$\tau_p = c + \sigma_n \tan \phi$$

Where ϕ is called the angle of internal friction and it describes the rate of increase of peak strength with normal stress (σ_n). τ_p is the peak shear stress or shear strength and c is cohesive strength.

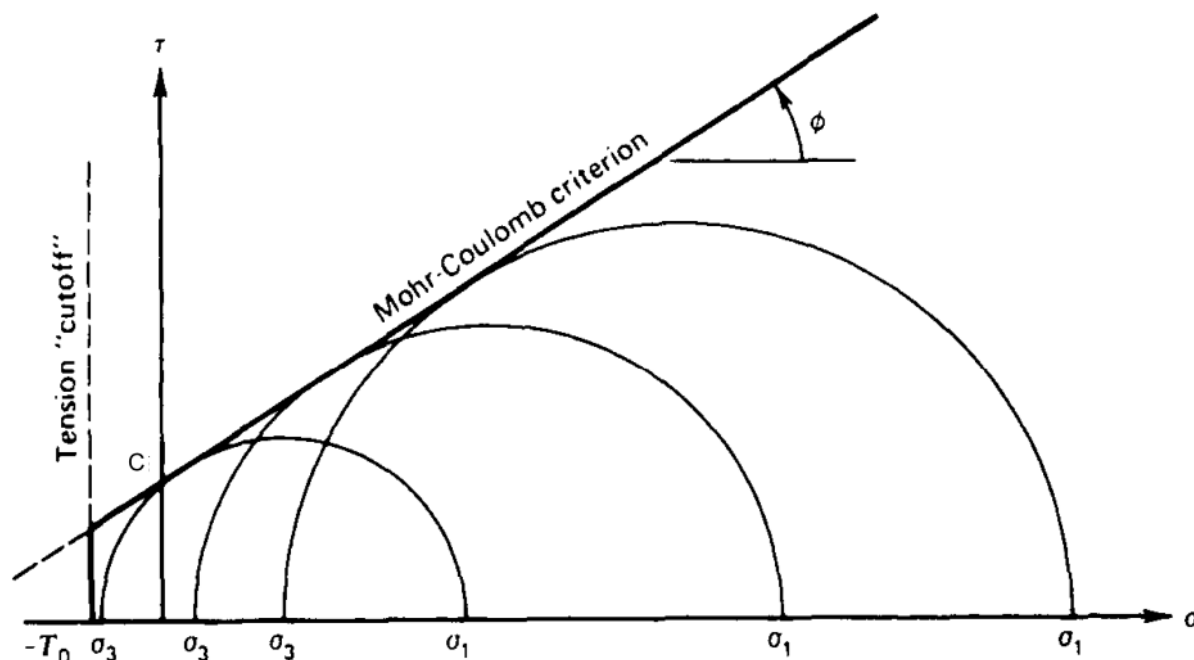


Figure 2-9: The Mohr-Coulomb failure criterion with a tension cutoff (Goodman, 1989)

Goodman (1989) explained that failure occurs when the applied shear stress less the frictional resistance associated with the normal stress on the failure plane becomes equal to a constant of the rock, c . But, the equation 2-9 loses its physical validity when the value of σ_n crosses into the tensile region because it would not be reasonable to consider the frictional resistance associated with tensile stress. However, the Mohr-Coulomb criteria has the simplified solution and it could be used by extrapolating the Mohr-Coulomb line into the tensile region up to the point where minor principle stress (σ_3) becomes equal to the uniaxial tensile strength $-T_0$, and σ_3 can never be less than $-T_0$ which represents the “tension cutoff” (Goodman, 1989).

Relationship between Hoek-Brown and Mohr-Coulomb Failure Criteria

Since most geotechnical software is still written in terms of Mohr-Coulomb failure criteria, it is necessary to determine the equivalent friction angles and cohesive strengths for rock mass and stress range (Hoek et al., 2002). This is done by fitting an average linear relationship to the curve generated by solving equation 2-5 for a range of minor principle stress values defined by $\sigma_t < \sigma_3 < \sigma'_{3max}$, as illustrated in figure 2-11. The fitting process involves balancing the area above and below the Mohr-Coulomb plot. Here σ_t is tensile strength and σ'_{3max} is the upper limit of confining stress over which the relationship is considered and has to be determined for each individual case (Hoek et al., 2002).

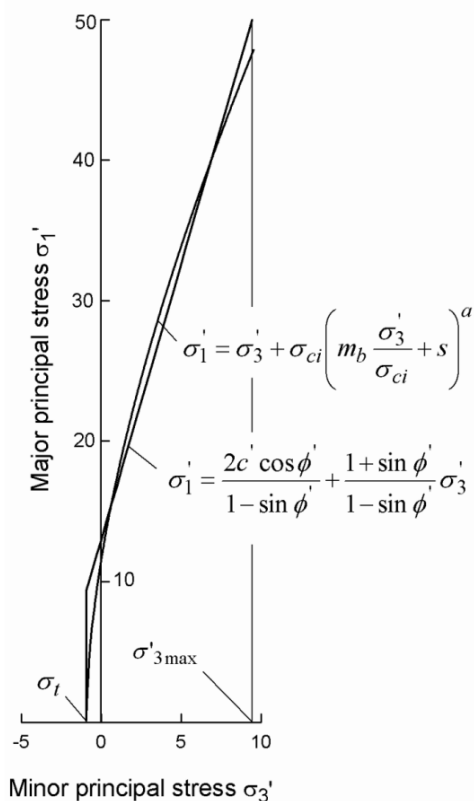


Figure 2-11: Relationship between major and minor principle stresses for Hoek-Brown and equivalent Mohr-Coulomb criteria (Hoek et al., 2002).

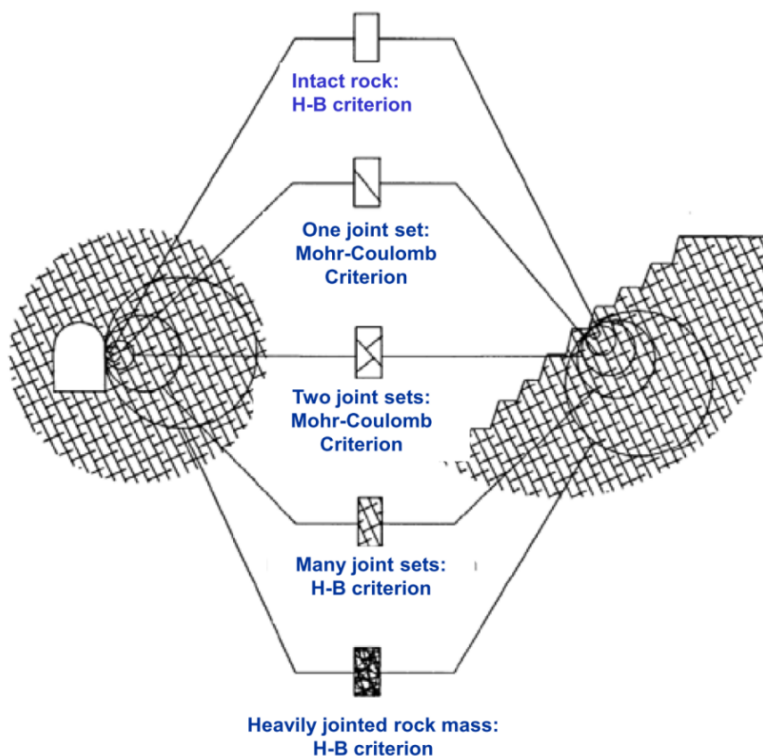


Figure 2-10: Selection of failure criteria according to rock mass condition (Panthi, Spring 2012)

Figure 2-10 shows the selection between Hoek-Brown and Mohr-coulomb failure criteria according to jointing of rock mass. In this figure, it can be clearly seen that the Mohr-Coulomb failure criteria is only applicable for the rock mass having one or two joint sets while in the other cases, Hoek-Brown criterion is applicable.

2.3.6 Rock mass strength estimation

The strength of rock is often influenced by discontinuities and foliation or schistosity planes and the orientation of these features relatively to the direction in which the strength is assessed. Hence the rock mass strength and deformation are different from that of intact rock. An intact rock specimen is usually strong and homogeneous with few discontinuities and much stronger than the rock mass. Hence, a small specimen does not represent the rock mass strength and deformation, but there is a distinct scale effect, which is explained earlier in section 2.3.2. The rock mass strength is very difficult to estimate in the field or by testing in laboratory. Therefore, many authors have suggested different empirical formula for the estimation of rock mass strength. Table 2-3 shows the different empirical relationships and respective authors. In the table, we can see that the RMR value, Q-value and unconfined compressive strength of intact rock (σ_{ci}) are essential to estimate the rock mass strength using these equations.

Table 2-3: Empirical formula for estimation of rock mass strength (Panthi, 2006)

Proposed by	Empirical relationship
Bieniawski (1993)	$\sigma_{cm} = \sigma_{ci} \times \exp\left(\frac{RMR - 100}{18.75}\right)$
Hoek et al. (2002)	$\sigma_{cm} = \sigma_{ci} \times \frac{(m_b + 4s - a(m_b - 8s))(m_b/4 + s)^{a-1}}{2(1 + a)(2 + a)}$
Barton (2002)	$\sigma_{cm} = 5\gamma \times Q_c^{1/3} = 5\gamma \left[\frac{\sigma_{ci}}{100} \times Q \right]^{1/3} = 5\gamma \left[\frac{\sigma_{ci}}{100} \times 10^{\frac{RMR-50}{15}} \right]^{1/3}$
Panthi (2006)	$\sigma_{cm} = \frac{\sigma_{ci}^{1.5}}{60}$

Where; σ_{cm} is the unconfined compressive strength of rock mass in MPa, σ_{ci} is the uniaxial compressive strength of intact rock in MPa, RMR is the Bieniawski's rock mass rating and the detail is given in Appendix B4, s and a are the material constant related to Hoek-Brown failure criteria (can be calculated using equations 2-7 and 2-8 respectively), GSI is the geological strength index, γ is the rock density in t/m^3 , Q_c is the normalized rock mass quality rating and Q is the rock mass quality rating. The detail of Q-system is given in section 6.2.2 and Appendix B5. However, in case of availability of Q-value; RMR and GSI value can be calculated using the equations 2-10 and 2-11 proposed by Barton (1995) and Hoek and Diederichs (2006) respectively. The equations are;

$$RMR = 15 \times \log Q + 50 \quad 2-10$$

$$GSI = RMR - 5 \quad 2-11$$

According to Marinos and Hoek (2001), in case of very weak, highly fractured and schistose rocks, the test specimen will contain discontinuities in the form of bedding and schistosity planes or joints. The laboratory test carried out in such samples will result in a strength value that is lower than the σ_{ci} required for input into the Hoek and Brown criteria. On the other hand, GSI value also considers the effect of discontinuities. Hence, Hoek and Brown criteria will impose a double penalty on the strength and will give unrealistically low values for the rock mass strength (Marinos and Hoek, 2001).

2.3.7 Rock mass deformability estimation

The modulus of deformation of rock mass (E_m) may be defined as the ratio of stress to corresponding strain during loading of rock mass, including elastic and inelastic behavior where as the modulus of elasticity of intact rock (E_{ci}) is the ratio of applied stress and corresponding strain within the elasticity limit. The jointed rock mass does not behave elastically. Hence, the term modulus of deformation is used instead of modulus of elasticity. The deformation modulus of jointed rock mass is very low compared to the elasticity modulus of intact rock.

Table 2-4: Empirical formula for rock mass deformation modulus in GPa (Panthi, 2006)

Proposed by	Empirical relationship
Sarafim and Perera (1983)	$E_m = 10^{\left(\frac{RMR-10}{40}\right)}$
Hoek et al (2002)	$E_m = \left(1 - \frac{D}{2}\right) \sqrt{\frac{\sigma_{ci}}{100}} 10^{\left(\frac{GSI-10}{40}\right)}$
Barton (2002)	$E_m = 10 \times \left(\frac{Q \times \sigma_{ci}}{100}\right)^{1/3}$
Panthi (2006)	$E_m = \frac{1}{60} \times E_{ci} \times \sigma_{ci}^{0.5}$
Hoek and Diederichs (2006)	$E_m = E_{ci} \times \left(0.02 + \frac{1 - D/2}{1 + e^{((60+15D-GSI)/11)}}\right)$

According to Palmström and Singh (2001), the deformation modulus may be measured directly in the field using the methods such as Plate Jacking Test (PJT), Plate Loading Test (PLT), Goodman Jack Test (GJT), Flat Jack Test (FJT), Cable Jack Test (CJT), Radial Jack Test (RJT) and Dilatometer Test (DT). However, all these methods are time-consuming and imply notable cost and operational difficulties. Also, the values obtained from different tests often differ considerably. Therefore, many authors have proposed empirical equations for estimating the rock mass deformation modulus which are given in Table 2-4.

3 STRESS INDUCED INSTABILITY IN TUNNELING

3.1 INTRODUCTION

The design of an underground structure in rock differs from other types of structural design in the nature of loads operating in the system. In conventional surface structures, geometry of the structure and its operating duty define the loads imposed on the system. For an underground rock structure, the rock medium is subject to initial stress prior to excavation. The final, post-excavation state of stress is the result of initial state of stress and stresses induced by excavation. Since induced stresses are directly related to the initial stresses, specification and determination of the pre-excavation state of stress is a key to any design analysis (Brady and Brown, 2007).

According to Goodman (1989), generally, near the surface in hilly regions, in situ stress may approach zero at some points and in other cases, the in situ stresses lie close to the rock strength to maintain equilibrium state. In the former case, rocks may fall from the surface because of jointing and weak rock mass where as in the later case, disturbance of the stress field by rock excavations, such as underground and even in surface sometimes, may trigger violent release of stored energy (Goodman, 1989). Because of this reason, there will be stress induced instability in tunneling.

3.2 ROCK STRESSES

Stress is the intensity of internal forces setup in a body under the influence of a set of applied surface forces. Due to the weight of overlying material, confinement and pass stress history, any undisturbed rock mass in situ contains nonzero stress condition.

3.2.1 In situ rock stresses

The virgin i.e. initial state of stress, generally represent the resultant of the following components (Nilsen and Thidemann, 1993);

- Gravitational stresses
- Topographical stresses
- Tectonic stresses
- Residual stresses

Discussion of these stresses can be found in many text books. The most important stress related parameters for the stability analysis of underground openings are magnitudes and directions of major and minor principle stresses (Panthi, 2006). Due to the gravity of earth, there are two components of the gravitational stresses i.e. horizontal and vertical components. When surface is horizontal, the vertical gravitational stress at a depth z is:

$$\sigma_v = \sigma_z = \gamma H \quad 3-1$$

In an elastic rock mass with a Poisson's ration of ν , the horizontal stresses induced by gravity are;

$$\sigma_h = \sigma_x = \sigma_y = \frac{\nu}{1-\nu} \gamma H \tag{3-2}$$

The total horizontal stress is given by (Panthi, Spring 2012),

$$\sigma_h = \frac{\nu}{1-\nu} \gamma H + \sigma_{tec} \tag{3-3}$$

Where, σ_v and σ_h are the vertical and horizontal stresses in MPa, σ_{tec} is the tectonic stresses due to plate tectonic movement, γ is the specific weight of rock mass in MN/m^3 , H is overburden depth in meters.

Figure 3-1 (left) shows that the measured vertical stresses are in fair agreement with the simple prediction given by calculating the vertical stress due to the overlying weight of rock at a particular depth from the equation 3-1. At shallow depths, there is a considerable amount of scatter which may be associated with the fact that these stress values are often close to the limit of the measuring accuracy of most stress measuring tools. On the other hand, the possibility that high vertical stresses may exist cannot be discounted, particularly where some unusual geological or topographic feature may have influenced the entire stress field (Hoek and Brown, 1980).

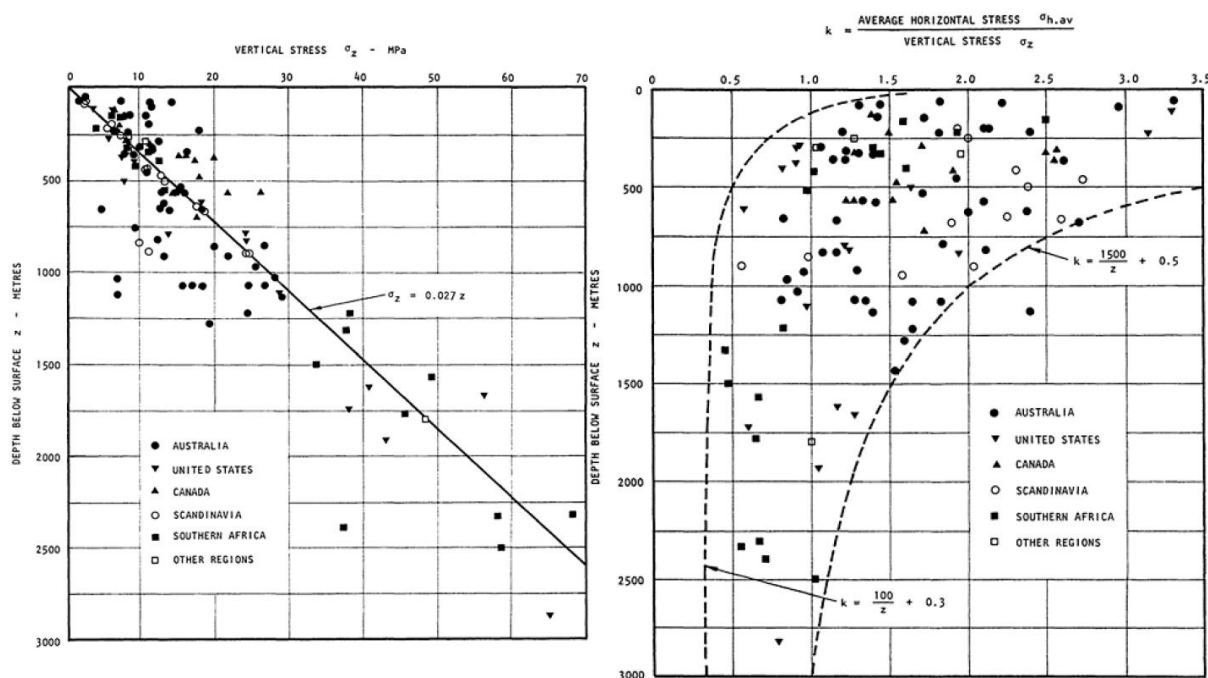


Figure 3-1: Plot of vertical stresses against depth below surface (left) and variation of ratio of average horizontal stress to vertical stress with depth below surface (right) (Hoek and Brown, 1980).

Figure 3-1 (right) gives a plot of k , the ratio of average horizontal to vertical stress, against depth below surface. It is seen that, for most of values plotted, the value of k lies within the limits defined by,

$$\frac{100}{z} + 0.3 < k < \frac{1500}{z} + 1.5 \tag{3-4}$$

The plot shows that, at depths of less than 500 meters, horizontal stresses are significantly greater than vertical stresses. For depths in excess of 1 kilometer (3280 feet), the average horizontal stress and the vertical stress tend to equalize, as suggested by Heim's rule (Hoek and Brown, 1980). If very high horizontal stresses existed at depths in excess of 1 kilometer, these would have induced fracturing, plastic flow and time-dependent deformation in the rock, and all of these processes would tend to reduce the difference between horizontal and vertical stresses (Hoek and Brown, 1980).

Tectonic stresses

Due to the convergence of the Indian and the Asian tectonic plates, the Himalayan region has been undergoing persistent compression for more than 50 million years. As a result, the Himalaya is one of the most seismically active regions of the world. By analyzing the earthquake regime of the Himalaya, Sarkar and Chander (2003) concluded that the plate subduction process in this region is causing large, moderate and small scale earthquakes. The annual rate of long-term tectonic stress change induced by the subduction process is estimated to be in the order of few kilo-Pascals. The compressional tectonic deformation and active reverse faulting mechanism have considerable influence on the magnitude of major tectonic principal stress in the Himalaya.

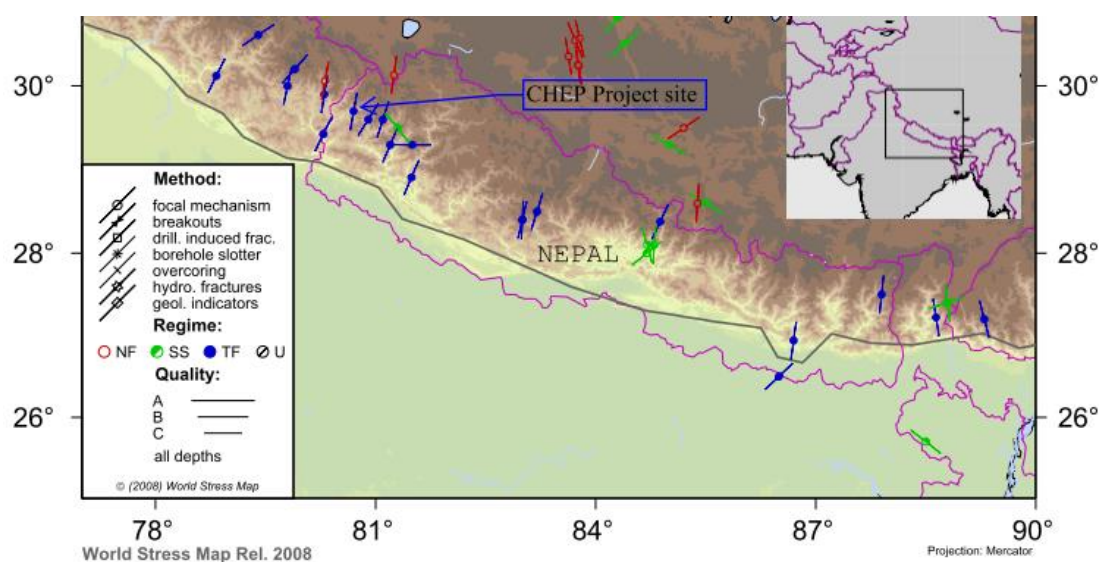


Figure 3-2: Stress map of the Himalaya and adjacent region (World Stress Map, 2008)

As shown in Figure 3-2, the tectonic principal stress in the Nepal Himalaya is oriented horizontally with Northeast-Southwest trend (Panthi, 2006). The direction of tectonic stress can be found from the Figure 3-2. The estimation of magnitude of tectonic stress at the particular site needs stress measurement data. It is very difficult to find the measured data in Himalayan region especially in Nepal. In case of tunnel projects, which have already been built, measurement of tunnel wall deformation will help to determine the stress at tunnel location. From these data, tectonic stress can be calculated using equation, 3-1, 3-2 and 3-3.

3.2.2 Stresses surrounding underground openings

When an underground excavation is made in a rock mass, the stresses which previously existed in the rock are disturbed, and new stresses are induced in the rock in the immediate

vicinity of the opening. One method of representing this new stress field is by means of *principal stress trajectories* which are imaginary lines in a stressed elastic body along which principal stresses act (Hoek and Brown, 1980).

According to Kirsch solution, the redistribution of stresses around a circular opening in an elastic material in isostatic stress conditions ($\sigma_h = \sigma_v = \sigma$) may be expressed as shown in Figure 3-3.

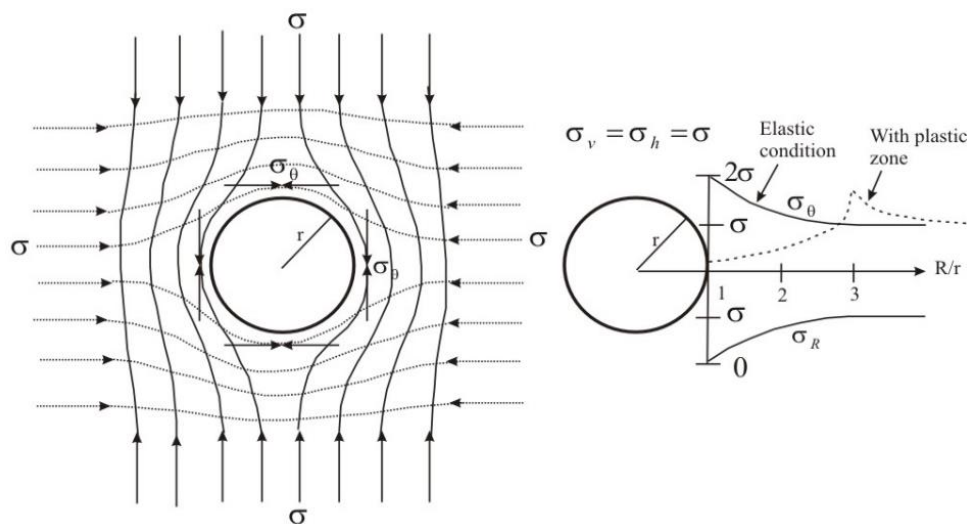


Figure 3-3: Stress trajectories in rock mass surrounding a circular opening (left) and tangential and radial stress distribution in elastic and non elastic conditions (right) (Panthi, 2006).

As shown in Figure 3-3 (right), the tangential stresses (σ_θ) and the radial stress (σ_R) at the periphery of a circular opening in fully isostatic stress condition and for elastic rock material will be twice and zero times the isostatic stress respectively. Stresses become normalized as the ratio between radial distance (R) and opening radius (r) increases. The magnitudes of σ_θ and σ_R are:

$$\sigma_\theta = \sigma \times \left(1 + \frac{r^2}{R^2}\right) \quad 3-5$$

$$\sigma_R = \sigma \times \left(1 - \frac{r^2}{R^2}\right) \quad 3-6$$

However, the stress conditions are seldom isostatic and different magnitudes of major principal stress (σ_1) and minor principal stress (σ_3) give variation in the magnitude of tangential stresses. According to the Kirsch solution the tangential stress will reach its maximum value ($\sigma_{\theta\max}$) where the σ_1 direction is tangent to the contour, and its minimum value ($\sigma_{\theta\min}$) where the σ_3 direction is tangent. The actual values will be as follows:

$$\sigma_{\theta\max} = 3\sigma_1 - \sigma_3 \quad 3-7$$

$$\sigma_{\theta\min} = 3\sigma_3 - \sigma_1 \quad 3-8$$

These equations are valid for homogeneous, isotropic and elastic rock mass having widely spaced and tight joints. In weak and anisotropic rocks, the gradual reduction in strength caused by destruction and cracking by the tangential stresses drives the zone of broken rock deeper into the contours forming a plastic zone. In such rock mass, as shown in the Figure 3-3 right with dotted lines, the maximum tangential stresses are moved further until the elastic zone is reached. Therefore, a solution for stresses and displacements derived from the theory of plasticity may provide a useful basis for the analysis in such rock mass condition (Goodman, 1989 in (Panthi, 2006)).

3.2.3 Rock stress estimation

There are no standard formulas that can calculate the total stress in the rock mass. In situ stress measurement is necessary to find the magnitude and direction of stresses. Once the stress is measured, the equation 3-3 can be used to back calculate the tectonic stress.

3.2.4 In situ stress measurements

To be able to analyze the potential problems due to rock stresses, it is necessary to obtain information about magnitudes and directions of the principal stresses. Reliable information of this issue can be obtained only by carrying out rock stress measurements (Nilsen and Thidemann, 1993). In situ rock stress measurement generally is carried out according to one of the following three main principles;

- The overcoring techniques
- Flatjack testing
- Hydraulic fracturing

The first two are normally carried out in underground openings and are applicable during and after construction of the project. On the other hand, as a result of the considerable development of methodology during the last decade, the hydraulic fracturing technique is being applied today in drillholes to depths of 100-200 meters and more. The detail of these principles are explained in Nilsen and Ozdemir (1999).

3.3 TUNNEL STABILITY PROBLEMS

When the stress around the tunnel periphery exceeds the rock strength, there will be stress induced stability problems in the tunnel. There are mainly two reasons for the instability of tunnel caused by the induced stress.

3.3.1 Problems due to tensile stress

If the value of minimum tangential stress given by the equation 3-8 is negative i.e. the region is in tensile stress field, there will be radial jointing of the rock mass in that area. In most cases a tensile jointing will not have much influence on the rock stability. For high pressure tunnels it is more important that secondary jointing and opening of existing joints may increase the water leakage out of the tunnel (Nilsen and Thidemann, 1993).

3.3.2 Problems due to high compressive stress

If the compressive tangential stress, given by the equation 3-7, exceeds the strength of the rock, there will be mainly two forms of instability problems depending upon the rock mass characteristics.

Rock burst/Rock spalling

If the compressive tangential stress exceeds the strength of the rock, fracturing parallel to the tunnel contours will be the result in hard rock. The fracturing process is often accompanied by loud noises from the rock, a phenomenon commonly referred to as rock burst. At moderate stress levels the fracturing will result in a loosening of thin rock slabs, often referred to as rock slabbing or spalling. If the tangential stress is very high, the rock burst activity may be quite dramatic. In extreme cases it may have the character of popping of large rock slabs with considerable force and speed. Rock burst activity is most intensive at the working face immediately after excavation. Experience shows that the most difficult area is the section 10-20 m closest to the working face (Nilsen and Thidemann, 1993). However the analysis and risk assessment of rock burst or spalling is not an objective of this research. There will be more focus on the next type of problem i.e. tunnel squeezing.

Tunnel squeezing or plastic deformations

In soft rocks the stress problems will not be characterized by rock burst or spalling. Because of the plastic nature of such rocks the potential problem here will be squeezing. In extreme cases reductions of the original tunnel diameter of several tens of centimeters due to squeezing have occurred in most of the Himalayan region (Panthi, 2006) and even in Central Europe (Nilsen and Thidemann, 1993). The analysis and risk assessment of this type of problem is discussed in more detail in the following chapters.

3.4 REVIEW ON SQUEEZING PHENOMENON

In 1995, the International Society for Rock Mechanics (ISRM) Commission defined rock squeezing as: 'Squeezing of the rock is the time dependent large deformation, which occurs around the tunnel, and is essentially associated with creep caused by exceeding a limiting shear stress. Deformation may terminate during construction or continue over a long time period' (Shrestha, 2006).

Squeezing phenomena have been observed in tunnels and caverns in various geological environments around the world. As described by Kovari (2000), the Alpine geologist Heim warned in his 1878 article that 'for each rock one needed to envisage a column so high that its weight exceeded the strength of the rock and therefore the foot of the column would be crushed' (Shrestha, 2006). Heim assumed that 'the internal friction would be so reduced under the all round pressure that a stress redistribution would occur without cleavage and the rock begins to flow, just like ice flows in a glacier'. Wiesmann in 1912 discovered the error in the reasoning of Heim. Firstly, it is not the uniaxial, but the triaxial, compressive strength that applies to the behavior of the rock surrounding the tunnel: 'The bearing capacity of enclosed bodies, this is the governing rock strength'. Secondly, the behavior of a rock in a plastic state cannot be compared to that of a fluid. In a viscous (Newtonian) fluid it is only a

question of time until a hydrostatic stress state develops. Due to internal friction, however, rocks behave quite differently.

According to Panet (1996), the convergence of tunnel are to be analyzed taking into account the immediate convergence due to the advance of the face and the time-dependent convergence due to the rheological behavior of the rock mass (Shrestha, 2006). After the advance of the tunnel face, if the stress developed around the opening exceeds the strength of the rock mass, the rock mass starts squeezing instantaneously. This is called 'Instantaneous squeezing'. If the accumulated stress does not exceed the rock mass strength but is sufficient to cause creep, it will cause convergence towards the tunnel. It is called 'Secondary squeezing'. Thus squeezing may take place in one of two stages and it depends on tangential stress level, rock mass properties and tunnel shape (Shrestha, 2006).

3.4.1 Instantaneous Squeezing

By taking the reference from Bray (1967), Panthi (2006) explained that when an underground opening is excavated, the existing stress regime is disturbed. As the stress cannot pass through the opening, it redistributes itself around the opening. This causes concentration of stress along the contour of opening that is shown in Figure 3-3 (left). Weak rocks such as shale, slates and phyllite, and weakness / fracture zones, behave very differently from isotropic and stronger rocks when subjected to tangential stresses. In weak rock mass such as shale, slates and phyllite, and weakness / fracture zones, when the strength is less than induced tangential stresses along the tunnel periphery, gradual formation of micro-cracks along the schistosity or foliation plane will take place. As a result, a visco-plastic zone of micro-fractured rock mass is formed deeply into the walls as shown in Figure 3-4, and the induced maximum tangential stresses are moved beyond the plastic zone. As a result, a time dependent inward movement of rock material (illustrated by dotted lines in Figure 3-4) will take place and support in the opening will experience gradual build up of pressure. In this figure, r is tunnel radius, R is radius of visco-plastic zone and p_i is the support pressure.

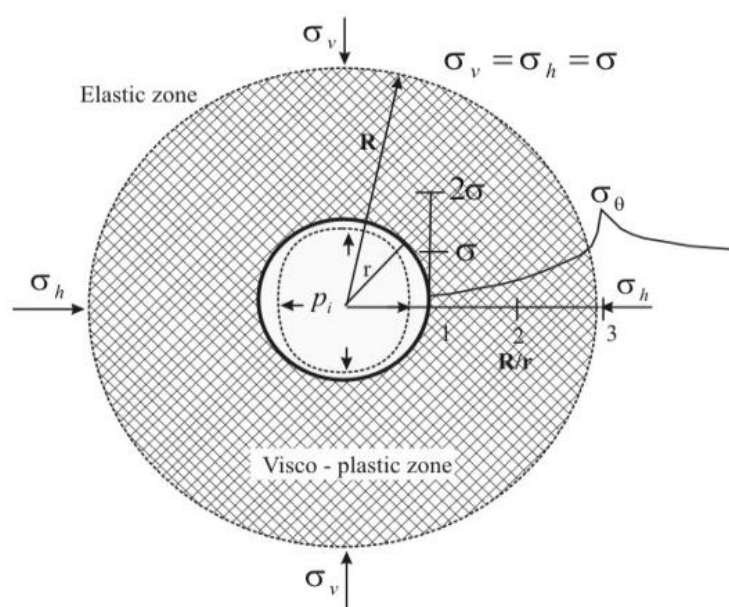


Figure 3-4: An illustration of squeezing in a circular tunnel (Panthi, 2006).

Hence, this kind of stress failure condition caused by overstressing is 'Instantaneous squeezing'. Squeezing problems normally occur at the areas of maximum tangential stress. However, if the minimum tangential stress is very low, it may also cause a problem (Shrestha, 2006).

3.4.2 Squeezing by creep

As defined by the ISRM, squeezing is time-dependent deformation, essentially associated with creep caused by exceeding a limiting shear stress. The complete stress-strain curve can also be used to predict rock failure as a result of creep. As shown in Figure 3-5, the locus of a creep test in stress-strain graph is a horizontal line. If the initial stress in the rock is close to the peak load, any creep will terminate in rupture when the accumulated strain intersects the falling part of the complete stress-strain curve.

A creep test started at A will terminate in a rupture at point B in a relatively short time. A creep test begun at C will terminate in a rupture at D after a much longer time. And a creep test initiated at E below the critical stress level G will approach point F and stops at a finite strain without rupture after a long time. Below T (creep threshold) there is no creep. If a number of creep tests are performed, each one for a different value of the applied stress (between level T and U), the results obtained can be plotted by giving the terminal locus of long term creep test (TU). The line T-U is the terminal locus of long term creep tests. Above level U (or G), the minimum creep rate (secondary) increases with stress level and the test terminates with tertiary creep and fracture when the accumulated strain has reached a finite value, given by the descending part of the curve.

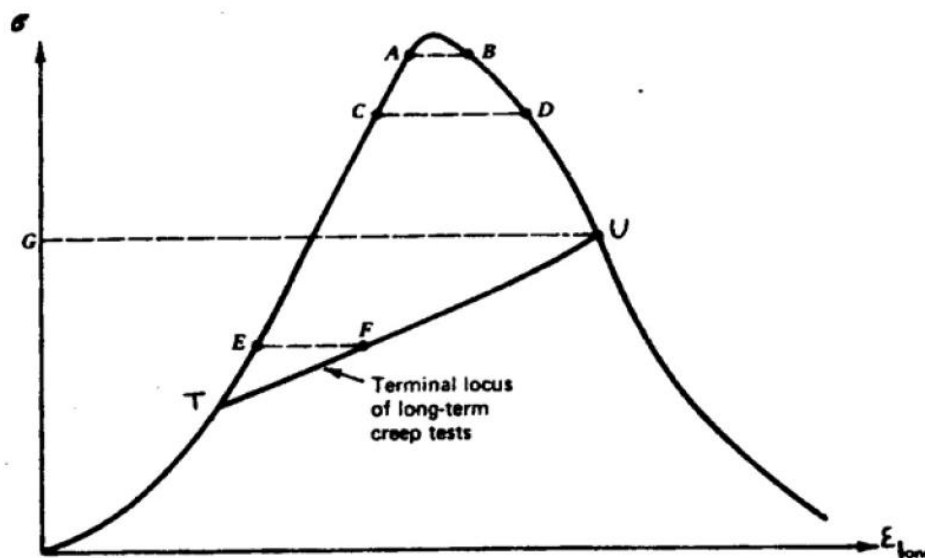


Figure 3-5: Creep in relation to the complete stress-strain curve (Goodman, 1989)

This shows that rock mass may creep to failure even if it has not failed immediately after the excavation. Failure takes place as the creep line intersects the falling part of the stress-strain curve. This is called 'secondary squeezing'. Time dependency is absent in tests with axial stress (σ_1) less than 40% of uniaxial compressive strength (q_u) and secondary creep is unimportant when σ_1 is less than 60% of q_u (Goodman, 1989).

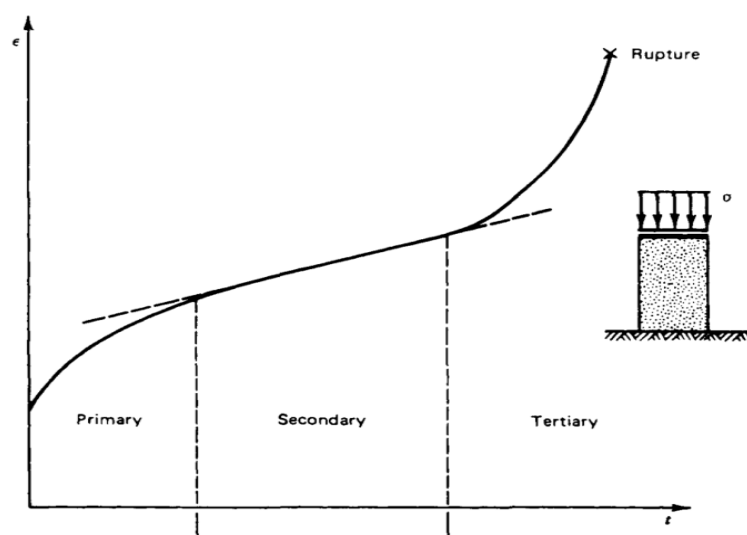


Figure 3-6: Regions of behavior in creep (Goodman, 1989)

The strain-time curve for a creep test has a very characteristic form. Initially, as the load is applied, the elastic strain occurs virtually instantaneously. As time passes under constant stress, the rate of strain decreases and the period of decelerating strain rate is called primary creep. The primary creep phase is followed by an extended period of slow (almost steady-state) deformation called secondary creep. At the end of this stage, the strain rate begins to accelerate and the material rapidly fails. The final stage of accelerating deformation is called tertiary creep. Creep in rock masses is associated with crack propagation. During the primary creep phase the rock 'acclimatizes' to stress and crack propagation slows to a stable, almost constant rate. During the 'steady' secondary creep stage, the material is damaged more and more until finally, in the tertiary stage, uncontrolled accelerating crack propagation leads to failure. Creep is important at low pressures only in a few rock types: shale, soft chalks and evaporite rocks (e.g. rock salts, gypsum and anhydrites) (Shrestha, 2006).

3.4.3 Factor influencing the squeezing phenomenon

According to Shrestha (2006), squeezing ground conditions are influenced by many factors which contribute in different degrees. On the basis of analysis and case studies, many authors have identified and recognized those factors in different ways. All those factors are compiled and mentioned and described below:

- Stress condition
- Strength and deformability of the rock mass
- Rock type
- Water pressure and porosity of rock mass
- Orientation of the geological structures
- Construction procedures and support systems

The ratio of rock mass strength to in situ stress plays a major role. Hence weak or strongly foliated or crushed rock may lead to squeezing even for low overburden. Low rock mass strength gives low value for the ratio of rock mass strength to in situ stress causing overstressing condition. In addition, high deformability causes large deformation. Thus the

rock mass strength and deformability could have direct contribution to the squeezing phenomenon.

Phyllite, schist, serpentine, claystone, tuff, certain types of flysch, and weathered clayey and micaceous metamorphic rocks are typical examples of squeezing rock types. According to Grimstad (2000) in Shrestha (2006), fault crushed zone is also a common location for squeezing problem, for example Lærdal tunnel in Norway.

The most important effect of the water is the high pore water pressure. The pressure also increases when there is clay in a discontinuity plane which is located in the vicinity of the tunnel. Reduction of water pressure may result in the reduction of the squeezing potential with time (Shrestha, 2006). On the other hand, increase of the rock porosity reduces the mechanical strength of the rock, which will result more squeezing.

If the tunnel alignment is parallel to foliation or near to fault line, there will be more squeezing than for the tunnel axis perpendicular to them. The orientation of other structural features such as schistosity plane, joints etc could also have great influence in squeezing. Overbreak due to buckling of schistose layers will occur mainly where the schistosity is parallel to the tunnel perimeter and for nearly vertically dipping layers a vertical sidewall is unfavorable.

Shrestha (2006) explained that the selection of a suitable construction procedure may have beneficial effects on squeezing. The heading and benching method could have great advantage in squeezing environment. A minimal support pressure may be necessary to stabilize the rock. Steel sets in combination with shotcrete or concrete and a circular cross-section may provide much higher support pressures than a dense pattern of rock bolts (Steiner, 1996).

3.5 CONCLUDING REMARKS

In the Himalaya region, basically in Nepal, squeezing phenomenon is very common in hydropower tunnels. Because of very weak, highly schistose and fractured rock types and high tectonic stress squeezing has been experienced even in the lower overburden. Hence, analysis of squeezing phenomenon to find the correct deformation values could be a challenge to tunnel engineers in this region for the successful tunneling. One of the most important tasks for the squeezing analysis is to define the correct stress value. Stress measurement is very important in this regards. The topic of this thesis is also chosen on the basis of this fact. One of the hydropower projects, CHEP, has been chosen for the analysis where there is significant tunnel squeezing. The problem is believed to be due to overstress of rock mass that means rock mass strength is less than induced tangential stress around the tunnel periphery.

Hence, squeezing is considered as a convergence phenomena caused by overstressing and deformation characteristics of the rock mass. Time dependent phenomenon can also be studied by using rheological parameters but this is not included in this thesis. Thus, only the instantaneous squeezing has been analyzed further.

4 THE CASE: CHAMELIYA HYDROELECTRIC PROJECT (CHEP)

In this thesis, the case study has been carried out for the ‘Chameliya Hydroelectric Project’ which is located in far western region of Nepal. The case has been taken on the basis of the excessive squeezing of headrace tunnel. The project is in the final stage of construction but the headrace tunnel has already been broken through. Squeezing of the rock inside the tunnel has been severe problems in the Himalayan region; many tunnel projects are affected in this region. Squeezing related data has been collected and some of the available approaches have been used to analyze the squeezing phenomena that occurred in the headrace tunnel.

4.1 PROJECT DESCRIPTION

4.1.1 General

To cope with the growing power demands and to develop related industries in far western region of Nepal, Government of Nepal has given high priority to this project (NEA, 2001). The project was identified by Nepal Electricity Authority (NEA) and planned to have a daily peaking run of river project with an installed capacity of 30MW for daily 6 hours.

The information about the project in this report has been taken from review study report (NEA, 2001) and the latest developments from the project site during construction phase. The project is currently in the final stage of construction. The review study report is based on the following documents of previous work executed by NEA and local consultants (NEA, 2001):

- Techno-Economic Feasibility Study (1996, METCON)
- Review Report on Chameliya Hydropower Project (1996, NEA)
- Report on Geotechnical Studies (1998, NEA)
- Upgraded Feasibility Study (NEA, 1997)
- Interim Detail Design Report (1998, NEA)
- Detail Engineering Study Report (1999, NEA)
- Environmental Impact Assessment Final Report (1999, NEA)

The conclusion of the review study, from the report NEA (2001), is that the development of this project will accelerate the electrification of this region and thus will help to develop power based industries and will also supply power to the construction of large projects under planning in this region. This is only the project in this area which is in under construction and there are no other projects that have been built.

4.1.2 Project Location

Chameliya River is one of the major tributaries of Mahakali River which borders to India. The Chameliya Hydroelectric Project is located on the Chameliya River in Darchula district of the far western region of Nepal and has installed capacity of 30 MW. It is located at about 270 km North West of Dhangadi. Dhangadi is one of the major business centers in the western region. The location map of the project site is shown in Figure 4-1.

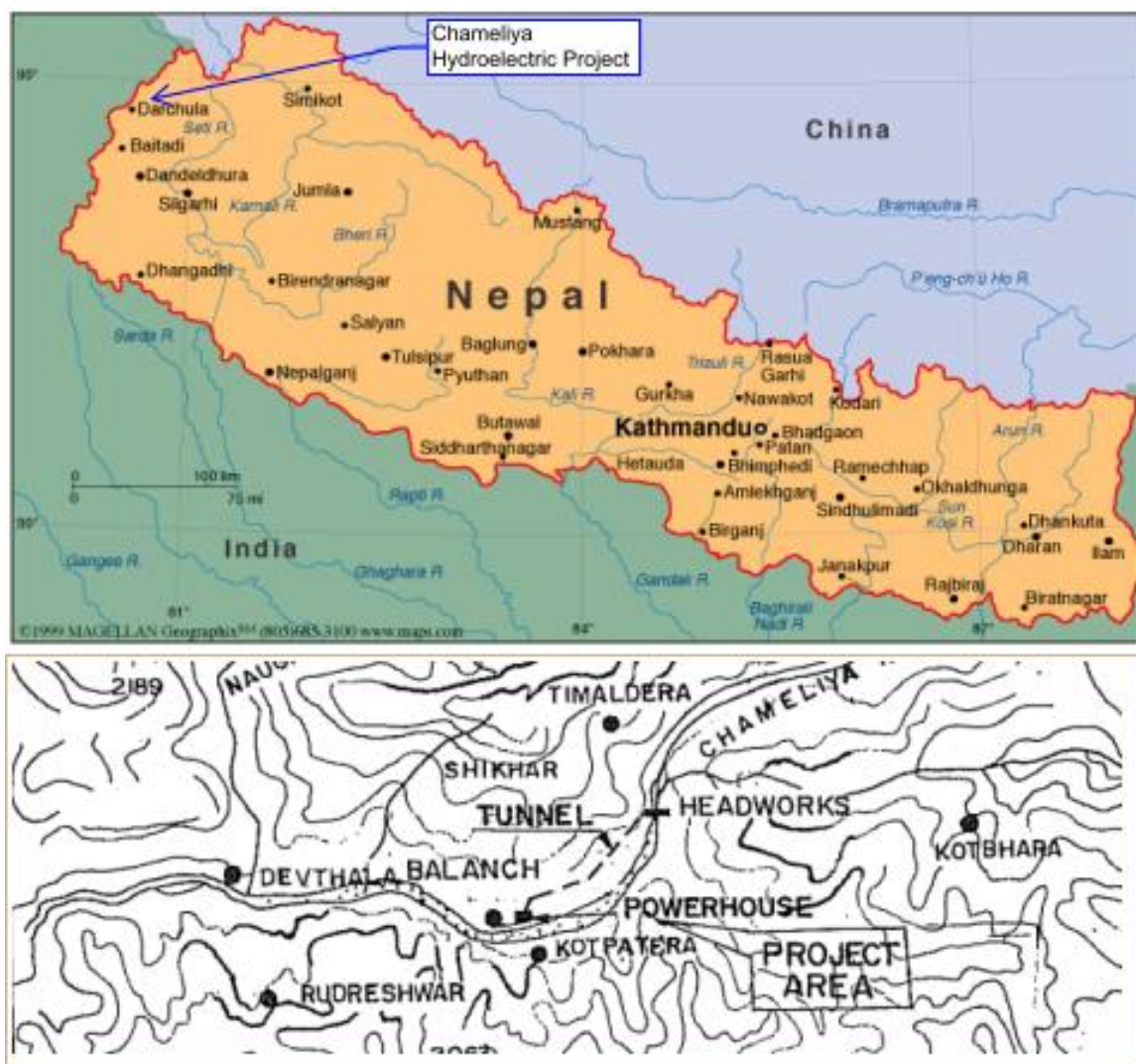


Figure 4-1: Project area location map (NEA, 1997)

4.1.3 Project layout features

The layout of the project components is shown in Figure 4-2. The dam consists of a non-overfall concrete gravity spillway section with two gates and will be located at Bitule, Seri VDC of Darchula district. The maximum height of dam is 54m and crest length is 88m. The desanding basin is located underground on the right side of the river and is designed for two caverns. Each cavern size is 12.0m wide, 25.0 m high and 80.0 m long. It accommodates flushing channel, to remove the deposited sediments.

The alignment of headrace tunnel was determined in considerations of economics, engineering and tunnel stability. The cross-section of headrace tunnel is a horse shoe type with diameter of 5.2m/4.2m depending upon the rock qualities and total length of the tunnel is 4067m. The surge shaft is located underground at the downstream of the headrace tunnel and is restricted orifice type. The penstock consists of both concrete lined and steel lined tunnels. The concrete lined tunnel consists of vertical part and horizontal part. The penstock has a diameter of 3.7 to 1.8m and a length of 464.8m.

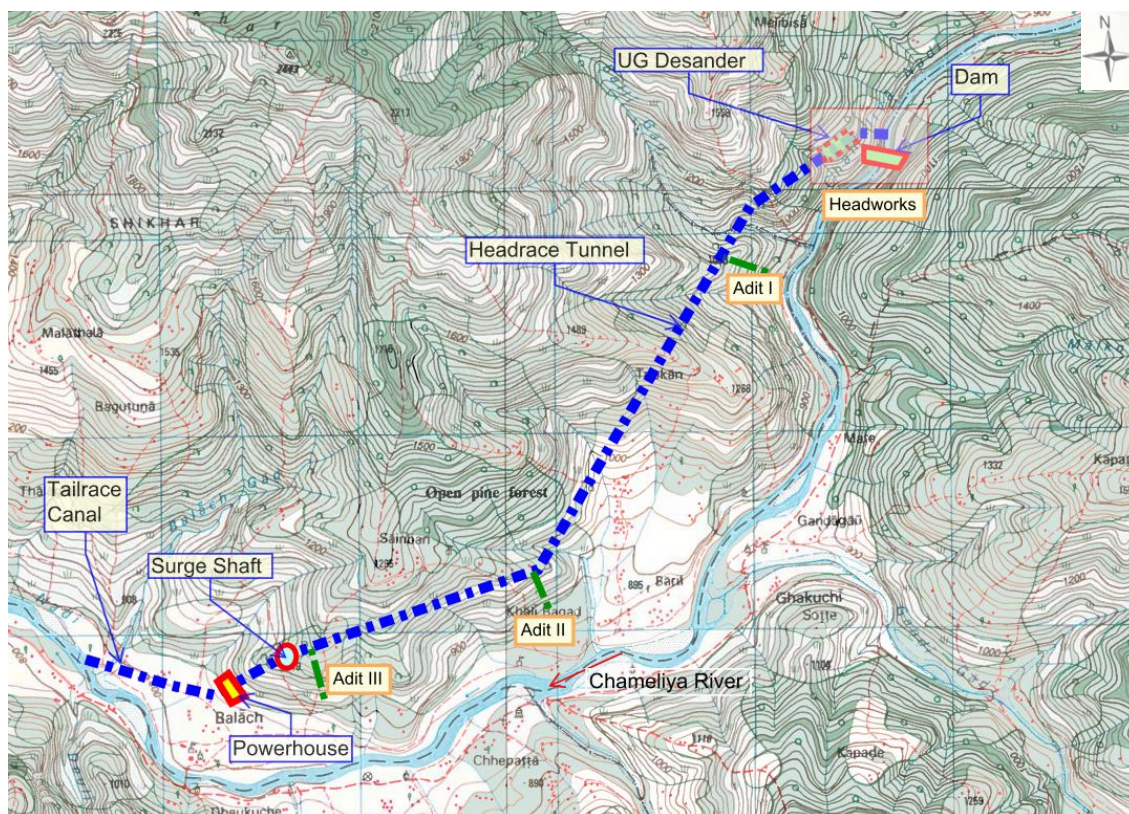


Figure 4-2: Layout of project components

The powerhouse lies over the Balanch terrace on the right bank of the Chameliya River. It will accommodate two units of francis turbines and generating equipments of 15MW capacity each. The powerhouse is reinforced concrete box type and a semi underground substructure with the dimensions of 37.5m length, 23.5m width and 27.4m height. The tailrace channel passes along medium and low level cultivated terraces. The water from powerhouse outlet will be conveyed through a 617m long box tailrace channel back to the Chameliya River near the Balanch-Chameliya confluence. The salient features of the project are given in Appendix A1.

4.2 REGIONAL GEOLOGY

Nepal lies in the Himalayan region. The concept behind the formation of Himalaya region is the key to understand geology of Nepal. Numbers of researchers have worked to describe the formation of Himalaya. By taking the reference from Patrick (2001), Panthi (2006) explained that the Himalaya was formed as a result of the collision of major lithospheric as well as intervening minor plate fragments and arch units from the late Mesozoic times to present date.

According to Panthi (2006), the Himalayan belt, as a result of compressional and extensional faulting, has several litho-tectonic units with Northwest-Southeast general trend. The altitude varies greatly in the Himalaya, which starts from approximately 100 meters above sea level at its South and reaches to its maximum 8,848 meters above sea level (the Mount Everest).

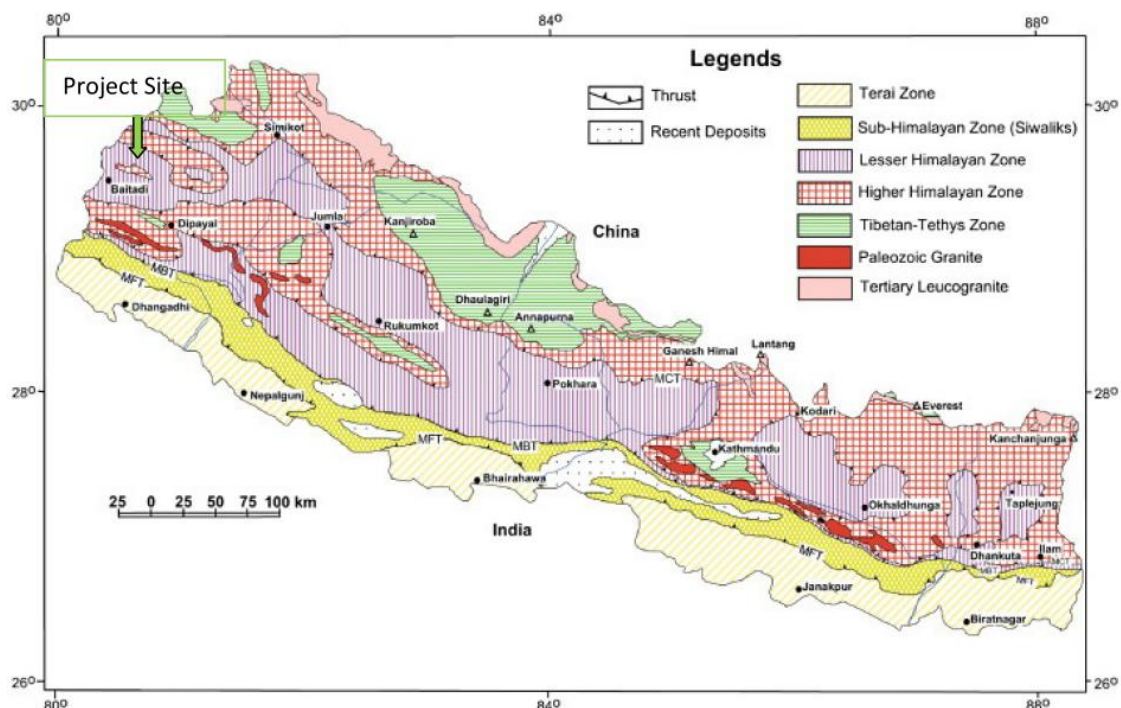


Figure 4-3: Geological map of Nepal (Dahal and Hasegawa, 2008)

As shown in Figure 4-3, from South to North, the Himalaya can be sub-divided into five major tectonic subdivisions; the Gangetic plane (Terai), the Siwaliks zone, the lesser Himalayan zone, the higher Himalayan zone and the Tibetan-Tethys zone. These tectonic zones are all characterized by special lithology, tectonics, geological structures, and geological history and are made up by different rock types (Figure 4-4). The major rock types in the Himalaya within the five tectonic zones are given in Table 4-2.

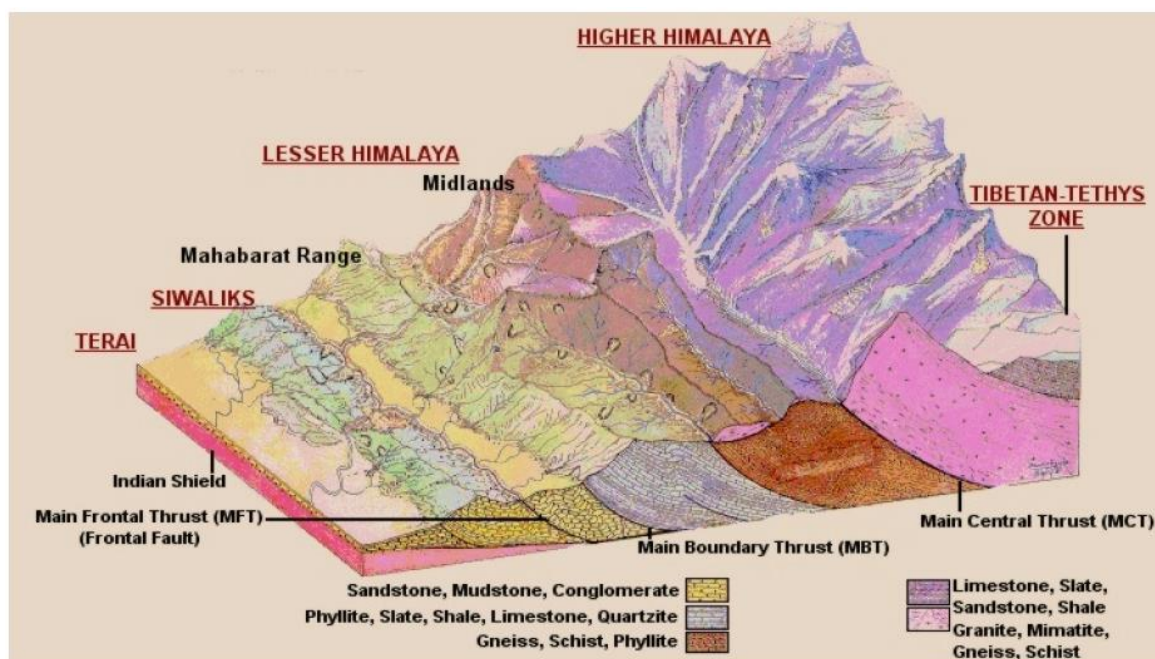


Figure 4-4: Block Diagram of the Himalaya giving different litho-tectonic units (Deoja, 1991)

The project area is located in Western-central part of Lesser Himalayan Zone having an average width of 165 km that extends throughout the length of Nepal Himalayan (Figure 4-3). The lesser Himalayan zone is a fold and thrust belt bounded by the Main Boundary Thrust (MBT) in the South and the Main Central Thrust (MCT) in the North (Figure 4-3 and Figure 4-4). The stratigraphy of the region nearby and within the project area is shown in Table 4-1.

Table 4-1: Regional Stratigraphy (NEA, 1997)

Surkhet Group		Suntar formation	
-----Unconformity-----			
Midland Group	Lakharpata Subgroup	Lakharpata formation	
		Syangja formation	
		Sangram formation	
		Galyang formation	
	-----Thrust-----		
	Ranimatta subgroup	Ranimatta formation	
	Kusma formation		
	Ulleria formation		
-----Thrust-----			
Dadeldhura group		Syllyanigad formation	

Table 4-2: Types of Himalayan rocks and their geomorphic units (Panthi, 2006)

Geomorphic Units	Width (km)	Altitude (m)	Main Rock Types	Age
Gangetic plane and inner Terai valleys	20-50	100-200	Alluvial deposits, coarse gravel at the foot of the Siwaliks mountain.	Recent
Siwaliks zone	15-30	200-1,000	Sandstone, mudstone, siltstone, shale, conglomerates etc.	Mid-Miocene to Pleistocene
Lesser Himalayan zone	70-165	200*-5,000	Shale, slate, phyllite, limestone, dolomite, marble, schist, quartzite, gneiss and granite.	Precambrian to Mesozoic
Higher Himalayan zone	10-60	>5,000	Gneiss, schist, marble, granite, quartzite, amphibole etc.	Precambrian
Tibetan-Tethys zone	-----	>2,500	Gneissic schist, marble, shale, slate, limestone, sandstone etc.	Late Proterozoic to early Cambrian
* In the lesser Himalayan valleys the elevation ranges from 200 to 2000 meters.				

The rock sequence of project area are very similar to those of the central Nepal midland zone (NEA, 1997). The main rock types in the region are shale, slate, phyllite, limestone, dolomite, schist, quartzite etc (Table 4-2).

4.3 GEOLOGY AND ENGINEERING GEOLOGY OF THE PROJECT AREA

The project area is covered by meta-sedimentary rock of Surkhet group and Midland group. The main rocks are siliceous dolomite, sandstone, calcareous slate, dolomite and dolomite intercalated with slate (NEA, 1997). The general trend of rock is about east to west and dips steeply north at dam site and gently at hill slope of powerhouse site.

Regarding the geological structures, the project site is located 60 km north of Main Boundary Thrust (MBT) and close to the Main Central Thrust (MCT) in the midland zone. The rocks in this area are folded and faulted. Two faults are inferred across the tunnel alignment. A thrust fault in the contact of dolomite and sandstone near Bhel Gad lies about 600m downstream of dam site. The fault extends in the left bank of Chameliya Gad with highly fractured rock zone. Another fault in the contact of dolomite and slate is inferred and passes through Baril village, following large flow of spring to the right bank of Chameliya Gad.

4.3.1 Geological investigations

In 1996, METCON Consultant in association with Bhutan Engineering Co. and Butwal Power Company prepared feasibility report. At that time, core drilling and seismic refraction survey were done in few selected sites. The summary of core drilling and seismic refraction survey is given in Table 4-3 and Table 4-4. The detail of drawings and results of the investigations can be found in the report, NEA (1998).

Table 4-3: Summary of core drilling (NEA, 1998)

S.N.	Location and Drill Hole No.	Depth, m
1	Dam Axis, DDH-1	30
2	Dam Axis, DDH-2	30
3	Dam Axis, DDH-3	30.25
4	Surge shaft, DS-1	39.5
5	Dam Axis, DP-2	27.5
	Total	157.25

Table 4-4: Summary of seismic refraction survey (NEA, 1998)

Profile No.	Location	Length, m
SLD-1	Along Dam Axis	115
SLD-2	32 m downstream of Dam Axis	115
SLD-3	Downstream of Dam axis, right bank terrace	115
SLD-4	Downstream of Dam axis, right bank terrace	115
SLD-5	Downstream of Dam axis, right bank terrace	115
SLD-6	Upstream of Dam axis, left bank terrace	115
SLD-7	Upstream of Dam axis, left bank terrace	115
SLP-1	Powerhouse site Balanch	115
SLP-2	Powerhouse site Balanch	115
SLP-3	Powerhouse site Balanch	115
SLP-4	Powerhouse site Balanch	345
SLP-5	Powerhouse to surge tank site	600
SLP-6	Penstock site	115
SLP-7	Penstock site	115
SLP-8	Penstock site	115
SLP-9	Penstock site	115
SLP-10	Penstock site	115
SLP-11	Penstock site	115
SLP-12	Penstock site	115
SLP-13	Surge tank site	115
SLT-1	Adit-2 site	225
SLB-1	Balanch Bridge site	115
	Total Length	3355

In addition to these subsurface investigations, surface investigations such as geological mapping of project area, discontinuities surveys, landslide survey and slope stability study, and rock mass classification, etc were also done. Based on these investigations, the rock types and their properties and characteristics in each project components have also been discussed. The engineering geology of the project components of CHEP are described further in this chapter. The information given in the following sections will be based on the Upgraded Feasibility Report (NEA, 1997) and Geotechnical Report (NEA, 1998).

4.3.2 Headworks area

The headworks consists of dam site and desanding basin.

Dam site

The main rock type in the dam site is light gray to pink, massive, cryptocrystalline and brittle, good quality siliceous dolomite. The rock trends almost east to west with vertical dip. The RMR and Q value were estimated to be equal to 63 and 13.3 respectively. Both these values correspond to good rock quality.

Desanding Basin

The main rock type in this area is also siliceous dolomite and is slightly weathered in the surface. The quality of rock is good and the compressive strength value measured by using Schmidt hammer test is reported to be 60 MPa, which seems to be low observing the rock quality. The general trend of the rock is east to west with vertical dip.

4.3.3 Headrace tunnel alignment

According to the feasibility report (NEA, 1997), the headrace tunnel passes across five different rock types as siliceous dolomite, sandstone, slate, dolomite and dolomite intercalated with slate. The main geological structures encountered are shear zone and faults.

On the other hand, figure 4-5 shows the geological plan and profile along tunnel alignment of the project, which was made after the tunnel had been broken through. There are large discrepancies in rock types. The figure shows that the main rock types along the headrace tunnel alignment are dolomite, dolomite intercalated with slate, talcosic dolomite and dolomite intercalated with phyllite, which are different than that mentioned at the time of feasibility study. The rock mass classification was made based on Q-system at both times. There are also large discrepancies in rock class and support types. In more detail, the quality of rock mass is explained further in section 4.4.

4.3.4 Surge shaft and vertical shaft area

A restricted orifice type surge shaft is proposed inside Balanch hill formed by light grey, slightly weathered, fair quality dolomite intercalated with slate. The rock trends $N270^{\circ}$ and dips 30° towards north. The portal area of aeration gallery is proposed on the left bank slope of Amroda Khola. A vertical core was drilled from the rock face at surge shaft area i.e. DS-1 in Table 4-3. The core was highly fractured and has poor core recovery (average recovery 30%).

The rock has been classified as fair quality rock and R2 type support was estimated (the detail of support types is discussed further in this chapter). The proposed vertical shaft (penstock shaft) also passes across this rock. The geo-technical parameters are same as estimated in headrace tunnel from chainage 2+307 to 4+067m which is discussed in section 4.4.

4.3.5 Powerhouse area

The site was proposed in medium level terrace, right bank of Chameliya River in Balanch village. A borehole DP-2 was drilled in the proposed site to a depth 27.50m and bedrock could not be penetrated. The recovery is poor and mainly high grey and white color quartzite and dolomite boulders, cobbles and gravels are recovered. Later during construction, powerhouse was shifted to the hill side just to be sure that there is bedrock below foundation.

About 200m long tailrace canal passes over low level terrace deposit characterized mainly by quartzite, dolomite and gneiss boulders to gravel size material in sandy soil. The outlet of the canal will be about 10m upstream from the confluence of Balanch Gad and Chamaliya River. The open cut along canal was estimated to be more than 15m deep.

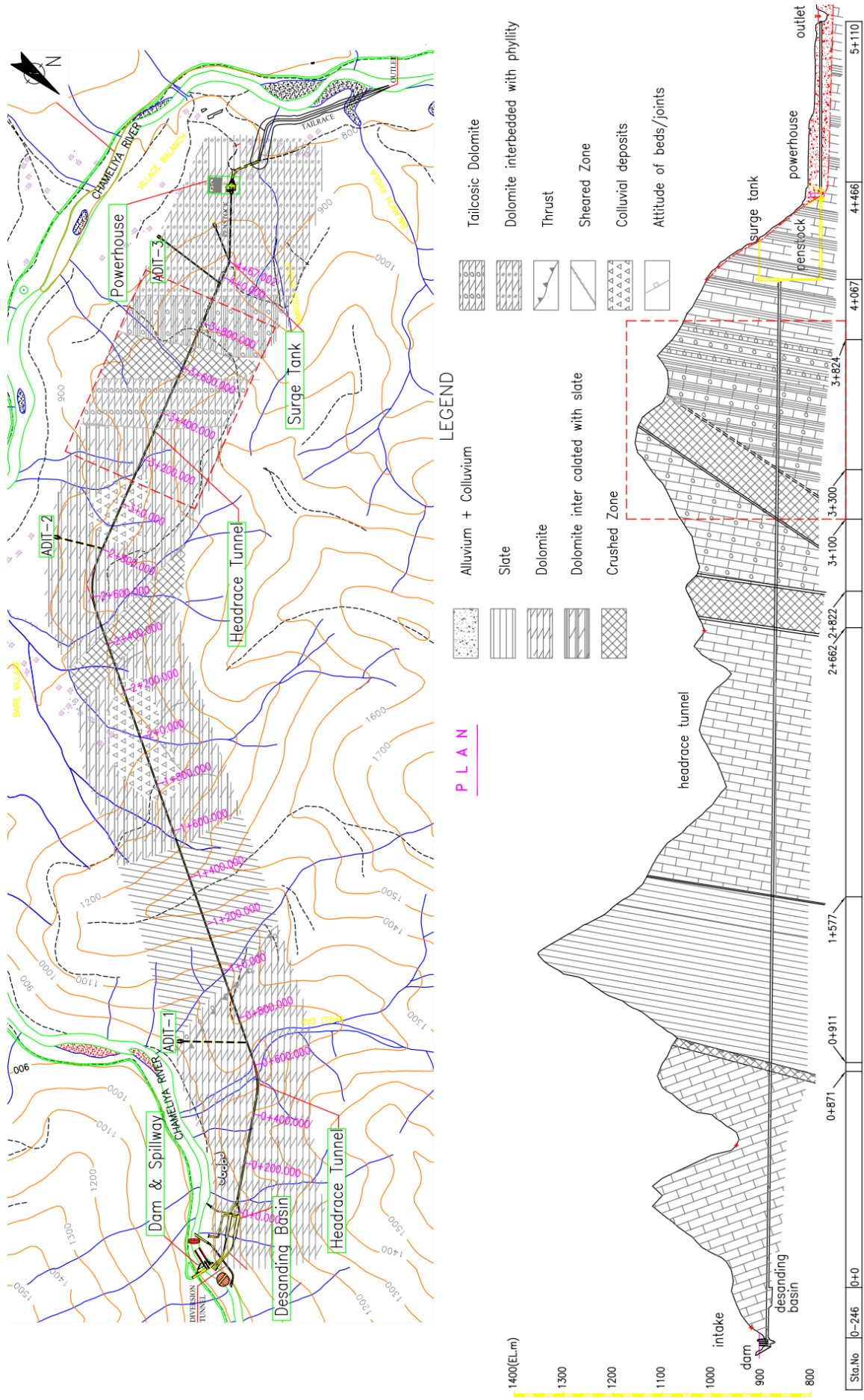


Figure 4-5: Geological Plan and Profile along headrace tunnel alignment of CHEP (Source: Latest information from CHEP site office, 2012)

4.4 ROCK MASS CONDITION ALONG HEADRACE TUNNEL

During planning phase investigations, the rock mass quality along the headrace tunnel alignment was estimated based on surface and very few subsurface investigations. The tunnel has already been broken through. During excavation, the rock mass condition has been found very different from that was found during investigation. Hence, there are large discrepancies between predicted and actual rock mass condition and support application. It is very difficult to quantify these discrepancies along whole tunnel alignment because the project has not provided the whole tunnel mapping that was done during excavation. Therefore only the rock mass quality that was predicted during planning phase investigation is discussed further.

According to NEA (1997), the rock mass classification was made based on Q-system. The detail of Q system is given in section 6.2.2. The support class is estimated for each rock quality class Q1 to Q4 as R1 to R4. The summary of rock mass classification is given in Table 4-5 the predicted percentage of different classes of rock encountered in headrace tunnel is shown in Figure 4-6.

Table 4-5: Geology of tunnel and rock support class (NEA, 1997)

Chainage (m)		Rock mass quality (Q-value)	Rock mass class	Rock support class	Rock type
From	to				
0+000	0+587	Good (18)	Q1	R1	Siliceous dolomite
0+587	0+607	Very Poor (0.1)	Q4	R4	Thrust zone
0+607	0+707	Poor (2)	Q3	R3	Sandstone
0+707	1+557	Fair (5)	Q2	R2	Calcareous Slate
1+557	1+707	Fair (5.4)	Q2	R2	Dolomite
1+707	2+307	Fair (5)	Q2	R2	Calcareous Slate
2+307	4+067	Fair (5)	Q2	R2	Dolomite intercalated with slate

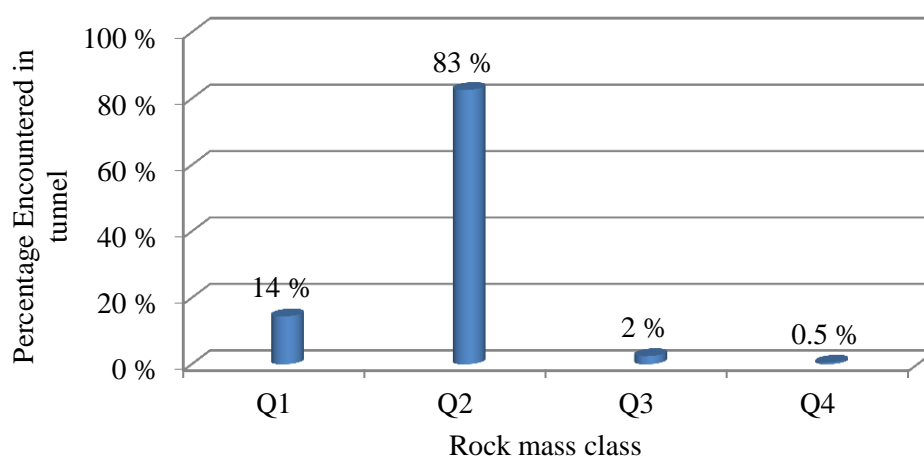


Figure 4-6: Predicted rock classes along headrace tunnel (NEA, 1997)

The rock quality in most of the section of tunnel is fair i.e. Q2 (Figure 4-6) that means support, R2, with rock bolts and shotcrete is sufficient to address the problems if any. But, actually during tunneling, the Q-value has been found even less than 0.01 (extremely poor) in

some of the sections (Table 7-1) that may need steel ribs, lattice girders and even concrete linings in addition to shotcrete and rock bolts. The detail of support systems during tunneling is discussed in section 4.6. This indicates that there is huge deviation in the quality of actual rock mass compared with predicted one.

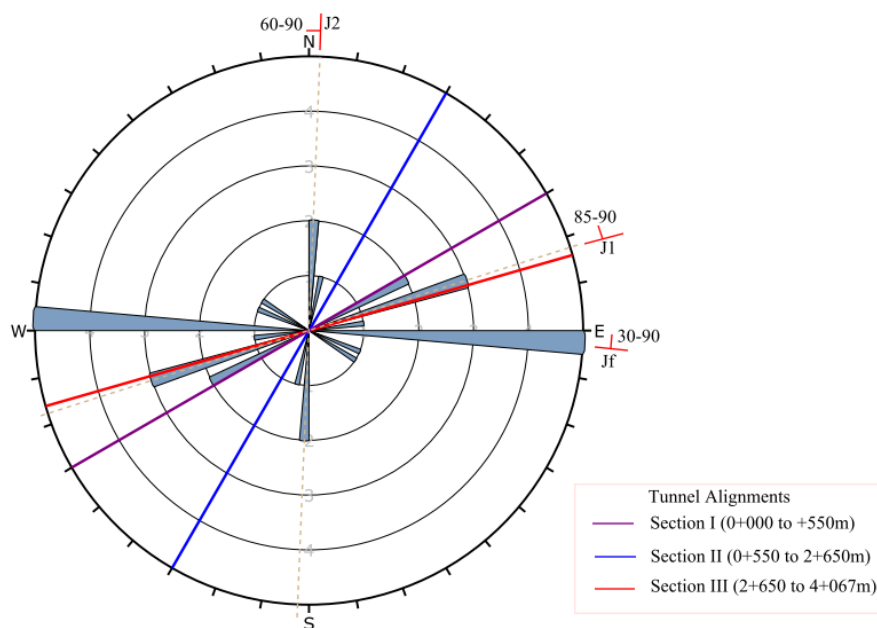


Figure 4-7: Orientation of main joint sets and headrace tunnel alignment of CHEP ((NEA, 1997)

As shown in Figure 4-7, there are three sections of headrace tunnel alignment. The 1st section is from chainage 0+000 to 0+550m and is favorably aligned with respect to foliation joints (Jf) but there is parallel random joint set too, which may cause some tiny problems. Section II is the most favorable alignment with respect to any joint sets. Section III is favorably aligned with respect to foliation joints but it is parallel to joint set J1, which is not favorable as it can cause some instability problems. There are three main joint sets and many random joints. Since dolomite is the most dominant rock type along the tunnel, the foliation joints is represented by this rock type.



Figure 4-8: Rock mass condition at different chainage along headrace tunnel of CHEP

Figure 4-8 shows the thinly foliated and fractured dolomite (left) and highly sheared and fractured talcosic phyllite with some bands of dolomite in the section between adit 2 and adit 3 (right). The rock mass condition in tunnel sections from chainage 0+000 to 3+100 is quite good with some exception (Figure 4-8, left) while in the section from chainage 3+100 to the end of tunnel is extremely poor in general (Figure 4-8, right).

4.5 INSTABILITY ALONG HEADRACE TUNNEL

During tunnel excavation, the headrace tunnel had to cross the different rocks, weakness zones and faults. In the tunnel section from chainage 0+000 to 3+100m there were minor stability problems such as rock spalling, several instances of mud flows etc. These problems had been addressed using the appropriate support system such as shotcrete with wire mesh, rock bolts etc. But in the tunnel section from chainage 3+100 to 3+900m, there is severe squeezing problem. In this tunnel section, actual geology is found significantly different from predicted one. The rock mass quality is extremely poor and rock type is talcosic phyllite. Figure 4-9 shows the typical tunnel section between adit 2 and adit 3 where there is significant floor heaving and wall convergence. There were several instances of large mud flows, floor heaving at few locations, poor invert conditions and the excavation work had been stopped at several locations for long periods. Due to severe squeezing and associated deformation, tunnel cross section has reduced considerably in several stretches of tunnel. At several locations in this section, the tunnel wall closure (deformation) is well over 1.0 m and the maximum is recorded above 2.0 m. The worst affected length of the tunnel is about 550m. Due to the excessive deformation, temporary supports were provided at several locations, steel ribs and lattice girders are buckled at several locations and shotcrete lining is also cracked.



Figure 4-9: Tunnel squeezing in headrace tunnel of CHEP: Significant floor heave (left) and wall closure in hill side (right)

Now, squeezing in most of the sections is stabilized but it is active at some places. The continuation of squeezing in some section could result in further reduction of cross section. The deformed tunnel profile is being surveyed with the total station continuously from time to time. Closure of tunnel wall has been measured in the tunnel sections using these data. The

detail of deformation measurement and tunnel wall closure at particular tunnel section are described in section 7.2.1 and Figure 7-3.

4.6 TUNNEL EXCAVATION AND SUPPORT MEASURE

The headrace tunnel excavation was started in June 2008 and completed in May 2012. Tunnel section from chainages 0+000 to 3+100m was excavated by adopting the conventional drill and blast methodology. But for the sections with severe squeezing problems, different methods were attempted to be applied such as over excavation but unsuccessful, fore-poling, sequential excavation (top heading and benching), excavation through light controlled blasting and manual excavations etc

Table 4-6: Predicted support type based on rock mass quality (Q-value)

Rock mass Quality (Q)	$10 \leq Q$	$4 \leq Q < 10$	$1 \leq Q < 4$
Support Pattern	Type-R1	Type-R2	Type-R3
Remarks	Enforce a spot bolting in fragile part	Pattern bolting untensioned D25, L=3.0@1.50 Upper 120°	Pattern bolting untensioned D25, L=3.0@1.50 Upper 180°
Rock mass Quality (Q)	$0.1 \leq Q < 1$	$Q < 1$	$Q < 0.1$
Support Pattern	Type-R4	Type-R5	Type-R6
Remarks	Pattern bolting untensioned D25, L=3.0@1.50 Upper and side wall 240°	Type-R4 pattern and lattice girder support	Type-R4 pattern and steel rib support

During the excavation, different supports had been applied at the face. The main support types that were applied are R5 and R6 as per site conditions where Q-value is less than 0.1. Table 4-6 shows the type of support applied based on rock mass quality (Q-value). The detail of support types, steel ribs, rock bolts and tunnel support pattern is given in appendix A2, A3 and A4. For the reinforcement, lattice girder is used in support type R5 whereas steel ribs is used in R6. Supports were applied at the face of tunnel to improve the working condition for next sequence.



Figure 4-10: Several instances of tunnel excavation in CHEP at squeezing part

Figure 4-10 shows the photographs that were taken during excavation and after excavation. The figure illustrates support application at face (top left), application of fore poling (top right), instance of mud flow (bottom left) and application of temporary support at heavy squeezing section (bottom right). The steel ribs and fore poling were applied at the face of tunnel and shotcrete with wire mesh was applied afterwards. The squeezing phenomenon has still happened even though the careful measures were taken. The right bottom's photograph in Figure 4-10 shows the squeezed condition of tunnel where all the support measures have been yielded.

5 REVIEW OF PROJECTS WITH SIMILAR INSTABILITY PROBLEMS

The aim of this thesis is to analyze squeezing phenomenon in the tunnel. In chapter 4, the case 'CHEP' has been described and the problems associated with this project have been pointed out. Squeezing phenomenon is found to be the most severe problem in the headrace tunnel of the case. The handling of tunneling in heavily squeezed ground is very challenging task and probably the most difficult one. Hence, in order to facilitate the understanding of problem and find out the appropriate solution to the problem, two cases histories has been taken into consideration where there was severe squeezing problems in the tunnel. The author of this thesis believes that these projects will certainly help to explore more on the squeezing phenomenon.

The two cases, one from the Himalayan and another from the Andes, are Kaligandaki "A" Hydroelectric Project in Nepal and Yacambú-Quibor tunnel in Venezuela respectively. Both the projects are already constructed and are in operation phase now. Each of them has tunnel as water conveyance system. In both projects, there was severe squeezing problem in tunnel. The geology of these project areas is more or less comparable with that of CHEP. In Kaligandaki "A" project, there was squeezing problem in the tunnel sections with graphitic phyllite (with low compressive strength) as rock type. Similarly, in Yacambú-Quibor tunnel, a very severe squeezing problem was faced in the tunnel sections with very weak graphitic phyllites as rock type. The case, CHEP, is also facing the very severe squeezing problem in the tunnel stretch where there is talcosic phyllite as main rock type. Hence, in all the above mentioned cases, the squeezing problem occurred in very weak phyllite (certainly with different mineralogical composition in each case). The detail of these two cases histories, associated geology and stability problems are discussed further in this chapter.

5.1 KALIGANDAKI "A" HYDROELECTRIC PROJECT, NEPAL

The Kaligandaki "A" hydroelectric project is located in the western part of Nepal about 200 km west of Kathmandu, Nepal (Figure 5-1). This project is the largest run-of-river scheme in Nepal. It has an installed capacity of 144 MW and is capable of generating 842GWh electrical energy annually. To generate this energy, the project utilizes a 45 kilometers long loop of a relatively flat bedded Kaligandaki river in a shortcut. The water is diverted by a concrete gravity dam with a height of 43 meters and is conveyed through approximately 6 km long headrace tunnel, a vertical penstock tunnel of 97 meters height and a semi underground powerhouse (Figure 5-2). The excavated cross section of the headrace tunnel is approximately 60 square meters with horse-shoe shape and 8.4 meters diameter. The final fully concrete lined shape of the headrace tunnel is circular and has 7.4 meters diameter. The project is a medium head scheme (net head 115 meters) with a rated design discharge of 141 m³ /s (Panthi, 2006).



Figure 5-1: Location map of Kaligandaki “A” Hydroelectric Project, Nepal

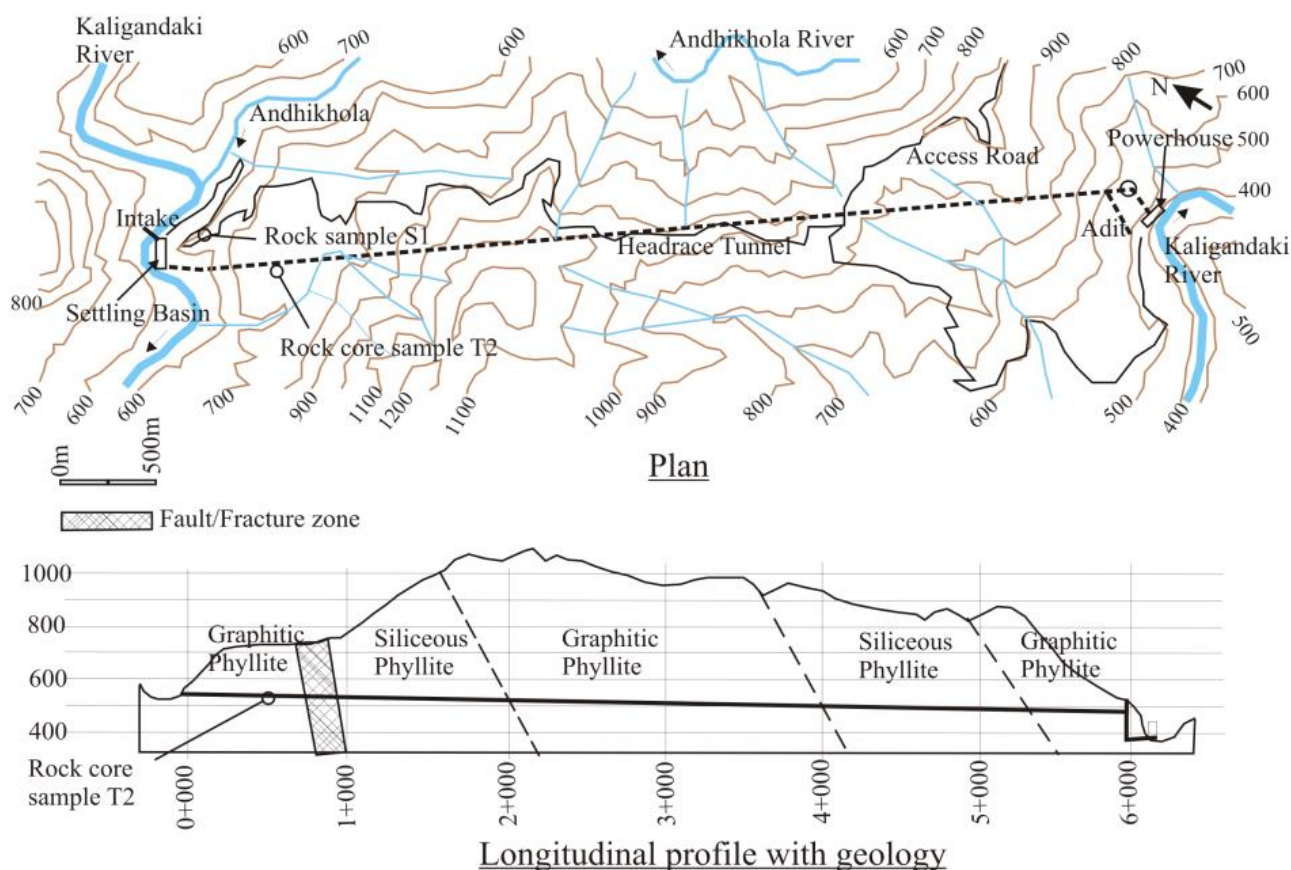


Figure 5-2: Project topography and longitudinal profile with geological description of Kaligandaki “A” hydroelectric project (Panthi, 2006)

The civil work contract was awarded to Impregilo SpA of Italy in January 1997 and the project was completed in the summer of 2002. This project is owned by Nepal Electricity Authority (NEA), an undertaking of the His Majesty's the Government of Nepal.

5.1.1 Project Geology

Geologically, the project area lies in the lesser Himalayan highly deformed rock formation and is relatively close to the Main Boundary Thrust (MBT). The rocks in the project area are mainly comprised of Precambrian to lower Paleozoic shallow marine sediments. Rocks in this group are mainly represented by dark slate, graphitic and siliceous phyllite and siliceous dolomite (Figure 5-3). The headrace tunnel of the project mostly passes through highly deformed graphitic phyllite, siliceous phyllite and phyllitic slate intercalation (Figure 5-2). The first few hundred meters upstream section of the headrace tunnel consists of highly fractured and weathered siliceous dolomite in intercalation with graphitic phyllite. The mineral composition of these rocks and the degree of metamorphism vary considerably (Panthi, 2006).

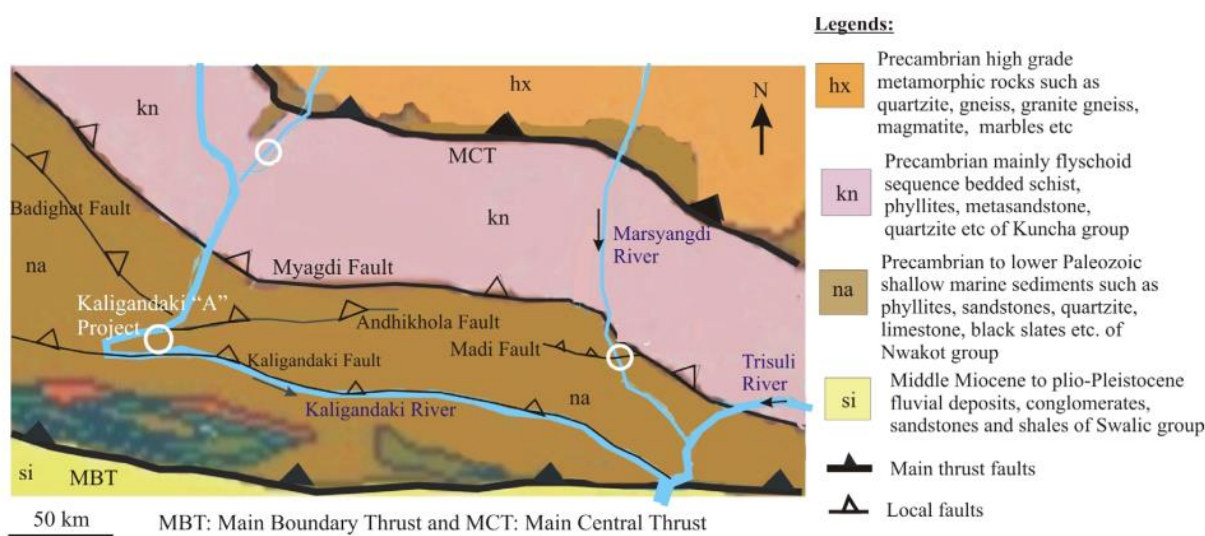


Figure 5-3: Geological environment of Kaligandaki “A” Hydroelectric Project (Panthi, 2006)

Figure 5-3 shows that the project area is very close to several local faults, namely Badighat, Andhikhola and Kaligandaki faults. The branch of Andhikhola fault crosses the headrace tunnel at about 700 meters from the intake (Figure 5-2).

5.1.2 Rock mass conditions

The planning phase investigation and predictions of the rock mass conditions along the headrace tunnel indicated that the upstream one kilometer section of the headrace tunnel would meet small fault and weakness zones. It was predicted that the tunnel might be subjected to heavy squeezing at this upstream section. The rest of the tunnel alignment was assumed to have fair to good quality rock mass except for some sections with highly sheared and deformed rock mass. It is interesting to note that most of the engineering geological investigations conducted during pre-construction phases were at headworks and powerhouse areas. The geological investigations along the headrace tunnel alignment were limited only to

engineering geological mapping and petrographic and mineralogical analysis of a limited number of rock samples. Accordingly, the estimated temporary tunnel rock support was also relatively small in comparison to as built. However, the rock mass observed during excavation was found to be very weak, highly sheared, thinly foliated and intensely folded (Panthi, 2006).

As a result of active tectonic movement and presence of several local faults, the rock mass in the area has been subjected to shearing, folding and faulting. In addition, the maximum elevation difference between the top of the hill and the tunnel alignment is as much as 600 meters and more than 80 percent of the tunnel alignment has overburden exceeding 200 meters. During tunnel excavation, most of the rock mass along the tunnel alignment was found to be of poor to extremely poor quality and demanding heavy rock support. As a result, considerable deviations between predicted and actual rock mass quality were witnessed and the need for tunnel rock support exceeded considerably what was predicted at planning (Panthi, 2006).

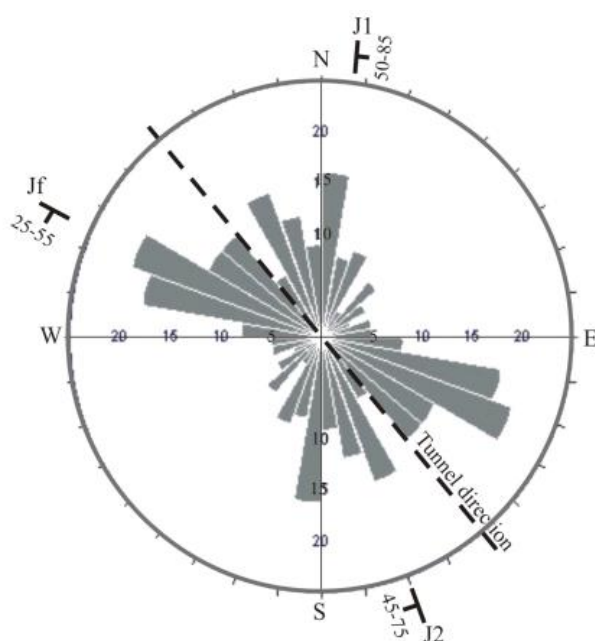


Figure 5-4: Orientation of main joint sets and Kaligandaki “A” headrace tunnel (Panthi, 2006)

As Figure 5-4 indicates, the orientation and dip of the joints sets are highly scattered due to extreme folding and shearing giving no distinct joint system except for foliation joints. In general, the foliation joints are oriented with strike varying from $N85^{\circ}$ to 140° E with dip angles between 25-55 degrees towards Southwest. The alteration and weathering of discontinuity surfaces are considerable and the joints are filled with highly sheared clay, quartz and calcite veins.

5.1.3 Tunnel stability problems

There were two major factors that played significant roles for stability at the Kaligandaki headrace tunnel. The first was related to very weak and thinly foliated phyllite with

high degree of strength anisotropy that led to considerable reduction on the self supporting capability of the rock mass. As a result of this, frequent small to medium scale tunnel collapses occurred. The second one was related to tunnel squeezing. Due to high overburden stress and the presence of weak phyllite rock mass, especially graphitic phyllite with low compressive strength, the tunnel squeezed severely at many locations (Figure 5-5).

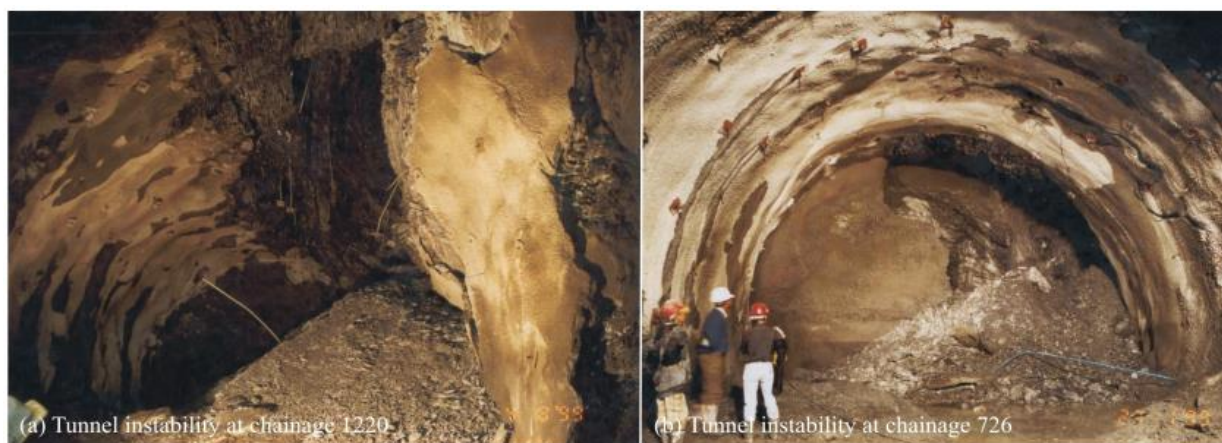


Figure 5-5: Collapse due to strength and stress anisotropy (left) and cracks formed by high squeezing pressure (right) (Panthi, 2006).

Kaligandaki headrace tunnel experienced severe squeezing problem in an about two kilometers long tunnel section between chainage 1+964 and 4+032. At this section, the headrace tunnel passes through highly schistose graphitic phyllite, and has overburden ranging from 425 to 620 meters. In that tunnel section convergence readings were made by using tape extensometer. The horizontal convergence measured in this tunnel stretch was mostly highest for the BC line (Figure 5-6, right). The calculated tunnel strains along BC line for respective instrumentation chainage are shown in Figure 5-6 (left).

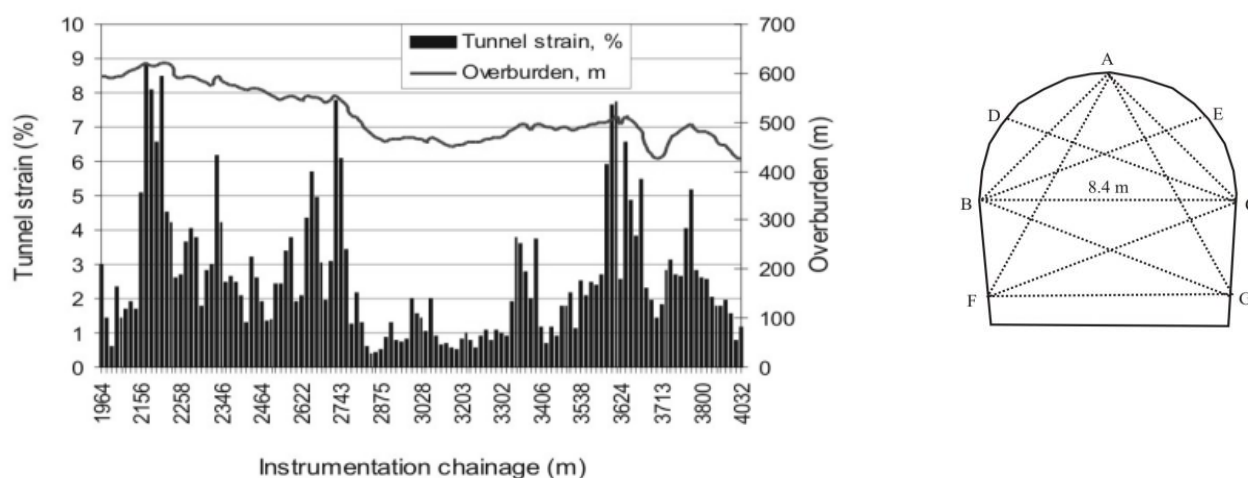


Figure 5-6: Horizontal strain (%) between chainage 1964 and 4032 in Kaligandaki headrace tunnel (left), typical tunnel section indicating tape extensometer measuring point (right) (Panthi, 2006)

The magnitudes of horizontal tunnel strain vary considerably within this section of the headrace tunnel (Figure 5-6, left). The figure also illustrates that even within similar overburden height there is a considerable difference in degree of tunnel squeezing. This suggests that the quality of rock mass, and in particular rock mass strength, varies greatly within short tunnel distances (Panthi, 2006).

5.2 YACAMBÚ-QUIBOR TUNNEL, VENEZUELA

The Yacambú-Quibor tunnel is located in the state of Lara in Venezuela. The tunnel is 4.0m average diameter and 23.3m long and will transfer 347 million m³ water per year from the wet tropical Orinoco basin, on the eastern bank of Andes, to semi-arid Quibor valley on the western flank of Andes. The agricultural and urban requirements of this semi-arid agricultural area, near the city of Barquisimeto, exceed currently available fresh water supplies and have resulted in a significant depletion of aquifers in the Quibor region (Hoek and Guevara, 2009a).

The main technical issues in this tunnel were the severe squeezing problems in very weak graphitic phyllites present in that area at depths of up to 1270 m below surface. Initial attempts to use an open-face TBM in 1976 failed as did attempts to use heavy support to resist squeezing. It was only after the introduction of yielding support in about 1991 that reasonable progress was made. Difficulties continued with floor heave in sections of the tunnel in which horseshoe profiles were used, even after the introduction of yielding support. Eventually, in 2004, slow but steady progress was achieved after the Owner and the Contractor agreed that only a circular section would be used and emphasis was placed on developing a routine construction procedure, irrespective of the rock conditions encountered at the face. Finally, The tunnel was broken through on 27th July 2008 after 32 years of technical, financial, contractual and political problems (Hoek and Guevara, 2009a). There were altogether eight phases of contracts to complete the tunnel excavation.

5.2.1 Project Location and Geology

The location map of the project site is shown in Figure 5-7 and is located in Barquisimeto. The layout plan and cross section of the project is shown in Figure 5-8. The north-western region of South America and Panama is one of the most tectonically complex land regions on earth as illustrated in Figure 5-9. Four major plates interact in the region. The Andes follow the north-south Nazca/South American plate boundary to the south but curve eastward in the north and they are influenced by this complex tectonic junction. In particular, in the region of Yacambú-Quibor project (circle in the upper right of the Figure 5-9) a triangle of strike-slip and transpressional faults (including the Bocono) react to accommodate the mismatch in movement of the surrounding plates. The phyllitic rock mass which dominates the mountain range in the Yacambú-Quibor area ranges from strong and reasonably massive silicified phyllites in the dam area to severely tectonically deformed *graphitic phyllite* along most of the tunnel alignment (Hoek and Guevara, 2009a). The Yacambú-Quibor project is located in the circled area in the upper right of the Figure 5-9.



Figure 5-7 Location map of Yacambú-Quibor tunnel project, Venezuela (Hoek and Guevara, 2009a)

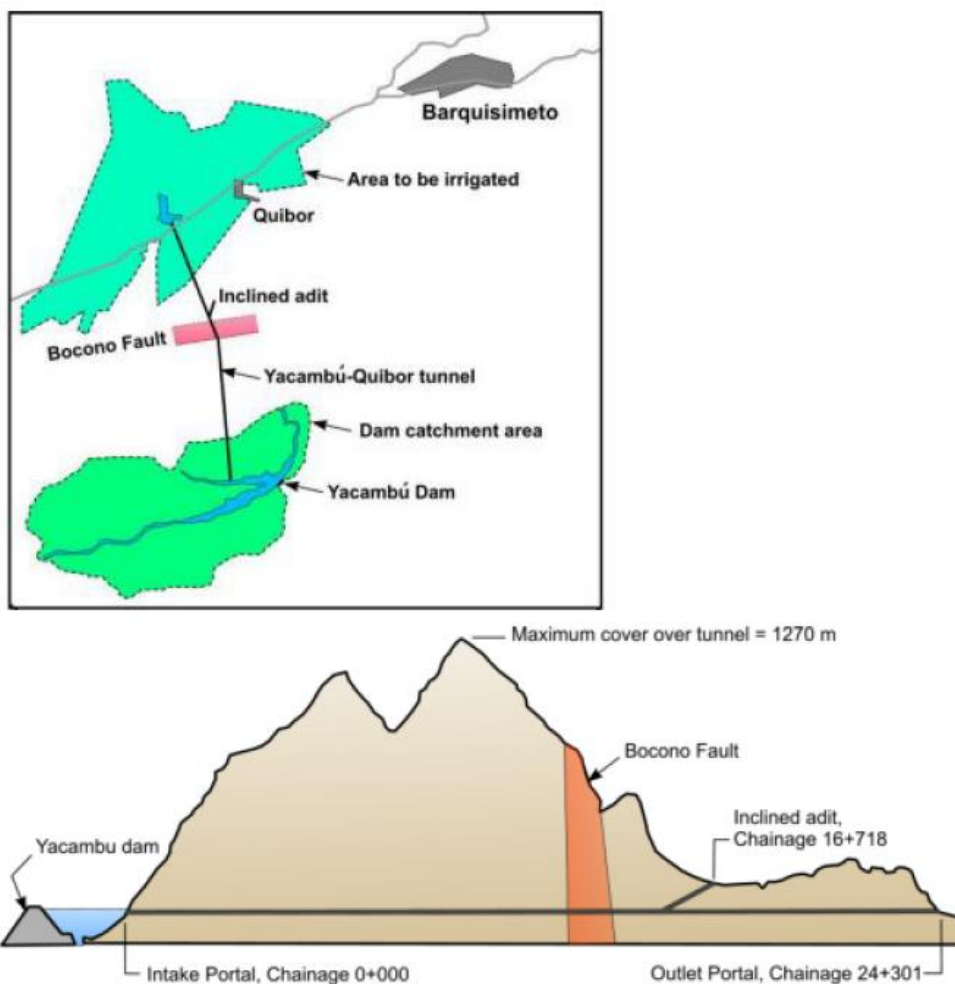


Figure 5-8 Plan and cross section along tunnel alignment of Yacambú-Quibor project, Venezuela (Hoek and Guevara, 2009a)

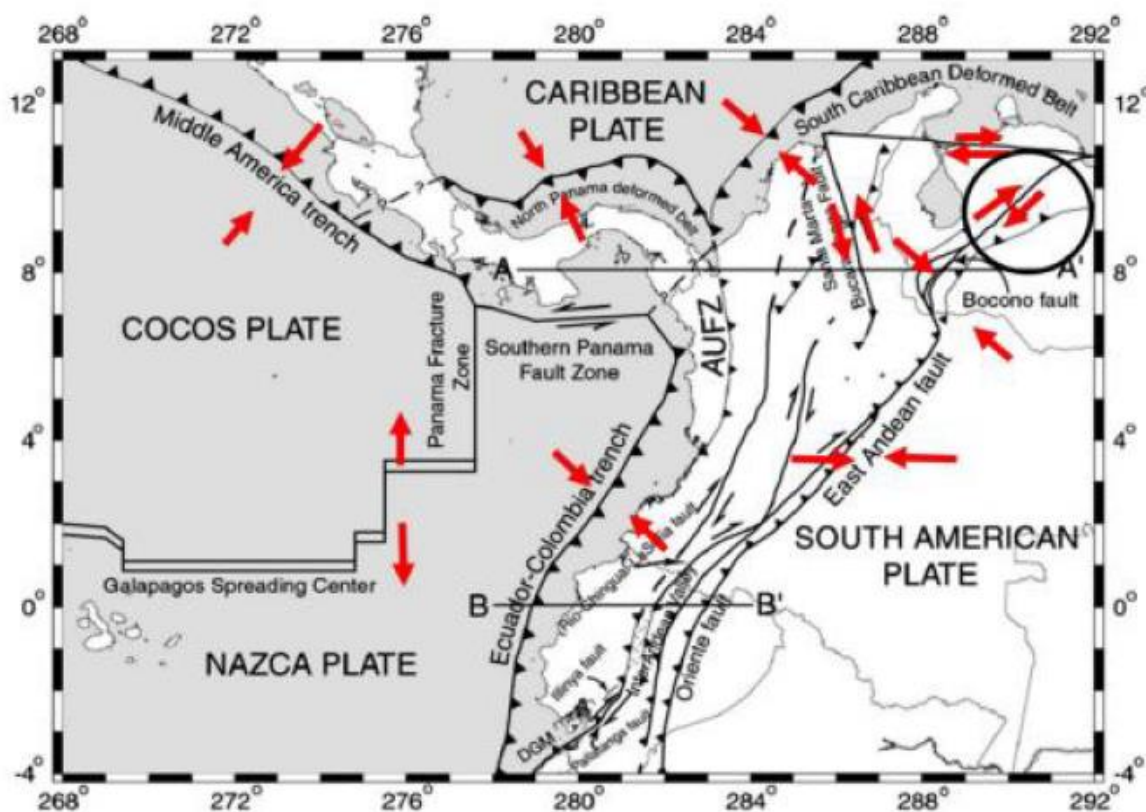


Figure 5-9: Tectonic plates in the south-western region of South America and Panama (Hoek and Guevara, 2009a).

Most of the detailed geology along the tunnel alignment was revealed at the time of excavation of tunnel and it was found that rather than the silicified phyllite anticipated on the basis of the dam site investigation, a highly tectonically deformed graphitic phyllite in high proportion of rock which behaves in a different way than the silicified phyllite (Hoek and Guevara, 2009a).

5.2.2 Rock mass properties

The 32 years required for the excavation of the Yacambú-Quibor tunnel coincided with significant developments in the field of rock engineering. The rock mass classification systems of Barton et al. (1974) and Bieniawski (1973) had only been introduced two years before the start of construction and were virtually unknown in the Americas. Numerical analyses techniques for underground excavation design were in their infancy and personal computers only became available in the early 1980s. European techniques for dealing with squeezing conditions Rabcewicz (1964) were seldom used in the Americas and were only used on a regular basis at Yacambú-Quibor from about 1990 onwards.

According to Hoek and Guevara (2009b), descriptive methods for estimating rock mass properties, required for support design calculations, were gradually replaced by rock mass classification methods based on detailed geological observations. Table 5-1 shows an example of one of the early descriptive classifications.

Table 5-1: Classification of Yacambú-Quibor rock units (Hoek and Guevara, 2009a)

CLASS	TYPE OF ROCK	CHARACTERISTICS
A	Predominance of silicified phyllite with small amounts of calcareous and/or graphitic phyllite.	Cemented layers from 5 to 10 cm in thickness with high strength and high deformation modulus.
B	Predominance of calcareous silicified phyllite with intervals of graphitic phyllite.	Cemented layers from 2 to 3 cm in thickness with average strength and average deformation modulus.
C	Graphitic phyllite with some intervals of silicified phyllite.	Thin lamination from 0.1 to 1 mm with low strength and highly deformable.
D1	Tectonically deformed, folded and sheared in Classes A, B and C.	Behaves as homogeneous rock mass with zero volume change during deformation
D2	As for D1 with clay gouge in contacts.	Highly plastic deformation with zero volume change

A critical component of the rock mass strength determination in the Hoek-Brown failure criterion is the uniaxial compressive strength σ_{ci} of the intact pieces of rock that make up the rock mass. In the case of the graphitic phyllite encountered in the Yacambú-Quibor tunnel, it proved to be difficult to arrive at a consensus on how the strength should be estimated in the field. Most geologists on the project were inclined to assign very low values of 5 to 15 MPa on the basis of the poor appearance of the rock mass and the slickensided nature of the surfaces. However, back analyses of the tunnel behaviour suggested that this value should be closer to 50 MPa. A maximum UCS of approximately 100 MPa was found for specimens tested normal to schistosity while a minimum of approximately 15 MPa is given for tests on specimens with the schistosity inclined at about 30° to the loading direction. These results are typical for highly schistose rocks and it is not unreasonable to assume an average UCS of 50 MPa for the intact strength of the individual rock pieces when they are more or less randomly oriented in the rock mass, on the scale of the tunnel (Hoek and Guevara, 2009a).

5.2.3 Tunnel stability problems

The main tunnel stability problem in Yacambú-Quibor tunnel was squeezing. Hoek (2001) explained that the maximum tunnel strain percentage was more than 30% and it was extreme squeezing. The instability was controlled by yielding steel sets. The photographs in Figure 5-10 and Figure 5-12 show some glimpse of instability caused by tunnel squeezing.



Figure 5-10: Floor heave about 100m behind the Intake drive TBM in 1979 at a depth of 400 to 425 m below surface (Hoek and Guevara, 2009a) (left) and Mining out the remains of a tunnel boring machine trapped by squeezing of the tunnel during a stoppage of the drive (Hoek, 2001) (right).

According to Hoek and Guevara (2009a), the section of the tunnel between chainage 12750 to 12850 was constructed in 2000 as a circular section with a lining illustrated in Figure 5-11. This lining consisted of WF 6 x 20 steel ribs spaced at 0.8 m with two sliding joints with 30 cm openings, giving a radial convergence of 3.7% strain before locking. These ribs are encased in 40 MPa shotcrete of 0.45 m thickness, reinforced by a layer of 100 x 100 x 7 mm weldmesh. The sequence of construction of this lining is not clear in the available documents.

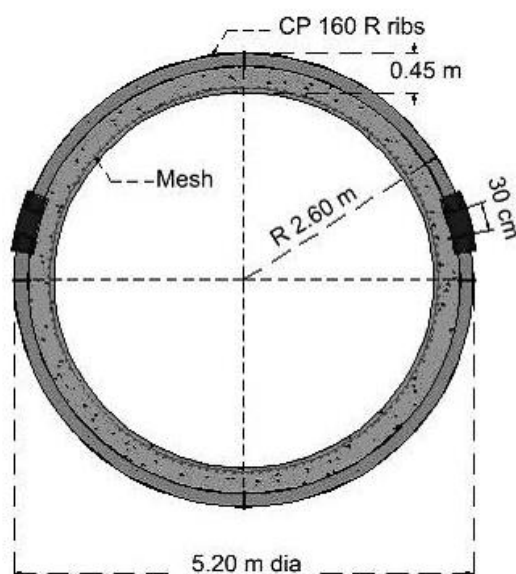


Figure 5-11: Geometry of lining used between Chainage 12750 and 12850 (Hoek and Guevara, 2009a)

After about 2 years of service the extensometers registered a sudden increase in deformation in this tunnel section. This was followed by progressive deterioration and eventual collapse of the lining as illustrated in Figure 5-12.



Initial damage with cracking of the shotcrete and loss of alignment of the track.



After removal of the cracked shotcrete, significant deformation of the WF 6 X 20 steel ribs could be observed.



In spite of having placed rings of rockbolts to isolate the damaged section, failure propagated to the roof of the section after removal of the damaged shotcrete in the invert.



As the failure developed, with closures of up to 1 m being observed, it was decided to re-mine the tunnel and replace the lining. The photograph shows a repaired section of the tunnel in the foreground and the damaged tunnel in the background.

Figure 5-12: Evolution of the damage caused by squeezing between Chainage 12+750 and 12+850 (Hoek and Guevara, 2009a)

The damage shown in Figure 5-12 is one of the examples among the many such instances along headrace tunnel and after excavation. The support in this case did not work well even if it contained good combination of shotcrete, steel ribs and wire mesh, which may be either due to the faulty sequence of application of support or the combined support capacity is less than support pressure.

5.2.4 Design of support and final lining

According to Hoek and Guevara (2009a), based on many years of experience in constructing the Yacambú-Quibor tunnel it was determined that, for the deepest sections of the tunnel in poor quality rock, the tunnel would be circular in shape and that it would be lined with a high quality shotcrete lining. It was not practical to install and anchor rock bolts in these very weak rock masses and, hence, the only support design decisions were the thickness of the shotcrete lining and the method and timing of installation. Ideally the lining should be installed as close to the working face as possible in order to provide protection for the workmen. But in that case, the available capacity of support could be lower than that required for long term conditions and there the lining will be overstressed. Actually that had happened in Yacambú-Quibor tunnel. An obvious solution to this problem will be to delay the installation of the lining that means the installation of lining far from tunnel face for e.g. 15m. Unfortunately it is not practical to install the lining at 15 m behind the face since this would result in an unacceptable level of risk to those working in the tunnel. Consequently, if the benefits of delayed lining installation are to be realized, it is necessary to provide some form of safety cage to protect the workers until the shotcrete lining can be fully mobilized. This introduces the concept of yielding support that has been used by miners for many years and, as mentioned earlier, had been employed during the second contract in mining the inclined adit.

In the case of the Yacambú tunnel several yielding support systems were investigated during the early 1990s and the design finally adopted is illustrated in Figure 5-13 and Figure 5-14. The design of this system was based on the requirements that it could be constructed on site from readily available locally manufactured steel sections, it had to be easy to assemble in the limited space available at the tunnel heading and it had to provide sufficient capacity to protect the workmen in the event of a sudden convergence of the tunnel.

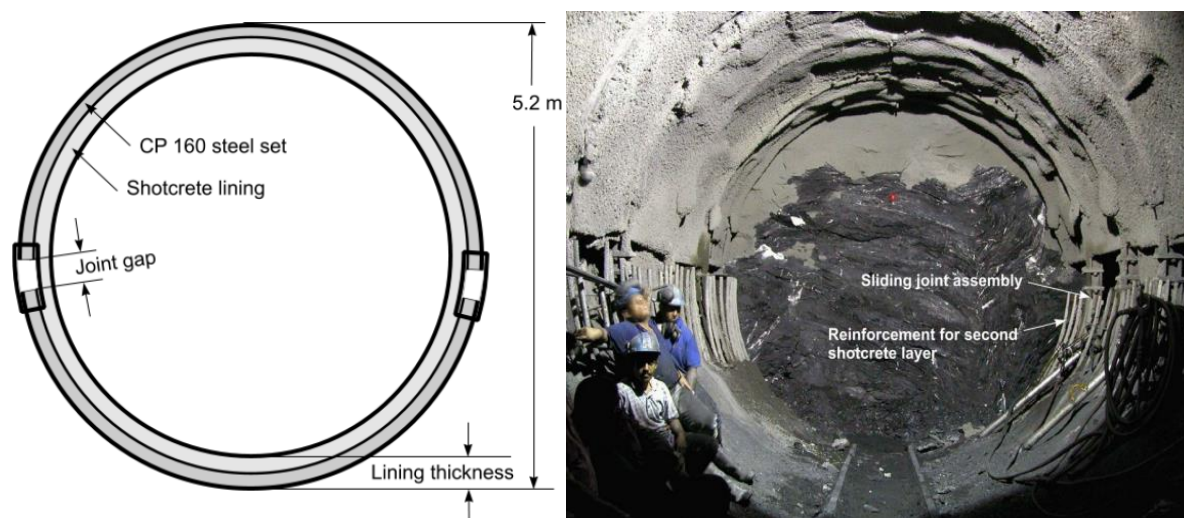


Figure 5-13: Design details of yielding support (left) and installation of circular lining such as that illustrated in figure 5-15 (right) (Hoek and Guevara, 2009a)



Figure 5-14: Details of one of the two sliding joints in the steel sets (left) and assembled steel set with two sliding joints (right) (Hoek and Guevara, 2009a)

Hoek and Guevara (2009a) mentioned that the yielding system was installed as close to the face as possible (Figure 5-14, right). In some cases where the stability of the face is a problem, the face was split and a very short top heading driven a distance of 1.5 to 3 m ahead of the following bench. The top half of the steel set was installed in the top heading and the sliding joints and lower half of the arch was installed as soon as the bench was removed. This short bench acted as a face buttress and it proved to be effective in maintain the stability of the face in the worst ground conditions.



Figure 5-15: Completed tunnel lining in one of the deepest sections between Chainages 10000 and 12000 in Yacambú-Quibor tunnel (Hoek and Guevara, 2009a)

Placing of the steel sets, generally at a spacing of 1 m, was followed by the immediate application of a 20 cm thick layer of shotcrete. This was sufficient to embed the 16 cm deep sets and to form a protective shell above the workers. A 1 m wide window was left on both

sides of the shotcrete shell to allow the sliding joints to move freely. This window was closed when the sliding gaps had closed or at a distance of about 15 m behind the face, whether or not the gaps had closed. Once the windows had been closed and the initial shell had been fully mobilized, a second inner shotcrete layer of up to 40 cm thick was placed to complete the lining. The appearance of the completed tunnel is shown in Figure 5-15.

Even with this support system, after 2 years of service there was sudden increase in deformation in tunnel sections between chainage 12+750 and 12+850. This was followed by progressive deterioration and eventual collapse of the lining (illustrated in section 5.2.3). Hoek and Guevara (2009a) explained that the shotcrete carries very little load under short term conditions and steel ribs carries practically all of the loading before the shotcrete lining was installed. However, failure of the steel ribs under long term loading conditions would result in a transfer of the load carried by the ribs onto the shotcrete lining and this would almost certainly overload the shotcrete. In addition, buckling of the steel ribs would cause local spalling of the shotcrete which would reduce its load carrying capacity. Afterward they claimed there would be the potential danger associated with incorrect installation sequencing of support elements which, when used correctly, are probably adequate for the loading conditions.

6 SQUEEZING ANALYSIS METHODS AND SUPPORT DESIGN

6.1 GENERAL

As already mentioned in the chapter 4, the main instability in the headrace tunnel of CHEP is tunnel squeezing. To apply appropriate tunnel excavation method and to support the tunnel in terms of immediate and long term basis, squeezing phenomenon and the rock support interaction in the tunnel should be assessed. For analysis and support design, many authors have proposed different approaches, which are discussed further in this chapter.

The methods that are used to predict the tunnel squeezing, include empirical methods such as Singh et al. (1992), Q-system (Grimstad and Barton, 1993), Goel et al. (1995), Palmstrom (1995); semi-analytical methods such as Hoek and Marinos (2000), Kovári (1998), Aydan et al. (1993); and analytical methods such as convergence confinement methods (Carranza-Torres and Fairhurst, 2000) and numerical methods such as the 2-dimensional elasto-plastic finite element program, Phase2. Among these methods, Singh et al. (1992), Q-system, Hoek and Marinos (2000), Carranza-Torres and Fairhurst (2000) and Phase2 are used in this thesis for the squeezing analysis. The selected methods are explained further in this chapter.

6.2 EMPIRICAL METHOD

The empirical methods are based on the experience and comparison of different case histories. There are three categories of empirical approaches based on the indicators used (Shrestha, 2006);

- Strength-stress ratio approach
- Strain estimation approach
- Rock mass classification approach

6.2.1 Singh et al approach

This method of analysis is based on the rock mass classification approach. Singh et al. (1992) developed an empirical relationship from the log-log plot between the tunnel depth (H) and the logarithmic mean of the rock mass quality, Q (Figure 6-1). 41 tunnel sections data were used to plot this figure. Out of 41 data, 17 data were taken from case histories in Barton et al. (1974) and 24 tunnel section data were obtained from tunnels in Himalayan region. A clear line of demarcation can be seen on the figure, which is in between the elastic and squeezing condition. The equation of this line is given as;

$$H = 350Q^{1/3} \quad 6-1$$

From Figure 6-1, it can be concluded that the squeezing phenomenon may occur in the rock mass when depth of overburden above tunnel section exceeds $350 Q^{1/3}$.

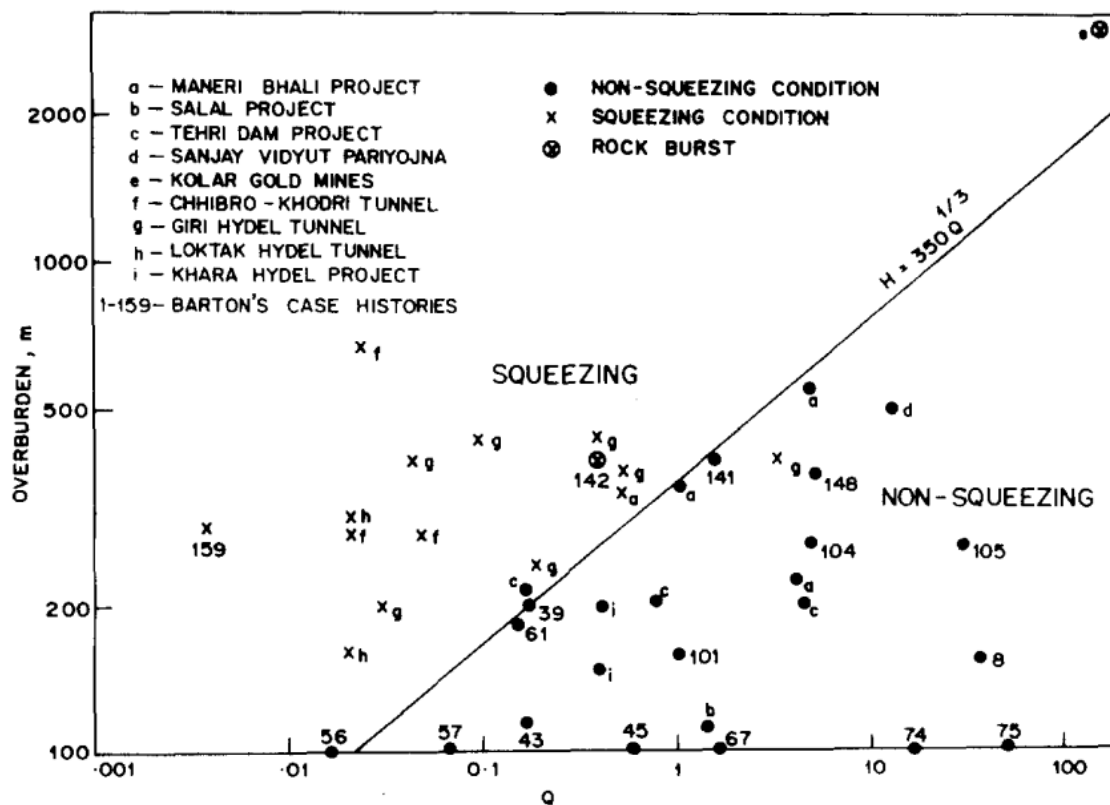


Figure 6-1: Criteria for predicting squeezing ground (Singh et al., 1992)

Although equation 6-1 is very simple and easy to use, difficulties have been experienced for the estimation of correct value of SRF (one of the term in Q) in some cases. The selection of SRF value is very sensitive for the correct estimation of Q-value.

6.2.2 Q-system

The Q-system for rock mass classification was developed at the Norwegian Geotechnical Institute (NGI) by Barton et al. (1974). Later, it was updated by Grimstad and Barton (1993) by including more than 1000 cases. It is a system for estimation of the required tunnel support, based on a numerical assessment of the rock mass quality using the following six parameters:

- Rock quality designation (RQD)
- Number of joint sets (J_n)
- Roughness of the most unfavourable joint or discontinuity (J_r)
- Degree of alteration or filling along the weakest joint (J_a)
- Water inflow (J_w)
- Stress condition given as the stress reduction factor (SRF)

The above mentioned six parameters are grouped to give the overall rock mass quality:

$$Q = \frac{RQD}{J_n} \times \frac{J_r}{J_n} \times \frac{J_w}{SRF} \tag{6-2}$$

The detail of estimation of these six parameters is given in appendix B5.

Singh et al. (1992) refers Q-system for the assessment of potential squeezing problem. Also, very briefly, Q-system itself addresses squeezing rocks on the basis of value of $\sigma_{\theta_{\max}}/\sigma_{\text{cm}}$ ratio. Where $\sigma_{\theta_{\max}}$ is maximum tangential stress and σ_{cm} is rock mass compression strength. According to Barton (2002), the squeezing condition is stated in Table 6-1.

Table 6-1: Squeezing condition according to Q-system (Barton 2002)

Squeezing rock: plastic flow of incompetent rock under the influence of high rock pressure	$\sigma_{\theta_{\max}}/\sigma_{\text{cm}}$	SRF
Mild squeezing rock pressure	1 - 5	5 - 10
Heavy squeezing rock pressure	> 5	10 - 20

The detail of squeezing condition and SRF estimation is given in appendix B5. $\sigma_{\theta_{\max}}$ can be estimated approximately using equation 3-7 whereas estimation of the value for σ_{cm} is a difficult task. According to Shrestha (2006), NGI (1997) also states ‘Cases of squeezing rock may occur for depth $H > 350 Q^{1/3}$ (Singh et al., 1992). Rock mass compression strength can be estimated as $\sigma_{\text{cm}} = 0.7 \gamma Q^{1/3}$ (MPa) where γ = rock density in kN/m^3 (Singh et al., 1993)’. But Shrestha (2006) claimed that these criteria lead to the loop of dependency in the following way: if the above mentioned equation is used to calculate σ_{cm} , it needs Q value which is found by estimating SRF value and; to estimate SRF value it should be known whether there is squeezing or not. To overcome this problem of loop of dependency, empirical relationships proposed by different authors that are explained in section 2.3.6 (Table 2-3) can be used. But, among these relationships, three out of four relationships still use Q-value. So, the relationship proposed by Panthi (2006) can be used to estimate σ_{cm} because it uses only the intact rock strength (σ_{ci}) as input parameter rather than Q-value.

Also, the Q-value is related to tunnel support requirement by defining the equivalent dimensions (D_e) of the underground opening. This equivalent dimension, which is a function of the size and type of the excavation, is obtained by dividing the span, diameter or wall height of the excavation (D_t) by a quantity called the excavation support ratio (ESR), given as:

$$D_e = \frac{D_t}{ESR} \quad 6-3$$

ESR considers type and use of the underground construction and its rating is done as per the table given in appendix B6. On the basis of the Q-value and D_e value, support requirement is estimated using support chart given by Palmstrom and Broch (2006), which is presented in appendix B6.

Furthermore, Barton et al. (1974) explained that the Q-value can also be used to estimate the support pressure. The chart given by Barton et al. (1974) to estimate support pressure is presented in appendix B7 where in addition to Q-value, one of the six parameter of Q-value i.e. J_r is also necessary.

6.3 SEMI-ANALYTICAL METHOD

The semi-analytical approaches that are used for the analysis of tunnel squeezing phenomenon are Kovári (1998), Aydan et al. (1993), Hoek and Marinos (2000), etc. Among them, Hoek and Marinos (2000) is described in this chapter and has been used for the analysis in this thesis.

6.3.1 Hoek and Marinos approach

According to Hoek and Marinos (2000), the ratio of uniaxial compressive strength (σ_{cm}) of the rock mass to the insitu stress (p_o) can be used as the indicator of the potential tunnel squeezing problems. They used Sakurai (1983) approach to determine the relationship between σ_{cm}/p_o and the percentage strain of the tunnel. The result of study based on the closed form analytical solutions for the circular tunnel in a hydrostatic stress field presented by Duncan Fama (1993) and Carranza-Torres and Fairhurst (1999) is shown in the figure 6.3. Hoek and Marinos (2000) used Monte Carlo simulations to determine the strain in the tunnels for a wide range of conditions. For this, they used 2000 iterations with assumed uniform distributions for the following ranges of parameters: In situ stress 2 to 20 MPa (80 to 800m depth), tunnel diameter 4 to 16 m, uniaxial strength of intact rock 1 to 30 MPa, Hoek and Brown constant m_i of 5 to 12, GSI of 10 to 35 and a dilation angle of 0 to 10. The simulation indicated that all tunnels follow a clearly defined pattern, which is well predicted by means of the equation included in Figure 6-2.

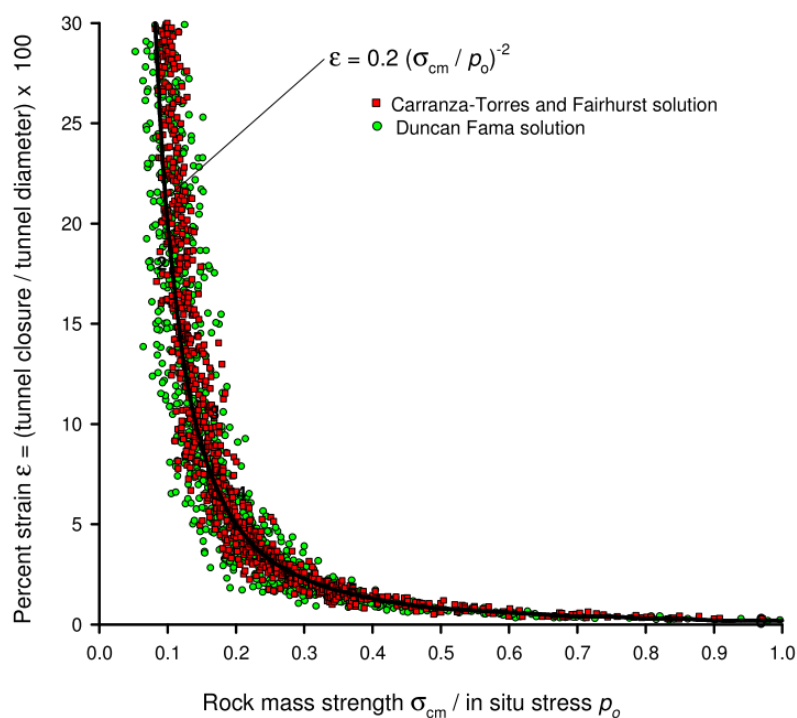


Figure 6-2: Plot of tunnel convergence against the ratio of rock mass strength to in situ stress in case of unsupported tunnel (Hoek and Marinos, 2000).

Hoek and Brown failure criteria proposed by Hoek et al. (2002), used for estimating strength and deformation characteristics of rock masses, assumes that the rock mass behaves

isotropically. However, Shrestha (2006) explained that even if the rock mass is heavily fractured, continuity of the bedding surfaces will have been disrupted and the rock may behave as an isotropic mass. Thus this criterion can be adapted to weak heterogeneous rock masses too.

The analysis presented above can be extended to cover tunnels in which an internal pressure is used to simulate the effects of support. Using a curve fitting process, Hoek and Marinos (2000) proposed following equations to determine size of the plastic zone and deformation of a tunnel in squeezing ground.

$$\frac{d_p}{d_o} = \left(1.25 - 0.625 \frac{p_i}{p_o}\right) \frac{\sigma_{cm}}{p_o} \left(\frac{p_i}{p_o}\right)^{-0.57} \tag{6-4}$$

$$\frac{\delta_i}{d_o} = \left(0.002 - 0.0025 \frac{p_i}{p_o}\right) \frac{\sigma_{cm}}{p_o} \left(2.4 \frac{p_i}{p_o} - 2\right) \tag{6-5}$$

Where, d_p = Plastic zone diameter, d_o = Original tunnel diameter in meters, δ_i = Tunnel sidewall deformation, p_i = internal support pressure, p_o = In situ stress = depth x unit weight and σ_{cm} = Rock mass strength. The rock mass strength can be estimated using empirical relationships given in Table 2-3.

Hoek and Marinos (2000) also suggested the classifications of squeezing severity based on the strain percentage. There are five classes of squeezing problems from few support problems to extreme squeezing problems i.e.; from A to E. The ranges of these classes and their description are shown in Figure 6-3 and Table 6-2.

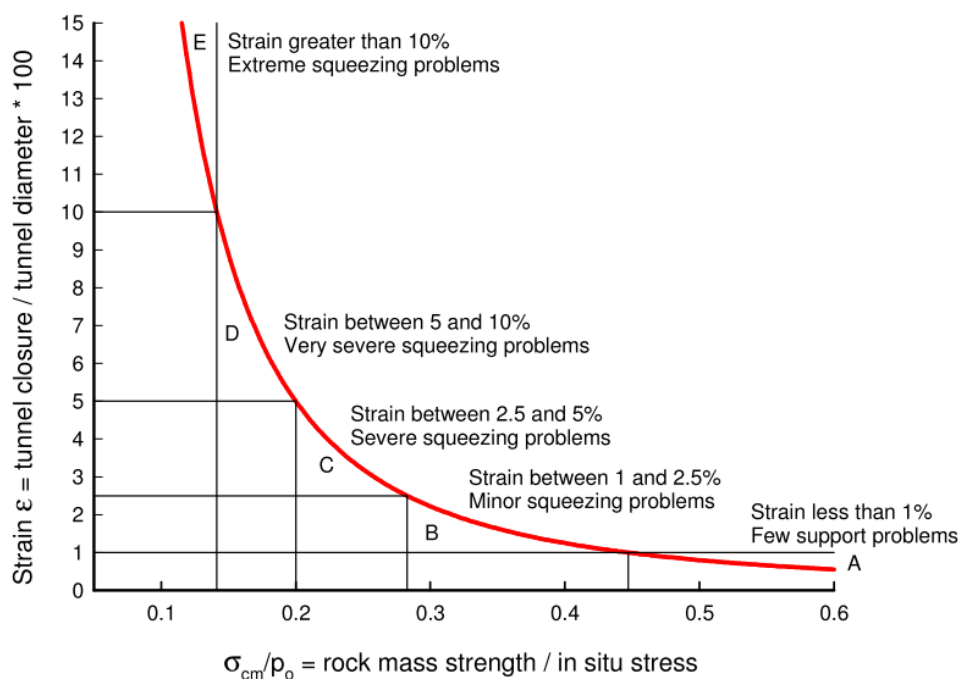


Figure 6-3: Approximate relationship between strain and the degree of difficulty associated with tunneling through squeezing rock in case of unsupported tunnel (Hoek and Marinos, 2000).

Table 6-2: Geotechnical issues associated with the squeezing severity classes and appropriate support types (Hoek and Marinos, 2000)

	Strain ϵ %	Geotechnical issues	Support types
A	Less than 1	Few stability problems and very simple tunnel support design methods can be used. Tunnel support recommendations based upon rock mass classification provide an adequate basis for design.	Very simple tunneling conditions, with rockbolts and shotcrete typically used for support.
B	1 to 2.5	Convergence confinement methods are used to predict the formation of a 'plastic' zone in the rock mass surrounding a tunnel and of the interaction between the progressive development of this zone and different types of support.	Minor squeezing problems which are generally dealt with by rockbolts and shotcrete; sometimes with light steel sets or lattice girders are added for additional security.
C	2.5 to 5	Two-dimensional finite element analysis, incorporating support elements and excavation sequence, are normally used for this type of problem. Face stability is generally not a major problem.	Severe squeezing problems requiring rapid installation of support and careful control of construction quality. Heavy steel sets embedded in shotcrete are generally required.
D	5 to 10	The design of the tunnel is dominated by face stability issues and, while two-dimensional finite analyses are generally carried out, some estimates of the effects of forepoling and face reinforcement are required.	Very severe squeezing and face stability problems. Forepoling and face reinforcement with steel sets embedded in shotcrete are usually necessary.
E	More than 10	Severe face instability as well as squeezing of the tunnel make this an extremely difficult three-dimensional problem for which no effective design methods are currently available. Most solutions are based on experience.	Extreme squeezing problems. Forepoling and face reinforcement are usually applied and yielding support may be required in extreme cases.

Although this approach can give useful indication of potential squeezing and support requirements for tunnels in weak ground, the solutions cannot be considered adequate for the final design purpose. The basic assumptions of this method is that the analysis is based on a simple closed-form solution for a circular tunnel in a hydrostatic stress field and support is assumed to act uniformly on entire perimeter of tunnel. These conditions are seldom met in the field, and tunnel shape and in situ stress conditions are seldom as simple as those

assumed. Therefore Hoek and Marinos (2000) recommended that, where there is significant potential squeezing problems, numerical analysis should be used in such cases.

6.4 ANALYTICAL METHOD

According to Carranza-Torres and Fairhurst (2000), the support requirement estimation in the vicinity of tunnel face is four dimensional problems. The three dimensional redistribution of forces around the excavation depends upon time and there is an uncertainty of nature of rock until and unless it is exposed in the face. They also explained that Labasse (1949) described the situations in two ways. First, the type of support to be used should be standardized i.e.; it must be limited to one or two types not to disturb the construction activities in underground. Second, in order to determine the precise solution in each face, there is necessity to study each cross-section separately where it would be necessary to carry out the test from each layer to determine its properties and influence of the properties on neighboring layers. For that, a number of experiments and mathematical analysis would be required which may take precious time during which the excavation would certainly have collapsed. This situation prevents the necessity to install the support immediately after excavation which may not allow time to carryout calculations and fabricate the support.

In order to overcome the above mentioned constraints, the analytical solutions have been proposed which may address the nature of interplay between the rock mass that may vary and the installed support, and the effect of variation in assumed rock properties on the support loads. Although there is no special analytical method available for squeezing condition only, the methods that are used for the general tunnel stability analysis can be used (Shrestha, 2006). Among different approaches available, convergence confinement method (CCM) of analytical solution, proposed by Carranza-Torres and Fairhurst (2000), is used in this thesis. The practical implementation of CCM to the rock masses is described in this chapter. This method can be described by the Hoek-Brown failure criteria (described in section 2.3.5) in order to define the strength and deformability properties of rock masses (Carranza-Torres and Fairhurst, 2000).

6.4.1 Convergence-Confinement Method (CCM)

Carranza-Torres and Fairhurst (2000) quoted that although the term CCM was developed in the 1960's and 70's, the method has been known at least since the paper by Fenner (1938). The application of CCM requires the knowledge of the deformation characteristics of the ground and of the support. CCM is the procedure that allows the load imposed on support installed behind the face of tunnel to be estimated. If the support is installed immediately in the vicinity of face, it does not carry out full load to which it is supposed to. The part of load is carried by face itself. As tunnel and face advance away from the support, face effect decreases and support must carry more loads. When the tunnel moves well away from face, the support will be subjected to full design load.

Figure 6-4 shows the problem that contains a cylindrical tunnel of radius R through a rock mass that is assumed to be subject initially to a uniform field far field stress σ_0 . A support is installed at a distance L from face at section A-A'. The support is assumed to be of unit length in the direction of tunnel axis. The radius R_{pl} indicates extent of failure zone that

developed around the tunnel. Main objective of the analysis is to determine the load that rock mass will transmit to the support at section A-A' from the time of installation until the time when face has moved ahead, sufficiently far that the face effect has disappeared.

For the simplicity, it is assumed that all the deformation occur in a plane perpendicular to the axis of tunnel. Radial displacement u_r and pressure p_i i.e. the reaction of support on the walls of the tunnel are uniform at the section. Figure 6-4c shows that the circular annular support of thickness t_c and external radius R is installed at the section A-A'. The pressure P_s represents uniform load transmitted by rock-mass to the support. For the compatibility of deformations at rock interface, radial displacements u_r in Figure 6-4b and Figure 6-4c must be equal.

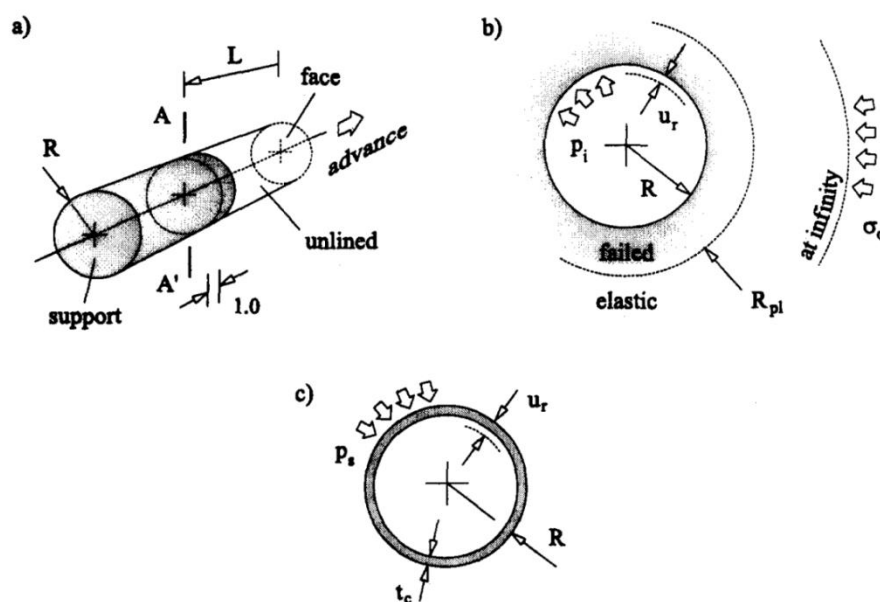


Figure 6-4: a) Cylindrical tunnel of radius R driven in the rock mass. b) Cross-section of the rock mass at the section A-A'. c) Cross-Section of the circular support installed at section A-A' (Carranza-Torres and Fairhurst, 2000).

Figure 6-5 shows the analogy to understand the basis of CCM in the sequences (a) to (c). Initially at the time t_0 , the support is installed at section A-A' at a distance L from face and ground has converged by the amount u_r^0 . It is assumed that, provided the face does not advance, rock mass transmits no load to the support $P_s^0 = 0$ at this stage. As the face advances more, ground and support deform together and support carries part of load that the face had been carrying. At time t , shown in figure 6.6b, the face reaches at a distance L_t from the support, the ground displaces by $u_r^t > u_r^0$ and the rock mass transmits the pressure P_s^t to the support. When the face has moved far enough from support, ground support system at section A-A' is in equilibrium and the support carries final load p_s^D . Finally, at time t_D , the effect of face has disappeared and the support and ground has converged together by u_r^D . From Figure 6-5, it could be realized that an analysis of the interaction of load-deformation characteristics of the system will be necessary to determine load transferred to the support. The system should consist of; the tunnel moving forward, the excavation section normal to tunnel axis and the installation of support at that section.

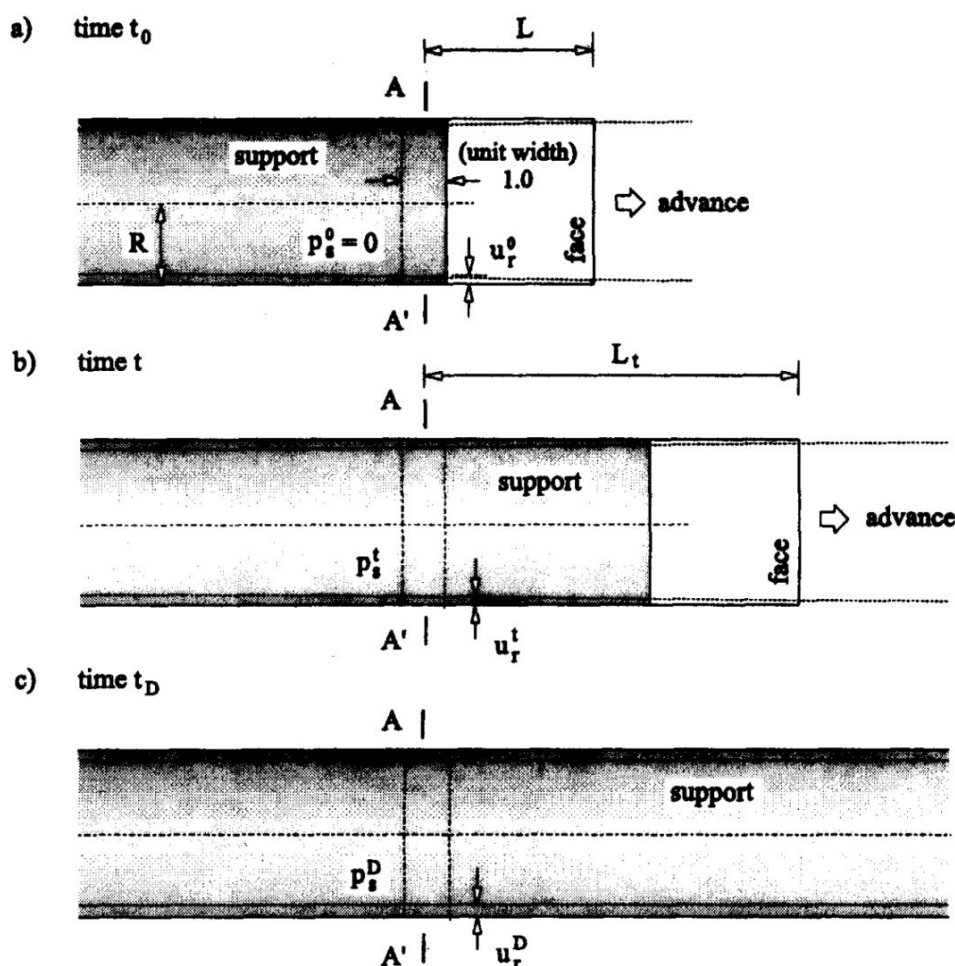


Figure 6-5: Loading of the support at section A-A' due to progressive advance of the tunnel face (Carranza-Torres and Fairhurst, 2000).

Based on the above explanations, Carranza-Torres and Fairhurst (2000) concluded that CCM has three basic components viz. the Longitudinal Displacement Profile (LDP), the Ground Reaction Curve (GRC) and the Support Characteristics Curve (SCC). The detail of these components is explained further in this chapter.

Longitudinal Displacement Profile (LDP)

LDP is the graphical representation of radial displacement that occurs along the axis of unsupported cylindrical excavation i.e. for the sections located ahead of and behind tunnel face. The upper diagram in Figure 6-6 represents the typical LDP. The diagram indicates that at some distance behind tunnel face the effect of face is negligibly small, so that beyond this distance the tunnel has converged by final value i.e. u_r^M . At some distance ahead of face, the tunnel excavation has no effect on the rock mass and the radial displacement is zero. Hence it provides insight into how quickly the support begins to interact with rock mass behind the face of tunnel.

The construction of LDP is very important task in CCM. According to Vlachopoulos and Diederichs (2009), in order to facilitate to construct the LDP, Panet (1995) derived the following equation based on plastic analysis;

$$u^* = \frac{u_R}{u_{max}} = \frac{1}{4} + \frac{3}{4} \left(1 - \left(\frac{3}{3+4X^*} \right)^2 \right) \tag{6-6}$$

Where; $X^* = X/R_T$; u_R is the radial displacement and u_{max} is the maximum short term radial displacement distant from face. This formula is used only to the positive value of the X i.e. behind the face.

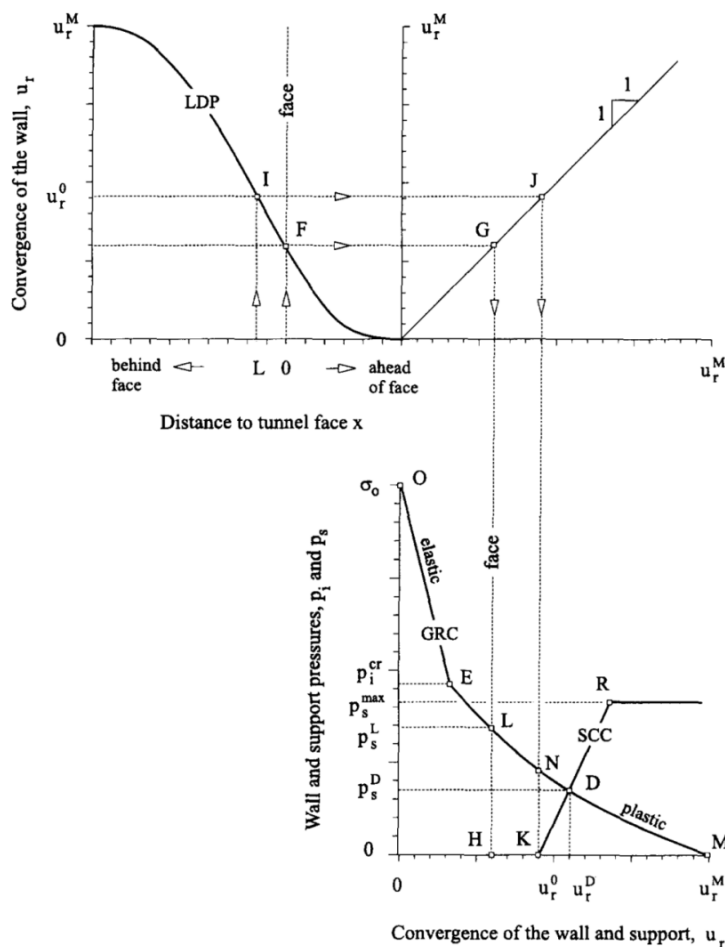


Figure 6-6: Schematic representation of Longitudinal Displacement Profile (LDP), Ground Reaction Curve (GRC) and Support Characteristics Curve (Carranza-Torres and Fairhurst, 2000)

Similarly, based on the measured value of the convergence in the vicinity of the face for the tunnel in Mingtam power cavern project by Chern et al. (1998), an empirical ‘best fit’ relationship to these actual measured data was proposed (Vlachopoulos and Diederichs, 2009);

$$u^* = \frac{u_R}{u_{max}} = \left(1 + e^{\left(\frac{-X^*}{1.1} \right)} \right)^{-1.7} \tag{6-7}$$

Both the relationship given above is reasonable for plastic analysis provided that the radius of plastic zone does not exceed 2 tunnel radii. However, there is the possibility of developing the plastic zone radius exceeding 2 tunnel radii. In order to account for the influence of increased overall yielding on the shape of the normalized LDP, the term normalized plastic

zone radius, $R^* = R_p/R_T$ (where, R_p is plastic zone radius and R_T is tunnel radius), is logical to use. Based on the analysis using Phase2 in plain strain cross section and axisymmetric models, Vlachopoulos and Diederichs (2009) proposed a new set of best fit relationships which are shown in following equations;

$$u_o^* = \frac{u_o}{u_{max}} = \frac{1}{3} e^{-0.15R^*} \quad 6-8$$

For $X^* \leq 0$ (in rock mass);

$$u^* = \frac{u}{u_{max}} = u_o^* \cdot e^{X^*} \quad 6-9$$

For $X^* \geq 0$ (in tunnel);

$$u^* = \frac{u}{u_{max}} = 1 - (1 - u_o^*) \cdot e^{-\frac{3X^*}{2R^*}} \quad 6-10$$

Where; $R^* = R_p/R_T$.

The relationships in the equations 6-8, 6-9 and 6-10 can be used to correlate the displacement to position to construct LDP. For 2D analysis, u_{max} and R_p need to be calculated prior to the sequenced analysis. The sequencing of the plain strain analysis can be accomplished through a core replacement technique (Vlachopoulos and Diederichs, 2009).

Ground Reaction Curve (GRC)

GRC is the relationship between decreasing internal pressure p_i and increasing radial displacement of tunnel wall u_r . The relationship depends upon mechanical properties of rock mass and can be obtained from the elasto-plastic solution of rock deformation around an excavation (Carranza-Torres and Fairhurst, 2000). The curve OEM in Figure 6-6 is the typical diagram of GRC.

According to Carranza-Torres and Fairhurst (2000), the uniform internal pressure p_i and far field stress σ_o can be scaled to give the scaled internal pressure P_i and scaled far field stress S_o respectively. Assuming that the rock mass satisfies Hoek-Brown failure criteria, P_i and S_i will be;

$$P_i = \frac{p_i}{m_b \sigma_{ci}} + \frac{s}{m_b^2} \quad 6-11$$

$$S_o = \frac{\sigma_o}{m_b \sigma_{ci}} + \frac{s}{m_b^2} \quad 6-12$$

Where the parameters σ_{ci} , m_i , s , a and m_b are explained in chapter 2 in Hoek-Brown failure criteria.

The point E in GRC of Figure 6-6 is the transition from elastic to plastic behavior of rock mass and corresponding pressure is the critical internal pressure, p_i^{cf} . For $p_i \geq p_i^{cf}$, the rock mass remains elastic and for $p_i < p_i^{cf}$, a plastic region of radius R_{pi} develops around the tunnel.

The scaled critical internal pressure, p_i^{cr} , is given by;

$$P_i^{cr} = \frac{1}{16} [1 - \sqrt{1 + 16S_o}]^2 \quad 6-13$$

and actual critical pressure is;

$$p_i^{cr} = \left[P_i^{cr} - \frac{s}{m_b^2} \right] m_b \sigma_{ci} \quad 6-14$$

In case of $p_i \geq p_i^{cr}$, the relationship between radial displacement u_r^{el} and internal pressure p_i elastic part of GRC is given by;

$$u_r^{el} = \frac{\sigma_o - p_i}{2G_{rm}} R \quad 6-15$$

Where G_{rm} is shear modulus of rock mass defined by the following equation;

$$G_{rm} = \frac{E_{rm}}{2(1+\nu)} \quad 6-16$$

Where, E_{rm} and ν are elastic modulus and Poisson's ratio of the rock mass which are defined in chapter 2.

For the case $p_i < p_i^{cr}$, the extent of plastic region R_{pl} that develops around the tunnel is given by;

$$R_{pl} = R \times e \left[2 \left(\sqrt{P_i^{cr}} - \sqrt{p_i} \right) \right] \quad 6-17$$

Where, R is the radius of tunnel.

Carranza-Torres and Fairhurst (2000) explained that a flow rule for the material is necessary to define the plastic part of GRC. Flow rule defines the relationship between strains that produce distortion and those that produce volumetric changes as the plastic deformation occurs in the material. The flow rule will be characterized by the dilation coefficient K_Ψ , which is computed from the dilation angle, Ψ , using the relation; $K_\Psi = (1 + \sin\Psi) / (1 - \sin\Psi)$. Where, the value of Ψ is one third of the internal friction angle, ϕ of the rock mass.

Hence the plastic part of the GRC is defined by the following expression;

$$\frac{u_r^{pl}}{R} \frac{2G_{rm}}{\sigma_o - p_i^{cr}} = \frac{K_\Psi - 1}{K_\Psi + 1} + \frac{2}{K_\Psi + 1} \left(\frac{R_{pl}}{R} \right)^{K_\Psi + 1} + \frac{1 - 2\nu}{4(S_o - P_i^{cr})} \left[\ln \left(\frac{R_{pl}}{R} \right) \right]^2 - \left[\frac{1 - 2\nu}{K_\Psi + 1} \frac{\sqrt{P_i^{cr}}}{S_o - P_i^{cr}} + \frac{1 - \nu}{2} \frac{K_\Psi - 1}{(K_\Psi + 1)^2} \frac{1}{S_o - P_i^{cr}} \right] \times \left[(K_\Psi + 1) \ln \left(\frac{R_{pl}}{R} \right) - \left(\frac{R_{pl}}{R} \right)^{K_\Psi + 1} + 1 \right] \quad 6-18$$

The equations 6-11 to 6-18 can be used to construct the GRC in elastic as well as plastic behavior of the rock mass.

Support Characteristics Curve (SCC)

SCC is defined as the relationship between increasing pressure p_i on the support and increasing radial displacement u_r of the support. It can be constructed from the elastic relationship between applied pressure and resulting displacement for the section of support of unit length in the direction of tunnel. The applied stress p_s can be expressed in terms of elastic stiffness of the support K_s and resulting closure u_r in the following way;

$$p_s = K_s u_r \quad 6-19$$

The plastic part of the SCC i.e. horizontal segment starting at point R in Figure 6-6, is defined by the maximum pressure p_s^{\max} that the support can accept before collapse. For different support system such as; concrete or shotcrete linings, ungrouted bolts and cables, steel ribs, lattice girders etc, the main task is to find the maximum pressure and elastic stiffness for the construction of SCC.

a. Concrete or Shotcrete Linings

The maximum pressure provided by the support in case of closed ring concrete or shotcrete is given by (Carranza-Torres and Fairhurst, 2000);

$$p_s^{\max} = \frac{\sigma_{cc}}{2} \left[1 - \frac{(R-t_c)^2}{R^2} \right] \quad 6-20$$

And the elastic stiffness is given by;

$$K_s = \frac{E_c}{(1-\nu_c)R} \frac{R^2 - (R-t_c)^2}{(1-2\nu_c)R^2 + (R-t_c)^2} \quad 6-21$$

Where,

σ_{cc} is the unconfined compressive strength of the shotcrete or concrete [MPa];

E_c is young's modulus for the concrete or shotcrete [MPa];

ν_c is Poisson's ratio for shotcrete or concrete;

t_c is the thickness of the ring [m];

R is the external radius of the support equal to that of tunnel [m].

b. UngROUTED bolts and cables

The Figure 6-7 shows the mechanically anchored bolts installed in the rock-mass surrounding a tunnel of radius R . The maximum pressure provided by the support system, assuming that the bolts are equally space in the circumferential direction, is given by;

$$p_s^{\max} = \frac{T_{bf}}{s_c s_l} \quad 6-22$$

And the stiffness is;

$$\frac{1}{K_s} = s_c s_l \left[\frac{4l}{\pi d_b^2 E_s} + Q \right] \quad 6-23$$

Where,

d_b is the bolt or cable diameter [m]

l is the free length of cable or bolt [m]

T_{bf} is the ultimate load obtained from a pull-out test [MN]

Q is a deformation load constant for the anchor and head [m/MN]

E_s is Young's modulus of bolt or cable [MPa]

s_c is the circumferential bolt spacing [m]

s_l is the longitudinal bolt spacing [m]

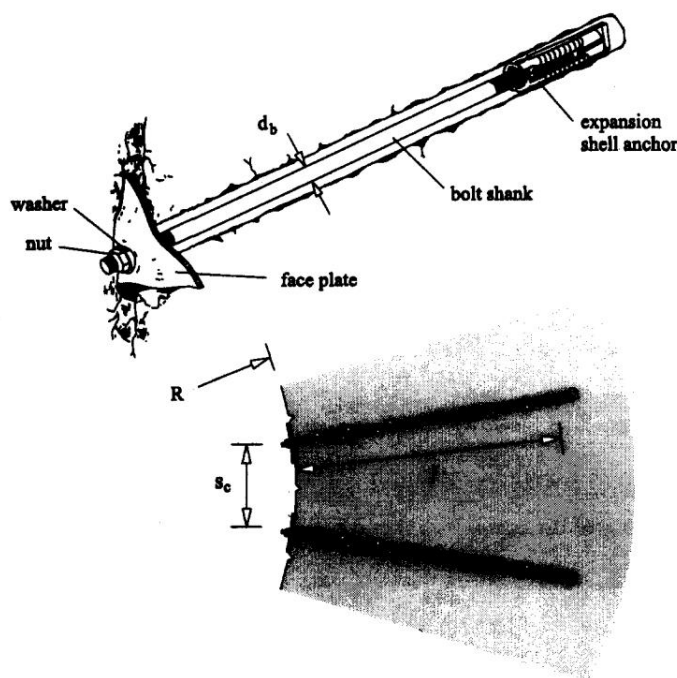


Figure 6-7: Representation of an ungrouted mechanical-anchored bolt (Carranza-Torres and Fairhurst, 2000)

c. Steel set support

The maximum support pressure of the set is (Hoek, 's Corner)

$$p_s^{max} = \frac{A_s \sigma_{ys}}{s_l R} \quad 6-24$$

And the stiffness is;

$$K_s = \frac{E_s A_s}{s_l R^2} \quad 6-25$$

Where

σ_{ys} is the yield strength of the steel [MPa]

E_s is the young's modulus of the steel [MPa]

A_s is the cross sectional area of the section[m²]

s_l is the set spacing along the tunnel axis[m]

R is the radius of the tunnel [m]

d. Lattice Girder Support

As shown in Figure 6-8, the curve number 8 and 9 are for 3 and 4 bar lattice girders respectively. The maximum pressure for these support types can be found from the diagram.

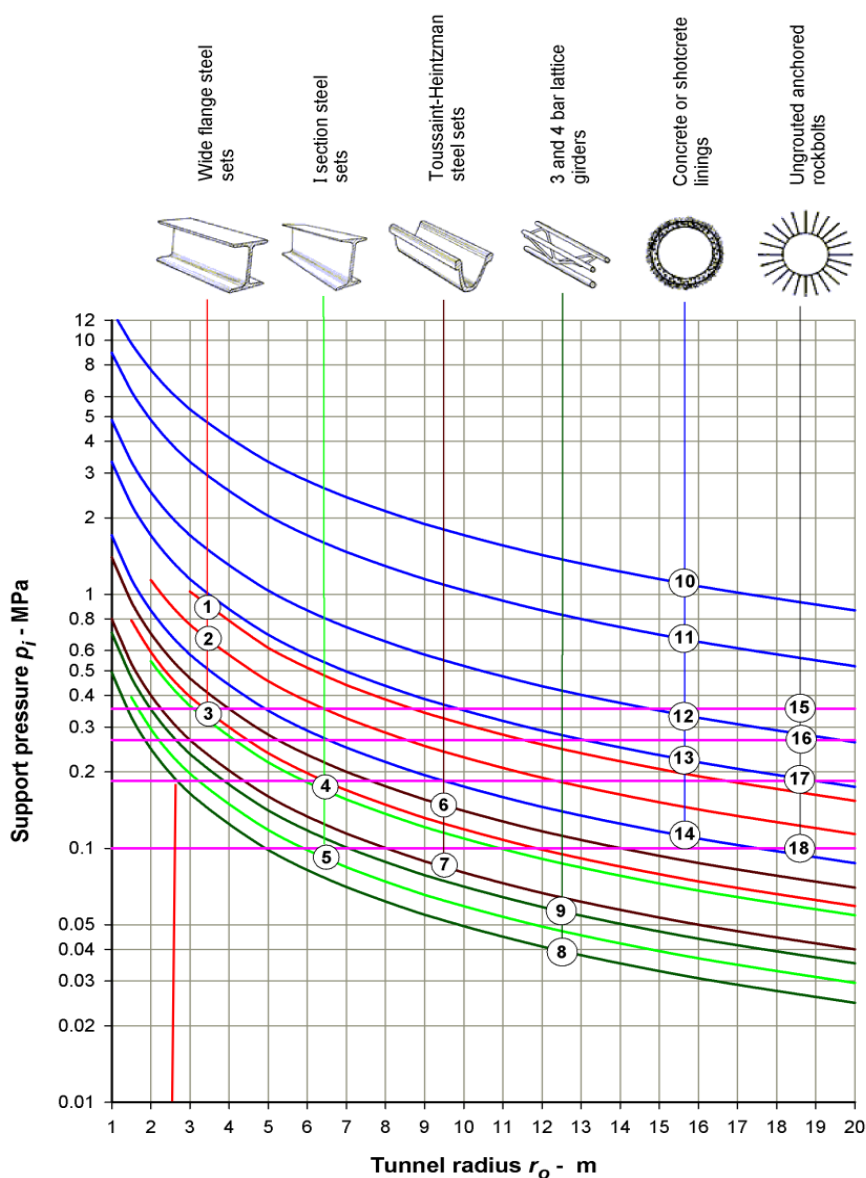


Figure 6-8: Maximum Support pressure versus tunnel radius for the different types of support (Hoek, Corner)

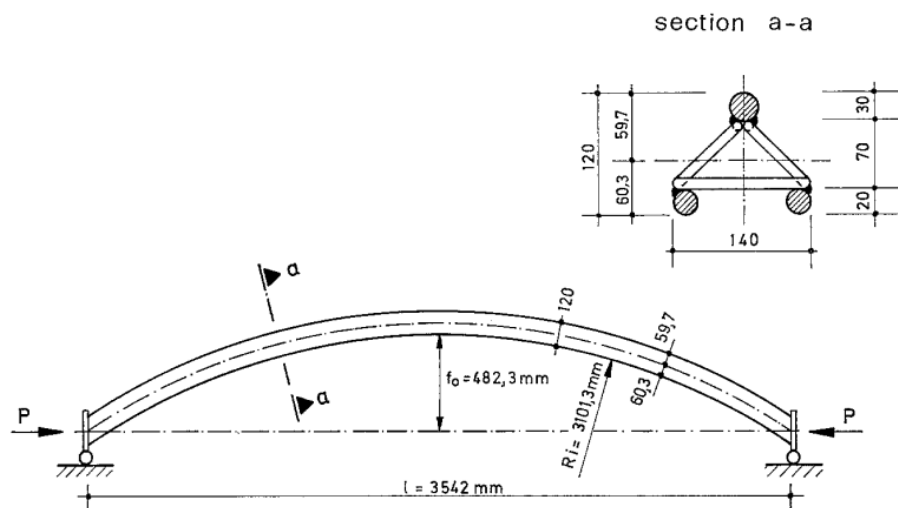


Figure 6-9: Loading test on lattice girder (Baumann and Betzle, 1984)

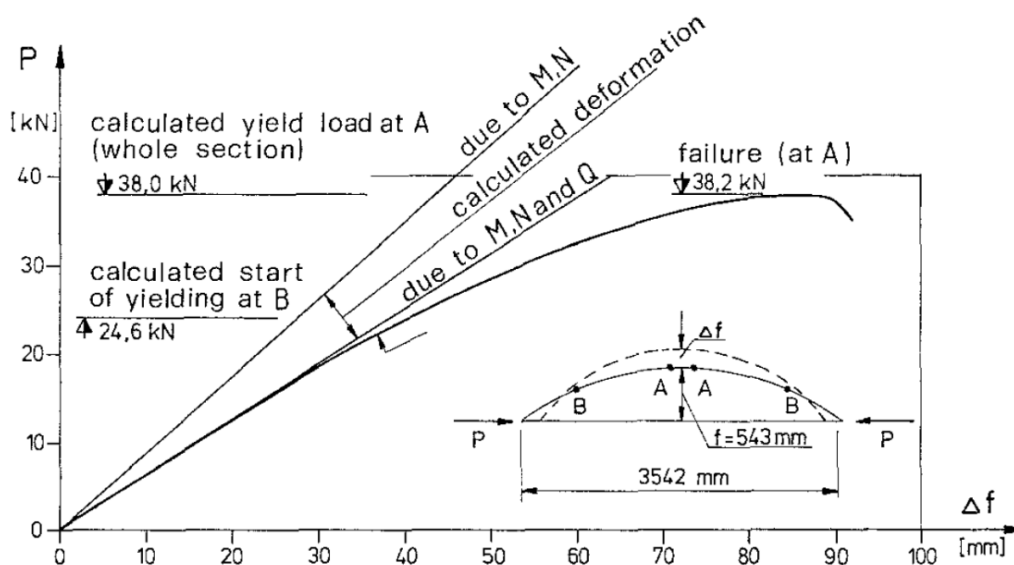


Figure 6-10: Measured and computed load-deformation deformation for the test girder (Baumann and Betzle, 1984)

Figure 6-9 shows the arrangement of loading test on the typical 3 bar lattice girder (Baumann and Betzle, 1984). The girder failed at a load of 38.2 kN by buckling of a lower chord shortly before the yield limit was reached. Altogether a maximum deformation of 83 mm was obtained as the girder reached failure. The yielding of girder starts at B when the load is 24.6kN and deformation is 40 mm. In case of 3 bar lattice girder, the maximum support pressure can be found from Figure 6-8 and the SCC can be constructed taking the deformation equal to 40 mm at yielding (Figure 6-10).

e. Combined effect of support system

In case there are more than one support is installed in the same location, their combined effect can be determined by adding the stiffness of the supports. For example, if two supports having the elastic stiffness K_{s1} and K_{s2} and maximum pressures p_{s1}^{\max} and p_{s2}^{\max} respectively are installed in the same location, their combined stiffness can be computed as $K_s^{eq} = K_{s1} +$

K_{s2} . The maximum possible elastic deformations for the two support systems are u_{r1}^{\max} and u_{r2}^{\max} respectively. The combined support system is assumed to fail at the point where one of the two supports achieves its maximum deformation i.e. the support with smallest deformation value. Hence the support with the lowest maximum deformation value, u_r^{\max} determines the maximum support pressure available for the supports acting together which can be calculated using equation 6-19.

6.4.2 Limitations of CCM

The CCM is based on two assumptions; first, the state of stress is often referred to as uniform or hydrostatic with constant magnitude and second, the tunnel cross section is circular (Carranza-Torres and Fairhurst, 2000). But in most of the cases, the far field stresses are unequal and tunnel cross section is non-circular. In these cases too, CCM can be used with some special assumptions that are described further in this section.

The measured values of vertical stresses σ_z as a function of depth z for different regions of the world can be expressed by the best fit relationship which is shown in Figure 3-1(left) is;

$$\sigma_z = 0.027 z \quad 6-26$$

Where, σ_z is expressed in MPa and z in meters. In this relationship, if the stress is assumed to be associated with the weight of overburden material, the factor 0.027 ought to be the density of rock mass in MN/m^3 . This value corresponds to the unit weight of silicates, a major components of many rocks (Carranza-Torres and Fairhurst, 2000).

The value of k as defined in section 3.2.1 can be expressed as;

$$k = \frac{\sigma_x}{\sigma_z} \quad 6-27$$

Where, σ_x is the mean horizontal stress in MPa. The Figure 3-1(right) indicates that the value of k varies from minimum of 0.5 to maximum of 3.5. This condition suggests that the principal stresses at the site are often unequal. In such cases, the average of two stresses can be taken as input to CCM as uniform far field stress i.e.;

$$\sigma_o = \frac{\sigma_x + \sigma_z}{2} \quad 6-28$$

The uniform state of stress assumed by the CCM can be expressed as $\sigma_o = \sigma_x = \sigma_z$ and $k = 1$.

The result obtained from CCM in case of non-uniform stress field can be verified with respect to the term limiting stress ratio, k_{lim} . If normal stress ratio, k is less than k_{lim} , the mean radius of plastic region around tunnel and the mean convergence at the crown and sidewall of the tunnel are same as the corresponding values obtained from CCM using the relationship in equation 6-27. If $k > k_{lim}$, there is no apparent relationship to the case of uniform loading (Carranza-Torres and Fairhurst, 2000). These situations are illustrated in Figure 6-11.

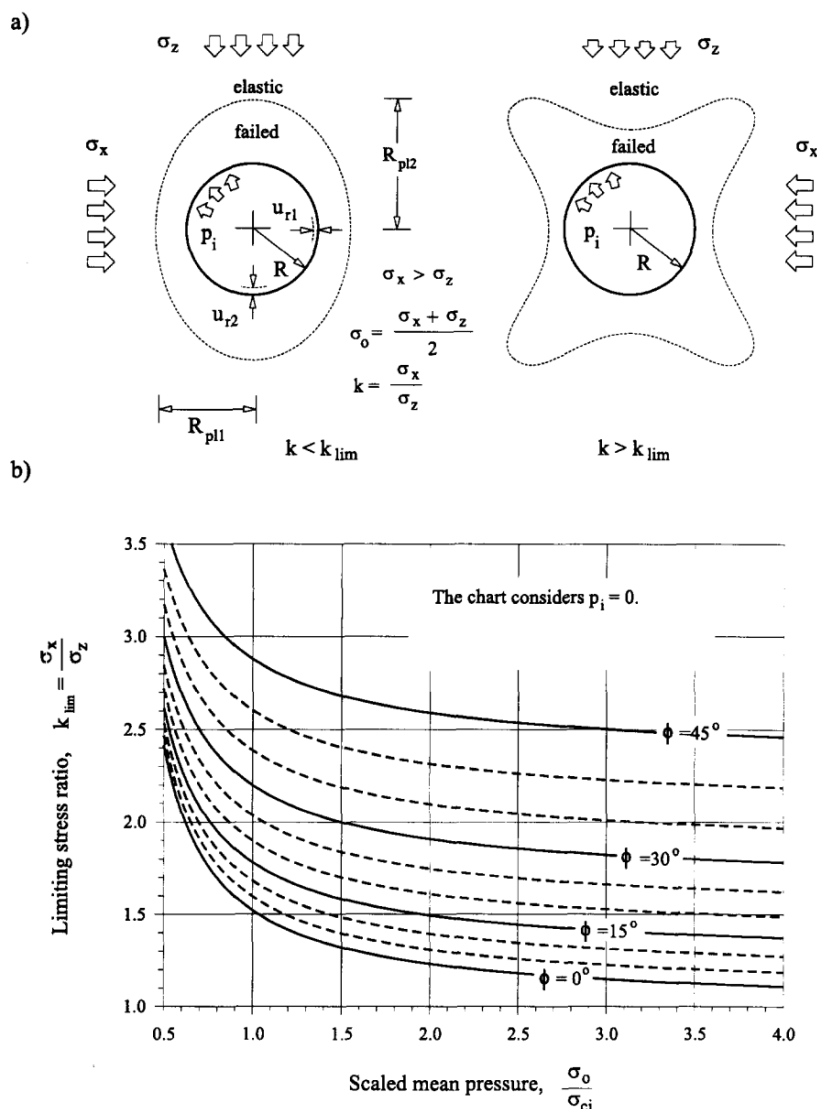


Figure 6-11: a) circular cavity in a Mohr-coulomb material subject to uniform internal pressure and unequal far field stress. b) limiting values of stress ratio k_{lim} as a function of scaled mean stress σ_o/σ_{ci} and friction angle ϕ (Carranza-Torres and Fairhurst, 2000).

For the case in which the cross section area of the tunnel is not circular, CCM can still be used to provide the first estimate of extent of failure zone and resulting convergence of wall. In such a case, the shape of the tunnel can be considered as circular with the radius equal to the average value of minimum and maximum dimension of the section. Carranza-Torres and Fairhurst (2000) described that the mean extent of failure zone and mean convergence of wall for the non-circular tunnel are comparable to the values that are obtained from CCM with equivalent circular section.

6.5 NUMERICAL ANALYSIS

6.5.1 General

Although the numerical modeling cannot be used directly to analyze the squeezing phenomenon in the tunnels, its application can be utilized to find the deformation of the

tunnel in squeezing environment and the results can be compared with the results that have been found from analytical, semi-analytical and empirical approaches. In an analytical approach, the rock mass is assumed to be simple homogeneous material and its use is limited to simple geometry of the underground excavations. Similarly, the empirical analyses are based on the practical aspects, measurements and experiences and have limited use. But in reality, every ground condition is unique and should be defined separately that means the rock mass has complexity in nature. In such cases, the numerical analysis will help to define the complex nature of the rock mass and geometry of opening and results from which can be found as close to the reality. The advantages of numerical analysis over the other analysis are;

- it is quantitative analysis,
- it provides better understanding of mechanism,
- it can be used to verify the results obtained from other methods,
- it provides the extension of measurement results from field and laboratory, etc.

Numerical modeling means discretization of rock mass into a large number of individual elements and powerful computers are used to handle such a huge amount of data. In rock engineering, the numerical analyses are used mainly to analyze the rock stresses and deformations (Nilsen and Palmström, 2000). There are two categories of numerical models;

a. Continuous models

Rock mass is modeled as a basically continuous medium, only a limited number of discontinuities (joints, faults etc) may be included here. This is the most commonly used category of numerical models. The methods belonging to this category are; Finite Element Method (FEM), Boundary Element Method (BEM) and Finite Difference Method (FDM). The most common programs of this category are; ABAQUS, ANSYS, BESOL, PHASE2, FLAC3D etc.

b. Discontinuous models

Rock mass is modeled as system of individual blocks interacting along their boundaries. These models represent the nature of the rock mass more close to the reality. The methods belonging to this category are referred to as the Distinct Element Method (DEM), Discontinuous Displacement Analysis (DDA). The most common program of this category is UDEC.

6.5.2 Selection of the computer program

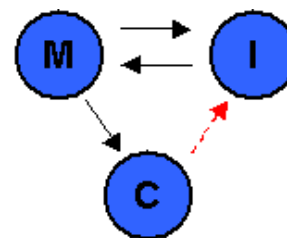
The main objective the numerical analysis in this thesis is to analyze the model to determine the deformation of rock mass around tunnel in weak rock mass condition where the squeezing phenomenon has already been occurred. Another objective is the back calculation of the rock mass parameters on the basis of the measured deformation. Among the different computer programs, the Finite Element Method, Phase² has been selected for the squeezing and support analysis. The background of the selection of this program is explained further in this chapter.

6.5.3 The Phase² Program

The Phase² is a 2-dimensional windows based program and is very popular for the analysis of underground/surface excavation in rock mass or soil. The program code is used for a wide range of geotechnical engineering projects including complex tunneling problems in weak rock, stress analysis, tunnel design, slope stability, support design and groundwater seepage analysis etc. Complex multi staged models can easily be created and analyzed quickly. This program is user friendly, easy to operate and easy to understand. Some of the basic features in Phase2 program are listed below;

- Elasto-Plastic Analysis,
- Constant or gravity field stress,
- Staged model,
- Plain strain or Axisymmetric analysis,
- Support analysis (Bolts, concrete or shotcrete liners, steel sets, lattice girders etc),
- Multiple material,
- Load splitting,
- Core replacement technique,
- Slope stability analysis,
- Ground water seepage analysis etc.

There are three basic components of the program i.e. model, compute and interpret. Model is the pre-processing module used for entering and editing the model boundaries, support, in-situ stresses, boundary conditions, material properties, and creating the finite element mesh. Model, compute and Interpret will each run as standalone programs. They also interact with each other as illustrated in the schematic diagram as shown on the right side.



- Compute and interpret can both be started from within model.
- Compute must be run on a file before results can be analyzed with interpret (red arrow).
- Model can be started from interpret.

6.5.4 Input parameters for Phase²

In phase², field stress can be constant or gravity stress. The gravity field stress option is used to define a gravity stress field which varies linearly with depth from a user-specified ground surface elevation. Gravity field stress is typically used for surface or near surface at shallow depth elevations and the areas where there is the effect of topography in the stress magnitudes and directions. Stress ratio is calculated with the help of Poisson's ratio. The locked in stress is also calculated from the tectonic stress as in plane and out of plane locked in stresses.

In addition, the material parameters such as unconfined compressive strength of intact rock (σ_{ci}), Hoek-Brown constant (m_i), Geological strength index (GSI), Young's Modulus of intact rock (E_i), Poisson's ratio (ν), density of the rock mass (γ) of the rock mass are the inputs to

Phase² as material properties. Similarly, the input parameter for different types of support will be discussed in chapter 7.

6.5.5 Interpretation of the results

The principle stresses can be displayed and see the result. The stress level could be checked in particular location of the analysis. The major and minor principle stress and angle between stresses with horizontal can be used to calculate the vertical and horizontal stress at that point and the result can be compared with the gravity stress and tectonic stress.

The strength factor of the rock mass around the tunnel can be displayed with contours. With the elastic analysis if the strength factor is greater than 1 everywhere around the tunnel, the result will be the same even if the plastic analysis has been done. Hence there is necessity of plastic analysis if the strength factor is less than one around the tunnel with elastic analysis.

The value of vertical, horizontal, total displacement can be displayed with the contour around the tunnel. The value can be compared with the result obtained from analytical, semi-analytical method and also with the measured convergence.

6.5.6 3D tunnel simulation using the core replacement technique in Phase2

This features of Phase2 is used to simulate the three dimensional excavation of a tunnel. In three dimensions, the tunnel face provides support. As the tunnel advances, the face effect will be reduced eventually and the support will receive more pressure from the ground that was taken by face initially. This procedure can be used to determine the amount of deformation prior to support installation. The point of support installation has been found by the comparison of displacement in LDP and GRC.

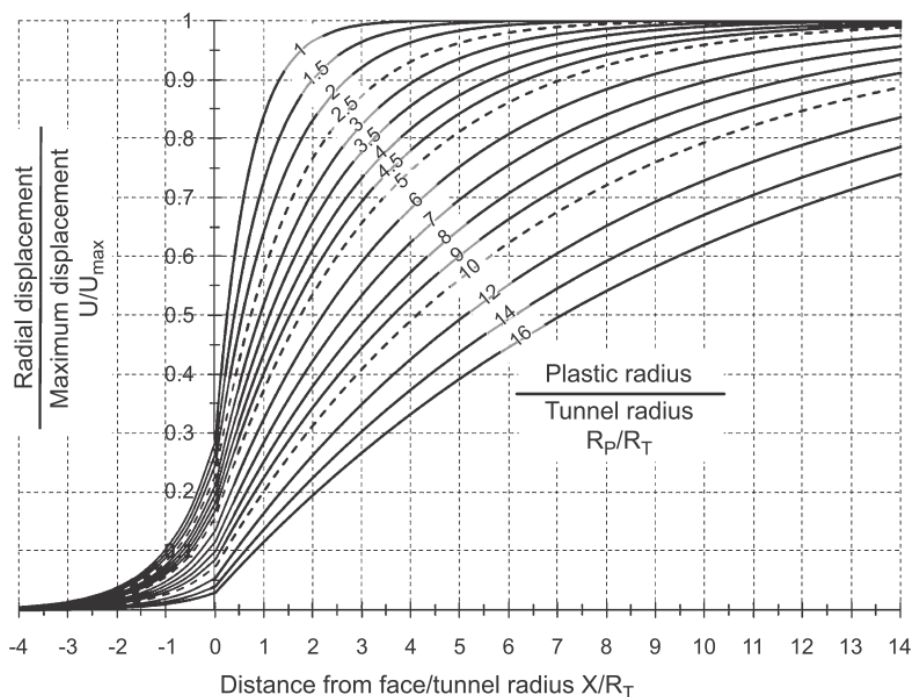


Figure 6-12: LDP templates to be used as an alternative to equations 6-8, 6-9, 6-10 (Vlachopoulos and Diederichs, 2009)

To use the graph given in Figure 6-12, two pieces of information from the finite-element analysis are necessary i.e. the maximum tunnel wall deformation, u_{\max} , far from the tunnel face and radius of plastic zone far from the tunnel face. Both of these values can be computed from a plane strain analysis with zero internal pressure inside the excavation. Then the displacement of wall at the point of support application can be found using Figure 6-12.

The next step is to determine the core modulus that yields a displacement equal to that at the point of support application. It is important to maintain the same location as is used to determine u_{\max} , since the location of maximum displacement can change depending on the magnitude of the internal pressure. This can be seen in this model as larger core moduli produce larger displacement in the sidewall while smaller core moduli produce larger displacements in the roof and floor. To determine the internal pressure that yields displacement equal to that at the point of support application, the displacement versus stage for a point on the tunnel under consideration of the excavation will be plotted.

6.6 CONCLUDING REMARKS ON THE SQUEEZING ANALYSIS TECHNIQUES

Using the semi-analytical and empirical methods, the extent of squeezing phenomenon can be found primarily. Although the analytical and numerical approaches cannot be used directly to analyze the squeezing phenomenon, more detail analysis can be done indirectly using these methods. Singh et al (1992) method gives the condition of ground whether there will be squeezing or not but it does not give the amount of tunnel wall deformation and support pressure. The difficulty in this method is the estimation of correct value of SRF (one of the term in Q) in some cases. The selection of SRF value is very sensitive for the correct estimation of Q -value.

Hoek and Merinos (2000) method gives the amount of tunnel wall deformation and also considers the support pressure. But it does not consider the tunnel wall deformation at the time of support application and also does not specify the yielding of support. It considers the vertical stress due to gravity but does not consider the effect of topography and tectonic stress. However, it can be used to get the useful information at the beginning of analysis. It also gives the grade of squeezing phenomenon in terms of tunnel closure percentage.

The analytical method, CCM, is quite useful method to find the tunnel wall deformation and support pressure required to maintain the deformation within the specified limit. The deformation of the tunnel wall at the time of support application can be calculated with the help of LDP. It gives the information regarding the yielding of different types of supports with factor of safety. The limitations of CCM are discussed in section 6.4.2.

Although the numerical modeling cannot be used directly to analyze the squeezing phenomenon in the tunnels, its application can be utilized to find the deformation of the tunnel in squeezing environment and the results can be compared with the results that have been found from analytical, semi-analytical and empirical approaches. The numerical analysis will help to define the complex nature of the rock mass and geometry of opening and results from which can be found as close to the reality.

7 SQUEEZING ANALYSIS

7.1 GENERAL

Tunnel squeezing is one of the major problems in Chameliya Hydroelectric Project. The deformation of tunnel was measured at different time at the tunnel sections where there is squeezing problem. The measured data quality is not good and the data are very random. In this thesis, latest data have been used as measured deformation and compared with the result obtained from different method of squeezing analysis. Regarding rock mass parameters, no tests were performed during the study period and even at the time of excavation. Q-value was estimated at the face of tunnel during face mapping, and rock types and support types were also mentioned. Other parameters such as unconfined compressive strength of the intact rock, young's modulus of intact rock, density of the rock, Poisson's ratio etc were not tested but they are mentioned in feasibility report of CHEP. Hence in this thesis, these parameters have been estimated using the information from different literatures, feasibility reports, and the tested data of similar type of rock mass. In addition to this, some of them are estimated from discussion with Supervisor.

Using the information from chapter 6, following methods and approaches have been used for the analysis of squeezing phenomenon in the headrace tunnel of CHEP such as empirical method; Singh et al (1992) and Q-system, semi-analytical method; Hoek and Marinos (2000) approach, analytical method; Carranza-Torres and Fairhurst (2000) approach using Hoek and Brown criteria and numerical analysis: Phase2 model. There are more than one approaches available for each method. In this thesis, at least one approach from each method has been used. The methodology and the equations that are used for each approach are followed from chapter 6. A number of sections have been selected for the analysis along the headrace tunnel based on the information available such as rock mass parameters. In each selected sections, squeezing has been predicted first using Singh et al (1992), Q-system and Hoek and Marinos (2000) approaches. The more detail study has been performed in the sections where there is high degree of squeezing and significant amount of measured deformation.

The main challenge in squeezing analysis will be to estimate the correct value of rock mass parameters. In this thesis, initially the parameters are estimated based on the information from different literatures. Limited tests have been done for very few types of rock from Nepal Himalaya. It is difficult to estimate the rock mass parameters based on these data. So, the information from other countries with similar rock types and condition has also been taken as basis. After defining the initial input parameters, Hoek and Marinos (2000) approach has been used to calculate the deformation of tunnel wall and the results have been compared with measured deformation. Because of significant discrepancy in results, unconfined compressive strength of intact rock has been back calculated from measured deformation using the same approach. Then, Phase² analysis for the selected four sections of tunnel has been performed using back calculated strength as input. Deformation values obtained from Phase2 analysis has been compared with measured values and significant discrepancy in values has been found. Hence, Phase2 program was rerun for several times by changing rock

mass parameters until the difference is within permissible limit. The rock mass parameters that gave best result have been considered as more correct values. The procedure that has been used for refining the rock mass parameters is outlined in the form of flowchart (Figure 7-1).

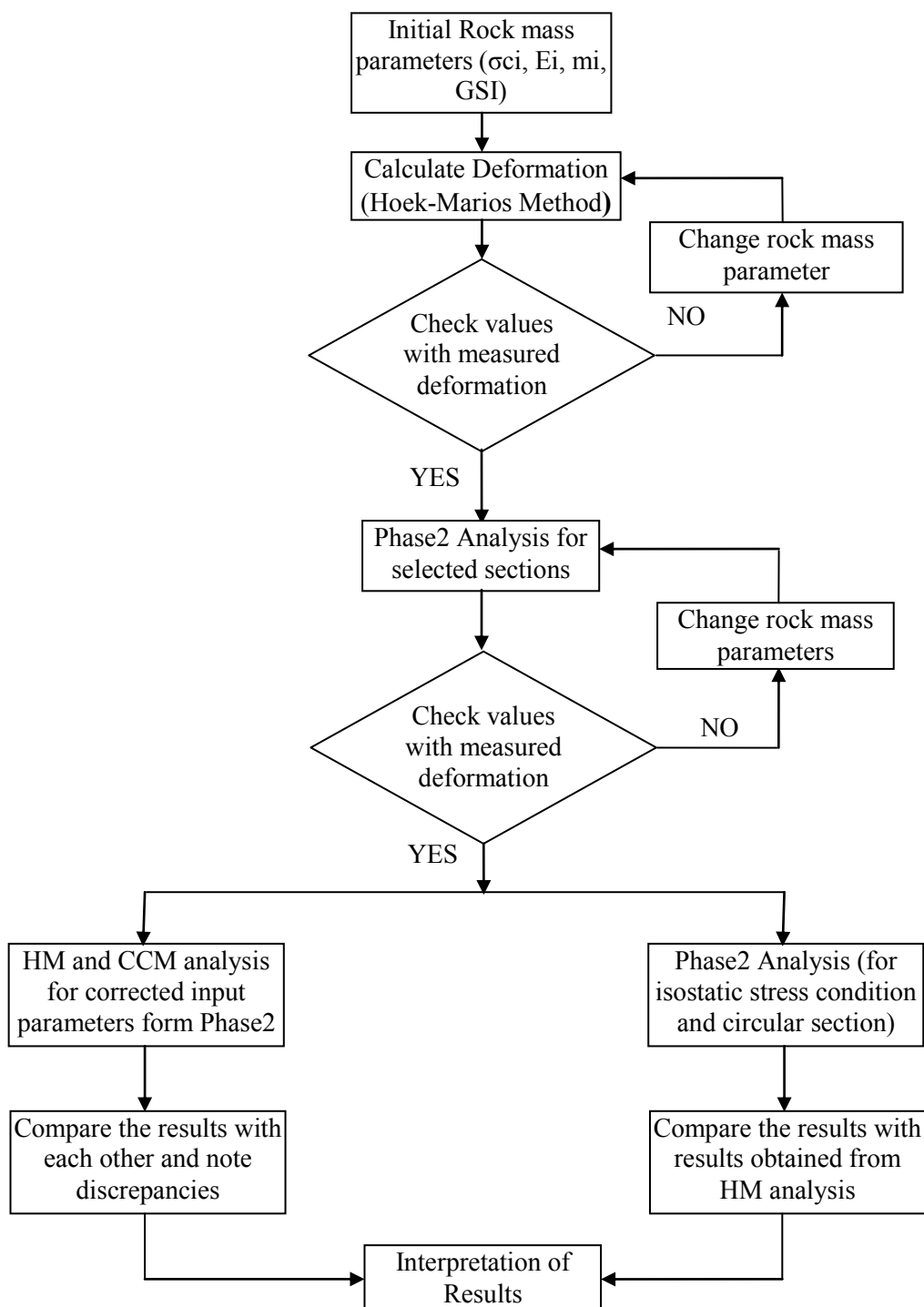


Figure 7-1: Flowchart of the methodology applied for the estimation of more accurate rock mass parameters. (Note: HM is Hoek and Marions (2000) and CCM is Convergence Confinement Method)

Furthermore, Hoek and Marinos (2000) and CCM approaches have been used to calculate the deformation using corrected input parameter. The results have been compared with that obtained from Phase2 and also with the measured value. Again, Phase2 program has been used to find the deformation considering the isostatic stress condition and circular section of tunnel. The results have been compared with the initial results obtained from Hoek and Marinos (2000) approach.

7.2 INPUT DATA COLLECTION

Inputs to each methods and approaches are rock mass parameters. Main sources of input data are; feasibility reports, information from project site, literatures related to similar rock mass condition and case histories etc. The data has been collected accordingly.

7.2.1 Data collection from field

A short field visit was conducted from 21th June 2012 to 2nd July 2012 to the project site of Chameliya Hydroelectric Project, Darchula District, Nepal. Tunnel logs, convergence measurement data and photographs were collected from field. Feasibility reports, related drawings and other project related reports were collected from main office located in Kathmandu, the capital city of Nepal.

Tunnel logs

Tunnel log of each tunnel face was recorded just after each excavation and mucking. The log includes graphical representation of geological structures, rock types, weathering condition and attitudes. It also includes estimated value of Q-value and required rock support type. A typical tunnel log sheet is given in Figure 7-2 at tunnel face at chainage 3+404m.

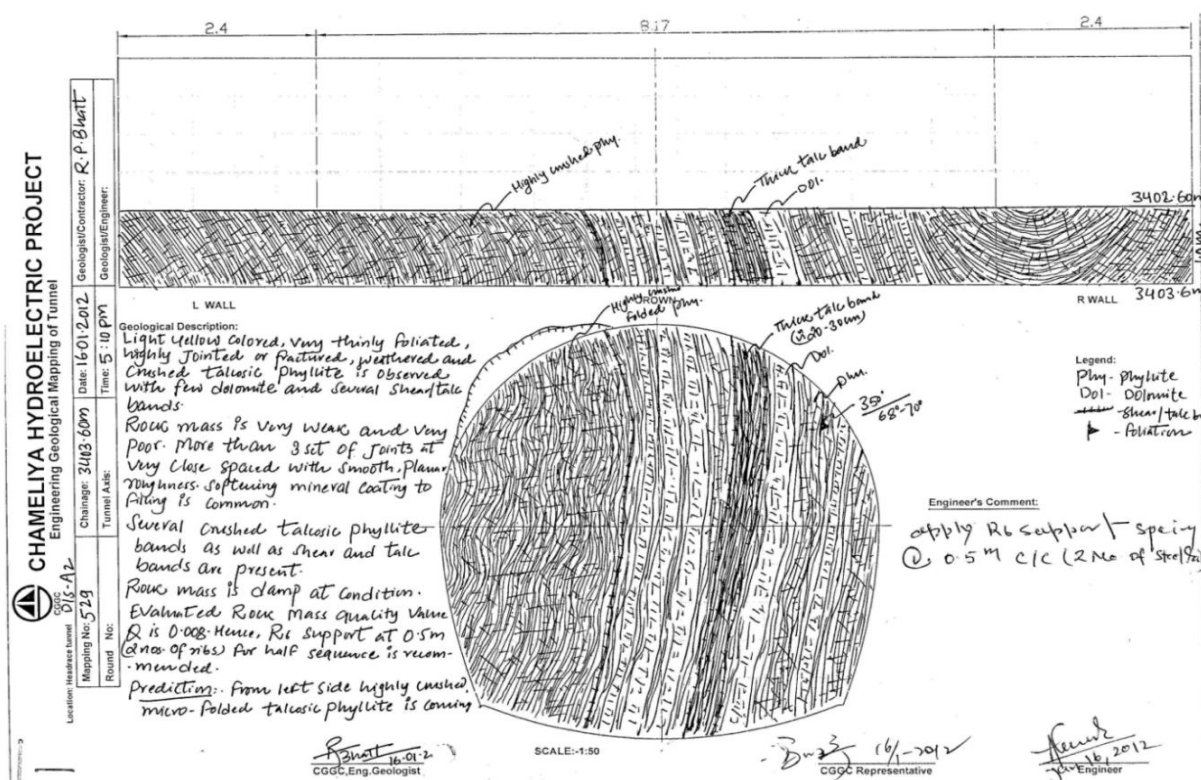


Figure 7-2: A typical tunnel log of CHEP headrace tunnel at chainage 3+404

The squeezing related data are extracted from the tunnel logs of seventeen tunnel sections. The tunnel sections for the squeezing analysis were selected based on rock types and availability of tunnel logs at that particular section. The extracted data are presented further in this chapter (Table 7-1). The Q-value is further converted into RMR and GSI values using formula given by Barton (1995) and Hoek and Diederichs (2006) respectively (equation 2-10 and 2-11).

Convergence measurements

Total length of headrace tunnel is 4067m. Squeezing problem has been noticed in the tunnel section from chainages 3+100 to about 3+940. CHEP project carried out convergence measurement for these sections only. The project measured the deformation at different time from 2011 to 2012 using total station and plotted the sections with measured values. In this thesis, the convergence at wall has been found by measuring the displacement of wall with respect to original section of tunnel (Figure 7-3). The project has not used any extensometers for the measurement.

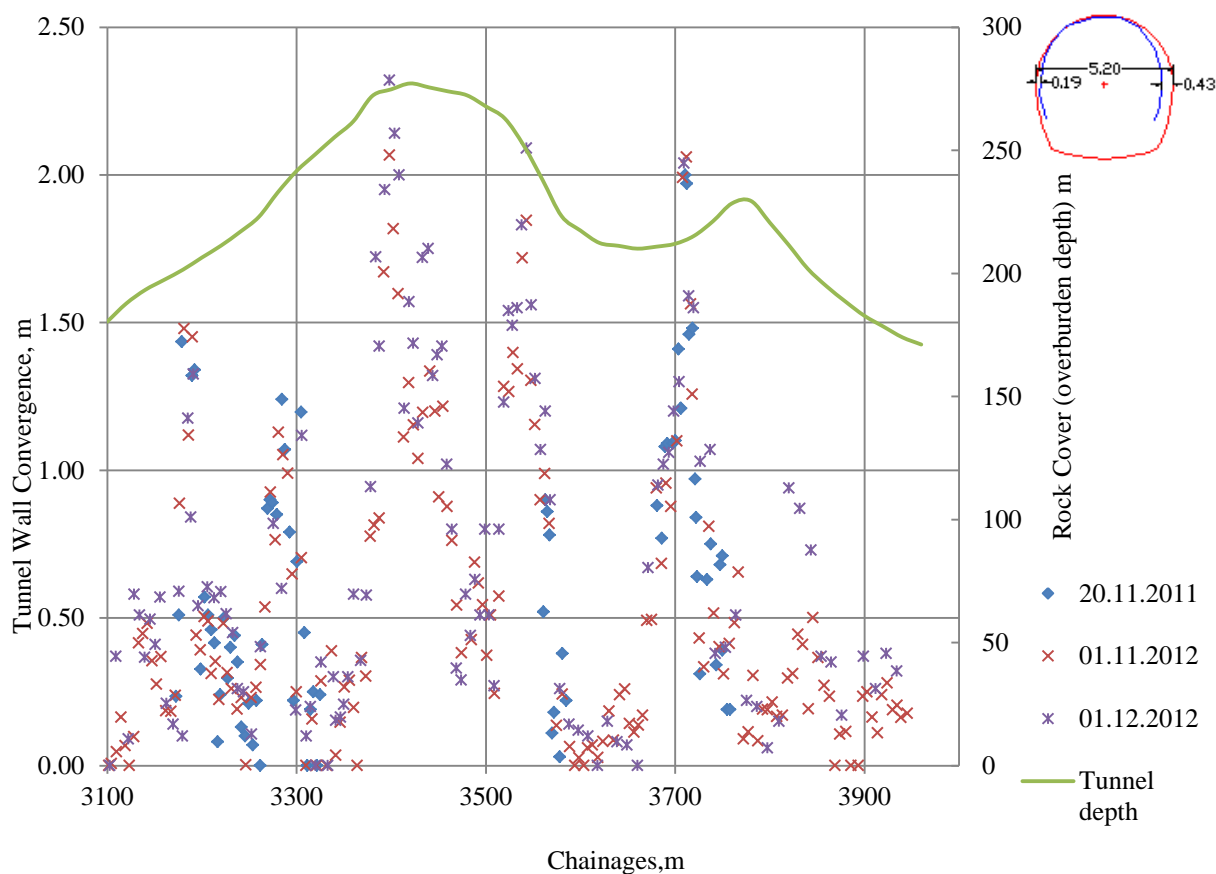


Figure 7-3: Convergence measurement data in headrace tunnel of CHEP at different time and typical tunnel section for the extraction of convergence data (right top corner of figure).

The maximum convergence has been recorded as 2.32m in 3+398m chainage. For the selected sections, latest data has been used. The list of measured tunnel wall convergence for some selected sections is presented further in this chapter (Table 7-1).

7.2.2 Rock mass parameters estimation

Different literatures such as books, scientific papers, publications, class notes, internet search, websites, feasibility report of CHEP etc have been studied and information from which have been used to estimate the initial values of rock mass parameters. The estimation is based on similar case histories, rock types, rock mass condition etc. Each parameter is described further in this chapter.

Density and Poisson's ratio

The rock types along the tunnel sections considered for the study are dolomite, talcosic phyllite and slate. The density of dolomite and talcosic phyllite are taken to be 2.82 and 2.72 t/m³ (Table 2-1) and that of slate is taken to be 2.73 t/m³ (Singh and Seshagiri Rao, 2005). The Poisson's ratio of dolomite and talcosic phyllite are considered as 0.15 and 0.1 (Panthi, 2006) and that of slate is considered as 0.22 (NEA, 1997).

Uniaxial compressive strength of intact rocks, σ_{ci}

The uniaxial compressive strength of intact, σ_{ci} , is also estimated from the literatures because no tests were performed in the field. σ_{ci} of dolomite and slate are taken as 60 and 45 MPa respectively (NEA, 1997) and that of talcosic phyllite is 39 MPa (Panthi, 2006). The weathering effect is considered further in these values for different weathering grade mentioned in tunnel log. Detail of weathering effect in rock mass strength is mentioned in section 2.3.2.

Young's modulus of elasticity of intact rocks, E_i

According to NEA (1997), young's modulus of intact rock, E_i , of dolomite is 26 GPa in first stretch of tunnel and 10 GPa in second stretch of tunnel and that of slate is 8.4 GPa. E_i value of talcosic phyllite can be taken as 7 GPa (Discussion with main Supervisor, May 8, 2013).

Hoek and Brown constant, m_i

According to appendix B1, values of m_i are taken as 10, 8 and 8 for dolomite, slate and talcosic phyllite respectively.

Disturbance factor, D

The basis of selection of disturbance factor is described in appendix B3. The value of D is taken as less than 0.8 in case of blasting of tunnel and zero in case of excavation.

Tectonic stress

Tectonic stress is taken as 3.5 MPa in the direction N 8⁰ E. The direction of tectonic stress is shown in Figure 3-2. Tunnel alignment is in the direction of N 74⁰ E. So, the angle between tectonic stress and tunnel alignment is 66⁰. Phase² program has been used to verify the tectonic stress value. The result of Phase² analysis is illustrated in Figure 7-4.

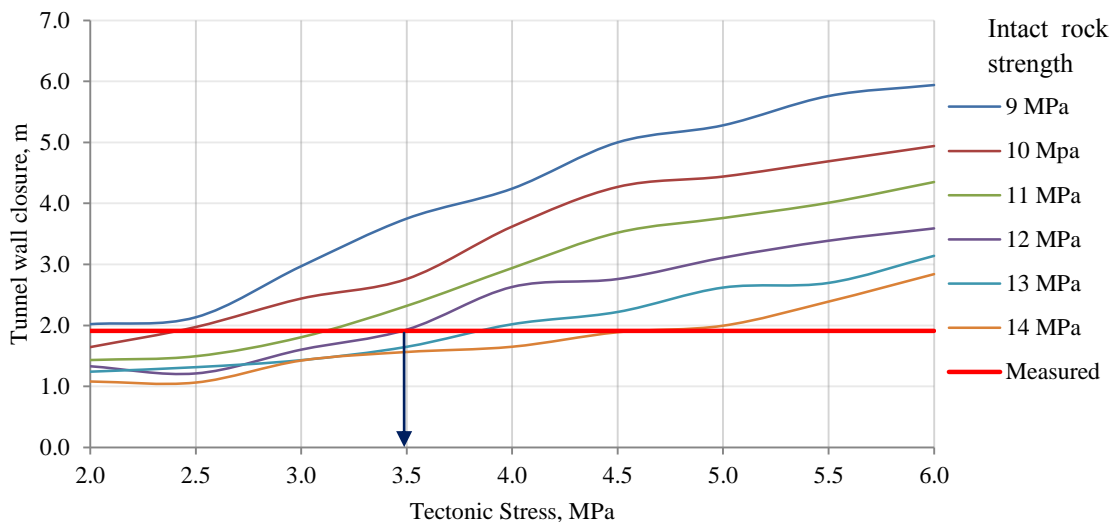


Figure 7-4: Matching the tunnel wall closure with measured value for different value of tectonic stress and intact rock strength combinations in Phase² program (Tunnel section at chainage 3+404)

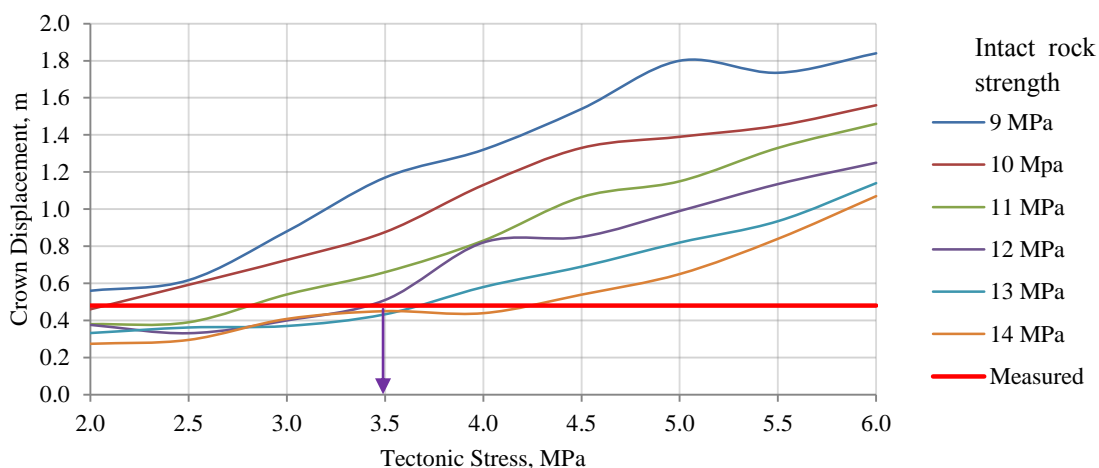


Figure 7-5: Matching the crown displacement with measured value for different value of tectonic stress and intact rock strength combinations in Phase² program (Tunnel section at chainage 3+404m)

Phase2 program has been used to find the tunnel wall closure and crown displacement for value of different tectonic stress and intact rock strength combinations in tunnel section at chainage 3+404m (Figure 7-4 and Figure 7-5). The program has been run by making the model similar to the prototype in field. Same support has been applied in the analysis that had already been applied in field. The figures show that both the values match at 3.5MPa tectonic stress and 12MPa strength. Detail of Phase² analysis is described further in this chapter.

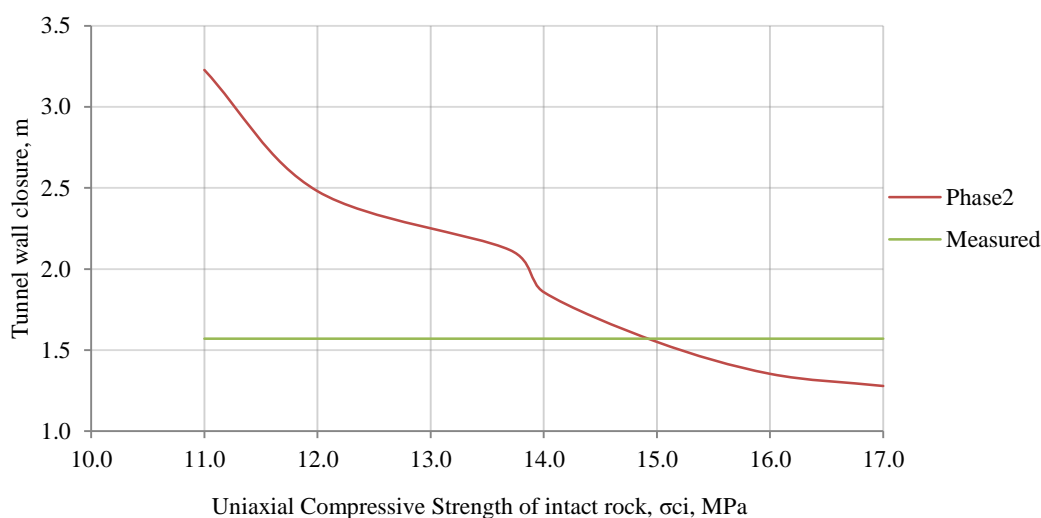


Figure 7-6: Verification of tunnel wall closure with measured value for 3.5 MPa tectonic stress in Phase² program (Tunnel section at chainage 3+420m)

Further, tunnel wall closure has been found in tunnel section at chainage 3+420m using phase2 program for 3.5MPa tectonic stress and different value of intact rock strength (figure 7-6). The value from Phase² analysis matches with measured value for intact rock strength of 15MPa. Here the intact rock strength is comparable with the estimated value which is 11MPa (Table 7-1).

7.2.3 Selection of representative sections for analysis

It is very much time consuming to analyze the whole section of the tunnel. Therefore number of sections of the tunnel has been selected based on overburden height, rock types, availability of tunnel logs at that particular section, highest, medium and lowest value of convergence measurement and overburden height. The first four sections have been taken at the stretch having dolomite as rock type and there is highest overburden depth too. After that one section has been taken at the stretch having slate as rock type. Again four sections have been considered in dolomite; two of them are in strong dolomite and another two sections are in highly fractured and sheared dolomite where there is significant convergence has been measured. The last eight sections are considered in highly fractured, thinly foliated talcosic phyllite with few bands of dolomite. In that last stretch, there is significant squeezing problem and high value of tunnel wall convergence has been measured. The sections are taken considering highest, medium and lowest value of measured convergence and also considering highest, medium and lowest value of overburden depth in that stretch. The detail of the selected sections is given in Table 7-1.

7.2.4 Summary of input data for selected tunnel sections

Based on above mentioned procedure, input data i.e. the rock mass parameters are listed in Table 7-1. These values are considered in different methods of squeezing analysis as per their requirements as input data. In Table 7-1, applied support types are considered based on the information given in tunnel logs. Details of these support types are given in appendix A2, A3 and A4. The support capacity has been calculated based on support drawings and

specifications. Some of the specifications are also taken from literatures. The detail of support capacity for each support type is described in section 7.4.2.

Table 7-1: Input parameters for squeezing analysis of selected tunnel sections

Chainage	Rock Type	Weathering pattern	Weathering grade	Strength reduction %	Overburden depth, m	Density, t/m ³	poisson's ratio	Q-Value	Intact Strength, σ_{ci} , MPa	Reduced Strength σ_{cr} , MPa	Young's modulus of rock, E_i (Gpa)	Constant, m_i	RMR value	GSI	measured tunnel wall convergence, m	Applied Support
0+180	Dolomite, Joint, Shear band, Water dripping	slightly weathered	II	0 %	140.2	2.82	0.150	0.25	60	60	26	10	41	36		R3
0+310	Dolomite, Joint, Shear band, Water dripping	slightly weathered	II	0 %	220.7	2.82	0.150	0.08	60	60	26	10	34	29		R4
0+410	Dolomite, shear band, Joint	slightly weathered	II	0 %	232.5	2.82	0.150	1.12	60	60	26	10	51	46		R2
1+340	Dolomite, Joint, Water dripping	slightly weathered	II	0 %	464.0	2.82	0.150	0.5	60	60	26	10	45	40		R3
1+430	Slate, Bedded, Joint	slightly weathered	II	0 %	131.1	2.73	0.220	0.62	45	45	8.4	8	47	42		R2
2+368	Dolomite, Shear band	moderately weathered	II	40 %	129.4	2.82	0.150	0.005	60	36	10	10	15	10		R5
3+103	Med. To strong dolomite	slightly weathered	II	0 %	181.2	2.82	0.150	1.25	60	60	10	10	51	46	0.004	R3
3+172	Highly fractured and heavily jointed Dolomite	highly weathered	IV	80 %	199.7	2.82	0.150	0.02	60	12	10	10	25	20	0.238	R5
3+190	Dolomite, Fractured, Shear band	highly weathered	IV	89 %	217.5	2.82	0.150	0.013	60	7	10	10	22	17	1.328	R5
3+296	Brownish, grey to green colored, thinly foliated phyllite within very thin band of dolomite	Highly Weathered	IV	65 %	252.2	2.78	0.100	0.01	39	14	7	8	20	15	0.65	R6
3+314	Very weak thinly foliated Phyllite with some bands of dolomite	Highly Weathered	IV	50 %	246.3	2.78	0.100	0.01	39	20	7	8	20	15	0.198	R6
3+404	Light yellow coloured, very thinly foliated, highly jointed or fractured and crushed talcosic phyllite with few dolomite and several shear/talc bands	Highly weathered	IV	75 %	283.9	2.78	0.100	0.008	39	10	7	8	19	14	1.91	R6
3+420	Light yellow coloured, very thinly foliated, fractured and crushed talcosic phyllite with few bands of dolomite	Highly weathered	IV	73 %	284.5	2.78	0.100	0.008	39	11	7	8	19	14	1.57	R6
3+681	Light yellow to brownish to green coloured, jointed or fractured, very thinly foliated talcosic Phyllite with few thin quartz bands	Highly weathered	IV	75 %	210.8	2.78	0.100	0.01	39	10	7	8	20	15	0.952	R6
3+733	Light yellow coloured, highly jointed or fractured, thinly foliated talcosic Phyllite with Grey coloured jointed and fractured dolomite and quartzite bands	Moderately weathered	III	65 %	237.7	2.78	0.100	0.01	39	14	7	8	20	15	0.57	R6
3+764	Light yellow coloured, jointed or fractured, thinly foliated Phyllite alternatively with Grey fractured dolomite. Phyllite is more than dolomite	Moderately weathered	III	70 %	230.0	2.78	0.100	0.015	39	12	7	8	23	18	0.51	R5
3+795	Light yellow coloured, jointed or fractured, thinly foliated Phyllite . At right wall dolomite and phyllite present	Moderately weathered	III	40 %	222.6	2.78	0.100	0.015	39	23	7	8	23	18	0.062	R5

7.2.5 Rock mass strength calculation

Rock mass strength has been calculated using the different empirical relationships proposed by different authors. The equations of four such approaches that are used for the calculation is given in Table 2-3 (chapter 2). In Hoek and Marinos (2000) approach, equation 6-6 has been used to back calculate the rock mass strength from measured deformation. Figure 7-7 shows comparison chart of rock mass strength estimation for the selected tunnel sections. The input data required for different approaches are given in Table 7-1.

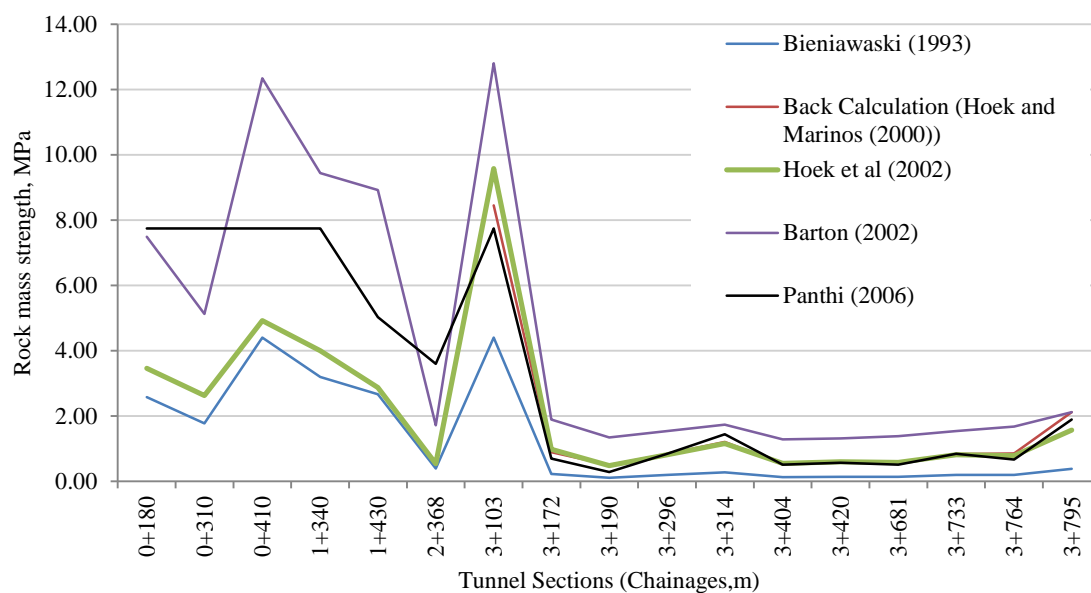


Figure 7-7: Rock mass strength estimation using five different methods for the selected tunnel sections

Figure 7-7 shows that Barton (2002) gives the highest values for each section (except 2+368) whereas Bieniawski (1993) gives the lowest values for all the sections. Panthi (2006) gives the values almost average of all approaches and Hoek et al (2002) gives the values more or less equal to that obtained from Hoek and Marinos (2000) approach for the last eleven sections. Panthi (2006) has been used to estimate the rock mass strength in Q-system (in section 6.2.2) to overcome the problem of loop of dependency in squeezing predicting criteria proposed by Grimstad and Barton (1993). Further in this chapter, equations suggested by Hoek et al (2002) have been used to estimate rock mass strength in Hoek and Marinos (2000) approach.

7.2.6 Rock mass modulus calculation

Rock mass modulus has been calculated using the different empirical relationships proposed by different authors. The equations of five such approaches that are used for the calculation is given in Table 2-4 (chapter 2). Figure 7-8 shows comparison chart of rock mass strength estimation for the selected tunnel sections. The input data required for different approaches are given in Table 7-1.

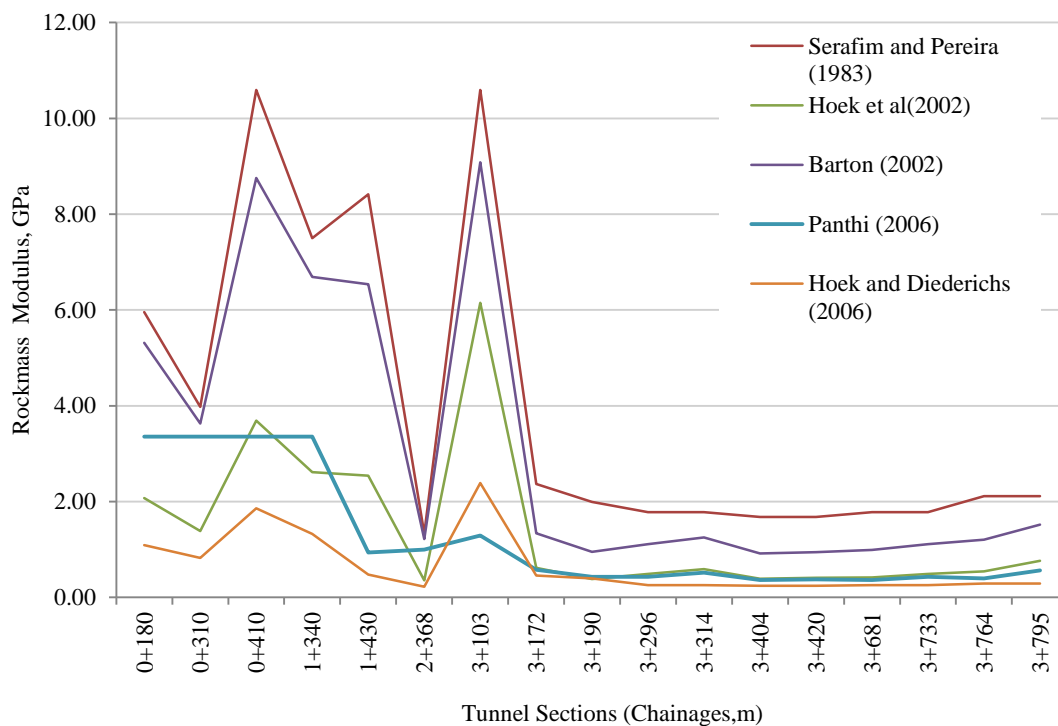


Figure 7-8: Rockmass Modulus estimation using five different methods for selected tunnel sections

Figure 7-8 shows that Serafim and Pereira (1983) give the highest values for all sections where as Hoek and Diederichs (2006) gives the lowest values for all the sections (except 3+103). Panthi (2006) gives almost reasonable values for all the sections with little bit lower values in last 11 sections. Further, in the squeezing analysis, Panthi (2006) has been used to calculate the rock mass deformation modulus.

7.3 ROCK MASS CLASSES AND SUPPORT TYPE

Rock mass classification system, i.e. Q-system proposed by Barton et al. (1974), has been used to classify the rock mass quality based on Q-values for the selected tunnel sections. According to Q-system, there are seven classes of rock mass quality from class A to class E depending upon the Q-values (appendix B6). But in the selected tunnel sections, four classes of rock mass have been noticed i.e. poor, very poor, extremely poor and exceptionally poor. The chart given in appendix B6 proposed by Grimstad and Barton (1993) has been used to find the required rock support type. For the estimation of rock support type, the Q-value and the ratio of span of tunnel and excavation support ratio (ESR). The value of ESR for different type of underground excavations is given in table in appendix B6.

Table 7-2 gives rock mass quality class and required support types based on Q-system. The table shows that rock mass is extremely to exceptionally poor in the tunnel sections where there is high degree of squeezing problem has been encountered in the field. High degree squeezing phenomenon in this rock quality has also been predicted by different approaches that are explained in section 7.4.1.

In CHEP case, span of the tunnel is 5.2 m and ESR can be taken as 1.6 because it is water tunnel for hydropower. The ratio between span and ESR can be calculated using equation 6-4 and it comes out to be equal to 3.25. Then, using Q-value and the ratio in support chart, the required support type has been predicted from (3) Sfr+B to (7) Sfr+RRS+B. The description of these support types is given in chart (appendix B6).

Table 7-2: Rock mass quality class and required support type based on Q-system and applied support type in actual field

Chainage	Rock Type	Overburden Depth	Q	Rock mass Classes	Span/ESR	Required support type	Applied support type
0+180	Dolomite	140.2	0.25	Very Poor	3.25	(4) Sfr+B	R3
0+310	Dolomite	220.7	0.08	Extremely Poor	3.25	(5) Sfr+B	R4
0+410	Dolomite	232.5	1.12	Poor	3.25	(3) Sfr+B	R2
1+340	Dolomite	464.0	0.5	Very Poor	3.25	(4) Sfr+B	R3
1+430	Slate	131.1	0.62	Very Poor	3.25	(4) Sfr+B	R2
2+368	Dolomite	129.4	0.01	Exceptionally Poor	3.25	(7) Sfr+RRS+B	R5
3+103	Dolomite	181.2	1.25	Poor	3.25	(3) Sfr+B	R3
3+172	Dolomite	199.7	0.02	Extremely Poor	3.25	(6) Sfr+B	R5
3+190	Dolomite	203.9	0.03	Extremely Poor	3.25	(6) Sfr+B	R5
3+296	Talcotic Phyllite	239.5	0.01	Exceptionally Poor	3.25	(7) Sfr+RRS+B	R6
3+314	Talcotic Phyllite	246.3	0.01	Exceptionally Poor	3.25	(7) Sfr+RRS+B	R6
3+404	Talcotic Phyllite	275.2	0.01	Exceptionally Poor	3.25	(7) Sfr+RRS+B	R6
3+420	Talcotic Phyllite	277.1	0.01	Exceptionally Poor	3.25	(7) Sfr+RRS+B	R6
3+681	Talcotic Phyllite	210.8	0.01	Exceptionally Poor	3.25	(7) Sfr+RRS+B	R6
3+733	Talcotic Phyllite	219.1	0.01	Exceptionally Poor	3.25	(7) Sfr+RRS+B	R6
3+764	Talcotic Phyllite	230.0	0.02	Extremely Poor	3.25	(6) Sfr+B	R5
3+795	Talcotic Phyllite	222.6	0.02	Extremely Poor	3.25	(6) Sfr+B	R5

Table 7-2 also shows the applied support type in the project site during excavation of the tunnel. The drawing and specifications of these supports are given in appendix A2, A3 and A4. For example, in table, it can be seen that R3 support is applied in the section where the predicted support from Q-system is (4) Sfr+B. In the last ten sections, the applied support types are more or less similar to that predicted from the Q-system. The applied supports were proposed based on Q-system.

7.4 SQUEEZING ANALYSIS

Squeezing analysis has been done in two stages. In 1st stage, squeezing problem has been predicted using Singh et al. (1992), Q-system and Hoek and Marinos (2000) approaches. In second stage, more detail analysis has been done, at the sections where there is significant squeezing problem, using Hoek and Marinos (2000) approach, Carranza-Torres and Fairhurst (2000) approach and Phase2 program. In this stage, support pressure has also been estimated. The detail calculation of Hoek and Marinos (2000) is given in AppendixC0. The results of analysis and their comparison are explained further in this chapter.

7.4.1 Squeezing prediction criteria

There methods such as Singh et al (1992), Q-system (Grimstad and Barton, 1993) and Hoek and Marinos (2000) have been used to predict the squeezing phenomenon in headrace tunnel of CHEP. The result of the analysis is shown in Table 7-3.

Table 7-3: Squeezing prediction according to Singh et al (1992), Q-system (Grimstad and Barton, 1993) and Hoek and Marinos (2000)

Chamage	Rock Type	Overburden Depth, m	Q	Singh et al (1992)		Q-System (Barton and Grimstad, 1993)				Hoek and Marinos (2000)	
				limiting value of H, m	Squeezing condition	$\sigma_{\theta\max}$	σ_{cm}	$\sigma_{\theta\max}/\sigma_{cm}$	Squeezing condition	strain % without support, ϵ	Squeezing condition
0+180	Dolomite	140.2	0.25	220.49	NO	7.75	7.75	1.00	Mild Squeezing	0.25 %	Few Support Problems
0+310	Dolomite	220.7	0.08	150.81	YES	14.04	7.75	1.81	Mild Squeezing	1.08 %	Minor Squeezing
0+410	Dolomite	232.5	1.12	363.47	NO	14.96	7.75	1.93	Mild Squeezing	0.34 %	Few Support Problems
1+340	Dolomite	464.0	0.5	277.80	YES	33.05	7.75	4.27	Mild Squeezing	2.06 %	Minor Squeezing
1+430	Slate	131.1	0.62	298.45	NO	6.35	5.03	1.26	Mild Squeezing	0.30 %	Few Support Problems
2+368	Dolomite	129.4	0.005	59.85	YES	6.91	3.60	1.92	Mild Squeezing	8.74 %	Very severe squeezing
3+103	Dolomite	181.2	1.25	377.03	NO	10.96	7.75	1.41	Mild Squeezing	0.05 %	Few Support Problems
3+172	Dolomite	199.7	0.02	95.00	YES	12.40	0.69	17.90	Heavy Squeezing	6.42 %	Very severe squeezing
3+190	Dolomite	203.9	0.031	109.95	YES	12.73	0.28	45.04	Heavy Squeezing	31.43 %	Extreme Squeezing
3+296	Talcosec Phyllite	239.5	0.01	75.41	YES	15.67	0.84	18.65	Heavy Squeezing	14.49 %	Extreme Squeezing
3+314	Talcosec Phyllite	246.3	0.01	75.41	YES	16.21	1.44	11.29	Heavy Squeezing	6.77 %	Very severe squeezing
3+404	Talcosec Phyllite	275.2	0.008	70.00	YES	18.48	0.51	36.42	Heavy Squeezing	39.33 %	Extreme Squeezing
3+420	Talcosec Phyllite	277.1	0.008	70.00	YES	18.63	0.57	32.72	Heavy Squeezing	33.86 %	Extreme Squeezing
3+681	Talcosec Phyllite	210.8	0.01	75.41	YES	13.41	0.51	26.43	Heavy Squeezing	19.85 %	Extreme Squeezing
3+733	Talcosec Phyllite	219.1	0.01	75.41	YES	14.06	0.84	16.73	Heavy Squeezing	12.87 %	Extreme Squeezing
3+764	Talcosec Phyllite	230.0	0.015	86.32	YES	14.93	0.67	22.38	Heavy Squeezing	12.85 %	Extreme Squeezing
3+795	Talcosec Phyllite	222.6	0.015	86.32	YES	14.34	1.89	7.60	Heavy Squeezing	3.01 %	Severe Squeezing

Each analysis shows the mixed results for the first seven sections. But for rest of the sections, the results are more or less same. Singh et al (1992) shows that there will be squeezing in thirteen sections. According to Q-system, there will be mild squeezing in seven sections and heavy squeezing in ten sections. Similarly, according to Hoek and Marinos (2000) approach, there will be few support problems in four sections, minor squeezing in two sections, severe squeezing in one section, very severe squeezing in three sections and extreme squeezing in seven sections. On the other hand, in the field, squeezing phenomenon has been noticed only in last ten sections. The measured convergence in these ten sections is shown in figure 7-1. Thus all the above criteria are found to be conservative to define squeezing section. However,

it should be noted that the convergence was measured after the support application that means there will be contribution of tunnel support to minimize the convergence.

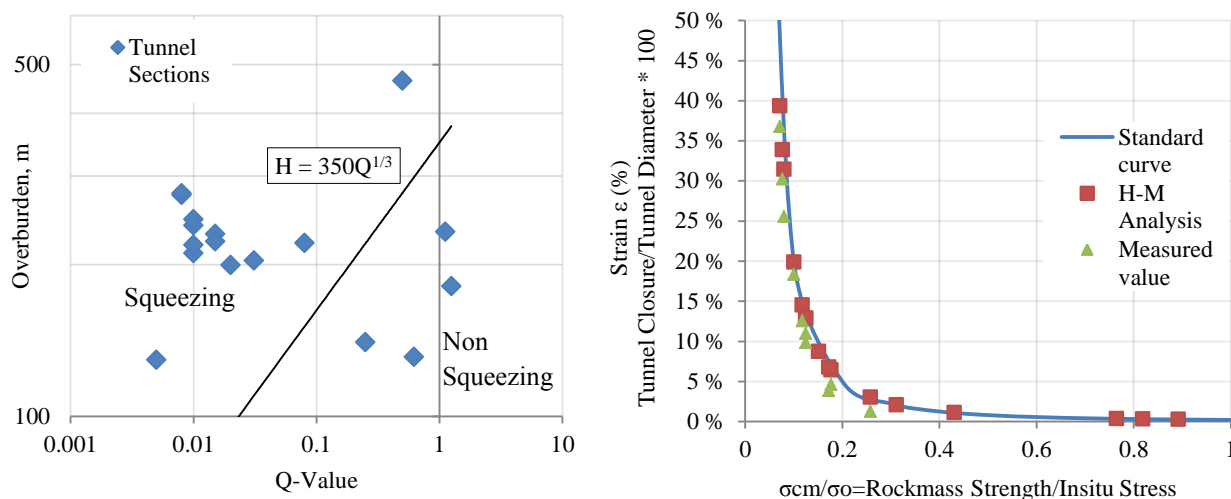


Figure 7-9: Squeezing and non-squeezing sections of tunnel according to Singh et al (1992) (left) and Squeezing classes for different sections of tunnel with respect to calculated strain % according to Hoek and Marinos (2000) for unsupported tunnel and measured strain % (right)

In conclusion, there is squeezing problem in headrace tunnel of CHEP and last ten sections have been selected for further analysis where there is significant squeezing. Hence, more detail analysis has been done only for the last ten sections, which is described further in this chapter. The graphical representation of result of the analysis is shown in Figure 7-9.

7.4.2 Rock support interaction using CCM

Convergence confinement method (CCM) is an analytical solution in which rock mass and support interaction can be understood using three basic components. It has been used to analyze the squeezing in the last ten tunnel sections. The three components are; Ground Reaction Curve (GRC), Load Displacement Profiles (LDP) and Support Characteristics Curve (SCC). Equations proposed by Carranza-Torres and Fairhurst (2000) has been used to construct GRC and SCC for different support types. The improved equations proposed by Vlachopoulos and Diederichs (2009) have been used to draw LDPs. The details of these equations are explained in chapter 6.

Figure 7-10 shows GRC and LDP for ten tunnel sections that are selected for detail analysis. The sample calculation of GRC and LDP of tunnel section at chainage 3+404m is presented in appendix C1 and C2 respectively. These GRC s and LDPs are used for the rock support interaction analysis.

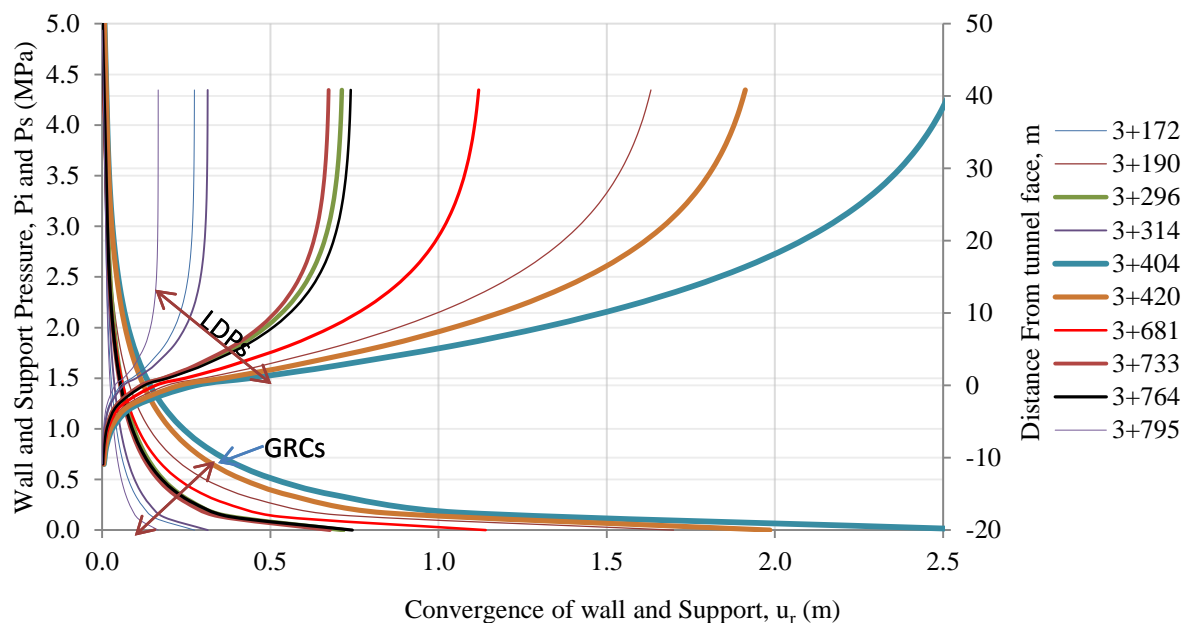


Figure 7-10: GRC and LDC of ten tunnel sections at different chainages

Support type R5 and R6 were used in ten tunnel sections during excavation. In the 1st two tunnel sections and last two tunnel sections, support type R5 was used whereas in the rest six sections, support type R6 was used (Table 7-2). Support R5 is the composition of rock bolts, shotcrete with wire mesh and lattice girder whereas support R6 is the combination of rock bolts, shotcrete with wire mesh and steel ribs. The effect of wire mesh has been neglected, so it has not been considered in this thesis. SCC for these two support types has been constructed using the equations given in chapter 6 in respective headings.

Table 7-4: Properties of rock bolts and shotcrete in R5 and R6 support types

Rock Bolts							Shotcrete			
Bolt Type	Bolt Length, m	Bolt Dia. mm	Bolt Modulus, E Mpa	Tensile Capacity MN	In-plane Spacing m	Out-of-plane spacing m	thickness, mm	young's Modulus, Mpa	Poisson's Ratio	Compressive Strength, Mpa
End Anchored	3	25	210000	0.254	1	1	100	20000	0.25	20

Table 7-4 shows the properties of rock bolts and shotcrete used in different support types. For both supports R5 and R6, properties of rock bolts and shotcrete are same. Support R5 is same for all the sections that it belongs to. But in support R6, the difference is spacing of steel sets in each sections. Table 7-5 shows the detail of composition of different support types used in selected tunnel sections. The properties of each support components have been used to calculate the maximum support capacity and maximum displacement at the time of yielding of each component, combined maximum support capacity and displacement at yielding (Table 7-6). 30% of support capacity has been reduced in maximum support capacity in order to account two main things; first, the practical difficulty in the installation of support and

second, tunnel shape and support are considered as circular in the analysis but in actual field tunnel shape is horseshoe type and invert is not supported.

Table 7-5: Detail composition of support type for selected tunnel sections

Chainage	Support Type	Rock Bolts	Shotcrete	Lattice Girder		Steel sets	
		Bolt Type	thickness, mm	Type	Spacing, m	Type	Spacing, m
3+172	R5	End Anchored	100	3 bar, bar size: 18, 26mm	1	-	-
3+190	R5	End Anchored	100	3 bar, bar size: 18, 26mm	1	-	-
3+296	R6	End Anchored	100	-	-	I-Beam W100 X 19.1	0.7
3+314	R6	End Anchored	100	-	-	I-Beam W100 X 19.2	0.7
3+404	R6	End Anchored	100	-	-	I-Beam W100 X 19.3	0.5
3+420	R6	End Anchored	100	-	-	I-Beam W100 X 19.4	0.35
3+681	R6	End Anchored	100	-	-	I-Beam W100 X 19.5	0.6
3+733	R6	End Anchored	100	-	-	I-Beam W100 X 19.5	0.6
3+764	R5	End Anchored	100	3 bar, bar size: 18, 26mm	1	-	-
3+795	R5	End Anchored	100	4 bar, bar size: 18, 26mm	1	-	-

Table 7-6: Maximum support pressure provided by the support system and maximum allowable displacement of support

		Rock Bolts		Shotcrete		Reduction in support capacity 30 %	
		Max support Pressure, MPa	Max Allowable Displacement, m	Max support Pressure, MPa	Max Allowable Displacement, m		
		0.18	0.044	0.50	0.0016		
Chainage	Support Type	Lattice Girder		Steel sets		Combined support	
		Max support Pressure, MPa	Max Allowable Displacement, m	Max support Pressure, MPa	Max Allowable Displacement, m	Max support Pressure, MPa	Max Allowable Displacement, m
3+172	R5	0.13	0.04	-	-	0.52	0.0016
3+190	R5	0.13	0.04	-	-	0.52	0.0016
3+296	R6	-	-	0.25	0.0032	0.64	0.0016
3+314	R6	-	-	0.25	0.0032	0.64	0.0016
3+404	R6	-	-	0.35	0.0032	0.69	0.0016
3+420	R6	-	-	0.50	0.0032	0.77	0.0016
3+681	R6	-	-	0.29	0.0032	0.66	0.0016
3+733	R6	-	-	0.29	0.0032	0.66	0.0016
3+764	R5	0.13	0.04	-	-	0.52	0.0016
3+795	R5	0.13	0.04	-	-	0.52	0.0016

The detail of maximum support pressure and maximum displacement calculation for tunnel section 3+404 is given in appendix C3. Figure C3.1 and C3.2 in appendix C3 show typical

SCC of support R5 and R6 for tunnel section 3+404m and 3+190m respectively. Similarly SCC for other tunnel sections can be constructed. These SCCs have been used in rock support interaction analysis.

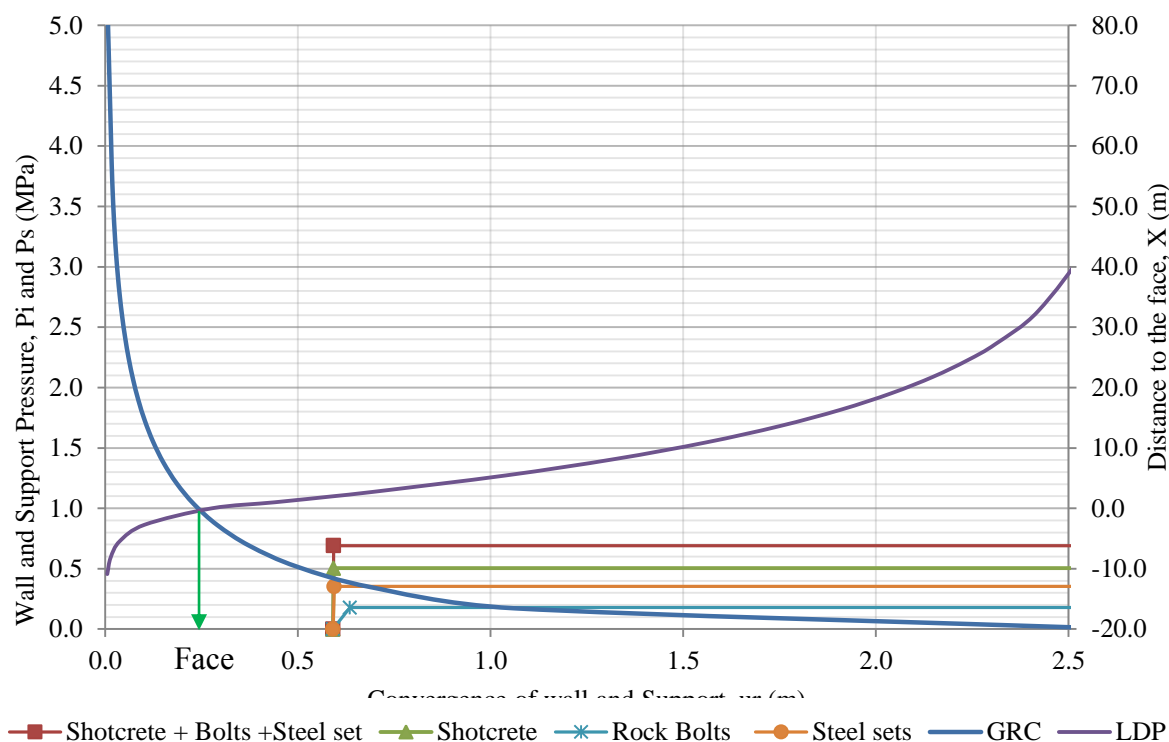


Figure 7-11: Interaction of GRC, LDP and SCC in tunnel section 3+404m

In Figure 7-11, if the support is applied at face of tunnel there will be 0.276m displacement at tunnel wall. At the face of tunnel, the maximum pressure that the support can experience is 0.9 MPa whereas the maximum support capacity for combined support (shotcrete + bolts + steel sets) is only 0.69 MPa. So the support will fail before it experiences 0.9 MPa pressure. Here, the residual support capacity of yielded support is assumed to be equal to 0.1 MPa as there were no strain gauges and load cells installed in the field to measure support pressure. At this point, the displacement of tunnel wall will be equal to 1.5m (57.7% strain).

To overcome the failure of support, either support capacity should be increased to the value more than support pressure when support is applied at tunnel face or the support can be applied at some distance behind tunnel face. Both of these solutions have some difficulties such as for the first case increase of support capacity can be achieved with concrete lining but application of concrete lining at the face of tunnel is very challenging work. And for the second case, tunnel size will be reduced to some extent more than acceptable limit but that could lead to total collapse if support is delayed and then support application will also be very challenging task.

In the Figure 7-11, the support is applied 2m behind the face. The tunnel wall deformation will be 0.591m i.e. 22.73% strain and support pressure will be 0.43 MPa. The rock bolts and steel sets will be failed before they reach their capacity. Shotcrete will sustain the support pressure with factor of safety (FOS) is equal to 1.16 (0.5/0.43) and combined support will be

working with FOS 1.6 (0.69/0.43). Similarly, tunnel wall deformation and support pressure have been estimated for other tunnel sections too.

Verification of CCM analysis

Theoretically, the main assumptions of CCM are; the stress field is isostatic and the tunnel shape is circular. But in CHEP case, there is non-uniform stress field and tunnel shape is horseshoe type. So, analysis has been done considering average stress (equation 6-28) and circular tunnel with radius equal to equivalent radius of the section (appendix C1). The result obtained from CCM in case of non-uniform stress field can be verified with respect to the term limiting stress ratio, k_{lim} (Section 6.4.2).

Table 7-7: Calculation of normal and limiting stress ratio in selected tunnel sections

Chainages m	Eq. tunnel radius, m	Intact rock strength, σ_{ci} (MPa)	Vert. stress, σ_z (MPa)	In plane Hz. stress, σ_x (MPa)	σ_o (MPa)	σ_o/σ_{ci}	k (σ_z/σ_x)	Friction angle, ϕ (degree)	k_{lim}	Remarks
3+172	2.72	12.00	5.52	4.17	4.85	0.40	1.32	10-20	2.6-2.7	$k < k_{lim}$
3+190	2.72	6.60	6.02	4.26	5.14	0.78	1.41	10-20	1.8-2.1	$k < k_{lim}$
3+296	2.72	13.65	6.88	3.96	5.42	0.40	1.74	10-20	2.6-2.7	$k < k_{lim}$
3+314	2.72	19.50	6.72	3.95	5.33	0.27	1.70	10-20	2.6-2.7	$k < k_{lim}$
3+404	2.72	9.75	7.74	4.06	5.90	0.61	1.91	10-20	2.5-2.6	$k < k_{lim}$
3+420	2.72	10.53	7.76	4.06	5.91	0.56	1.91	10-20	2.5-2.6	$k < k_{lim}$
3+681	2.72	9.75	5.75	3.84	4.79	0.49	1.50	10-20	2.6-2.7	$k < k_{lim}$
3+733	2.72	13.65	6.48	3.92	5.20	0.38	1.65	10-20	2.6-2.8	$k < k_{lim}$
3+764	2.72	11.70	6.27	3.90	5.09	0.43	1.61	10-20	2.6-2.9	$k < k_{lim}$
3+795	2.72	23.40	6.07	3.87	4.97	0.21	1.57	10-20	2.6-2.10	$k < k_{lim}$

Because of symmetry of problem, the axis of cavity is rotated through 90^0 , so, $k = \sigma_z/\sigma_x$ has been used instead of using equation 6-27. Table 7-7 shows that the normal stress ratio (k) is less than limiting stress ratio (k_{lim}) for all tunnel sections. Hence, mean radius of plastic region around tunnel and mean convergence at the crown and sidewall of the tunnel should be similar to the corresponding values obtained from CCM, which verifies the analysis of CHEP case using CCM.

7.4.3 Estimation of support pressure and capacity of support

Support pressure has been estimated using three different approaches i.e. Barton et al. (1974), Hoek and Marinos (2000) and CCM (Carranza-Torres and Fairhurst, 2000). Barton et al. (1974) uses Q-value to estimate the support pressure at wall (appendix B7). Equation 6-5 has been used in case of Hoek and Marinos (2000) approach and rock support interaction analysis (explained in section 7.4.3) has been applied in CCM.

Table 7-8 shows estimated support pressure using three different approaches. In case of Hoek and Marinos (2000) i.e. HM approach, the pressure has been estimated at 2% strain condition and at the measured tunnel closure. Similarly, in case of CCM, the pressure has been estimated at the face of tunnel, 1m behind tunnel face, 2m behind tunnel face, and 2% strain condition and at the point of measured tunnel closure (Table 7-8 and Figure 7-12). In CCM, the critical support pressure has also been estimated. The critical support pressure means the

pressure at point from where plastic behavior of rock material starts. The applied support capacity is taken from Table 7-6. The comparison of estimated support pressure by different approaches and applied support capacity is shown in Figure 7-12.

Table 7-8: Estimation of support pressure using three different approaches

Chainage	Support Pressure Estimation, Mpa							Support capacity Provided, Mpa	Measured Tunnel closure, m
	Barton (1974)	Hoek and marinos (2000)		CCM (Carranza-Torres and Fairhurst, 2000)					
		at 2% strain, ϵ (HM)	at measured convergence	p_r^{cr}	at face of tunnel	at 2% strain, ϵ	at measured convergence		
3+172	0.74	1.14	0.33	2.72	0.77	0.82	0.24	0.52	0.24
3+190	0.88	2.14	0.17	3.46	0.79	1.83	0.17	0.52	1.33
3+296	0.93	2.01	0.16	3.30	0.81	1.57	0.19	0.64	0.65
3+314	0.93	1.40	0.72	2.94	0.85	1.04	0.48	0.64	0.20
3+404	0.98	2.86	0.07	3.96	0.90	2.40	0.22	0.69	1.91
3+420	0.98	2.79	0.12	3.91	0.91	2.29	0.21	0.77	1.57
3+681	0.93	1.85	0.07	3.07	0.72	1.59	0.17	0.66	0.95
3+733	0.93	1.84	0.18	3.13	0.76	1.45	0.23	0.66	0.57
3+764	0.81	1.77	0.27	3.24	0.74	1.49	0.31	0.52	0.51
3+795	0.81	0.50	1.13	2.45	0.88	0.58	1.14	0.52	0.06

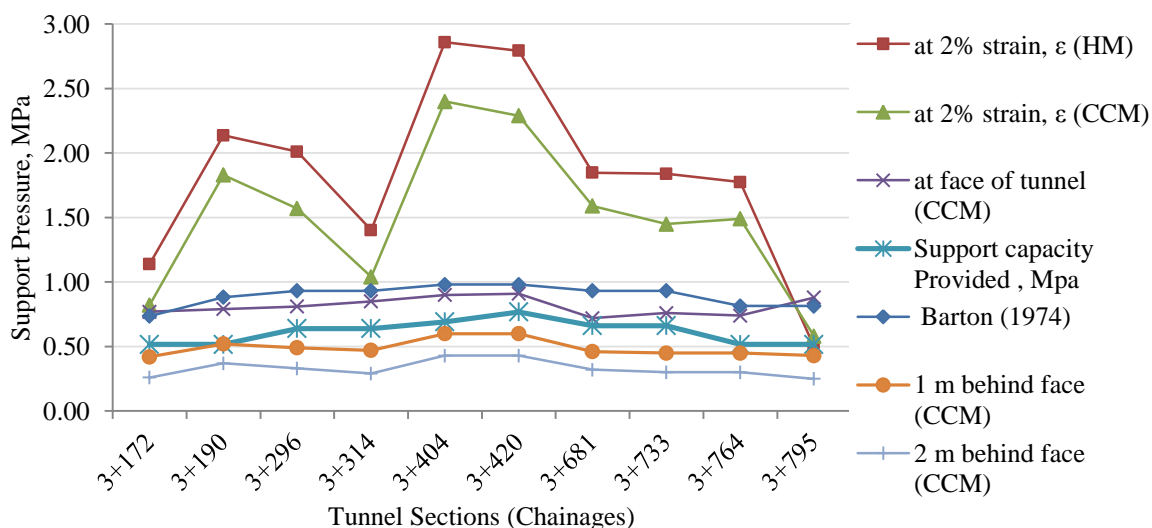


Figure 7-12: Comparison chart of estimated support pressure by three different approaches and applied support capacity

The support pressure at 2% strain condition given by both HM and CCM approaches are higher than the support pressure at tunnel face given by CCM. Hence it is very difficult to maintain the tunnel strain less than 2% in normal condition. To maintain tunnel strain level below the specified limit (for e.g. 2%), the rock mass properties could be improved before tunnel excavation using some special arrangements such as pre injection grouting, fore poling etc. In CHEP case, fore poling was used before excavation but it is very difficult to estimate the improvement of rock mass quality due to fore poling. Hence, the effect of fore poling is neglected in this thesis. After that, the only remaining possibility to maintain the minimum level of tunnel closure is to apply the support at tunnel face. But minimum strain will still be more than the specified limit i.e. 2%. The deformation calculation is explained further in section 7.4.5.

Furthermore, the support pressure estimated using Barton (1974) is more or less equal to that estimated at tunnel face using CCM. But in both cases, the support capacity is less than estimated support pressure that means if the support is applied at tunnel face, it will get ruptured. The similar situation should have happened in CHEP case where the support was applied at tunnel face and however later high deformation was observed. The support pressures estimated at 1m and 2m behind tunnel face using CCM are less than provided support capacity that means support will sustain these pressures without rupture but with different factor of safeties. In actual case, even if the support failed there will be certain residual support pressure. Two approaches have been used to estimate the residual support pressure at measured tunnel closure. The estimation of residual support pressure in actual field is very difficult task and no arrangement was provided to measure this pressure. Hence, the residual support pressure is assumed to be equal to 0.1 MPa for seven tunnel sections i.e. the case of support failure, 0.33 MPa for two sections with support R5 type (no support failure) and 0.4 MPa for one section with R6 support type (no support failure).

Table 7-9: Estimated residual support pressure using HM and CCM and assumed residual support pressure at different tunnel sections

Chainage	Residual Support Pressure Estimation at measured tunnel closure, MPa		Assumed Residual Support Pressure at site, p_i , MPa	Measured Tunnel closure, m
	HM	CCM		
3+172	0.33	0.24	0.33	0.24
3+190	0.17	0.17	0.10	1.33
3+296	0.16	0.19	0.10	0.65
3+314	0.72	0.48	0.40	0.20
3+404	0.07	0.22	0.10	1.91
3+420	0.12	0.21	0.10	1.57
3+681	0.07	0.17	0.10	0.95
3+733	0.18	0.23	0.10	0.57
3+764	0.27	0.31	0.10	0.51
3+795	1.13	1.14	0.33	0.06

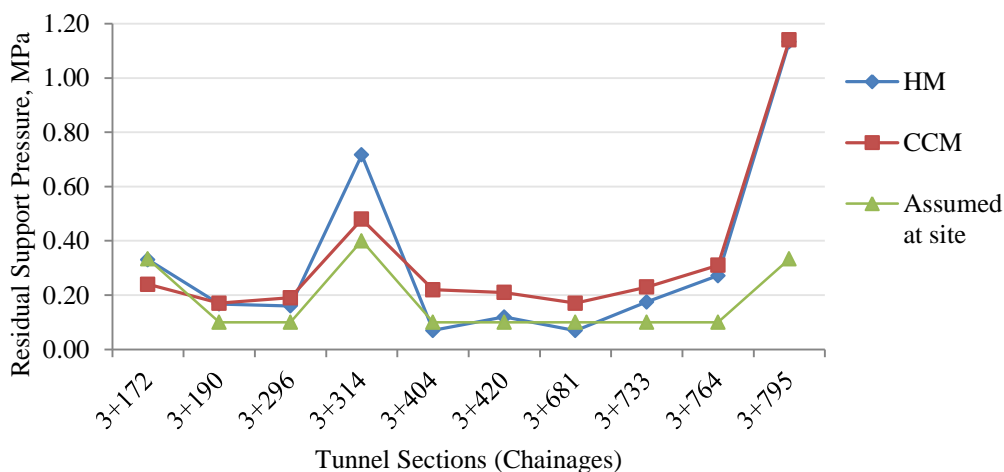


Figure 7-13: Comparison of residual support pressure estimated by HM and CCM with assumed pressure at CHEP site for different tunnel sections

Table 7-9 gives the value of estimated residual support pressure using HM and CCM approaches and assumed pressure in actual field. Also, Figure 7-13 compares the assumed value with estimated values. The figure shows that the assumed value is lower than estimated values most of the sections. The assumed pressure has been used in case of HM analysis further in section 7.4.5.

The support capacity has been estimated with 1.5 Factor of safety using Barton (1974) and CCM approaches. Using CCM, support capacity at tunnel face, 1m and 2m behind tunnel face has been estimated (Table 7-10).

Table 7-10: Support capacity estimation in case of Barton et al. (1974) and CCM with 1.5 factor of safety

Chainage	Required support capacity, MPa				Support capacity Provided, MPa	Measured Tunnel closure, m
	Barton (1974)	CCM				
		at face of tunnel	1 m behind face	2 m behind face		
3+172	1.10	1.16	0.63	0.39	0.52	0.24
3+190	1.32	1.19	0.78	0.56	0.52	1.33
3+296	1.40	1.22	0.74	0.50	0.64	0.65
3+314	1.40	1.28	0.71	0.44	0.64	0.20
3+404	1.47	1.35	0.90	0.65	0.69	1.91
3+420	1.47	1.37	0.90	0.65	0.77	1.57
3+681	1.40	1.08	0.69	0.48	0.66	0.95
3+733	1.40	1.14	0.68	0.45	0.66	0.57
3+764	1.22	1.11	0.68	0.45	0.52	0.51
3+795	1.22	1.32	0.65	0.38	0.52	0.06

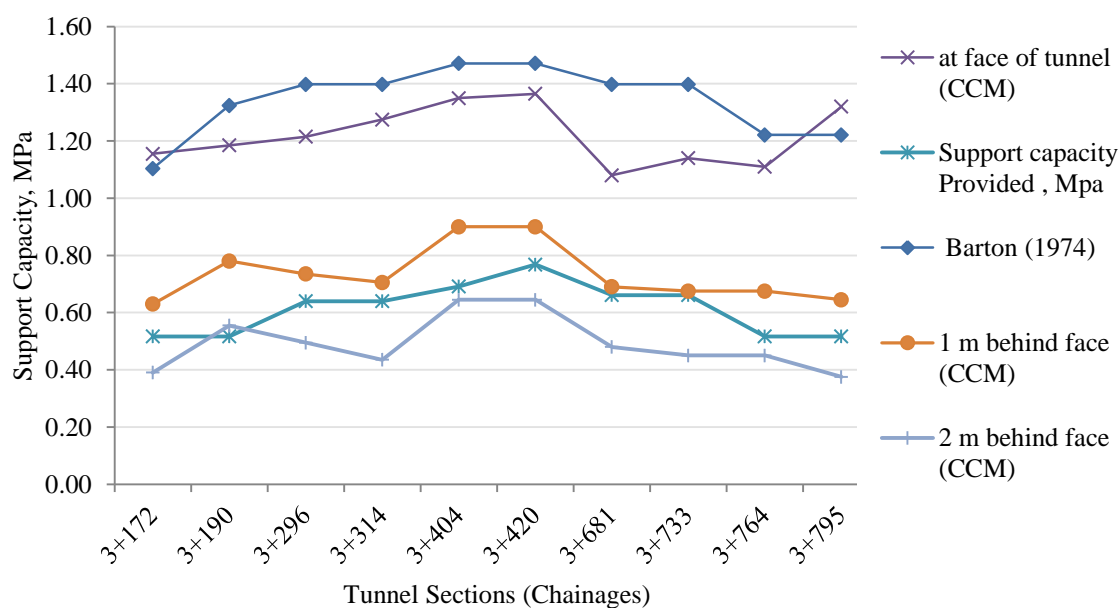


Figure 7-14: Comparison of estimated support capacity (1.5 FOS) with provided support capacity

Figure 7-14 shows that provided support capacity is less than estimated support capacity in three cases viz. Barton (1974), at face of tunnel and 1m behind the face of tunnel using CCM. The factor of safety 1.5 could have been achieved if the provided support was applied at 2m behind the face. But there could be complete collapse of tunnel in the case if support is delayed.

7.4.4 Deformation due to squeezing

The deformation due to squeezing in CHEP headrace tunnel has been calculated using two approaches viz. HM (Hoek and Marinos 2000) and CCM (Carranza-Torres and Fairhurst, 2000). Equations 6-4 and 6-5 are used in HM analysis and rock support interaction analysis is used in CCM analysis to find the deformation in tunnel wall due to squeezing pressure. In addition to deformation, plastic zone radius around the excavated tunnel has also been calculated.

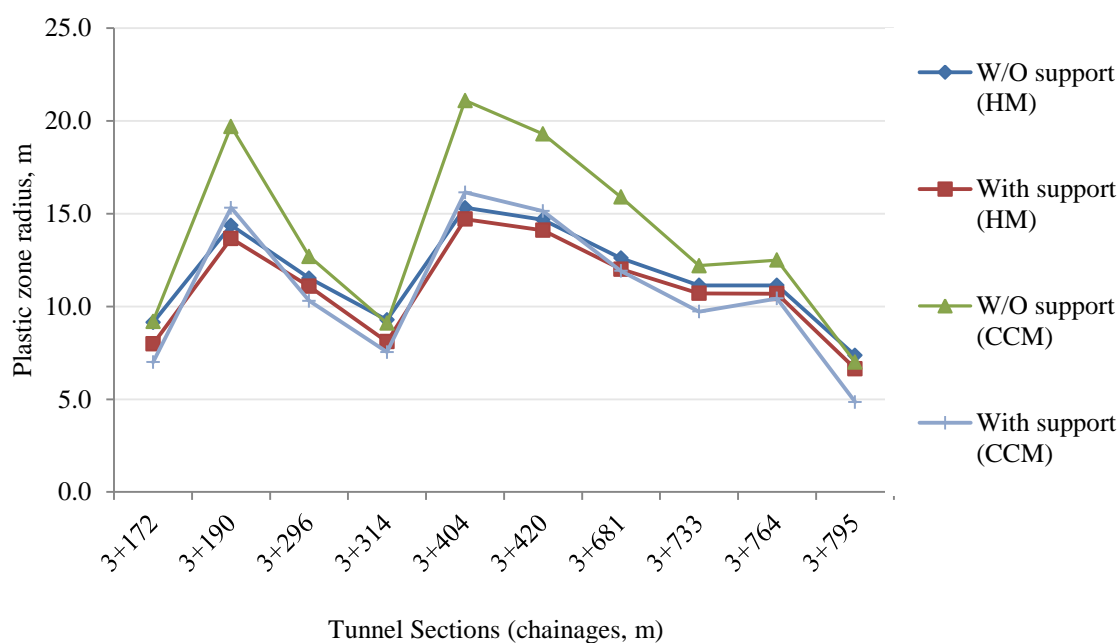


Figure 7-15: Plastic zone radius around the tunnel after excavation (with and without support) using HM and CCM approaches

Figure 7-15 shows that CCM gives highest plastic zone radius in the analysis without support. For other cases, similar values of plastic zone radius have been noticed. At higher value of plastic zone radius, higher tunnel wall deformation will be expected. The strain percentages in selected tunnel sections calculated by using HM and CCM for the cases with and without support are given in Table 7-11.

Table 7-11: Tunnel strain percentage (tunnel wall closure/tunnel diameter x 100) calculation using Hoek and Marinos (2000) and CCM approaches with and without support

Chainage	Overburden depth, m	Strain % = Tunnel Closure/Tunnel Diameter x 100						Measured strain
		Hoek and marinos (2000)			CCM (Carranza-Torres and Fairhurst 2000)			
		W/O support	Assumed support pressure, pi, Mpa	With support	W/O support	With support		
3+172	199.7	6.4 %	0.33	4.6 %	10.6 %	5.4 %	4.6 %	
3+190	217.5	31.4 %	0.10	27.8 %	65.3 %	38.5 %	25.5 %	
3+296	252.2	14.5 %	0.10	13.2 %	27.6 %	17.3 %	12.5 %	
3+314	246.3	6.8 %	0.40	4.9 %	12.1 %	7.7 %	3.8 %	
3+404	283.9	39.3 %	0.10	35.7 %	102.1 %	57.7 %	36.7 %	
3+420	284.5	33.9 %	0.10	30.8 %	76.4 %	46.2 %	30.2 %	
3+681	210.8	19.9 %	0.10	17.6 %	43.9 %	23.1 %	18.3 %	
3+733	237.7	12.9 %	0.10	11.7 %	26.0 %	15.4 %	11.0 %	
3+764	230.0	12.9 %	0.10	11.6 %	28.6 %	19.2 %	9.8 %	
3+795	222.6	3.0 %	0.33	2.3 %	6.4 %	2.4 %	1.2 %	

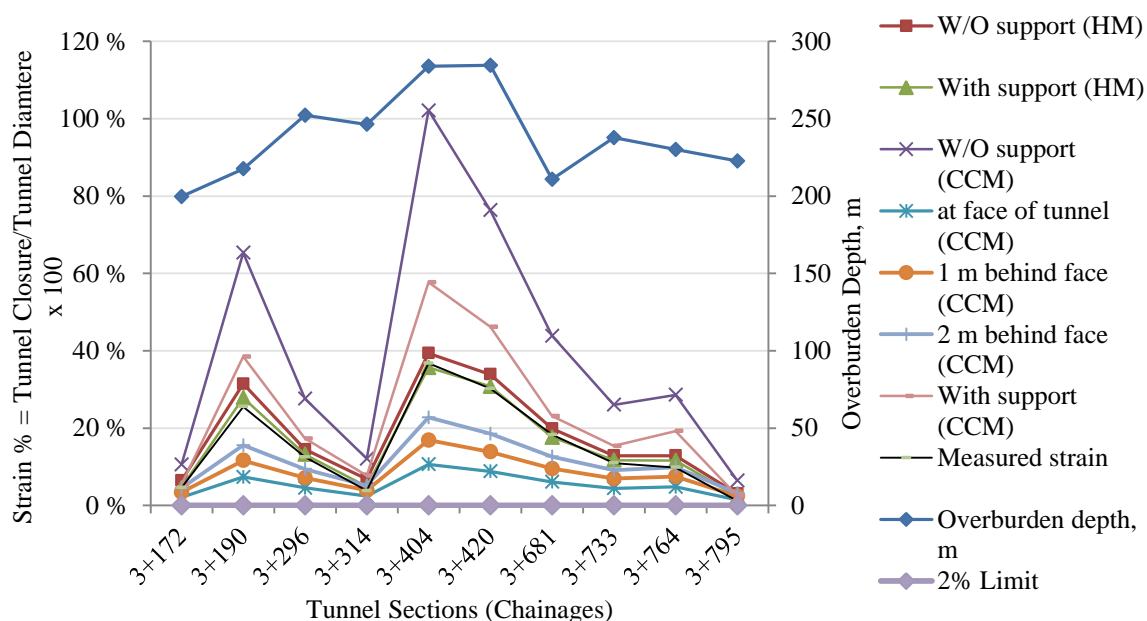


Figure 7-16: Comparison of strain percentage (with and without support) calculated using HM and CCM approaches with measured strain percentage

The highest values of tunnel wall deformation have been noticed in Figure 7-16 in case of the analysis without support using CCM for all tunnel sections. All the strain percentages are above 2% base line. Strain percentage at the face of tunnel (calculated using CCM) is lowest for all the sections but still higher than 2% base line that means there is no possibility of maintaining the tunnel section within the specified strain percentage in normal case. This could be achieved by improving the rock mass properties before tunnel excavation, which is already explained in section 5.4.4 in brief.

The measured tunnel strain is more or less equal to the strain calculated by HM approach in the case with support. The strain calculated by CCM in the case with support is slightly higher than measured value. The strain values; at tunnel face, 1m and 2m behind face are less

than measured value, which indicates that there could be the possibility of limiting strain value within these limits. For this, it will be necessary to provide supports with more capacity.

7.5 NUMERICAL ANALYSIS

Phase² program can be used to determine the deformation of tunnel wall closure. The value of tunnel wall closure will determine the condition of ground whether it is squeezed or not. In this thesis, Phase² program has been used to analyze squeezing phenomenon in CHEP case. At first, the back calculated intact rock strength along with other rock mass parameters has been taken as input to the program. The resulting deformation has been compared with measured deformation. The intact rock strength has been changed until the resulting deformation becomes equal to measured value. At that point, the intact rock strength value has been considered as more accurate value. The more detail procedure of using phase2 program in this thesis is explained in section 7-1 and Figure 7-1.

7.5.1.1 Back calculation of intact rock strength

For numerical analysis, four tunnel sections at different chainages have been selected. Among them, one section is selected in dolomite and three sections are taken in talcosic phyllite. The intact rock strength in each section is back calculated using Hoek and Marinos (2000) approach by taking measured strain percentage as input in equation 6-4. The back calculated strength is used as input in Phase2 model later in this chapter.

Table 7-12: Back calculation of intact rock strength using Hoek and Marinos (2000) approach

Chainage	Rock Type	Tunnel Depth	σ_0 , Mpa	σ_{ci} , MPa	Rock mass Strength, σ_{cm} , Mpa	Strength Stress ratio, σ_{cm}/σ_0	% strain w/o support, ϵ	Support Pressure, p_i , Mpa	Calculated % strain with support, ϵ	Measured % strain	σ_{ci} , Mpa, (Back calculation)
3+190	Dolomite	217.5	6.02	6.6	0.48	0.08	31.43 %	0.10	27.83 %	25.54 %	7
3+404	Talcosic phyllite	283.9	7.74	9.75	0.55	0.07	39.33 %	0.10	35.7 %	36.73 %	10
3+420	Talcosic phyllite	284.5	7.76	10.53	0.60	0.08	33.86 %	0.10	30.78 %	30.19 %	11
3+733	Talcosic Phyllite	237.7	6.48	13.65	0.81	0.12	12.87 %	0.10	11.69 %	10.96 %	14

Table 7-12 shows that the back calculated strength is more or less equal to estimated intact rock strength. The assumed residual support pressure, p_i , is taken from Table 7-9.

7.5.2 Input data in Phase2 program

For four tunnel sections, most of the input parameters are extracted from Table 7-1. The intact rock strength, σ_{ci} , is taken from Table 7-12 i.e. the back calculated value. In the program, field stress type is taken as gravity and initial element loading is considered as field stress and body force. Mohr-coulomb failure criterion is used to calculate the input data for material properties. The analysis has been done for both elastic and plastic material type.

Table 7-13: Input parameters for Phase2 analysis in each tunnel sections for both elastic and plastic analysis

Chainage	Rock Type	Field stress type	Initial element loading	Elastic type	Failure Criterion	Material type	Density, MN/m ³	Poisson's ratio	E _i Gpa	σ _{ci} Mpa	m _i	GSI	Stress Ratio	Support type
3+190	Dolomite	Gravity	Field stress and body force	Isotropic	Mohr coulomb	Elastic and plastic	0.028	0.150	7	7	10	17	0.176	R5
3+404	Talcotic phyllite	Gravity	Field stress and body force	Isotropic	Mohr coulomb	Elastic and plastic	0.027	0.100	7	10	8	14	0.111	R6
3+420	Talcotic phyllite	Gravity	Field stress and body force	Isotropic	Mohr coulomb	Elastic and plastic	0.027	0.100	7	11	8	14	0.111	R6
3+733	Talcotic Phyllite	Gravity	Field stress and body force	Isotropic	Mohr coulomb	Elastic and plastic	0.027	0.100	7	14	8	15	0.111	R6
Direction of Tectonic Stress						8 Degree, NE								
Direction of Tunnel Alignment						74 Degree, NE								
Angle between tectonic stress and tunnel alignment						66 Degree								
Tectonic Stress						3.5 Mpa								
Locked in Stress (in plane)						3.20 MPa								
Locked in Stress (out of plane)						1.42 MPa								

Table 7-13 gives input data required in phase2 program. The tectonic stress is taken as 3.5MPa. Phase2 program has already been used to estimate the tectonic stress for which more detail explanation is given in section 7.2.2.

Furthermore, RocLab software (www.rockscience.com) has been used to calculate the input parameters for material properties using Mohr-Coulomb failure criteria. Input data to the rock lab software are intact rock strength, GSI value, m_i, disturbance factor (D) and intact rock modulus (E_i). Output from the software is shown in Figure 7-17 for tunnel section at chainage 3+404m. Same principle has been used in other tunnel sections too.

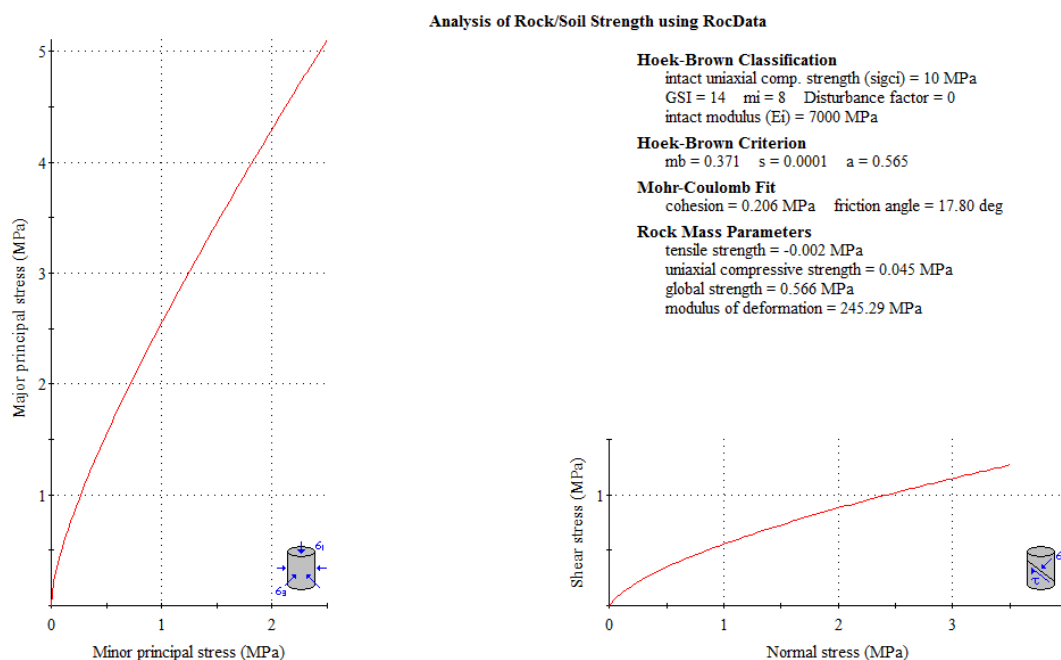


Figure 7-17: Typical output from rock lab software for tunnel section 3+404

Rock mass modulus has been calculated using the relationship given by Panthi (2006), which is explained more detail in section 7.2.6. For plastic analysis, the residual material parameters

has been taken as same as that for elastic analysis. The dilation angle has been considered one third of the friction angle as described in Phase² help.

Similarly, input data to the different support types are taken from Table 7-4 and Table 7-5. The drawings and specifications of different support types are given in appendix A2 and A3. Supports are applied only in crown and wall for whole analysis in order to follow the actual support application in field. The final lining i.e. concrete lining has not been applied in the model in order to match the analysis with actual situation and compare the displacement values with the values obtained from HM and CCM analysis and finally with measured value.

7.5.3 Phase2 model generation

The model for each tunnel sections has been created in Phase2 program. For the loading, field stress type is chosen as gravity and the option 'Use actual ground surface' has been selected to account for the effect of topography in stress development. The model has been generated for both elastic and plastic analysis and also for analysis with and without support application in each case. The typical Phase2 model for tunnel section 3+404 is shown in Figure 7-18 and closer look of excavation shape and support is shown in Figure 7-19.

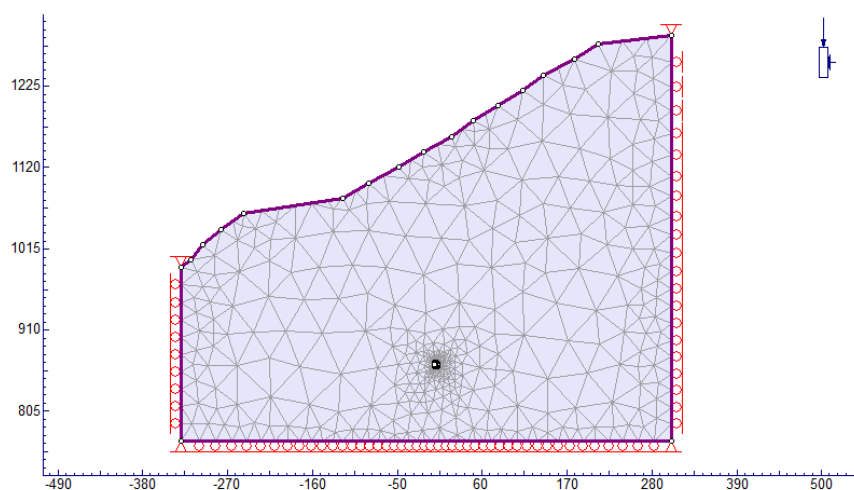


Figure 7-18: Finished model in Phase2 for tunnel section at chainage 3+404m

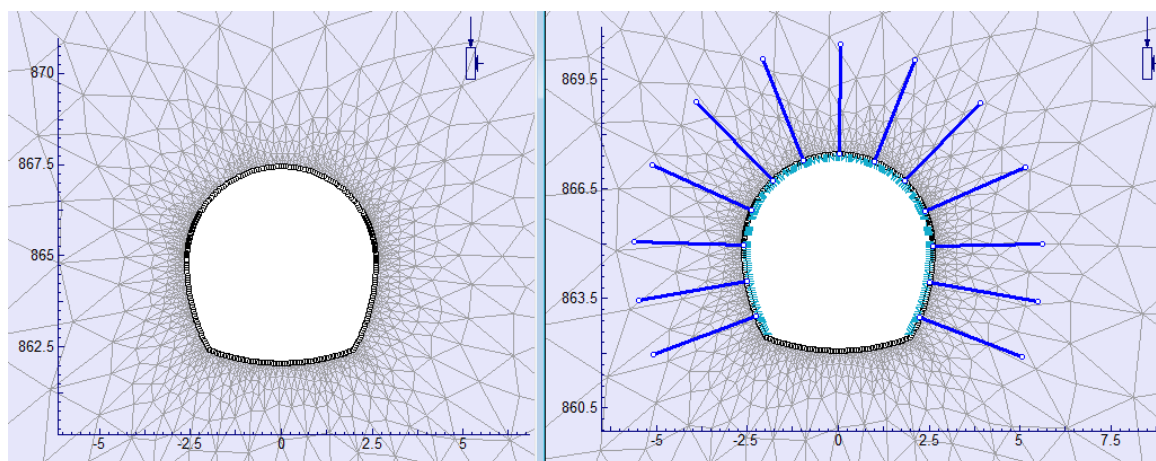


Figure 7-19: Closure view of tunnel excavation and support application for tunnel section at chainage 3+404m

Similarly, for other tunnel sections, the model has been generated and analyzed. The model generations for other tunnel sections are given in appendix D1.

7.5.4 Elastic Analysis

In elastic analysis, the material type is considered as elastic that means rock mass behaves elastically. The major concern of this analysis is to find the strength factor around tunnel periphery. In addition to strength factor, major principal stress and total displacement around tunnel contour has also been analyzed and compared for both the cases i.e. with and without support. The results are shown graphically in the following figures.

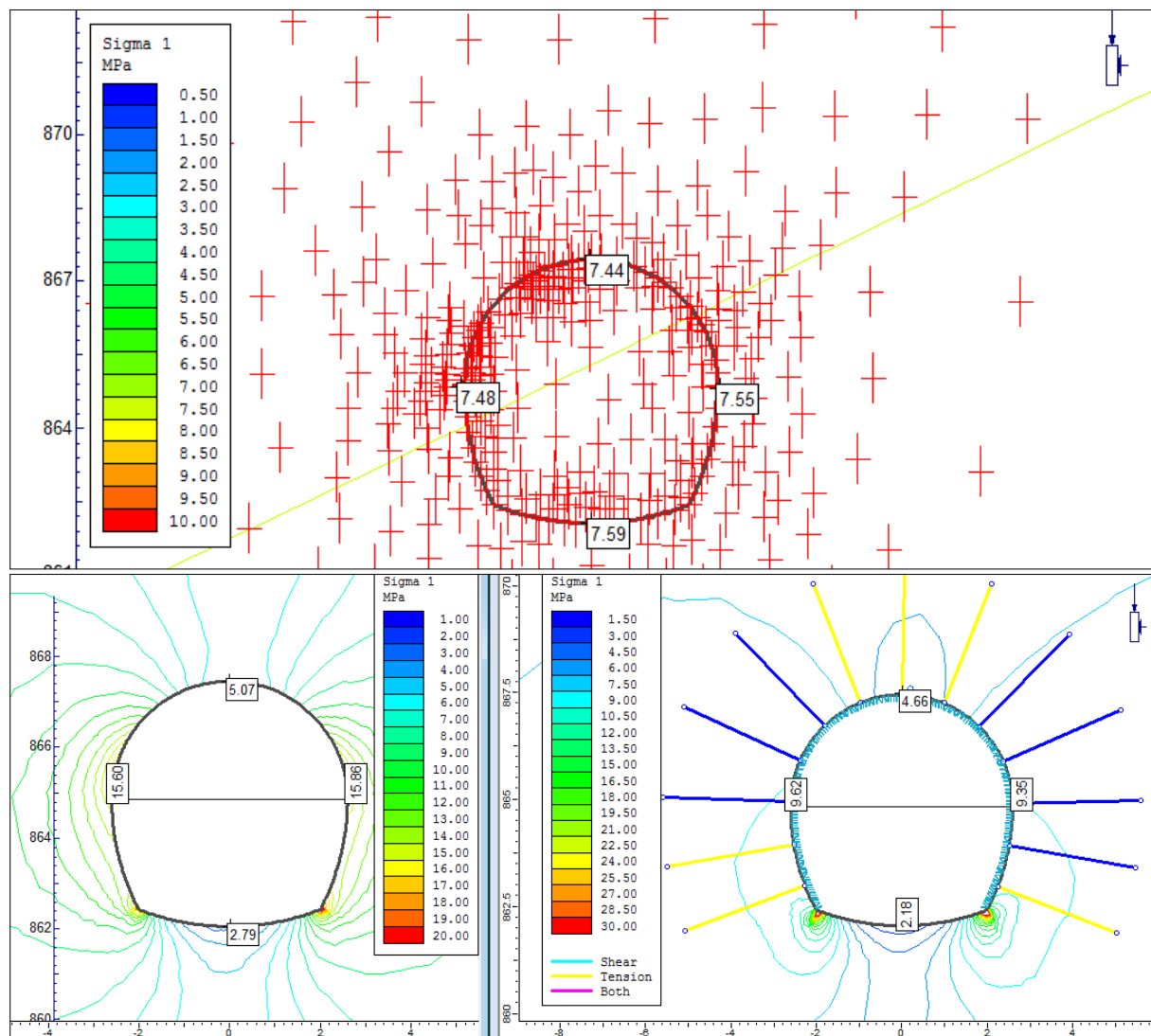


Figure 7-20: Major Principal Stress before excavation (top), after excavation (bottom left) and after excavation with support (bottom right) for section 3+404m (Elastic Analysis)

In Figure 7-20, it can be seen that the major principal stress is almost vertical that means there is not much effect of topography in stress development. After excavation, more stress is developed in side wall than in crown and invert. The result of analysis for other tunnel sections is shown in Appendix D2, D3 and D4.

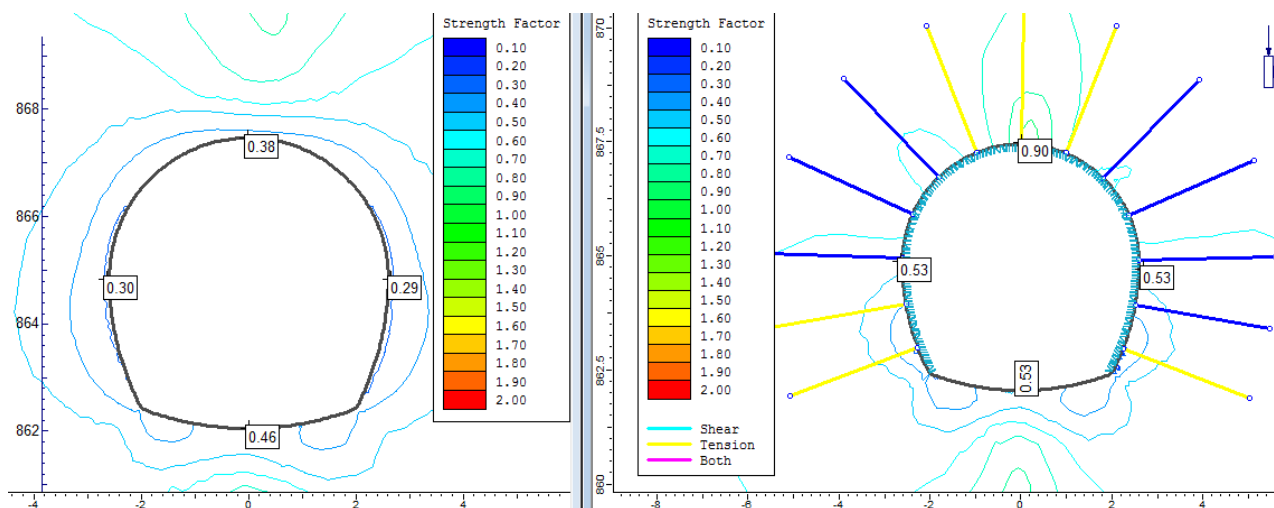


Figure 7-21: Strength factor before and after support application for section 3+404m (Elastic Analysis)

The strength factor is less than one around the tunnel contour in both cases (Figure 7-21). Results for other sections are given in Appendix D2, D3 and D4. If strength factor is less than one in elastic analysis, there will be failure of the material and for more additional information plastic analysis would be necessary (Phase2 tutorial no. 1). Strength factor is less than one for all the tunnel sections. Hence, plastic analysis has been done in each case and is discussed further in this chapter.

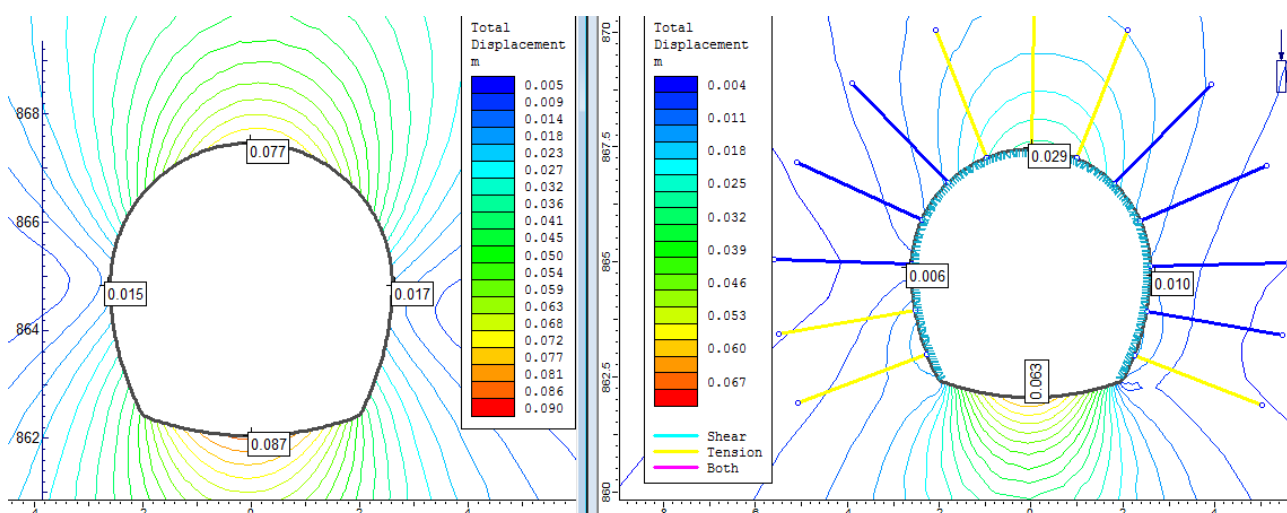


Figure 7-22: Total displacement before and after support application for section 3+404m (Elastic Analysis)

The displacement of wall, crown and invert is shown in Figure 7-22. The tunnel wall closure is very much less compared to measured value. Hence, more accurate result will be expected in plastic analysis. The displacement values in case of other sections are presented in Appendix D2, D3 and D4.

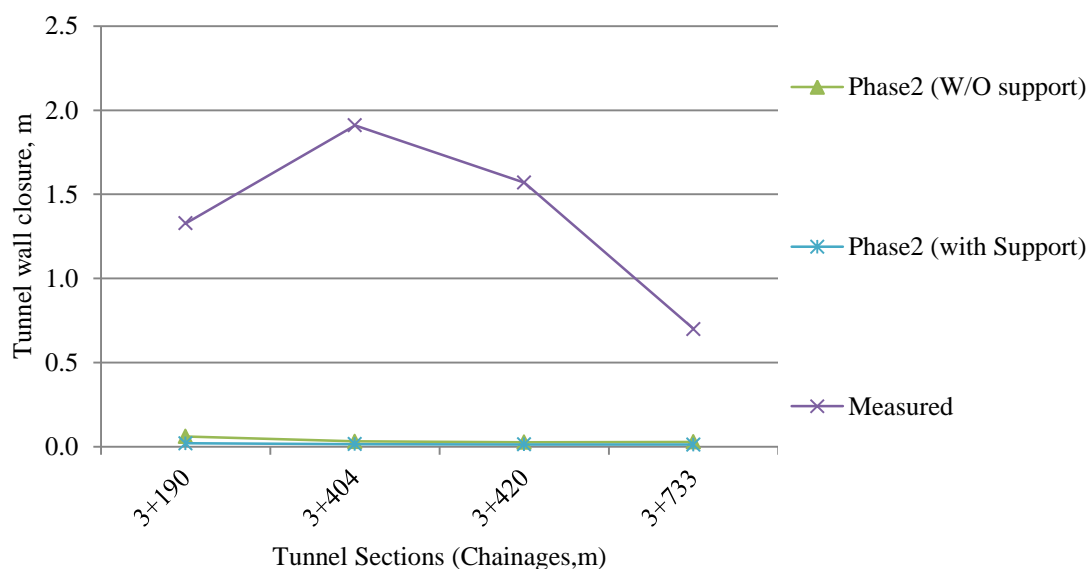


Figure 7-23: Tunnel wall closure at different tunnel sections from Phase² analysis (Elastic) and measured convergence

Figure 7-23 compares the tunnel wall closure from elastic analysis in phase2 at different tunnel sections with measured value. The analysis is for both the cases i.e. without and with support. The deformation values obtained from phase2 are low even in the range of millimeters. But the measured values are very high and in the range of meters. So, the elastic analysis is not representing the true analysis in CHEP case. Hence, the plastic analysis has been done for each tunnel sections further in this chapter.

7.5.5 Plastic analysis

The plastic analysis has been done for four tunnel sections to find the deformation around the tunnel with and without support. The deformation obtained from Phase² program has been compared with measured value. Then, the rock mass parameters are refined to match calculated deformation with measured value if there is discrepancy. The deformations in the tunnel were measured after the support application. Hence the result should be compared with that obtained in Phase² program after applying support. In order to follow the right order to apply the support in Phase² program, core replacement technique can be used. The detail of this technique is already explained in section 6.5.6.

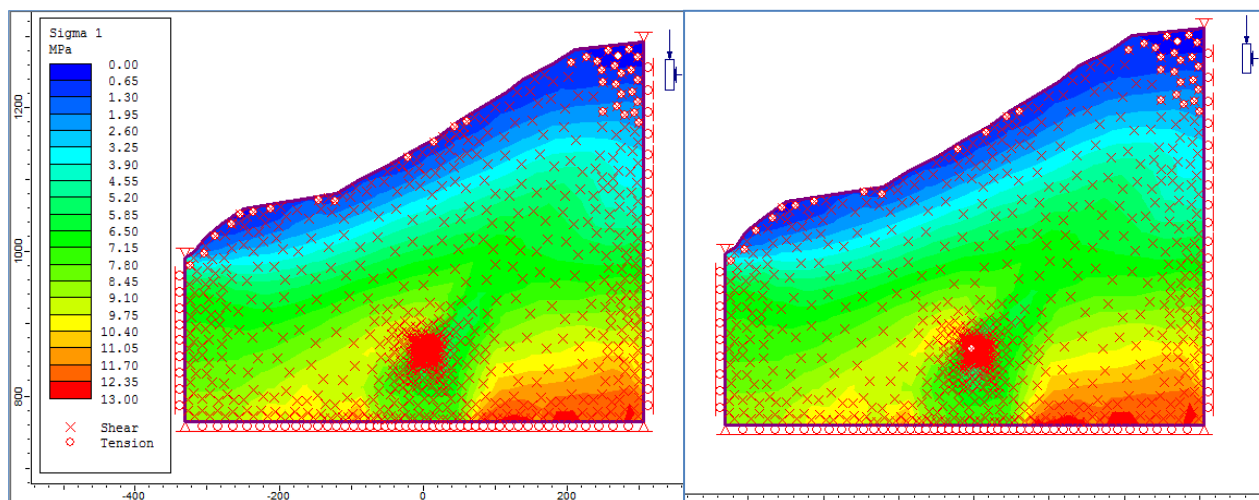


Figure 7-24: Sheared rock mass condition before tunnel excavation i.e. stage 1 (left) and after tunnel excavation i.e. stage 2 (right) in section at chainage 3+404m.

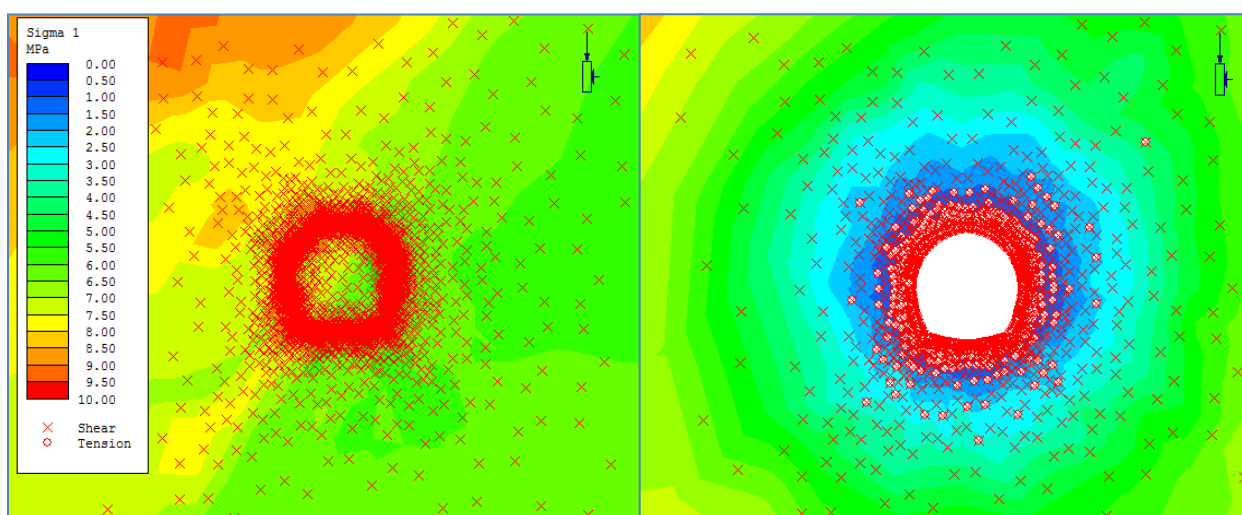


Figure 7-25: Closure view of sheared rock mass condition before (left) and after (right) tunnel excavation in section at chainage 3+404m.

One of the main tasks in core replacement technique is to find the plastic zone radius around tunnel after excavation. In order to find the plastic zone radius in Phase², the radius from centre of excavated tunnel is measured up to the point in surrounding rock mass where there is extent of failure in rock mass. But, in tunnel section at chainage 3+404m, the rock mass is already sheared before excavation (Figure 7-24). The closure view of sheared rock mass before and after excavation is shown in Figure 7-25. There is tensional failure around the tunnel after excavation but there is no clear line of demarcation of further shearing of rock mass due to opening of tunnel. Therefore it is very difficult to measure the radius of plastic zone in this tunnel section. Similar situation of rock mass condition has been found in case of other tunnel sections too. Hence, in this thesis, core replacement technique has not been used for the support application. The support is applied immediately after excavation (i.e. at stage 2 in all models) for all tunnel sections. The plastic analysis of tunnel section at chainage 3+404m is explained further in this chapter.

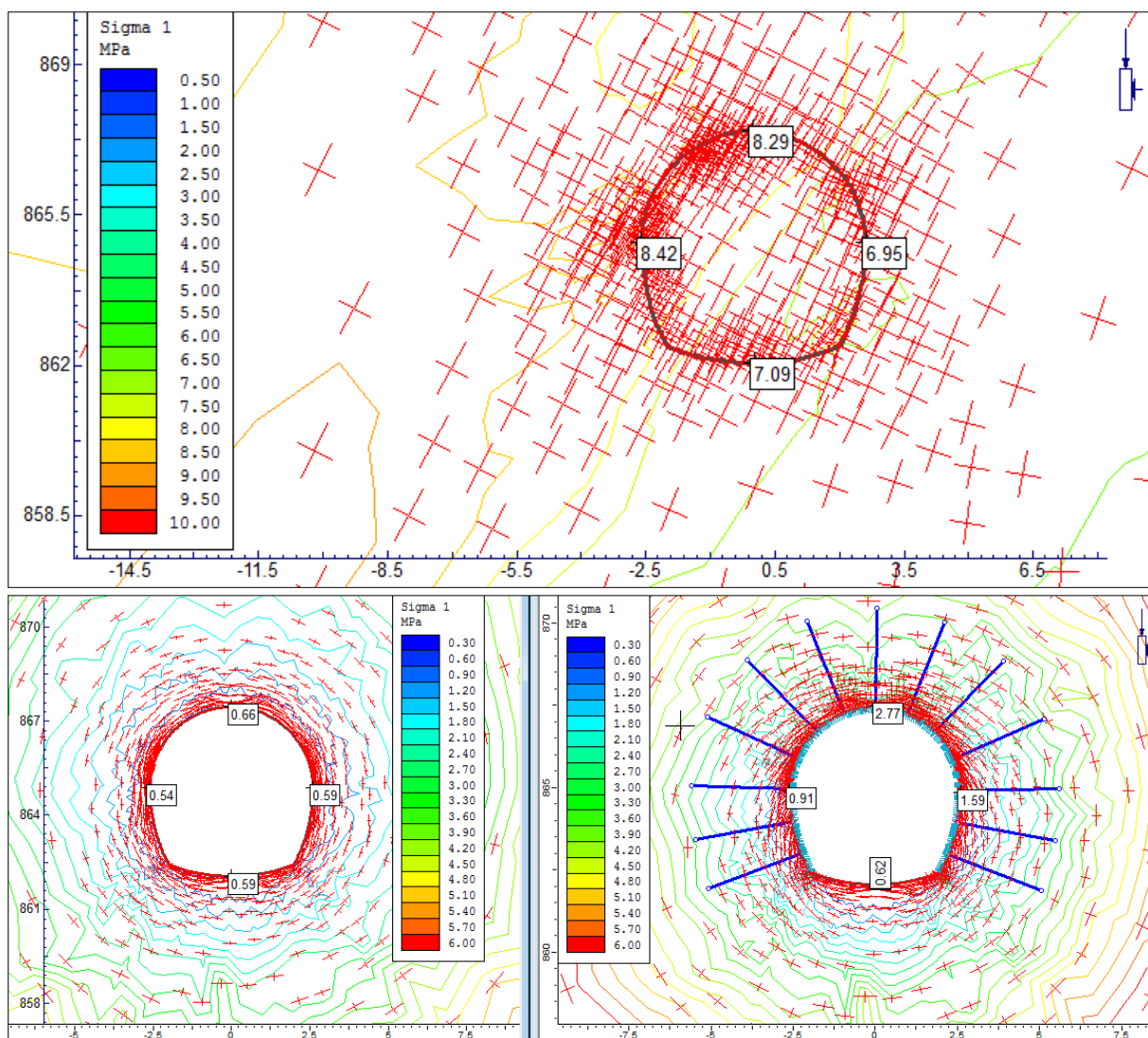


Figure 7-26: Major Principal Stress before excavation (top), after excavation without support (bottom left) and after excavation with support (bottom right) for section 3+404m (Plastic Analysis)

First of all the model was generated using the ground profile and tunnel shape (Figure 7-18). The input data from Table 7-13 and rock lab software were entered in the respective field. Then, the model was run and the result has been analyzed in the following ways.

Figure 7-26 (top) shows that there is significant effect of topography in stress development. The major principle stress at tunnel section is inclined towards hill side of section and significantly different around the contour of tunnel. Hence it is worthwhile to use the actual ground surface rather than using the constant field stress. Low value of stress is developed around the tunnel after excavation without support application (Figure 7-26, left) and a little bit higher value is developed due to support application (Figure 7-26, right).

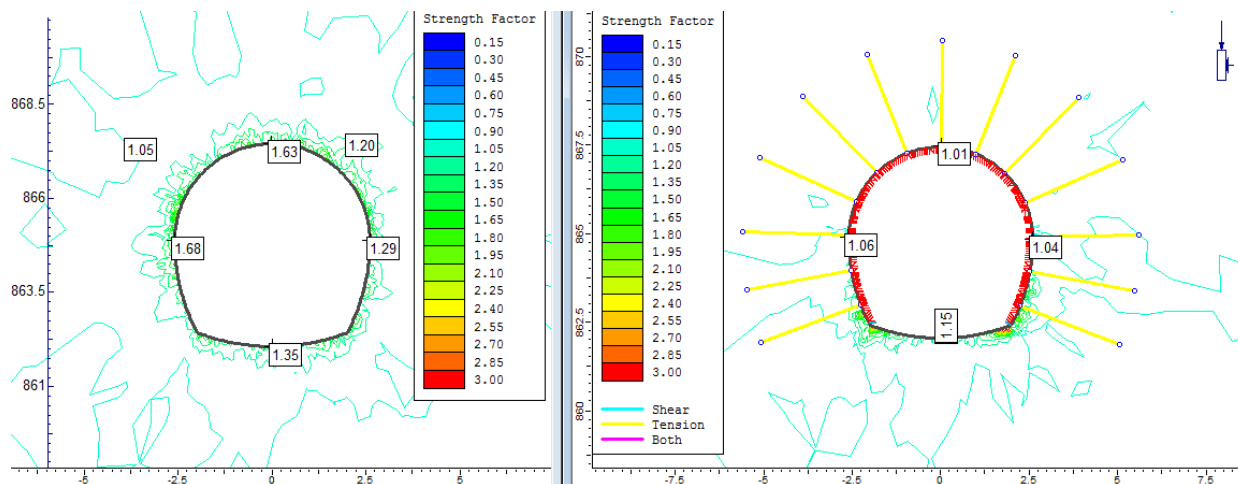


Figure 7-27: Strength factor before and after support application for section 3+404m (Plastic Analysis)

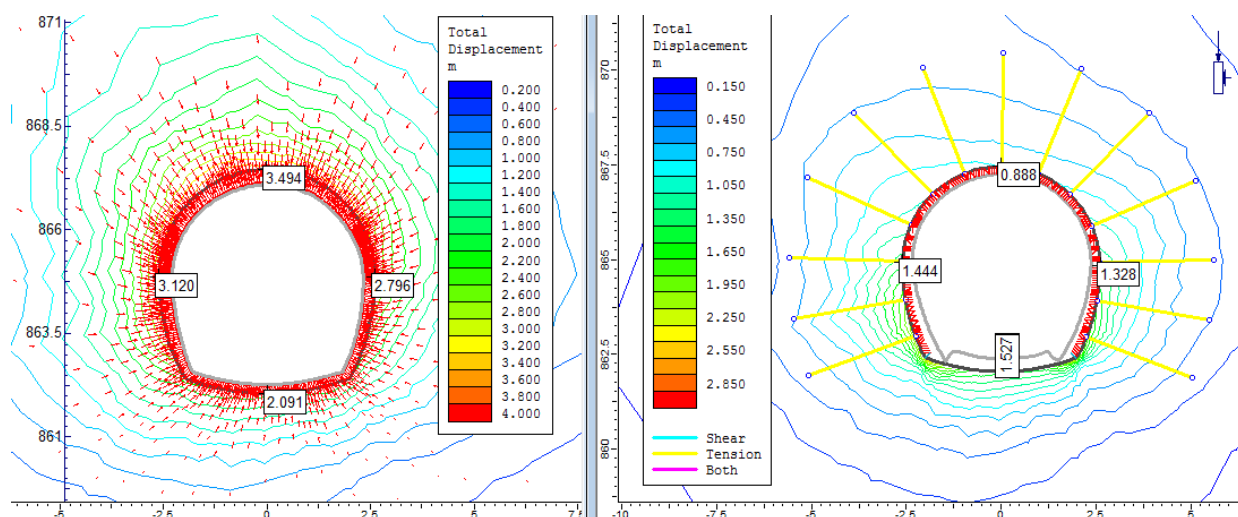


Figure 7-28: Total displacement before and after support application for section 3+404m (Plastic Analysis)

Figure 7-27 and Figure 7-28 show the strength factor and total displacement respectively. The analysis has been done for both cases i.e. with and without support. The strength factor is greater than one in both cases but higher in the case without support. The strength factor is reduced with the application of support. All the rock bolts and almost all the liner elements are ruptured. The total displacement is reduced with support application. The displacement at invert is not significantly reduced compared with wall and crown, which may be due to the reason that support is not applied at invert. However, the displacements are still significantly high even if the support is applied. The results of other sections are given in appendix D5, D6 and D7.

The main concern of the analysis is to calculate the displacement of tunnel. The displacement value will indicate whether there is squeezing or not. Table 7-14 shows the tunnel wall closure, crown and invert displacement in four tunnel sections from Phase² analysis with back calculated intact rock strength.

Table 7-14: Deformation of tunnel from Phase² program with back calculated intact rock strength from Hoek and Marinos (2000)

Chainages	Deformation, m										
	Without Support				With Support					Measured	
	No. of yielded elements	Tunnel wall closure	Crown	Invert	No. of yielded elements	No. of yielded Support elements	Tunnel wall closure	Crown	Invert	Tunnel wall closure	Crown
3+190	3330	11.99	6.520	3.77	3330	13 bolts and 239 liner	4.66	2.180	2.470	1.328	0.35
3+404	3256	5.9	3.494	2.091	3255	13 bolts and 238 liner	2.77	0.888	1.527	1.91	0.48
3+420	3282	6.5	3.376	2.38	3282	14 bolts and 236 liners	3.14	0.908	2.020	1.57	0.36
3+733	3233	1.4	0.690	0.44	3235	14 bolts and 235liners	0.689	0.190	0.400	0.7	0.1

The displacements with support obtained from Phase² analysis are significantly different from measured value. Therefore, intact rock strength is changed and the program is rerun again. The program has been rerun many times until and unless the displacements are more or less equal to measured value. Finally, the improved intact rock strengths are found and are given in Table 7-15. The Table 7-15 also shows corresponding displacement values, number of yielded elements, number of yielded support elements, etc.

Table 7-15: Improved rock mass properties and corresponding deformation values from Phase² program

Chainages	Improved σ_{ci} , Mpa,	Deformation, m										
		Without Support				With Support					Measured	
		No. of yielded elements	Tunnel wall closure	Crown	Invert	No. of yielded elements	No. of yielded Support elements	Tunnel wall closure	Crown	Invert	Tunnel wall closure	Crown
3+190	12.0	3322	2.05	0.950	0.807	3322	13 bolts and 239 liners	1.35	0.540	0.720	1.328	0.35
3+404	12.0	3250	4.0	2.200	1.5	3249	13 bolts and 238 liners	1.93	0.510	1.160	1.91	0.48
3+420	15.0	3272	2.8	1.480	0.98	3272	14 bolts and 236 liners	1.55	0.480	0.790	1.57	0.36
3+733	14.0	3233	1.4	0.690	0.44	3235	14 bolts and 235liners	0.689	0.190	0.400	0.7	0.1

As shown in Table 7-15, almost all the liner elements and bolt elements are failed. From phase2 analysis, it is difficult to estimate the support pressure. The support elements were also failed in the actual field. Hence, it can be concluded that the model with improved input parameters represents actual site condition. Figure 7-29 and Figure 7-30 clearly show that the tunnel wall closure with support is almost equal to measured tunnel wall closure and crown displacement with support is also almost equal to measured crown displacement. In that

situation, the intact rock strength and other input parameters are considered more accurate. The tables also show that the result with back calculated strength i.e. HM input without support is highest and not comparable with measured value, and the displacement is even more than tunnel diameter which is unacceptable. The analysis with improved input parameter, in the case without support, shows that the displacement value is high enough and represents the severe tunnel squeezing problems in all four sections.

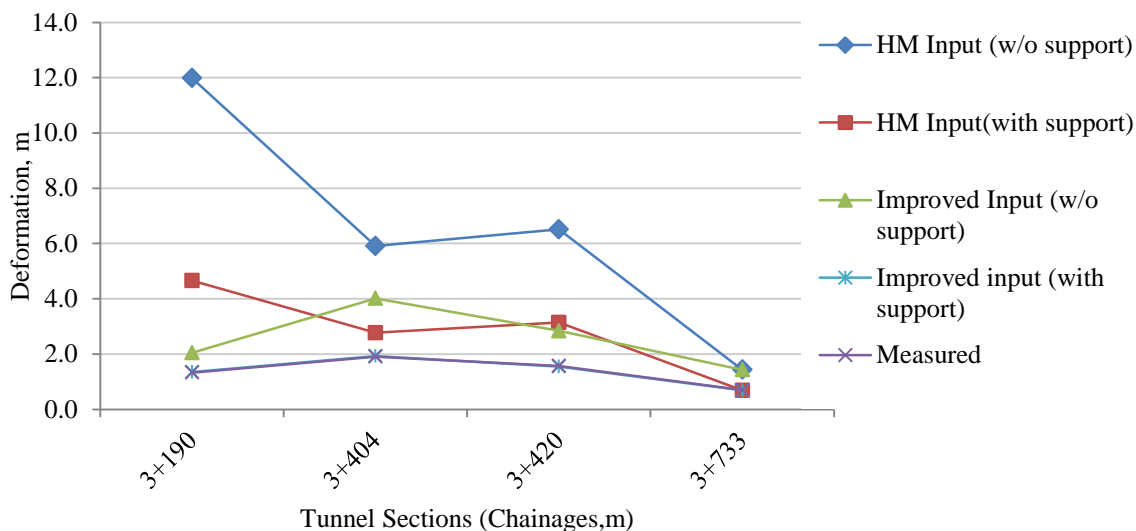


Figure 7-29: Total tunnel wall closure from Phase2 analysis and measured value for different tunnel sections

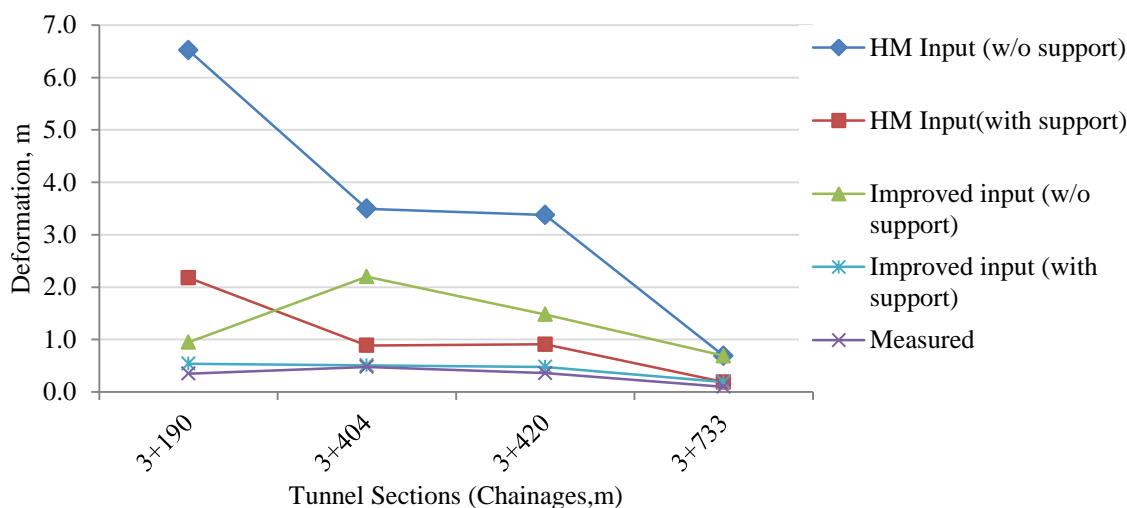


Figure 7-30: Crown displacement from Phase2 analysis and measured value for different tunnel sections

Figure 7-29 compares the improved rock strength with the back calculated strength using Hoek and Marinos (2000). The improved strengths are higher in first three sections and equal in last section. There is significant difference in first section, which may be either due to erroneous initial estimate of strength or due to measurement error in displacement. But in other sections, the difference could be acceptable. Here, in all analysis, the effect of water is

neglected. If the effect of water is considered in the analysis, intact rock strength will be higher for the same displacement value.

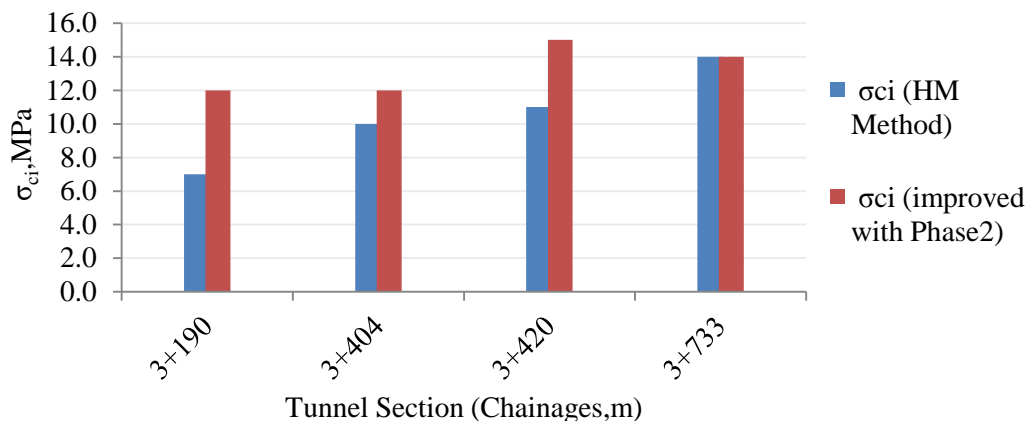


Figure 7-31: Comparison of intact rock strength back calculated from Hoek and Marinos (2000) with improved strength using Phase²

Rock mass quality in the squeezed tunnel stretch is weak, highly crushed and highly fractured. The analysis shows that the intact rock strength in that stretch will be in the range of 10 to 15 MPa. If it is compared with Appendix B0 (section 2.3.4), the table shows that grade of the rock is R2 and rock mass is weak.

7.6 COMPARISON OF THE RESULTS

The outputs obtained from different approaches are compared with each other and with measured value further in this section. Inputs to each method are the improved rock mass parameters. Four tunnel sections have been selected for the comparison. The analyses have been done for both the cases i.e. without and with support. The tunnel strain (%) has been found from the tunnel wall closure data that are already discussed earlier in this chapter. Here, tunnel strain (%) is the tunnel wall closure (%). For without support analysis, the result obtained from HM analysis has the lowest value and that obtained from phase2 has highest value (Figure 7-32).

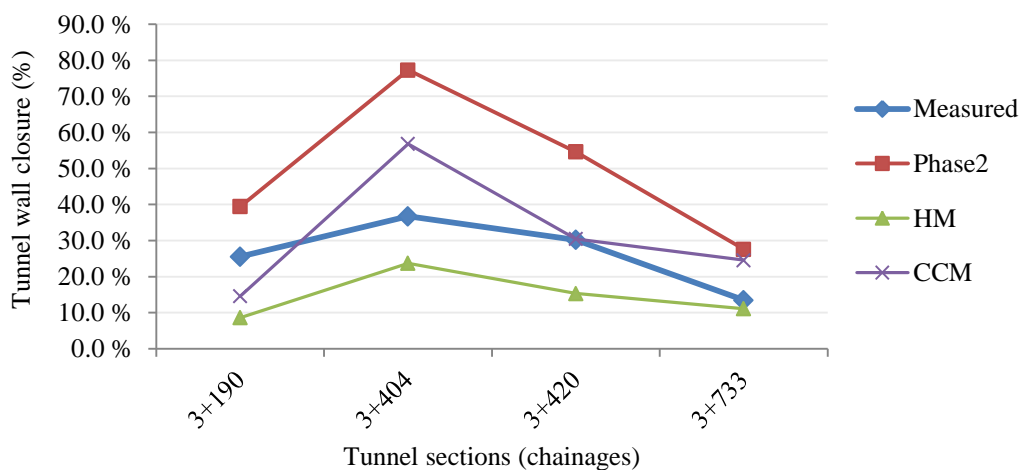


Figure 7-32: Tunnel wall closure in percentage without support from different methods using improved input intact rock strength

In the analysis with support, results obtained from Phase² is approximately equal to measured value whereas HM analysis shows the lowest values for all sections, and CCM analysis shows that for two sections, the results are more or less equal but for other two sections, it gives very low values compared with measured value (Figure 7-33).

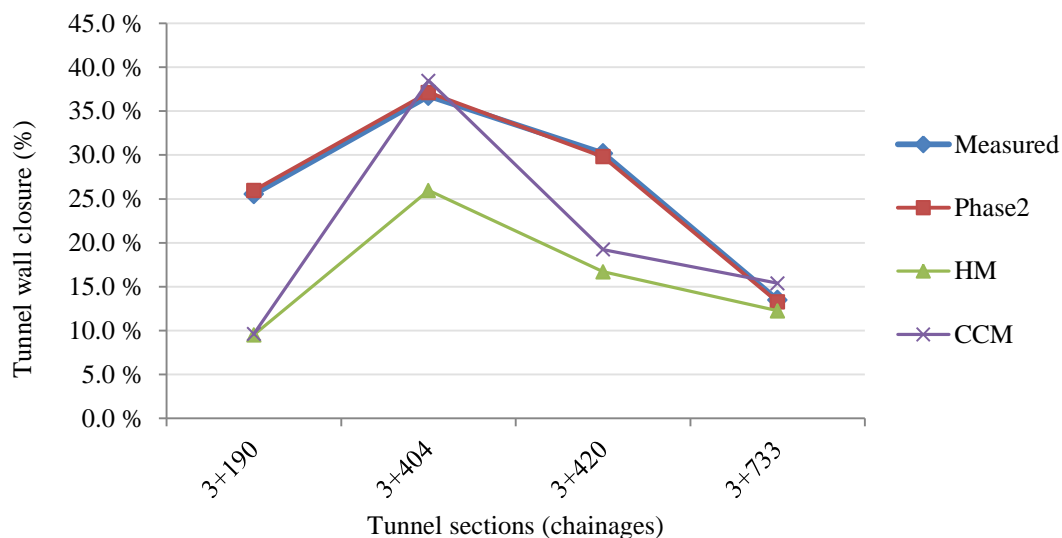


Figure 7-33: Tunnel wall closure in percentage with support from different methods using improved input intact rock strength

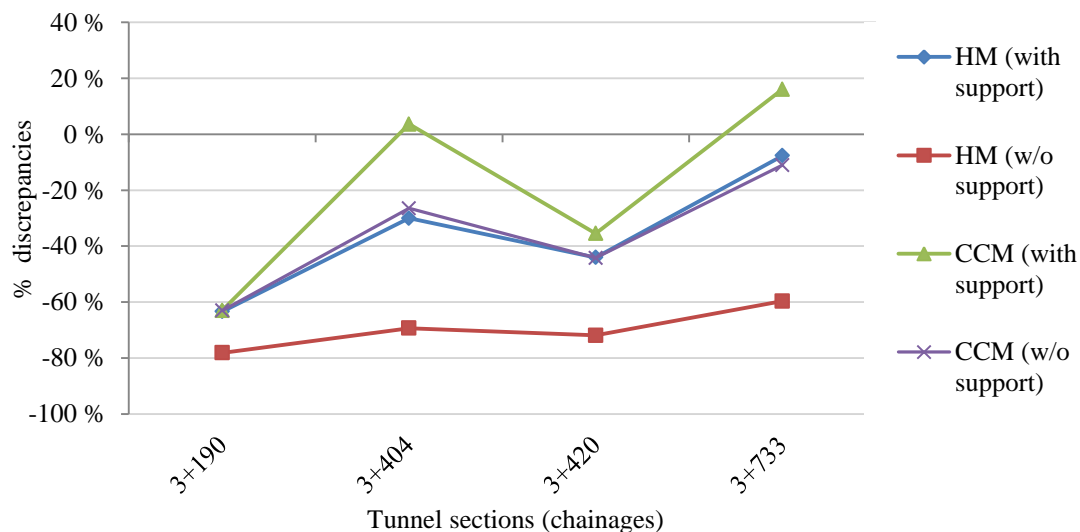


Figure 7-34: Discrepancies of results i.e. from HM and CCM with respect to Phase2 results for both cases; with support and without support

Figure 7-34 shows the difference (%) in the tunnel wall closure (%) obtained from HM and CCM analysis with respect to phase2 results for both the cases i.e. with and without support. There is more discrepancy in the result obtained from HM analysis than that from CCM analysis. In two sections, CCM analysis has comparatively less discrepancies. There are many reasons behind the discrepancy. One of the main reasons could be the different assumptions that are considered by each method. For e.g., HM analysis considers isostatic stress condition and circular tunnel section, CCM considers the initial stress equal to the

average of horizontal and vertical stress and circular tunnel section, and Phase² model considers the major and minor principle stresses developed due to gravity, topography and tectonic stress and real tunnel section i.e. horseshoe shape.

Furthermore, to verify the result obtained from HM analysis, Phase² program has been used by considering the constant isostatic stress field (equal to stress due to gravity) and circular tunnel section. The results are compared in both cases i.e. with and without support. Figure 7-35 shows the result of the analysis.

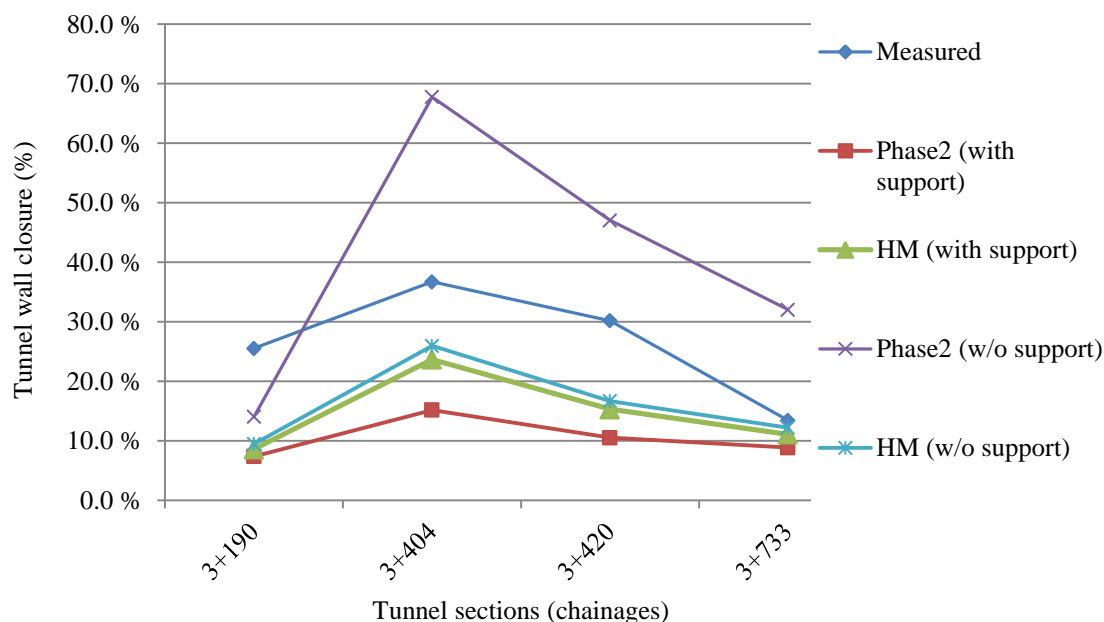


Figure 7-35: Comparison of Phase2 result with the deformation from HM analysis in case of isostatic stress condition and circular tunnel section in Phase2 model

The with support analysis shows that HM gives higher value than Phase² but the without support analysis shows that Phase² gives higher values than HM for all tunnel section.

8 EXISTING CHALLENGES AND POSSIBLE SOLUTIONS

The problems caused by squeezing in headrace tunnel of CHEP are already explained in chapter 4. Mainly, the problem is the reduction of tunnel cross section at several locations due to squeezing. To maintain the specified diameter, the tunnel has to be re-excavated in these locations. Importantly, squeezing in most of the sections has been stabilized but is active in some locations. In the active part, there will again be problem during re-excavation. In the squeezed part of the tunnel, concrete lining was proposed. But due to the excessive squeezing problem, the final concrete lining was not applied. Similar problems were encountered in Yacambú-Quibor tunnel, Venezuela. Solution of problems in Yacambú-Quibor tunnel is already explained in chapter 5.

8.1 RE-EXCAVATION OF SQUEEZED SECTION

Due to excessive deformations, the excavated profile has moved inside the design profile in several stretches, which would need reshaping of tunnel profile. There are also temporary supports erected at several places to retain squeezing. In addition to temporary support, there are also buckled and distorted steel ribs, lattice girders, invert struts and cracked shotcrete at several stretches. These will have to be removed before reshaping of profile which could result further deformation and instability. Hence, there are so many difficulties to re-excavate the tunnel to make it operational.

In the stretches where squeezing effect has ceased, the profile will be reshaped easily and a final lining will be installed afterwards. But, in the stretches where deformations are still continuing, reshaping will have to be done with some extra room for installing a deformable primary support to safeguard the crews and then final lining will be provided. The second situation is really a difficult problem during re-excavation.

8.2 FINAL LININGS

Reshaping of tunnel section could be done in two ways; in first option the tunnel will be to reshape again in horseshoe type and final concrete lining to be provided as specified in appendix A2, and in second option the tunnel to be made circular and final lining (shotcrete and steel ribs) to be provided afterwards. Both of these solutions are explained further in this chapter. Phase² program has been used to analyze the stability and to find the deformation of tunnel after the final lining.

8.2.1 Concrete lining in horse shoe shape

After reshaping of tunnel in horseshoe shape, the concrete lining as specified in appendix A2 will be applied. Phase² program has been used to analyze the stability and to determine the deformation around tunnel contour. For the analysis, four tunnel sections at chainage 3+290m, 3+404m, 3+420m and 3+733m has been chosen. For the first tunnel section, support type R5 was proposed where the concrete lining of thickness 0.3m was specified and for other three sections, support R6 with 0.4m concrete lining was proposed by the project. In phase2 model, the concrete lining having young's modulus 35000MPa, Poisson's ratio 0.2, compressive strength 35MPa and tensile strength 3MPa has been used. The effect of rock

bolts and shotcrete linings that were applied at the time of excavation has been neglected because most of them are already failed and most of them will be removed during re-excavation, however reapplication will be done at necessary sections.

The analysis shows that the deformation is within 3% in last three sections and maximum 6.5% in first section (Figure 8-1 and Figure 8-2). Figure 8-11 also shows that most of the liner elements are failed. The higher deformation value obtained in first section can be reduced by using 0.4m concrete lining instead of 0.3m.

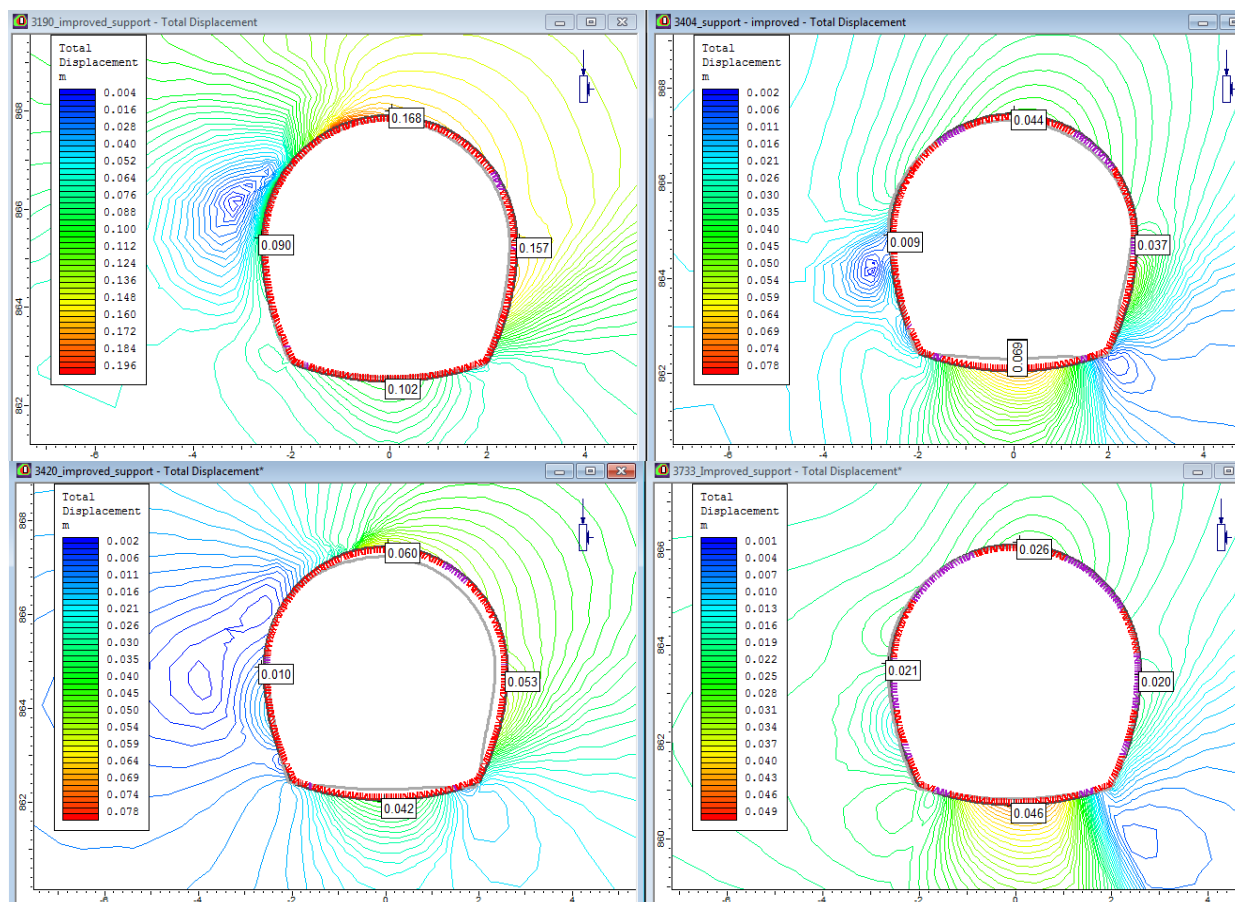


Figure 8-1: Deformation after concrete lining in tunnel sections at chainage 3+190m (top left), 3+404m (top right), 3+420m (bottom left) and 3+733m (bottom right)

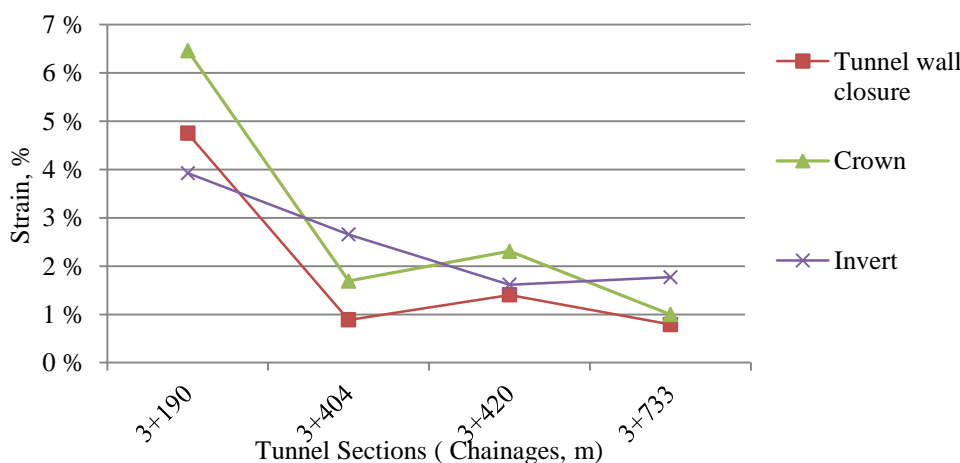


Figure 8-2: Tunnel strain (%) in different location of tunnel contour (with concrete lining)

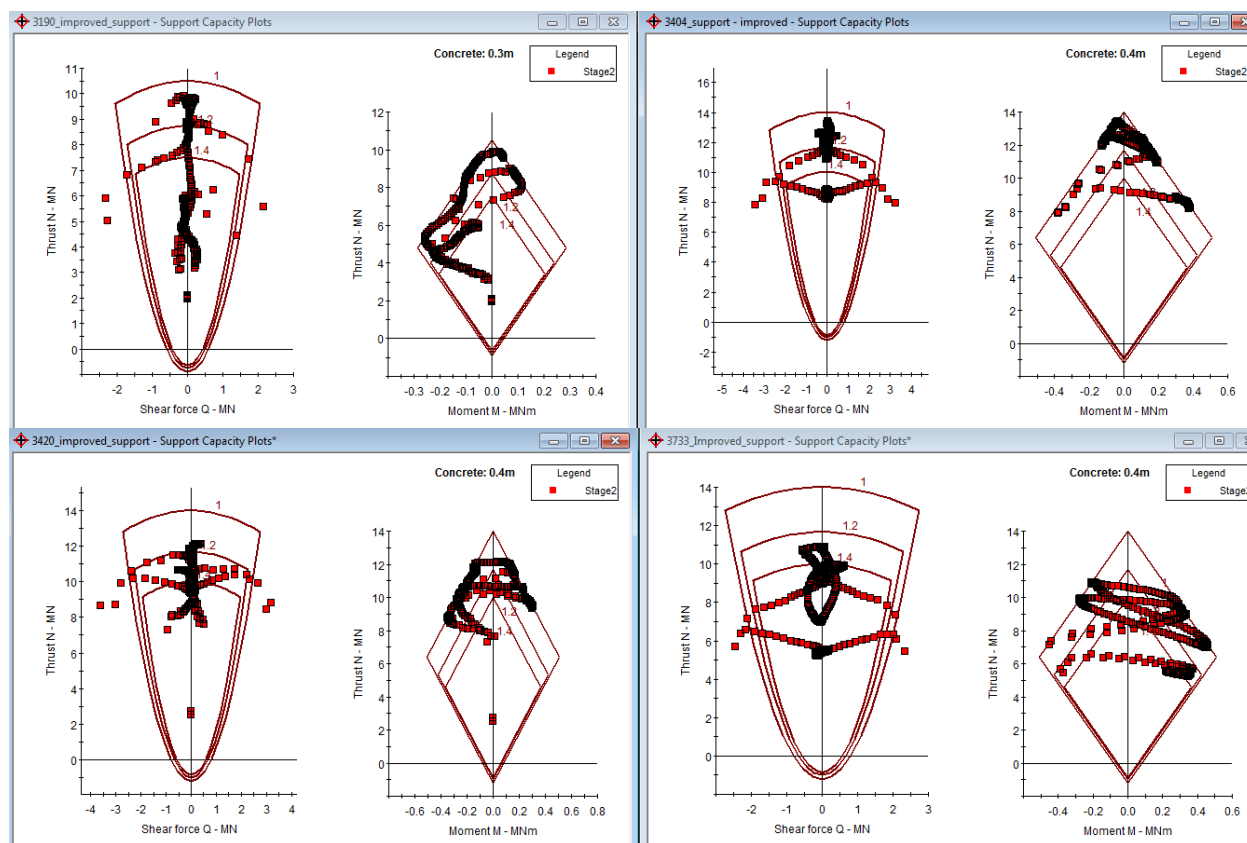


Figure 8-3: Support capacity plots of concrete lining in tunnel sections at chainage 3+190m (top left), 3+404m (top right), 3+420m (bottom left) and 3+733m (bottom right)

Some of the lining elements have factor of safety less than one, most of them have 1 to 1.4 and very few have more than 1.4 (Figure 8-3). Hence, the support capacity with factor of safety below 1.4 is inadequate that means there will be high chance that the support will fail in near future with the time dependent long term deformations.

8.2.2 Steel ribs and shotcrete lining in circular shape

Another solution to the squeezing section will be to apply the final lining after the reshaping of tunnel into circular shape with diameter 5.4m. Again, four same tunnel sections have been considered for the analysis as considered in section 8.2.1 and phase2 program has been used for the stability analysis and deformation calculation. The final linings will contain steel ribs and shotcrete with thickness 0.6m. The steel ribs will be W150x24 with spacing 0.8m and yield strength of 350 MPa. The shotcrete lining will consist of 0.6m thick; 25000MPa young's modulus, 0.25 Poisson's ratio, 30MPa compressive strength and 2MPa tensile strength. The same lining system with little different specifications was proposed in Yacambú-Quibor tunnel, Venezuela in squeezed section. Again, the effect of rock bolts and shotcrete linings that were applied at the time of excavation has been neglected because most of them are already failed and most of them will be removed during re-excavation.

The analysis shows that some of the lining elements are failed and rest are working well. The deformation is within 1% in last three sections but in first section it is from 2.5% to 3.5%

(Figure 8-4 and Figure 8-5). The higher deformations in this section will be due to very weak rock mass condition.

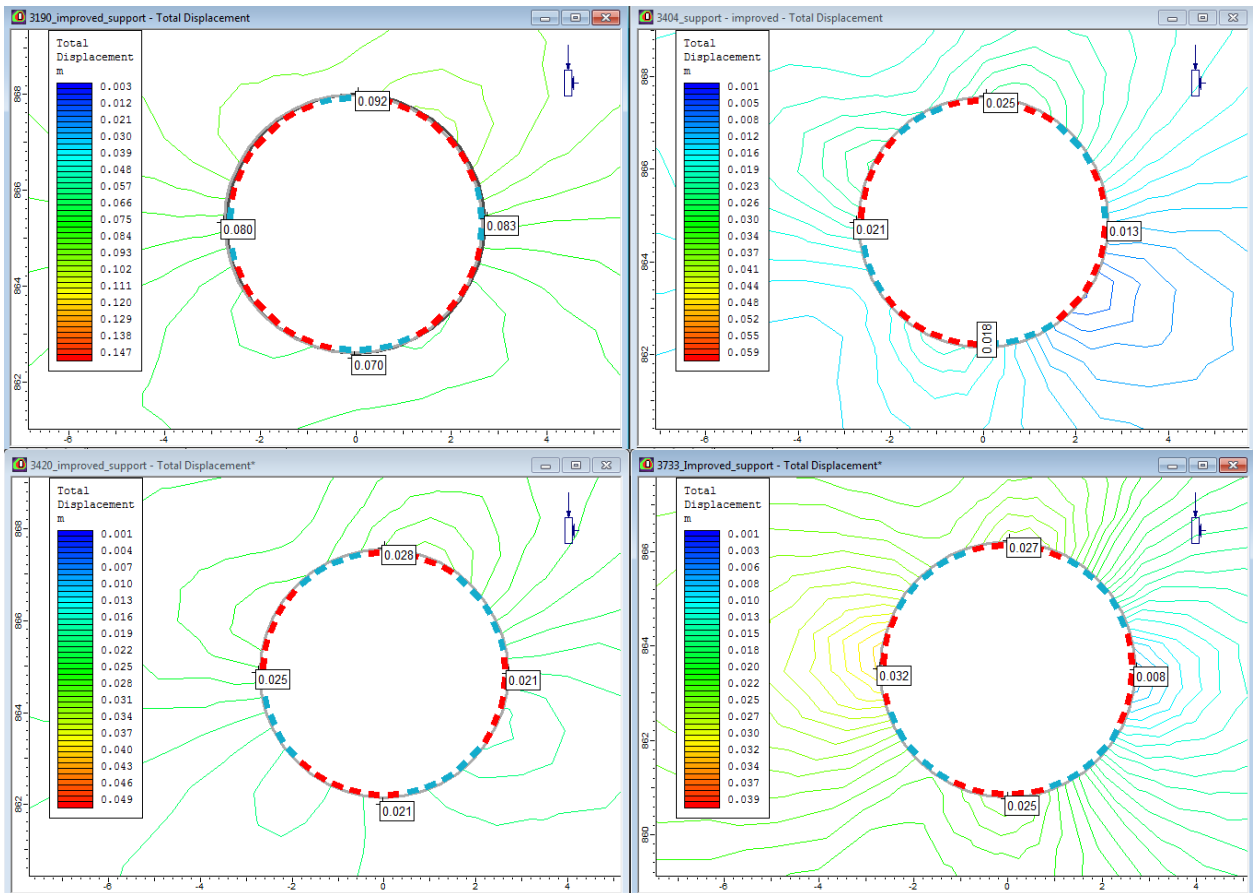


Figure 8-4: Deformation after final lining in tunnel sections at chainage 3+190m (top left), 3+404m (top right), 3+420m (bottom left) and 3+733m (bottom right)

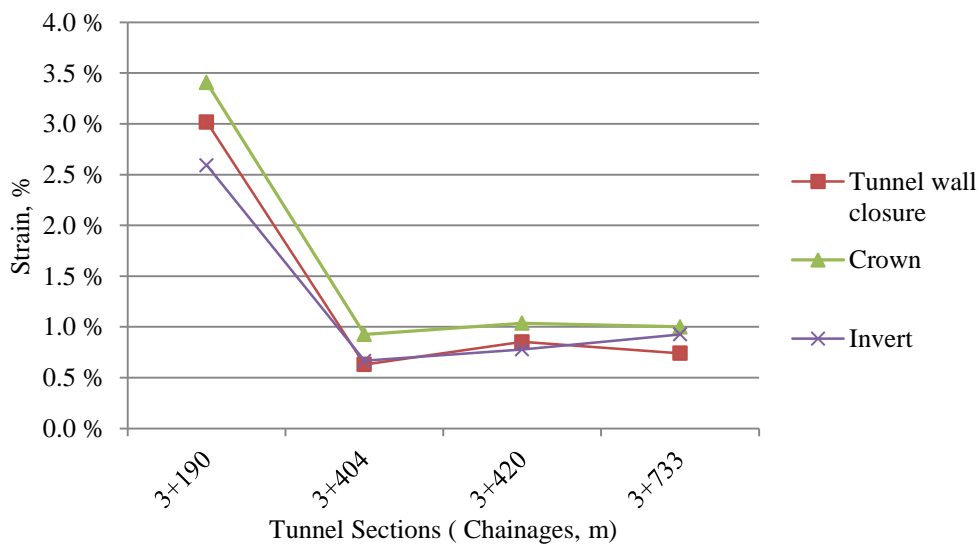


Figure 8-5: Tunnel strain (%) in different location of tunnel in circular shape (With steel ribs and shotcrete)

The support capacity plots of steel ribs and shotcrete for all tunnel sections are given in appendix D8. The plots show that the steel ribs works with factor of safety more than 1.4 that means it is safely working. But in case of shotcrete linings, most of the elements work within factor of safety 1 to 1.4, which may cause failure of lining elements with increase in deformation due to creeping (time dependent deformations). After application of full linings, the diameter of tunnel will be 4.2m which is acceptable.

8.3 COMPARISON BETWEEN THE POSSIBLE SOLUTIONS

Two different solutions have been proposed for the final linings after excavation. The first one was already proposed during the study phase of project and was concrete lining with horseshoe shape. The application of concrete lining will take more time to be stabilized and there will be the possibility of squeezing before the lining comes into work. So, utmost care should be taken during lining application. The second option is proposed based on the experience of Yacambú-Quibor tunnel, Venezuela to overcome squeezing problem. The final lining consists of steel ribs and shotcrete with circular shape. The analysis shows that second option works better than first option assuming that the situation will be maintained accordingly during real application. The difficulty in second option will be to make the tunnel in circular shape and to apply the support in right order.

9 CONCLUSIONS AND RECOMMENDATIONS

9.1 CONCLUSIONS

In the Himalaya region, squeezing phenomenon is very common in hydropower tunnels. Because of very weak, highly schistose and fractured rock types and high tectonic stress, squeezing has been experienced even in the lower overburden. Hence, analysis of squeezing phenomenon to find the correct deformation values could be a challenge to tunnel engineers in this region for the successful tunneling. One of the hydropower projects, CHEP, has been chosen for the analysis where there is significant tunnel squeezing. The problem is believed to be due to overstress of rock mass that means rock mass strength is less than induced tangential stress around the tunnel periphery.

The headrace tunnel of CHEP is facing squeezing problems in an about 800m long stretch, from chainage 3+100m to 3+900m, out of total length 4067m. The rock mass quality is extremely poor and rock type is talcosic phyllite in the squeezed section. At several locations in squeezing section, the tunnel wall closure (deformation) is well over 1.0 m and the maximum is recorded above 2.0 m. Due to severe squeezing and associated deformation, tunnel cross section has reduced considerably in several stretches of tunnel. The final concrete lining is not applied yet. The tunnel needs to be reshaped before applying the final lining and making the tunnel operational. Buckled and distorted steel ribs, lattice girders and invert struts and cracked shotcrete at several places would need rectification and temporary supports erected at several places would need to be removed.

In this study, four main methods have been used to analyze the squeezing phenomenon viz.; empirical methods such as Singh et al (1992) and Q-system (Grimstad and Barton, 1993), semi-analytical method such as Hoek and Marinos (2000), analytical method such as Convergence Confinement Method (Carranza-Torres and Fairhurst, 2000) and numerical program Phase². The inputs to squeezing analysis in each method are rock mass parameters and rock stresses. Therefore, quality of analysis largely depends upon the correct estimation of these input parameters. From the analysis, the tectonic stress value has been found to be equal to 3.5MPa in this area, but stress measurement will be necessary to verify this value. Following conclusions has been made from the squeezing analysis using different approaches;

- The main challenge that has been faced in squeezing analysis is the correct estimation of rock mass parameters. However, the input parameters have been estimated with the help of different reports, literatures and discussion with Supervisors. Q-value, estimated during face mapping, helped a lot in the analysis to use different methods.
- In CHEP headrace tunnel, in the beginning of analysis, seventeen tunnel sections at several locations have been taken into consideration. The squeezing prediction criteria, such as Singh et al (1992), Q-system and Hoek and Marinos (2000) approach, have shown that there is severe squeezing in last ten sections. Hence more detail squeezing analysis and support pressure estimation have been done for

these ten sections using Hoek and Marinos (2000), CCM and Barton et al. (1974) approaches. The HM and CCM analysis show that there will be significant amount of tunnel deformation to cause squeezing problems.

- Singh et al (1992) method gives the condition of ground whether there will be squeezing or not but it does not give the amount of tunnel wall deformation and support pressure. The difficulty in this method is the estimation of correct value of SRF (one of the term in Q) in some cases. The selection of SRF value is very sensitive for the correct estimation of Q-value. Also, this approach does not consider the rock mass strength.
- Hoek and Merinos (2000) method gives the amount of tunnel wall deformation and also considers the support pressure. But it does not consider the tunnel wall deformation at the time of support application and also does not specify the yielding of support. It considers only the isostatic stress condition but in reality there will be considerable difference in stresses in different directions. However, it can be used to get the useful information at the beginning of analysis. It also gives the grade of squeezing phenomenon in terms of tunnel wall closure percentage.
- The analytical method, CCM, is quite useful method to find the tunnel wall deformation and support pressure required to maintain the deformation within the specified limit. The deformation of the tunnel wall at the time of support application can be calculated with the help of LDP. It gives the information regarding the yielding of different types of supports with factor of safety. This approach considers the shape of tunnel with circular cross-section. For other shape tunnel shape, it uses equivalent diameter of tunnel section, which will not represent the reality.
- Phase² program has been used in four sections to improve the rock mass parameters taking the measured deformation as basis. From analysis, it is found that improved rock mass parameters are slightly different from estimated rock mass parameters. The improved value of intact rock strength has been found to be in the range of 10 to 15Mpa in the squeezed section. Then, deformation has been calculated using improved rock mass parameters as input to different approaches such as HM, CCM and Phase². All methods show that there is significant squeezing problem in all four tunnel sections but show slightly difference results.
- Although the numerical modeling cannot be used directly to analyze the squeezing phenomenon in the tunnels, its application can be utilized to find the deformation of the tunnel in squeezing environment and the results can be compared with the results that have been found from analytical and semi-analytical approaches. The numerical analysis will help to define the complex nature of the rock mass and geometry of opening, and the results can be found as close to the reality.
- Re-excavation and reshaping of tunnel profile is very difficult task in case of squeezed part of CHEP headrace tunnel. In addition to this, the final lining after excavation is another difficult task. In the stretches where squeezing effect has ceased, the profile will be reshaped easily. But, in the stretches where deformations are still continuing, reshaping will have to be done with some extra

room for installing a deformable primary support to safeguard the crews and then final lining will be provided. The second situation is really a difficult problem.

- Two different possible solutions have been studied for the final linings after excavation (concrete lining and shotcrete lining with steel ribs). The analysis shows that second option works better than first option assuming that the situation will be maintained accordingly during real application. The difficulty in second option will be to make the tunnel in circular shape and to apply the support in right order.

9.2 RECOMMENDATIONS

There are many limitations in this thesis. These limitations can be improved with some more efforts on the analysis. Following major points have been recommended for the further analysis;

- Stress measurement is necessary to verify the estimated value.
- Support characteristics curve for different support types can be improved by taking input parameters of the materials that were applied in actual field.
- Intact rock strength measurement is necessary to verify the estimated and back calculated value.
- The effect of water has not been considered in the analysis in this thesis. The results can be improved considering the water effect in the analysis that will give slightly higher value of rock mass strength for the same measured deformation.
- Correct timing and sequence of the support application could be done using convergence confinement analysis.
- Steel lining will be another possible solution to address the existing problem in squeezed part that may avoid the reshaping of tunnel profile.
- Optimization of hydraulically equivalent tunnel section for different final linings can be done further, which will result optimized tunnel size and lining option. This study will help to address whether there is necessary to increase the tunnel size or the squeezed tunnel size is enough to carry the specified amount of water.

REFERENCES

- Aydan, Ö., Akagi, T. and Kawamoto, T., 1993. The squeezing potential of rocks around tunnels; theory and prediction. *Journal of Rock Mechanics and Rock Engineering*.
- Barton, N., 1995. The influence of joint properties in modelling jointed rock masses, 8th ISRM congress.
- Barton, N., 2002. Some new Q -value correlations to assist in site characterisation and tunnel design. *International Journal of Rock Mechanics and Mining Sciences*.
- Barton, N., Lien, R. and Lunde, J., 1974. Engineering classification of rock masses for the design of tunnel support. *Journal of Rock mechanics*.
- Baumann, T. and Betzle, M., 1984. Investigation of the performance of lattice girders in tunnelling. *Rock mechanics and rock engineering*.
- Beavis, F., 1985. *Rock weathering. Engineering geology*. Blackwell Scientific, Melbourne.
- Bieniawski, Z., 1973. Engineering classification of jointed rock masses. *Journal of Civil Engineer in South Africa*.
- Bieniawski, Z.T., 1975. The point-load test in geotechnical practice. *Engineering Geology*, 9(1): 1-11.
- Brady, B.H. and Brown, E.T., 2007. *Rock mechanics: for underground mining*. Springer.
- Broch, E. and Franklin, J.A., 1972. The point-load strength test. *International Journal of Rock Mechanics and Mining Sciences & Geomechanics Abstracts*, 9(6): 669-676.
- Brown, E.T. and Brady, B.H.G., 1985. *Rock Mechanics for Underground Mining*.
- Carranza-Torres, C. and Fairhurst, C., 1999. General formulation of the elasto-plastic response of openings in rock using the Hoek-Brown failure criterion. *Int. J. Rock Mech. Min. Sci.*
- Carranza-Torres, C. and Fairhurst, C., 2000. Application of the Convergence-Confinement method of tunnel design to rock masses that satisfy the Hoek-Brown failure criterion. *Tunnelling and Underground Space Technology*.
- Chern, J., Shiao, F. and Yu, C., 1998. An empirical safety criterion for tunnel construction, *Proceedings of the Regional Symposium on Sedimentary Rock Engineering*, Taipei, Taiwan.
- Dahal, R.K. and Hasegawa, S., 2008. Representative rainfall thresholds for landslides in the Nepal Himalaya. *Geomorphology*.
- Deoja, B.B., 1991. Risk engineering in the Hindu Kush-Himalaya. *ICIMOD*.
- Duncan Fama, M., 1993. Numerical modelling of yield zones in weak rocks. *Journal of Comprehensive rock engineering*.
- Goel, R., Jethwa, J. and Paithankar, A., 1995. Indian experiences with Q and RMR systems. *Tunnelling and Underground Space Technology*.
- Goodman, R.E., 1989. *Introduction to rock mechanics*. Wiley, New York.
- Grimstad, E. and Barton, N., 1993. Updating of the Q system for NMT, *Proceedings of the International Symposium on sprayed concrete-Modern use of wet mix sprayed concrete for underground support*, Fagernes, Oslo, Norway.
- Gupta, A. and Seshagiri Rao, K., 2000. Weathering effects on the strength and deformational behaviour of crystalline rocks under uniaxial compression state. *Engineering geology*.
- Hoek, E., http://www.rockscience.com/hoek/corner/12_Tunnels_in_weak_rock.pdf.
- Hoek, E., 1990. Estimating Mohr-Coulomb friction and cohesion values from the Hoek-Brown failure criterion, In *Intl. J. Rock Mech. & Mining Sci. & Geomechanics Abstracts*

- Hoek, E., 2001. Big tunnels in bad rock. *Journal of Geotechnical and Geoenvironmental Engineering*.
- Hoek, E. and Brown, E.T., 1980. *Underground excavations in rock*. The Institute of Mining and Metallurgy.
- Hoek, E., Carranza-Torres, C. and Corkum, B., 2002. Hoek-Brown failure criterion-2002 edition, H Proceedings of NARMS-TAC.
- Hoek, E. and Diederichs, M., 2006. Empirical estimation of rock mass modulus. *International Journal of Rock Mechanics and Mining Sciences*.
- Hoek, E. and Guevara, R., 2009a. Overcoming squeezing in the Yacambú-Quibor tunnel, Venezuela. *Rock mechanics and rock engineering*.
- Hoek, E. and Guevara, R., 2009b. Overcoming squeezing in the Yacambú-Quibor tunnel, Venezuela. *Rock mechanics and rock engineering*, 42(2): 389-418.
- Hoek, E. and Marinos, P., 2000. Predicting tunnel squeezing problems in weak heterogeneous rock masses. *Tunnels and Tunnelling International*.
- Kovári, K., 1998. *Tunelling in Squeezing Rock*. Tunnel-Gutersloh.
- Marinos, P. and Hoek, E., 2001. Estimating the geotechnical properties of heterogeneous rock masses such as flysch. *Bulletin of Engineering Geology and the Environment*.
- NEA, 1997. Upgraded feasibility report, Chameliya Hydroelectric Project, Nepal. Nepal Electricity Authority.
- NEA, 1998. Report on Geotechnical Studies of Chameliya Hydroelectric Project, Nepal. Nepal Electricity Authority.
- NEA, 2001. Review Study Report, The detail design and preparation of tender documents of Chameliya Hydroelectric Project, Nepal. Nepal Electricity Authority: 468.
- NGI, 1997. Practical use of the Q-method. Norwegian Geotechnical Institute, Oslo, Report.
- Nilsen, B. and Ozdemir, L., 1999. Recent developments in site investigation and testing for hard rock TBM projects, Proceedings of the Rapid Excavation and Tunneling Conference.
- Nilsen, B. and Palmström, A., 2000. *Engineering geology and rock engineering*. Norwegian Group for Rock Mechanics.
- Nilsen, B. and Thidemann, A., 1993. *Rock Engineering*. Hydropower Development, 9. Tapir, Trondheim, Norway, 156 pp.
- Palmstrom, A., 1995. Rmi-a rock mass characterization system for rock engineering purposes.
- Palmstrom, A. and Broch, E., 2006. Use and misuse of rock mass classification systems with particular reference to the Q-system. *Tunnelling and Underground Space Technology*.
- Palmström, A. and Singh, R., 2001. The deformation modulus of rock masses—comparisons between in situ tests and indirect estimates. *Tunnelling and Underground Space Technology*.
- Panet, M., 1996. Two case histories of tunnels through squeezing rocks. *Rock mechanics and rock engineering*.
- Panthi, K.K., 2006. Doctoral Thesis. Analysis of engineering geological uncertainties related to tunneling in Himalayan rock mass conditions, NTNU, Trondheim, Norway.
- Panthi, K.K., Autumn 2012. Class notes on TGB5100 Rock Engineering AC, NTNU, trondheim, Norway.
- Panthi, K.K., Spring 2012. Lecture notes in Geology and Tunneling, NTNU, Trondheim, Norway.
- Rabcewicz, L.v., 1964. The new Austrian tunnelling method. *Water Power*.
- Sakurai, S., 1983. Displacement measurements associated with the design of underground openings, Proc. Int. Symp. Field Measurements in Geomechanics.

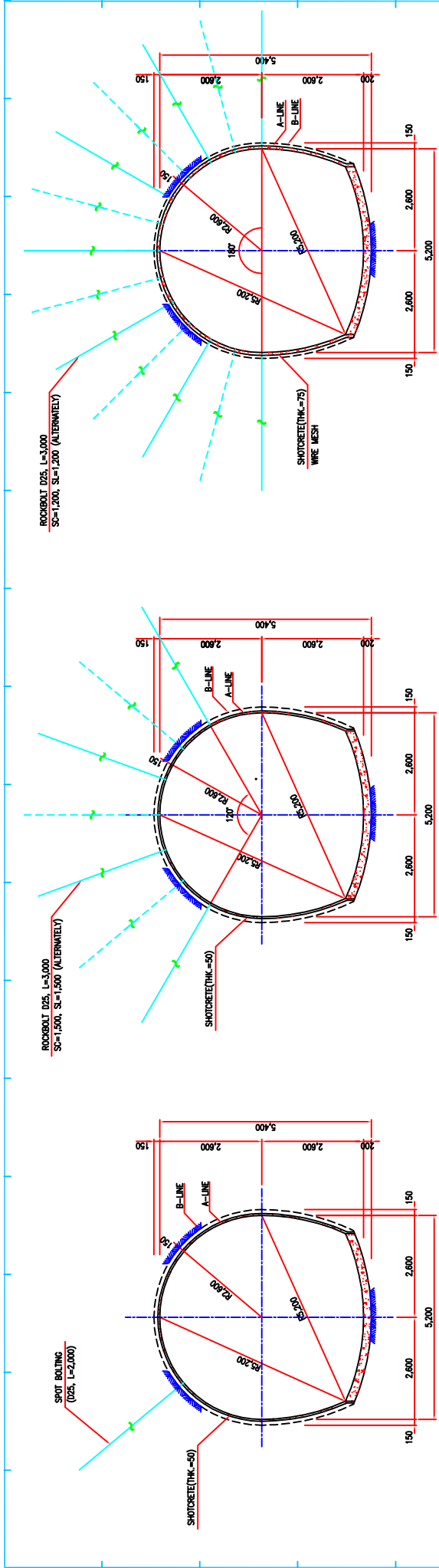
- Sarkar, I. and Chander, R., 2003. Role of static stress transfer in earthquake occurrence in the Himalaya. *Journal of Asian Earth Sciences*.
- Shrestha, G.L., 2006. Doctoral Thesis. Stress induced problems in Himalayan tunnels with special reference to squeezing, Norwegian University of Science and Technology, Trondheim, Norway.
- Singh, B., Jethwa, J., Dube, A. and Singh, B., 1992. Correlation between observed support pressure and rock mass quality. *Tunnelling and Underground Space Technology*.
- Singh, M. and Seshagiri Rao, K., 2005. Empirical methods to estimate the strength of jointed rock masses. *Engineering geology*.
- Steiner, W., 1996. Tunnelling in squeezing rocks: case histories. *Rock mechanics and rock engineering*.
- Vlachopoulos, N. and Diederichs, M., 2009. Improved longitudinal displacement profiles for convergence confinement analysis of deep tunnels. *Rock mechanics and rock engineering*.

APPENDIX A: PROJECT RELATED DOCUMENTS AND DRAWINGS

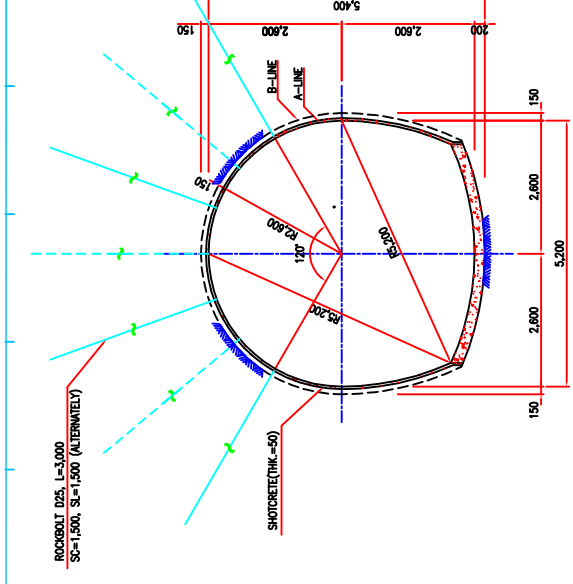
Appendix A1: Salient features of CHEP

General Type of Project Location Maximum gross head Rated net head Design flow Installed capacity	Run-of-river plant for 6hours daily peaking Darchula district 103.7 m 94.0 m 36 m ³ /sec (38.3% exceedence flow) 30 MW
Hydrology Catchment area Average annual flow 90% firm flow 95% firm flow Flood 100 years return period 1000 years return period 10000 years return period	835 km ² 46.6 m ³ /sec 13.2 m ³ /sec 11.3 m ³ /sec 500 m ³ /sec 710 m ³ /sec 970 m ³ /sec
Reservoir Minimum operating level Maximum operating level Active storage volume	EL. 880.0 m EL. 888.0 m 0.68 Mil.m ³
Dam & Spillway Type Dam crest elevation Crest length Height above foundation Spillway Gates, width/height Design flood Energy dissipator	Concrete gravity EL. 892.0 m 88.0 m Max. 54.0 m 2 radial gates, 7.0 m/13.5 m 710 m ³ /sec Stilling basin
Intake Type Width/height/number	side (orifice) 8.0m/3.0m/2
Desanding Basins Type number of caverns Width/height/length Nominal size of trapped particles	Underground desander in caverns 2 12m/25m/80m 0.25 m
Headrace Tunnel Type Length/diameter (internal)	Horseshoe pressure 4,067m/5.2 (4.2)m
Surge Tank Type Net diameter Height Max. upsurge/down surge	Restricted orifice 8.0m 48.4 m EL. 904.66m/EL. 877.7m

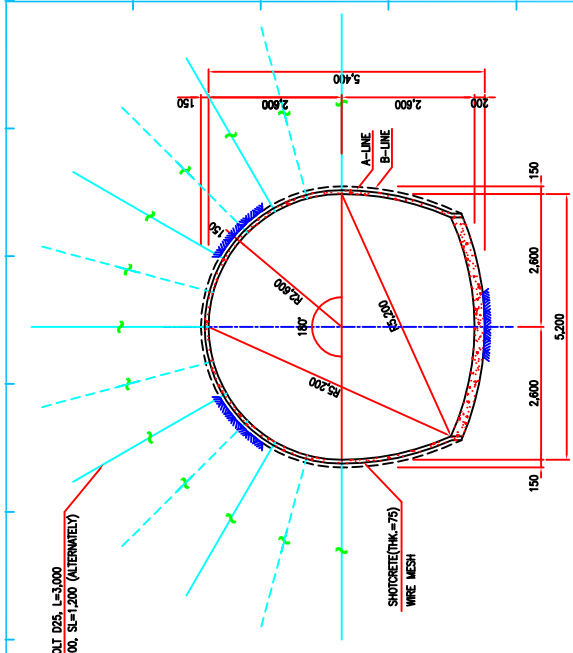
Penstock	
Type	Vertical and horizontal, concrete lined tunnel and embedded steel lined penstock
Concrete lined penstock	ver. L : 71.5m (ID = 3.9m)
Steel lined penstock	hor. L : 209.3m (ID = 3.9 m) L : 184.0 m ID : 3.7 - 2.5 - 1.8 m
Powerhouse	
Type	Semi-underground
Width/height/length	23.5m/27.4m/37.5m
Number of generating unit	2
Turbine	
Number and type	2/vertical shaft Francis
Rated discharge	36m ³ /sec
Rated net head	94.0m
Rated output	15.6MWX2
Rated speed	428.6rpm
Center line elevation	EL. 781.20m
Generator	
Number and type	2/3phase, synchronous
Rated output	16,200kVAX2
Rated voltage	11,000V
Rated frequency	50Hz
Power factor	0.9
Rated speed	428.6rpm
Tailrace channel	
Type	outdoor conventional type
Length/width	57m/47m
Transmission Line	
Route	CHEP to National grid at Attariya
length	131km
Voltage	132kV
Number of circuit	Single circuit
Energy generation	
Annual average energy	184.21 GWh
Annual on-peak energy	59.24 GWh
Annual off-peak energy	73.05 GWh
Annual secondary energy	51.92 GWh
Project Cost (cost T/L)	75.28 US\$ Mil
Specific capacity cost	2.509 US\$ / KW
Specific energy cost	5.81 US Cents / KWh
B/C (10% Discount rate)	1.46



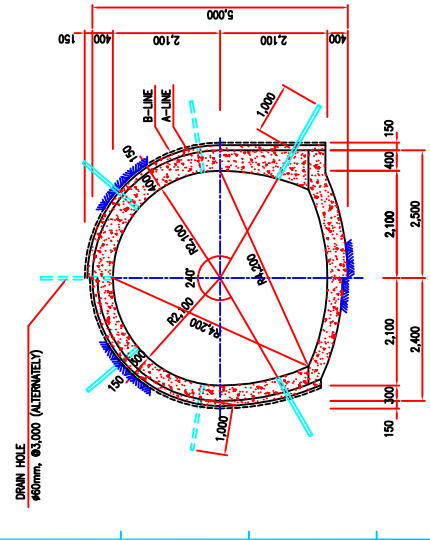
TYPE - R1



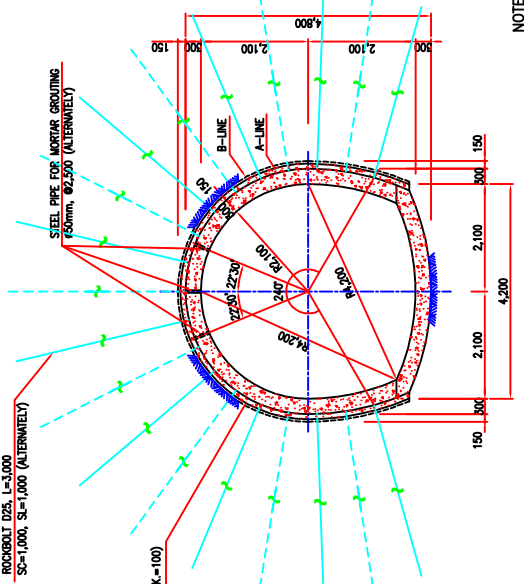
TYPE - R2



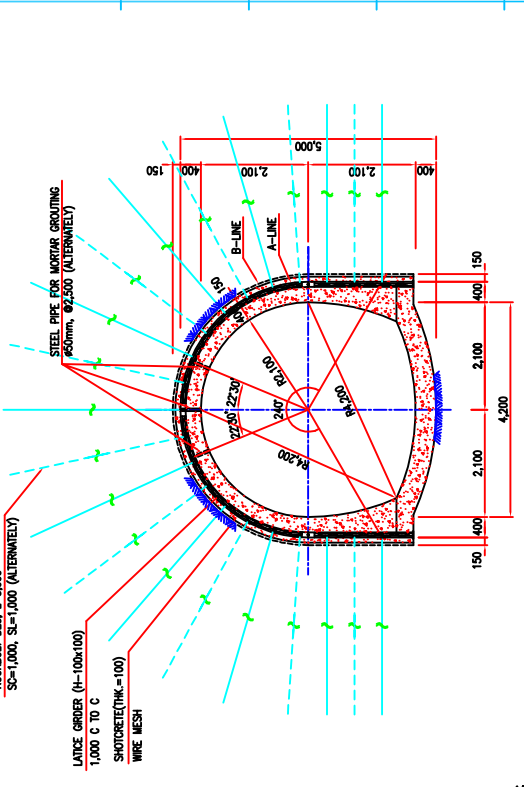
TYPE - R3



DETAIL OF DRAIN HOLE (R4 & R5)



TYPE - R4



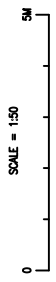
TYPE - R5

NOTES :

1. ALL DIMENSIONS ARE IN MILLIMETERS.
2. A-LINE : DESIGN LINE
B-LINE : PAY LINE
3. BACKFILL GROUTING FOR ROCK SUPPORT TYPE-R4 AND R5 ARE CONSTRUCTED WITH A 2.0kg/cm² PRESSURE.
3. IN HEADRACE TUNNEL, DRAIN HOLES ARE INSTALLED AT R4 & R5-TYPE AGAINST EXTERNAL WATER PRESSURE.
4. FOR DETAIL OF ROCKBOLT, SEE DWG. NO. CH-C-2901.
5. FOR DETAIL OF LATTICE GRIDER, SEE DWG. NO. CH-C-2902.

ROCK MASS QUALITY	SUPPORT TYPE	SHOTCRETE (mm)	ROCKBOLT	STEEL RIB OR LATTICE GRIDER	CONC'L LING (mm)
Good (10 ≤ Q)	R1	50	SPOT BOLTING	-	INVERT=200
Fair (4 ≤ Q < 10)	R2	50	PATTERN BOLTING	-	INVERT=200
Fair (1 ≤ Q < 4)	R3	75	PATTERN BOLTING	-	INVERT=200
Poor (0.1 ≤ Q < 1)	R4	100	PATTERN BOLTING	-	INVERT=300 ARCH=300
V. Poor (Q < 0.1)	R5	100	PATTERN BOLTING	LATTICE GRIDER SPACING (1.0m)	INVERT=400 ARCH=400

TUNNEL SUPPORT PATTERN



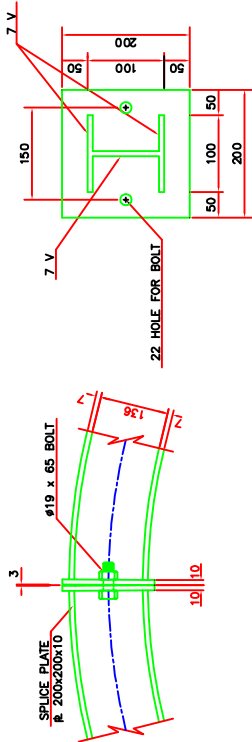
SCALE = 1:50

ORDER NO.	CLIENT : KOREA INTERNATIONAL COOPERATION AGENCY
PROJECT NO.	E/A : NEPAL ELECTRICITY AUTHORITY
DESIGNER	HYUNDAI ENGINEERING CO., LTD.
CHECKED	KOREA WATER RESOURCES CORPORATION
APPROVED	PROJECT : CHAMLIYA HYDROELECTRIC PROJECT
DATE DRAWN	TITLE : WATERWAY HEADRACE TUNNEL
SCALE	SUPPORT PATTERN OF HEADRACE TUNNEL
AS SHOWN	DWG. No. CH-C-2204

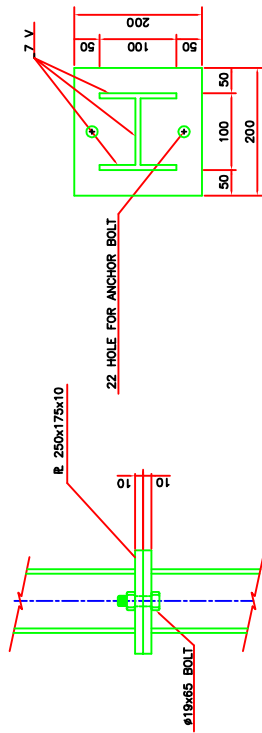
NO.	REVISIONS	DATE	BY	CHKD	APPD

DETAILS OF STEEL SUPPORT

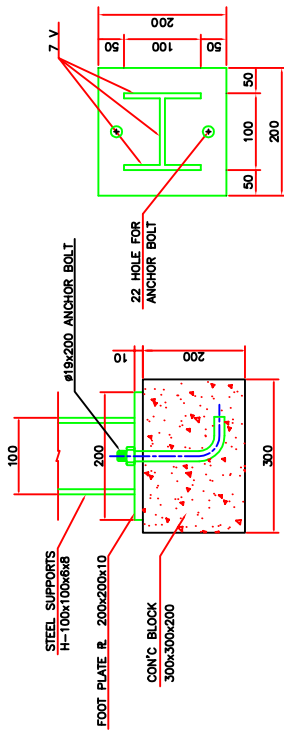
DETAILS OF SPLICE SUPPORT



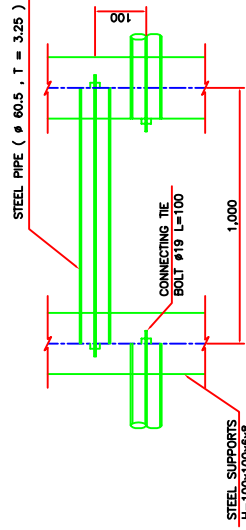
DETAILS OF INTERMEDIATE SPLICE PLATE



DETAIL OF FOOT PLATE



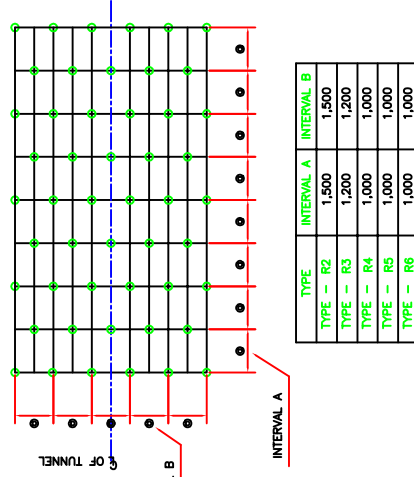
TIE BOLT AND STEEL PIPE



DETAILS OF ROCKBOLT

SUPPORT PATTERN	TYPE - R1	TYPE - R2	TYPE - R3
ROCKMASS QUALITY (Q)	$10 \leq Q$	$4 \leq Q < 10$	$1 \leq Q < 4$
REMARKS	Enforce a spot bolting in fragmented and unconsolidated shale part.	Pattern bolting using unretensioned D25, L=3,000 Upper 120'	Pattern bolting using unretensioned D25, L=3,000 Φ 1,200 Upper 180'
SUPPORT PATTERN	TYPE - R4	TYPE - R5	TYPE - R6
ROCKMASS QUALITY (Q)	$0.1 \leq Q < 1$	$Q < 0.1$	$Q < 0.1$
REMARKS	Pattern bolting using unretensioned D25, L=3,000 Upper and side wall 240'	Type-R4 pattern and lattice girder support.	Type-R4 pattern and lattice girder support.

ARRANGEMENT OF ROCKBOLT



NOTES ;

- UNLESS OTHERWISE SPECIFIED, ALL DIMENSIONS ARE IN MILLIMETERS.
- TUNNEL SUPPORT PATTERN MAY BE CHANGED ACCORDING TO GEOLOGICAL CONDITION.
- STEEL RIB ARE SUBSTITUTED FOR LATTICE GIRDER IN THE ROCK CONDITION, WHICH ARE REQUIRED MORE STRENGTH AS PORTAL AND WEAK ZONE.

ORDER No.	CLIENT : KOREA INTERNATIONAL COOPERATION AGENCY
PROJECT No.	E/A : NEPAL ELECTRICITY AUTHORITY
DESIGN No.	HYUNDAI ENGINEERING CO., LTD.
CONTRACT No.	KOREA WATER RESOURCES CORPORATION
PROJECT NAME	CHAMELITA HYDROELECTRIC PROJECT
TITLE	HEAVYWEAR WATERWAY
DWG. No.	DETAILS OF ROCK BOLT AND STEEL SUPPORT
SCALE	1:100
DATE DRAWN	09.08.2010
DATE APPD	10.08.2010
NO.	REV.

APPENDIX A3

TYPE - R4~R6

NO.	DATE	REV.	CHD	APPD	NO.	DATE	REV.	CHD	APPD	NO.	DATE	REV.	CHD	APPD

APPENDIX B: STANDARD CHARTS AND FIGURES

Appendix B0: Field estimates of uniaxial compressive strength of intact rock, σ_{ci} (Hoek and Marinos, 2000)

Grade*	Term	Uniaxial Comp. Strength (MPa)	Point Load Index (MPa)	Field estimate of strength	Examples
R6	Extremely Strong	> 250	>10	Specimen can only be chipped with a geological hammer	Fresh basalt, chert, diabase, gneiss, granite, quartzite
R5	Very strong	100 - 250	4 - 10	Specimen requires many blows of a geological hammer to fracture it	Amphibolite, sandstone, basalt, gabbro, gneiss, granodiorite, peridotite, rhyolite, tuff
R4	Strong	50 - 100	2 - 4	Specimen requires more than one blow of a geological hammer to fracture it	Limestone, marble, sandstone, schist
R3	Medium strong	25 - 50	1 - 2	Cannot be scraped or peeled with a pocket knife, specimen can be fractured with a single blow from a geological hammer	Concrete, phyllite, schist, siltstone
R2	Weak	5 - 25	**	Can be peeled with a pocket knife with difficulty, shallow indentation made by firm blow with point of a geological hammer	Chalk, claystone, potash, marl, siltstone, shale, rocksalt,
R1	Very weak	1 - 5	**	Crumbles under firm blows with point of a geological hammer, can be peeled by a pocket knife	Highly weathered or altered rock, shale
R0	Extremely weak	0.25 - 1	**	Indented by thumbnail	Stiff fault gouge

* Grade according to Brown (1981).

** Point load tests on rocks with a uniaxial compressive strength below 25 MPa are likely to yield highly ambiguous results.






Appendix B1: Hoek and Brown Constant, m_i

Rock type	Class	Group	Texture			
			Coarse	Medium	Fine	Very fine
SEDIMENTARY	Clastic		Conglomerates (21 ± 3) Breccias (19 ± 5)	Sandstones 17 ± 4	Siltstones 7 ± 2 Greywackes (18 ± 3)	Claystones 4 ± 2 Shales (6 ± 2) Marls (7 ± 2)
		Non-Clastic	Carbonates	Crystalline Limestone (12 ± 3)	Sparitic Limestones (10 ± 2)	Micritic Limestones (9 ± 2)
	Evaporites			Gypsum 8 ± 2	Anhydrite 12 ± 2	
	Organic					Chalk 7 ± 2
METAMORPHIC	Non Foliated		Marble 9 ± 3	Hornfels (19 ± 4) Metasandstone (19 ± 3)	Quartzites 20 ± 3	
	Slightly foliated		Migmatite (29 ± 3)	Amphibolites 26 ± 6	Gneiss 28 ± 5	
	Foliated*			Schists 12 ± 3	Phyllites (7 ± 3)	Slates 7 ± 4
IGNEOUS	Plutonic	Light	Granite 32 ± 3 Granodiorite (29 ± 3)	Diorite 25 ± 5		
		Dark	Gabbro 27 ± 3 Norite 20 ± 5	Dolerite (16 ± 5)		
	Hypabyssal			Porphyries (20 ± 5)	Diabase (15 ± 5)	Peridotite (25 ± 5)
	Volcanic	Lava		Rhyolite (25 ± 5) Andesite 25 ± 5	Dacite (25 ± 3) Basalt (25 ± 5)	
		Pyroclastic		Agglomerate (19 ± 3)	Breccia (19 ± 5)	Tuff (13 ± 5)

Appendix B2: Geological Strength Index, GSI

<p>GEOLOGICAL STRENGTH INDEX FOR JOINTED ROCKS (Hoek and Marinos, 2000)</p> <p>From the lithology, structure and surface conditions of the discontinuities, estimate the average value of GSI. Do not try to be too precise. Quoting a range from 33 to 37 is more realistic than stating that GSI = 35. Note that the table does not apply to structurally controlled failures. Where weak planar structural planes are present in an unfavourable orientation with respect to the excavation face, these will dominate the rock mass behaviour. The shear strength of surfaces in rocks that are prone to deterioration as a result of changes in moisture content will be reduced if water is present. When working with rocks in the fair to very poor categories, a shift to the right may be made for wet conditions. Water pressure is dealt with by effective stress analysis.</p>		<p>SURFACE CONDITIONS</p> <p>VERY GOOD Very rough, fresh unweathered surfaces</p> <p>GOOD Rough, slightly weathered, iron stained surfaces</p> <p>FAIR Smooth, moderately weathered and altered surfaces</p> <p>POOR Slackensided, highly weathered surfaces with compact coatings or fillings or angular fragments</p> <p>VERY POOR Slackensided, highly weathered surfaces with soft clay coatings or fillings</p> <p>DECREASING SURFACE QUALITY →</p>				
<p>STRUCTURE</p>		<p>DECREASING INTERLOCKING OF ROCK PIECES ↓</p>				
	<p>INTACT OR MASSIVE - intact rock specimens or massive in situ rock with few widely spaced discontinuities</p>	90	80	70	60	N/A
	<p>BLOCKY - well interlocked undisturbed rock mass consisting of cubical blocks formed by three intersecting discontinuity sets</p>	80	70	60	50	40
	<p>VERY BLOCKY- interlocked, partially disturbed mass with multi-faceted angular blocks formed by 4 or more joint sets</p>	70	60	50	40	30
	<p>BLOCKY/DISTURBED/SEAMY - folded with angular blocks formed by many intersecting discontinuity sets. Persistence of bedding planes or schistosity</p>	60	50	40	30	20
	<p>DISINTEGRATED - poorly interlocked, heavily broken rock mass with mixture of angular and rounded rock pieces</p>	50	40	30	20	10
	<p>LAMINATED/SHEARED - Lack of blockiness due to close spacing of weak schistosity or shear planes</p>	N/A	N/A	10	5	0

Appendix B3: Disturbance factor, D

Appearance of rock mass	Description of rock mass	Suggested value of <i>D</i>
	<p>Excellent quality controlled blasting or excavation by Tunnel Boring Machine results in minimal disturbance to the confined rock mass surrounding a tunnel.</p>	<p>$D = 0$</p>
	<p>Mechanical or hand excavation in poor quality rock masses (no blasting) results in minimal disturbance to the surrounding rock mass.</p> <p>Where squeezing problems result in significant floor heave, disturbance can be severe unless a temporary invert, as shown in the photograph, is placed.</p>	<p>$D = 0$</p> <p>$D = 0.5$ No invert</p>
	<p>Very poor quality blasting in a hard rock tunnel results in severe local damage, extending 2 or 3 m, in the surrounding rock mass.</p>	<p>$D = 0.8$</p>
	<p>Small scale blasting in civil engineering slopes results in modest rock mass damage, particularly if controlled blasting is used as shown on the left hand side of the photograph. However, stress relief results in some disturbance.</p>	<p>$D = 0.7$ Good blasting</p> <p>$D = 1.0$ Poor blasting</p>
	<p>Very large open pit mine slopes suffer significant disturbance due to heavy production blasting and also due to stress relief from overburden removal.</p> <p>In some softer rocks excavation can be carried out by ripping and dozing and the degree of damage to the slopes is less.</p>	<p>$D = 1.0$ Production blasting</p> <p>$D = 0.7$ Mechanical excavation</p>

Appendix B4: RMR Classification of rock mass (Bieniawski, 1989)

A. Classification parameters and their ratings

Parameters		Range of values or ratings							
1	Strength of Intact Rock	Point load strength index (MPa)	> 10	4 - 10	2 - 4	1 - 2	Low range uniaxial strength is preferred		
		Uniaxial compressive strength (MPa)	> 250	100-250	50-100	25-50	5- 25	1 - 5	< 1
	Rating	15	12	7	4	2	1	0	
2	Drill core quality, RQD (%)		90-100	75-90	50-75	25-50	< 25		
	Rating		20	17	13	8	5		
3	Spacing of discontinuities (m)		> 2	0.6-2	0.2-0.6	0.06-0.2	< 0.06		
	Rating		20	15	10	8	5		
4	Condition of discontinuities	Length, persistence (m)	< 1	1-3	3-10	10-20	> 20		
		Rating	6	4	2	1	0		
		Separation (mm)	none	< 0.1	0.1-1	1-5	> 5		
		Rating	6	5	4	1	0		
		Roughness	very rough	rough	slightly rough	smooth	slickensided		
		Rating	6	5	3	1	0		
		Infilling (gouge) (mm)	none	hard filling		soft filling			
		Rating	6	4	2	2	0		
Weathering	un-weathered	slightly weathered	moderately weathered	highly weathered	decomposed				
Rating	6	5	3	1	0				
5	Ground water	Inflow per 10 meter tunnel length (l/min)	none	< 10	10-25	25-125	> 125		
		ρ_w / σ_1	0	0.0-1	0.1-0.2	0.2-0.5	> 0.5		
		General conditions	dry	damp	wet	dripping	flowing		
		Rating	15	10	7	4	0		
here, ρ_w is joint water pressure and σ_1 is major principle stress									

B. Rating adjustment for discontinuity orientation

Tunnel alignment	very favorable	favorable	fair	unfavorable	very unfavorable
Rating adjustment	0	-2	-5	-10	-12

C. Rock mass classes determined from total ratings

Rating	100-80	80-61	60-41	40-21	< 20
Class No.	I	II	III	IV	V
Description	Very good	Good	Fair	Poor	Very poor

D. Meaning or rock mass classes

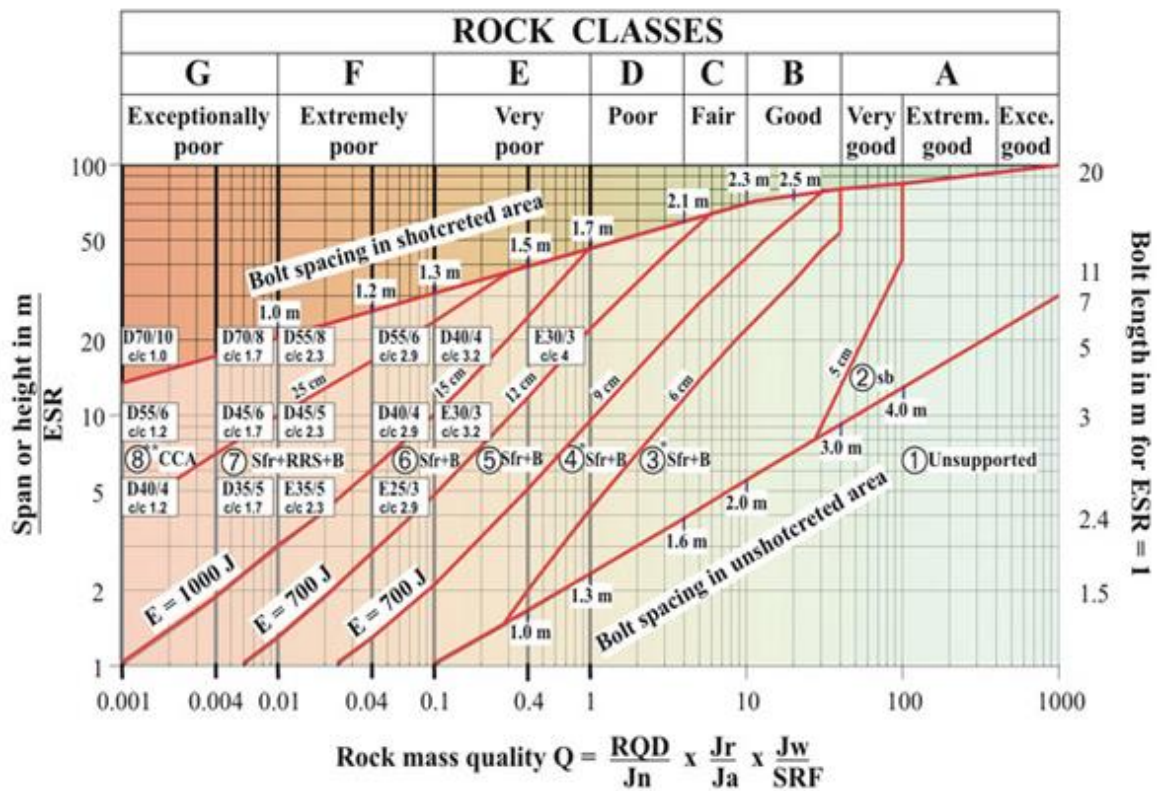
Class No.	I	II	III	IV	V
Average stand-up time	Can be estimated from Figure 4-4				
Cohesion of the rock mass (kPa)	> 400	3-400	2-300	1-200	< 00
Friction angle of the rock mass (degrees)	< 45	35-45	25-35	15-25	< 15

Appendix B5: Description of ratings for input parameters of Q-system (based on Barton, 2002)

RQD (Rock quality designation, %)		J_n (Joint set number)	
Very poor	0 - 25	Massive, no or few joints	0.5 - 1
Poor	25 - 50	One joint set	2
Fair	50 - 75	One joint set + random joints	3
Good	75 - 90	Two joint sets	4
Excellent	90 - 100	Two joint sets + random	6
<i>Notes:</i>		Three joint sets	9
(i) where RQD is reported or measured as ≤ 10 (including 0), a nominal value of 10 is used to evaluate Q.		Three joint sets + random	12
(ii) RQD intervals of 5 i.e. 100, 95, 90 etc., are successfully accurate.		Four or more joint sets, heavily jointed, sugar cube etc	15
		Crushed rock, earthlike	20
		<i>Note:</i> For tunnel intersections, use (3 x J _n) and for portals use (2 x J _n)	
J_r (Joint roughness number)			
<i>(a) Rock wall contact</i>		<i>(b) Rock wall contact before 10 cm shear</i>	
Discontinuous joints	4	Rough or irregular, undulating	1.5
Rough or irregular, undulating	3	Smooth, undulating	1
Smooth, undulating	2	Slickensided, undulating	0.5
Slickensided, undulating	1.5		
<i>© No rock wall contact when sheared</i>			
Zone containing clay minerals thick enough to prevent rock wall contact			1
Sandy, gravely or crushed zone thick enough to prevent rock wall contact			1
<i>Notes:</i> (i) Description refers to small-scale features and intermediate scale features, in that order (ii) Add 1.0 if the mean spacing of the relevant joint set is greater than 3 m. (iii) J _r = 0.5 can be used for planner, slickenside joints having lineations, provided these are oriented for minimum strength. (iv) J _r and J _a classification is applied to the joint set that is least favorable for stability both from the point of view of orientation and shear resistance, $\tau \approx \sigma_n \cdot \tan^{-1} (J_r/J_a)$			
J_a (Joint alteration number)			
<i>(a) Rock wall contact (no mineral fillings, only coatings)</i>		<i>θ_r (appr.)</i>	J_a
Tightly healed, hard, non-softening, impermeable filling i.e., quartz/epidote		-	0.75
Unaltered joint walls, surface staining only		25 - 35	1
Slightly altered joint walls, non-softening mineral coatings, sandy particles, clay free disintegrated rock ,etc.		25 - 30	2
Silty or sandy clay coatings, small clay fractions (non-softening)		20 - 25	3
Softening or low friction clay mineral coatings, i.e., kaolinite or mica. Also chlorite, talk, gypsum, graphite etc., and small quantities of swelling clay		8 - 16	4
<i>(b) Rock wall contact before 10 cm shear (thin mineral fillings)</i>			
Sandy particles, clay free disintegrated rock etc.		25 - 30	4
Strongly over-consolidated non-softening clay mineral fillings (continuous, but < 5mm thickness)		16 - 24	6

Medium or low over-consolidated non-softening clay mineral fillings (continuous, but < 5mm thickness)	12 - 16	8
Swelling clay fillings, i.e., montmorillonite (continuous, but < 5mm thick)	6 - 12	8 - 12
<i>(c) No rock wall contact when sheared (thick mineral fillings)</i>		
Zones or bands of disintegrated or crushed rock and clay	6 - 24	6, 8 - 12
Zones or bands of silty or sandy clay, small clay fraction (non-softening)	-	5
Thick, continuous zones or bands of clay	6 - 24	13 - 20
J_w (Joint water reduction factor)	<i>Approx. P (bars)</i>	
Dry excavations or minor inflow, i.e., < 5 l/min locally	< 1	1
Medium inflow or pressure, occasional outwash of joint fillings	1 - 2.5	0.66
Large inflow or high pressure in competent rock with unfilled joints	2.5 - 10	0.5
Large inflow or high pressure, considerable outwash of joint fillings	2.5 - 10	0.33
Exceptionally high inflow or pressure at blasting, decaying with time	> 10	0.2 - 0.1
Exceptionally high inflow or pressure continuing without noticeable decay with time	> 10	0.2 - 0.1
<i>Notes:</i> (i) The last four factors are crude estimates. Increase J_w if drainage measures are installed. (ii) Special problems caused by ice formation are not considered. (iii) For general characterization of rock masses distance from excavation influences. The use of $J_w = 1, 0.66, 0.5, 0.33$, etc. as depth increases from say 0-5, 5-25, 25-250 to >250m is recommended, assuming that RQD/J_n is low enough (0.5-25) for good hydraulic connectivity.		
<i>SRF (Stress Reduction Factor)</i>		
<i>(a) Weakness zones intersecting excavation, which may cause loosening of rock mass</i>		<i>SRF</i>
Multiple occurrence of weakness zones containing clay or chemically disintegrated rock, very loose surrounding rock at any depth		10
Single weakness zone containing clay or chemically disintegrated rock (depth ≤ 50 m)		5
Single weakness zone containing clay or chemically disintegrated rock (depth > 50m)		2.5
Multiple shear zones in competent rocks (clay free), loose surrounding rock at any depth		7.5
Single shear zone in competent rocks (clay free), (depth of excavation ≤ 50 m)		5
Single shear zone in competent rocks (clay free), (depth of excavation > 50m)		2.5
Loose, open joints, heavily jointed or sugar cube etc. at any depth		5
<i>Note:</i> Reduce these values of SRF by 25 - 50 % if the relevant shear zones only influence but do not intersect the excavation.		
<i>(b) Competent rock, rock stress problems</i>		σ_c / σ_1
Low stress, near surface, open joints		> 200
Medium stress, favorable stress condition		200 - 10
High stress, very tight structures. Usually favorable to stability, may be unfavorable for wall stability		10 - 5
Moderate slabbing after > 1 hour in massive rock		5 - 3
Slabbing and rock burst after a few minutes of excavation		3 - 2
Heavy rock burst and immediate dynamic deformations		< 2
		σ_1 / σ_c
		> 1
		SRF
		2.5
		1
		0.5 - 2
		5 - 50
		50 - 200
		200 - 400
<i>Notes:</i> (i) For strongly anisotropic virgin stress field (if measured): when $5 \leq \sigma_1 / \sigma_3 \leq 10$, reduce σ_c to $0.75 \sigma_c$ and when $\sigma_1 / \sigma_3 > 10$, reduce σ_c to $0.5 \sigma_c$. (ii) For general characterization of rock mass, overburden from excavation influences. The use of SRF 5, 2.5, 1 and 0.5 is recommended as depth increases from say 0-5, 5-25, 25-250 to > 250m respectively.		
<i>© Squeezing rock: plastic flow of incompetent rock under the influence of high rock pressure</i>		σ_1 / σ_c
Mild squeezing rock pressure		1 - 5
Heavy squeezing rock pressure		> 5
		SRF
		5 - 10
		10 - 20
<i>(d) Swelling rock: chemical swelling activity depending on pressure of water</i>		SRF
Mild swelling rock pressure		5 - 10
Heavy swelling rock pressure		10 - 15

Appendix B6: Q-system chart and various excavation support ratio categories (Grimstad and Barton, 1993)



REINFORCEMENT CATEGORIES

- 1) Unsupported
- 2) Spot bolting, **sb**
- 3) Systematic bolting,
- (and unreinforced shotcrete, 5-6 cm), **B(+S)**
- 4) Fibre reinforced shotcrete and bolting, 6-9 cm, **Sfr+B**
- 5) Fibre reinforced shotcrete and bolting, 9-12 cm, **Sfr+B**
- 6) Fibre reinforced shotcrete and bolting, 12-15 cm, **Sfr+B**
- 7) Fibre reinforced shotcrete > 15 cm + reinforced ribs of shotcrete and bolting, **Sfr+RRS+B**
- 8) Cast concrete lining, **CCA** or **Sfr+RRS+B**

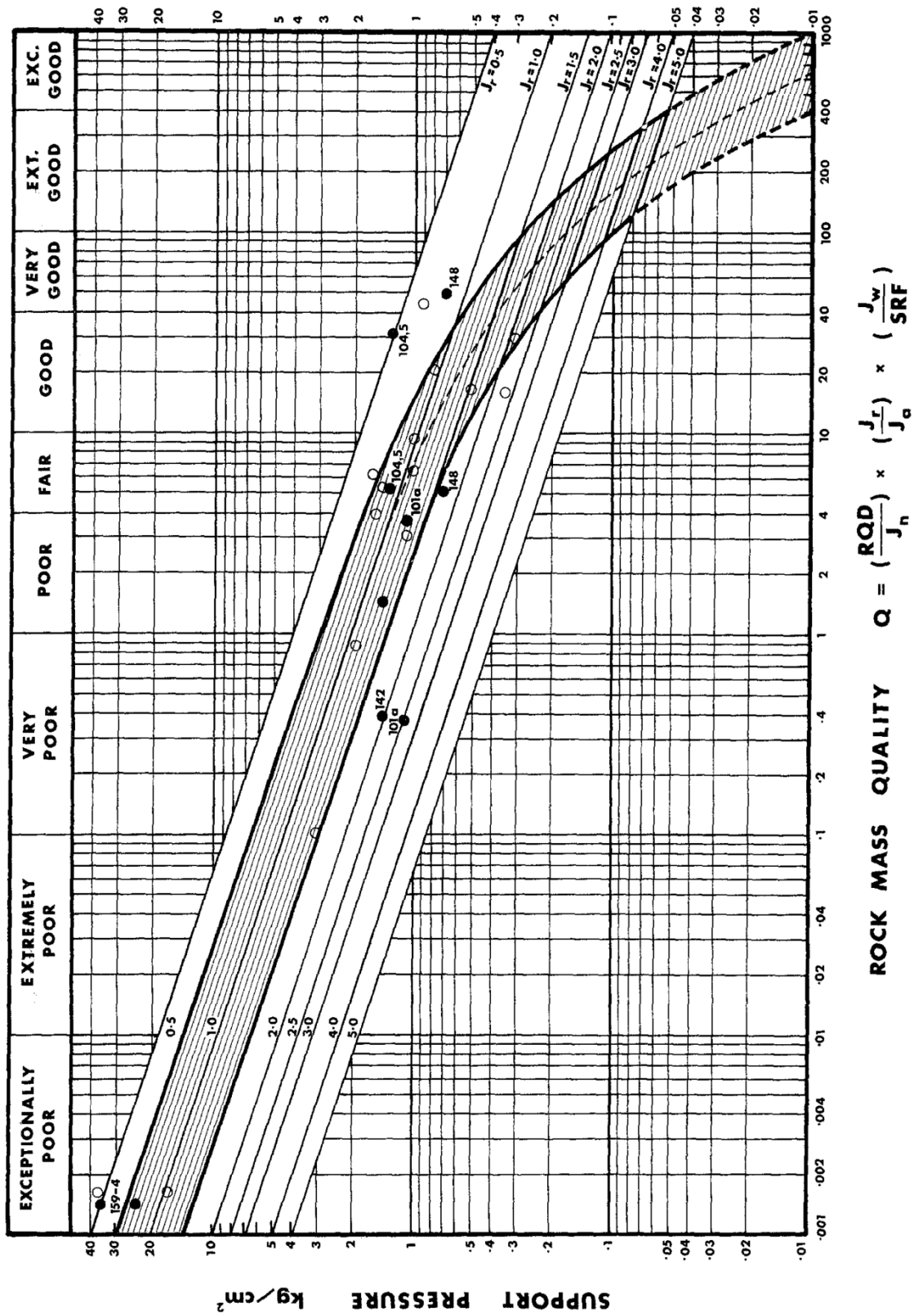
E) Energy absorption in fibre reinforced shotcrete at 25 mm bending during plate testing

$\left[\begin{matrix} D45/6 \\ \text{c/c } 1.7 \end{matrix} \right]$ = RRS with 6 reinforcement bars in double layer in 45 cm thick ribs with centre to centre (c/c) spacing 1.7 m. Each box corresponds to Q-values on the left hand side of the box. (See text for explanation)

*) Up to 10 cm in large spans
) Or **Sfr+RRS+B

Temporary mine openings	<i>ESR</i> = 3–5
Permanent mine openings, water tunnels for hydro power (excluding high pressure penstocks), pilot tunnels, drifts and headings for large excavations	1.6
Storage rooms, water treatment plants, minor road and railway tunnels, surge chambers, access tunnels	1.3
Power stations, major road and railway tunnels, civil defence chambers, portal intersections	1
Underground nuclear power stations, railway stations, sports and public facilities, factories	0.8

Appendix B7: Support pressure estimation chart using Q-value (Barton et al. 1974)



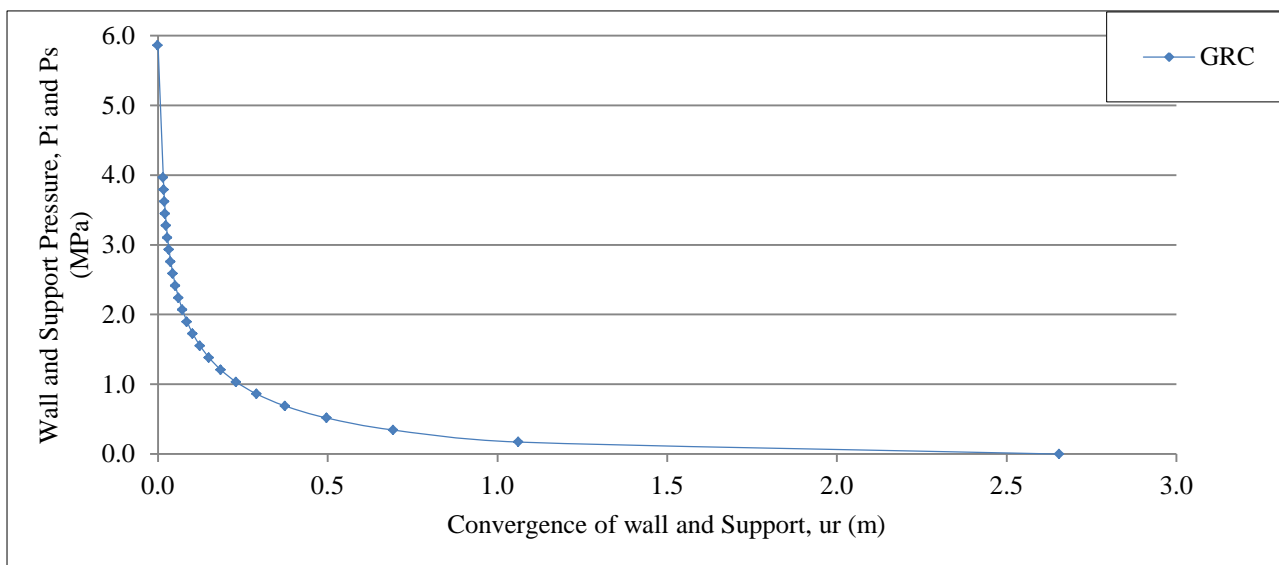
APPENDIX C: DETAIL OF CALCULATIONS AND RESULTS

Appendix C0: Detail of calculation for Hoek and Marinos (2000)

Chainage, m	Rock Type	Overburden, m	σ_0 , MPa	σ_{ci} , MPa	Q	m_i	GSI	a	Disturbance factor, D	s	mb	Rock mass Strength, σ_{cm} , MPa	Strength Stress ratio, σ_{cm}/σ_0	Calculated % strain without support, ϵ	Estimated Support Pressure, p_s , MPa	Calculated % strain with support, ϵ	Measured % strain	σ_{cm} , MPa, Back calculation	σ_{ci} , MPa, Back calculation
0+180	Dolomite	140.2	3.88	60.0	0.250	10	36	0.51	0.8	0.00006	0.222	3.46	0.892	0.25 %					
0+310	Dolomite	220.7	6.11	60.0	0.080	10	29	0.52	0.8	0.00002	0.146	2.63	0.43	1.08 %					
0+410	Dolomite	232.5	6.43	60.0	1.120	10	46	0.51	0.8	0.00028	0.402	4.92	0.76	0.34 %					
1+340	Dolomite	464.0	12.84	60.0	0.500	10	40	0.51	0.8	0.00011	0.281	4.00	0.31	2.06 %					
1+430	Slate	131.1	3.51	45.0	0.620	8	42	0.51	0.8	0.00015	0.253	2.87	0.82	0.30 %					
2+368	Dolomite	129.4	3.58	36.0	0.005	10	10	0.59	0.8	0.00000	0.047	0.54	0.15	8.74 %					
3+103	Dolomite	181.2	5.01	60.0	1.250	10	46	0.51	0.0	0.00248	1.454	9.58	1.91	0.05 %					
3+172	Dolomite	199.7	5.52	12.0	0.020	10	20	0.54	0.0	0.00014	0.574	0.97	0.18	6.42 %	0.33	4.62 %	4.58 %	0.89	11
3+190	Dolomite	217.5	6.02	6.6	0.013	10	17	0.55	0.0	0.00010	0.516	0.48	0.08	31.43 %	0.10	27.83 %	25.54 %	0.50	7
3+296	Talcosic Phyllite	252.2	6.88	13.7	0.010	8	15	0.56	0.0	0.00008	0.384	0.81	0.12	14.49 %	0.10	13.21 %	12.50 %	0.83	14
3+314	Talcosic Phyllite	246.3	6.72	19.5	0.010	8	15	0.56	0.0	0.00008	0.384	1.15	0.17	6.77 %	0.40	4.87 %	3.80 %	1.21	20
3+404	Talcosic Phyllite	283.9	7.74	9.8	0.008	8	14	0.57	0.0	0.00007	0.371	0.55	0.07	39.33 %	0.10	35.7 %	36.73 %	0.51	9
3+420	Talcosic Phyllite	284.5	7.76	10.5	0.008	8	14	0.57	0.0	0.00007	0.371	0.60	0.08	33.86 %	0.10	30.78 %	30.19 %	0.60	11
3+681	Talcosic Phyllite	210.8	5.75	9.8	0.010	8	15	0.56	0.0	0.00008	0.384	0.58	0.10	19.85 %	0.10	17.64 %	18.30 %	0.57	10
3+733	Talcosic Phyllite	237.7	6.48	13.7	0.010	8	15	0.56	0.0	0.00008	0.384	0.81	0.12	12.87 %	0.10	11.69 %	10.96 %	0.83	14
3+764	Talcosic Phyllite	230.0	6.27	11.7	0.015	8	18	0.55	0.0	0.00011	0.428	0.78	0.12	12.85 %	0.10	11.63 %	9.80 %	0.85	13
3+795	Talcosic Phyllite	222.6	6.07	23.4	0.015	8	18	0.55	0.0	0.00011	0.428	1.57	0.26	3.01 %	0.33	2.34 %	1.20 %	2.11	32

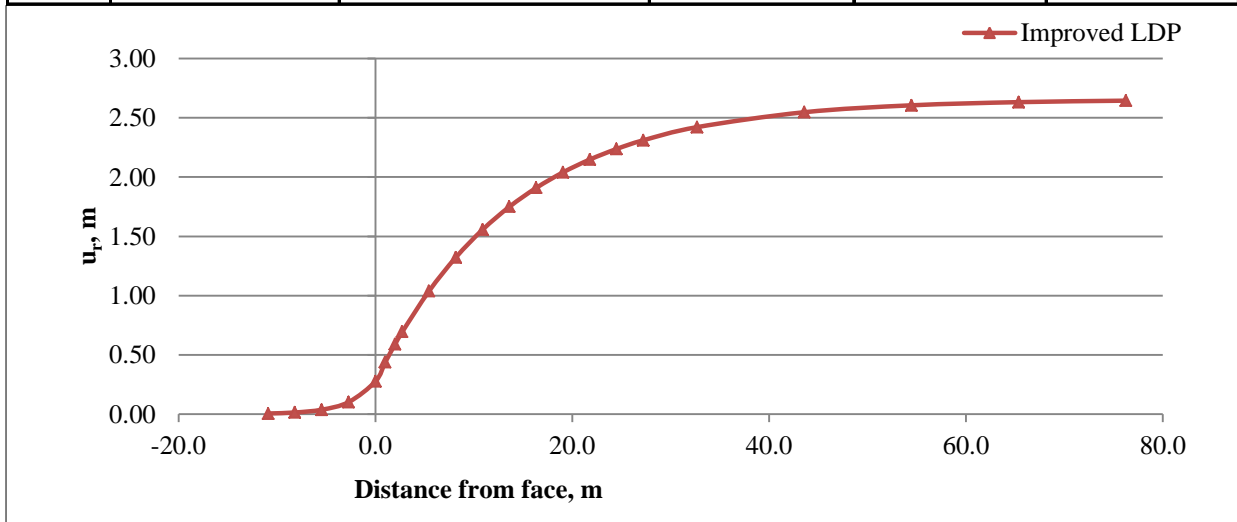
Appendix C1: Detail of calculation for Ground Reaction Curve for tunnel section at chainage 3+404m

			S.N.	Internal pressure, P_i, Mpa	Scalled Internal pressure, $P_{i, \text{Mpa}}$	Radius of Plastic region, $R_{pl, m}$	Elastic disp, u_r^{el}	Plastic disp, u_r^{pl}	Disp, u_r
Width of tunnel	w	5.2 m	1	5.857	1.620	-	0.000		0.000
Crosssection of Tunnel	A	23.3 m ²	2	3.964	1.097	-	0.016		0.016
Eq. Radius of Tunnel	R	2.7 m	3	3.792	1.049	2.9	0.000	0.017	0.017
Overburden	H	283.9 m	4	3.619	1.001	3.0	0.000	0.019	0.019
Unit wt. of Rock	γ	0.027 MN/m ³	5	3.447	0.954	3.1	0.000	0.022	0.022
Poisson's Ratio	ν	0.1	6	3.275	0.906	3.3	0.000	0.025	0.025
Strength of Intact rock	σ_{ci}	9.75 Mpa	7	3.102	0.858	3.5	0.000	0.028	0.028
Vertical Stress	σ_v	7.67 Mpa	8	2.930	0.811	3.7	0.000	0.032	0.032
Tectonic Stress	σ_{tec}	3.5 Mpa	9	2.757	0.763	3.9	0.000	0.038	0.038
Direction of stress		8 °N	10	2.585	0.715	4.1	0.000	0.044	0.044
Direction of alignment		74 °N	11	2.413	0.668	4.3	0.000	0.052	0.0515
Total Hz. Stress	σ_h	4.0 Mpa	12	2.240	0.620	4.6	0.000	0.061	0.061
Geological Strength Index	GSI	14	13	2.068	0.572	4.9	0.000	0.072	0.072
Intact rock parameter	m_i	8	14	1.896	0.525	5.2	0.000	0.086	0.086
Disturbance Factor	D	0	15	1.723	0.477	5.6	0.000	0.103	0.103
Rock mass parameter	m_b	0.371	16	1.551	0.430	6.0	0.000	0.124	0.124
	s	0.00007	17	1.379	0.382	6.4	0.000	0.151	0.151
	a	0.57	18	1.206	0.334	7.0	0.000	0.185	0.185
Modulus Ratio	MR	7.00	19	1.034	0.287	7.6	0.000	0.230	0.230
Intact rock modulus	E_i	7000 MPa	20	0.862	0.239	8.3	0.000	0.291	0.291
Rockmass Modulus	E_m	364.29 Mpa	21	0.689	0.191	9.2	0.000	0.374	0.374
RM Shear Modulus	G_m	165.6 Mpa	22	0.517	0.144	10.4	0.000	0.497	0.497
Initial stress field	σ_o	5.86 Mpa	23	0.345	0.096	11.9	0.000	0.693	0.693
Far field stress	S_o	1.620 Mpa	24	0.172	0.048	14.3	0.000	1.062	1.062
Scalled Crit. Int. Pressure	P_i^{cr}	1.097 Mpa	25	0.000	0.001	21.1	0.000	2.655	2.655
Actual Crit. Int. Pressure	p_i^{cr}	3.96 Mpa							
Dilation angle	Ψ	7.0 degree							
Dilation Coeff	K_Ψ	1.3							
	$K_{\Psi+1}$	2.3							
	$K_{\Psi-1}$	0.3							



Appendix C2: Detail of calculation for Longitudinal Displacement Profile for tunnel section at chainage 3+404m

Tunnel Radius	R	2.72 m		
Max. Disp	U_r^M	2.655 m		
Maximum normalized plastic zone radius	R^*	7.8		
Normalized displacement at face	u_0^*	0.104		
Point	$X^*=X/R$	Dist. to the Face, X,m	u_r , m	Remarks
1	-4.0	-10.9	0.005	Min
2	-3.0	-8.2	0.014	
3	-2.0	-5.4	0.037	
4	-1.0	-2.7	0.102	
5	0.0	0.0	0.276	Face
6	0.4	1.0	0.439	
7	0.7	2.0	0.591	
8	1.0	2.7	0.694	
9	2.0	5.4	1.039	
10	3.0	8.2	1.323	
11	4.0	10.9	1.557	
12	5.0	13.6	1.750	
13	6.0	16.3	1.909	
14	7.0	19.1	2.040	
15	8.0	21.8	2.148	
16	9.0	24.5	2.238	
17	10.0	27.2	2.311	
18	12.0	32.7	2.421	
19	16.0	43.6	2.547	
20	20.0	54.5	2.606	
21	24.0	65.4	2.632	
22	28.0	76.3	2.645	Max



Appendix C3: Detail of calculation for Support Characteristics Curve of support type R6 for tunnel section at chainage 3+404m

A. Shotcrete

Reduction in Support Capacity

30 %

Unconfined Compressive Strength	σ_{cc}	20	Mpa	Displacement, m	Support Pressure, Mpa
Young's Modulus	E_c	3.00E+04	Mpa	0.276	0
Radius of Tunnel	R	2.7	m	0.278	0.505
Thickness of Shotcrete	t_c	100	mm	2.655	0.505
Poisson's Ratio	ν	0.25			
Max support Pressure	P_s^{max}	0.721	Mpa		
Elastic Stiffness	K_s	445	Mpa/m		
Max Displacement	u_r	0.0016	m		

B. Rock Bolts

Bolt/cable dia.	d_b	0.025	m	Displacement, m	Support Pressure, Mpa
free length of bolt or cable	l	3	m	0.276	0
Ultimate load (pull out test)	T_{bf}	0.254	MN	0.320	0.178
Deformation load constant	Q	0.143	m/MN	2.655	0.178
Young's Modulus for bolt or cable	E_s	2.10E+05	Mpa		
Circumferencial bolt spacing	s_c	1	m		
longitudinal bolt spacing	s_l	1	m		
Max support Pressure	P_s^{max}	0.25	Mpa		
Elastic Stiffness	K_s	5.8	Mpa/m		
Max Displacement	u_r	0.0437	m		

C. Steel sets

Set spacing	s_l	0.5	m	Displacement, m	Support Pressure, Mpa
Cross sectional area	A_s	2.80E-03	m ²	0.276	0
Young's modulus of steel	E_s	2.10E+05	Mpa	0.279	0.35
Yield strength of steel	σ_{ys}	245.00	MPa	2.655	0.35
Max support Pressure	P_s^{max}	0.50	Mpa		
Elastic Stiffness	K_s	158.6	Mpa/m		
Max Displacement	u_r	0.0032	m		

D. Shotcrete + Bolts +Steel set (Combined support)

Elastic Stiffness	K_{sb}	609.3	Mpa/m	Displacement, m	Support Pressure, Mpa
Max Displacement	u_r	0.0016	m	0.276	0
Max support Pressure	P_{sb}^{max}	0.99	Mpa	0.278	0.691
				2.655	0.691

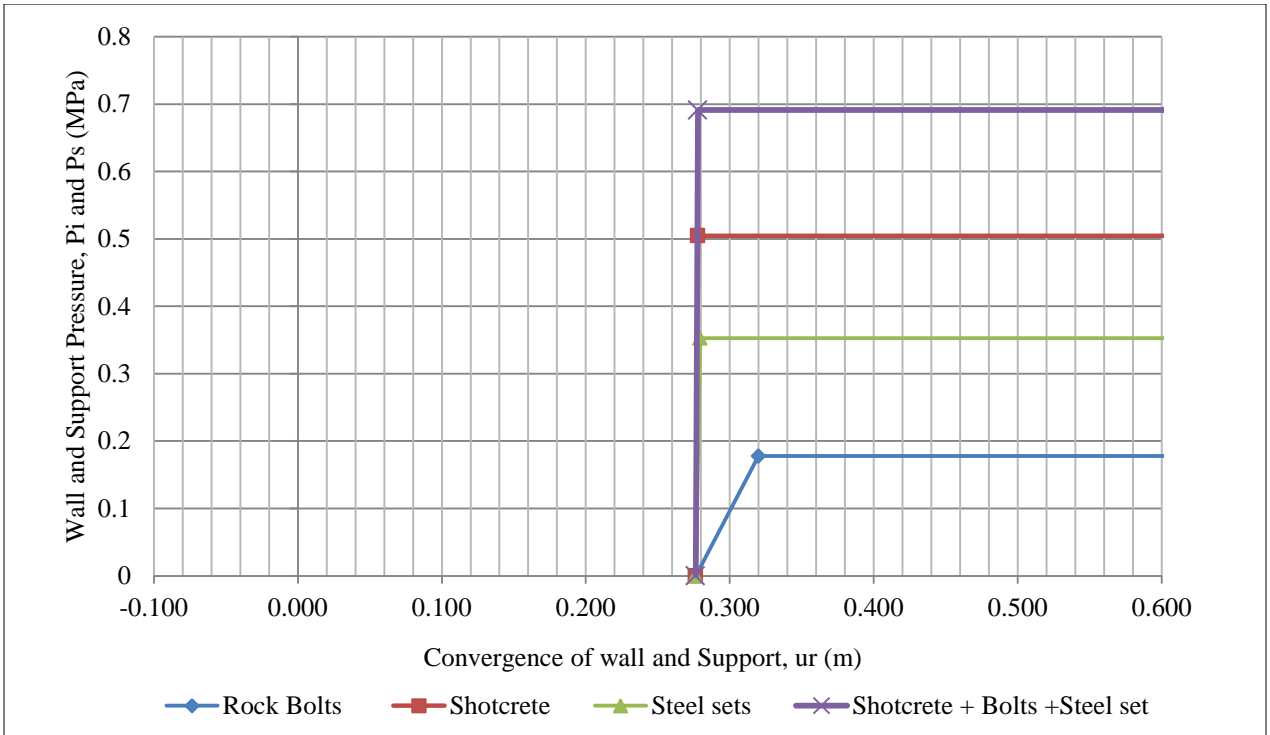


Figure C3.1: Support capacity curve for support type R6 at tunnel face (chainage 3+404m)

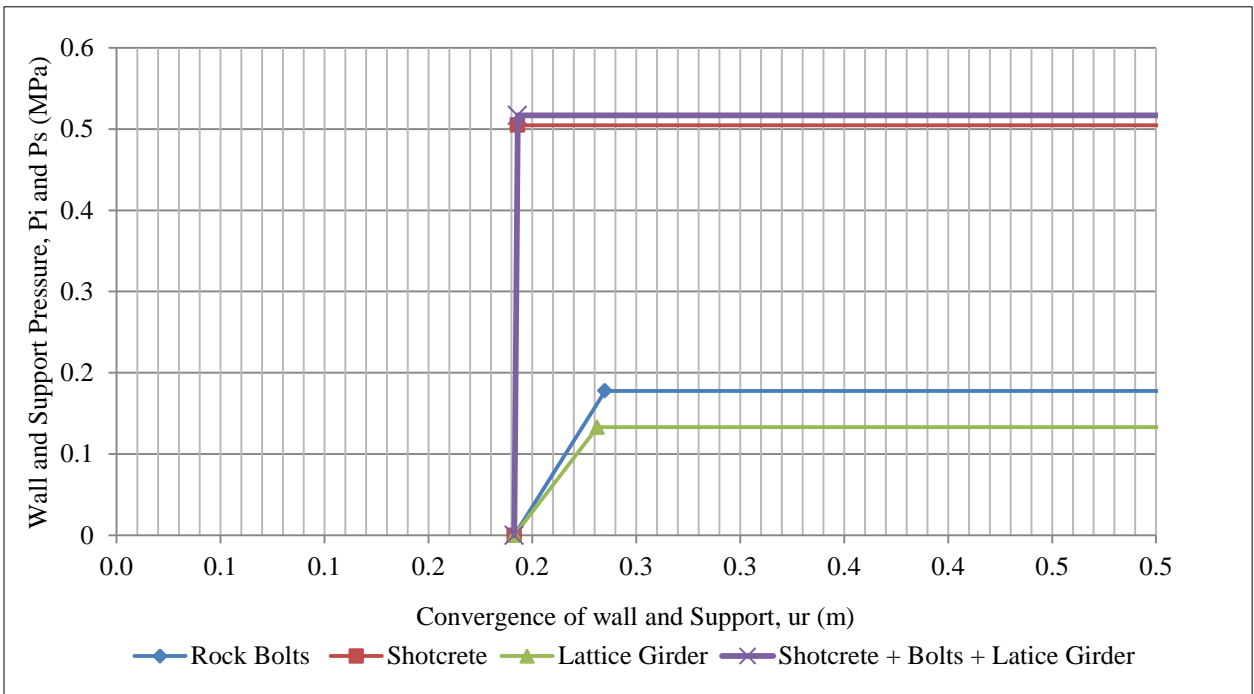


Figure C3.2: Support capacity curve for support type R5 at tunnel face (chainage 3+190m)

APPENDIX D: PHASE² MODELING AND RESULTS

Appendix D1: Model generation in three different tunnel sections

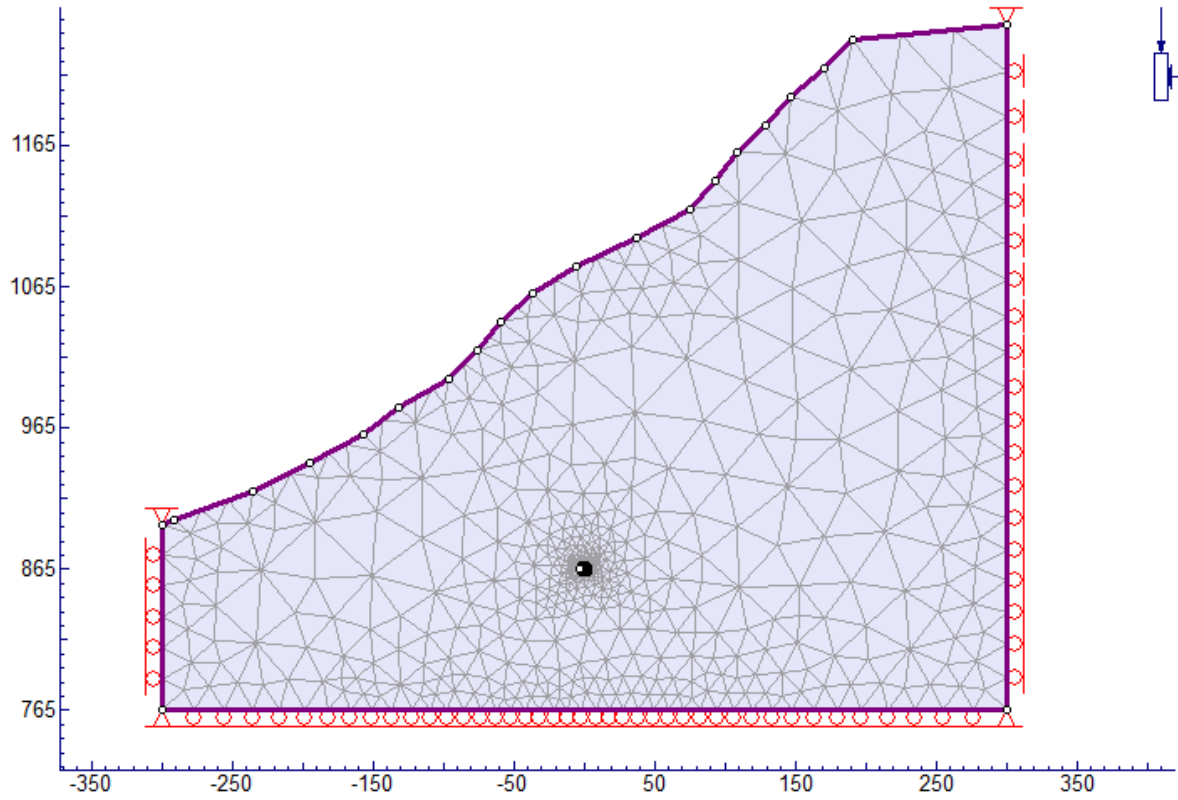


Figure D1.1: Model generation in tunnel section at Chainage 3+190

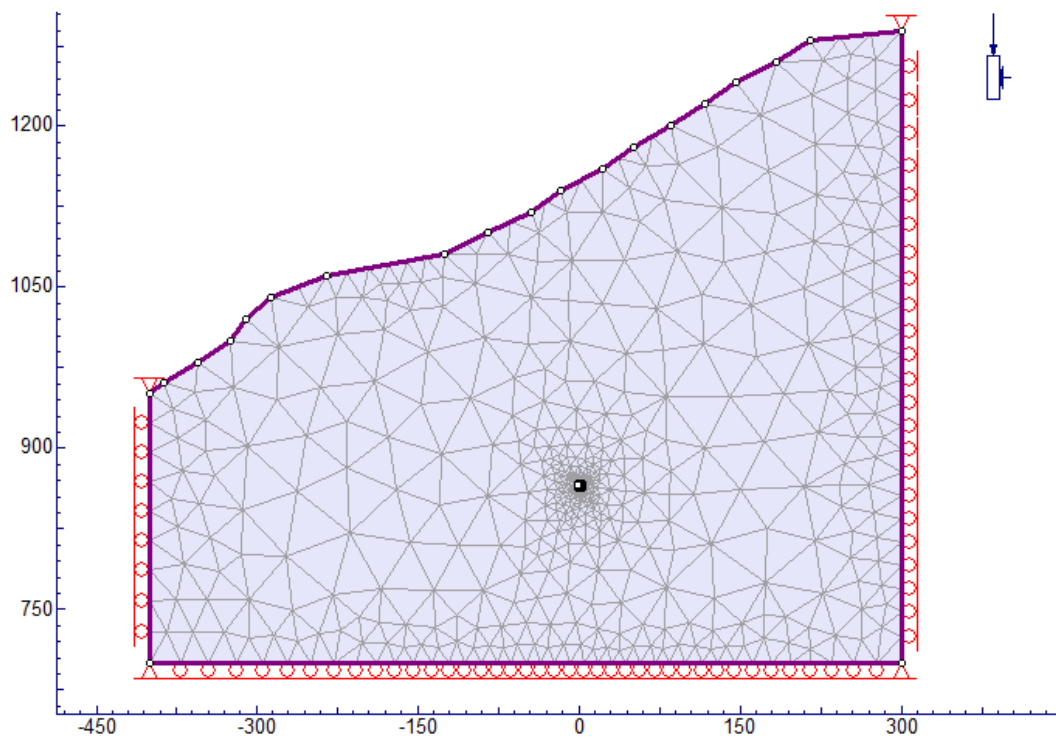


Figure D1.2: Model generation in tunnel section at Chainage 3+420

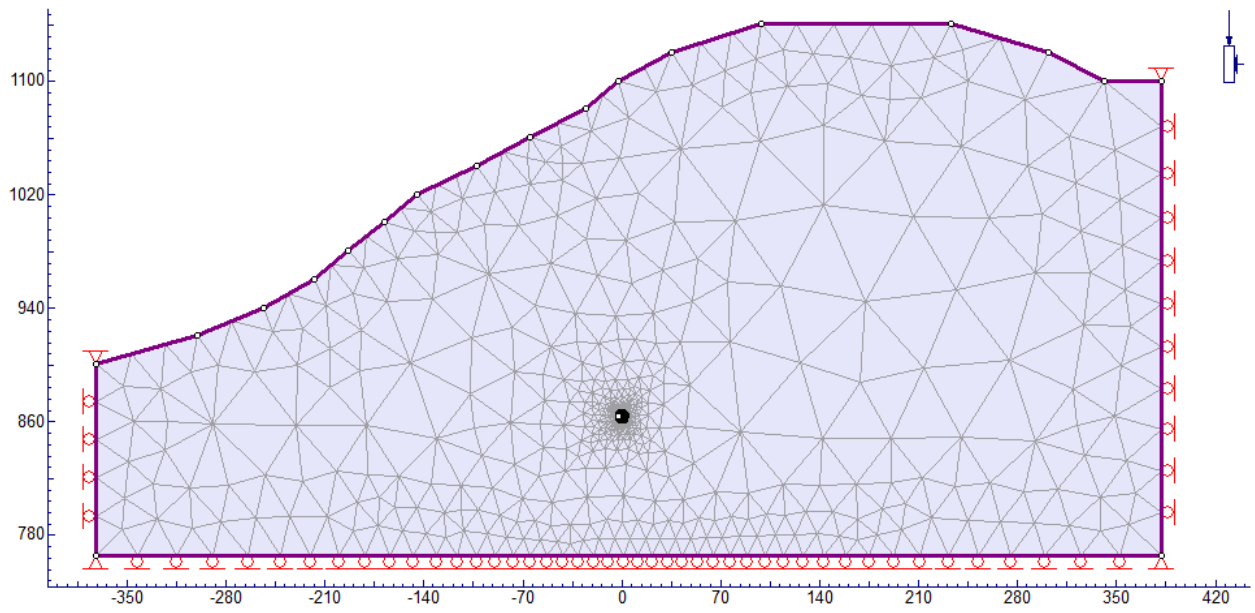
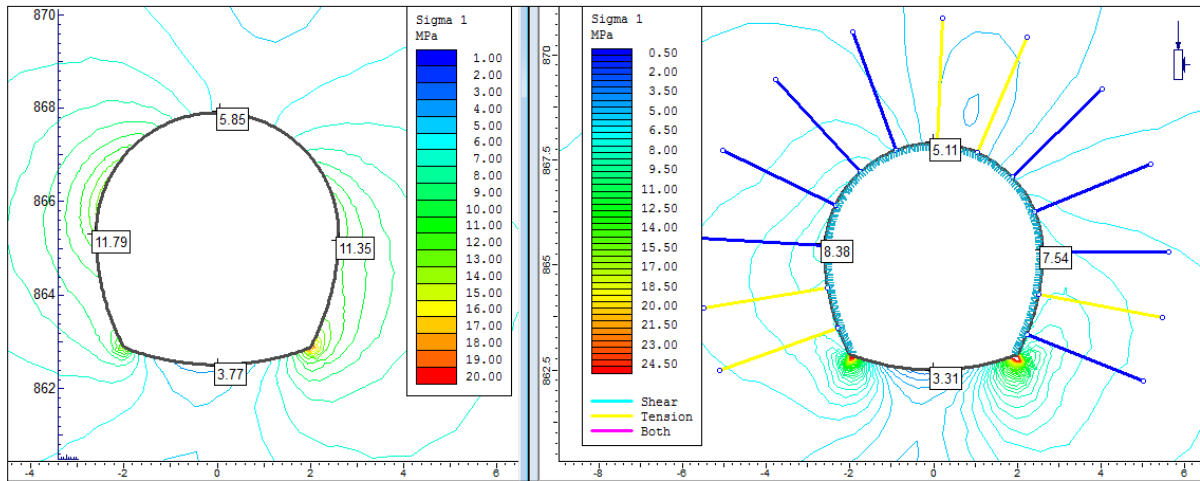


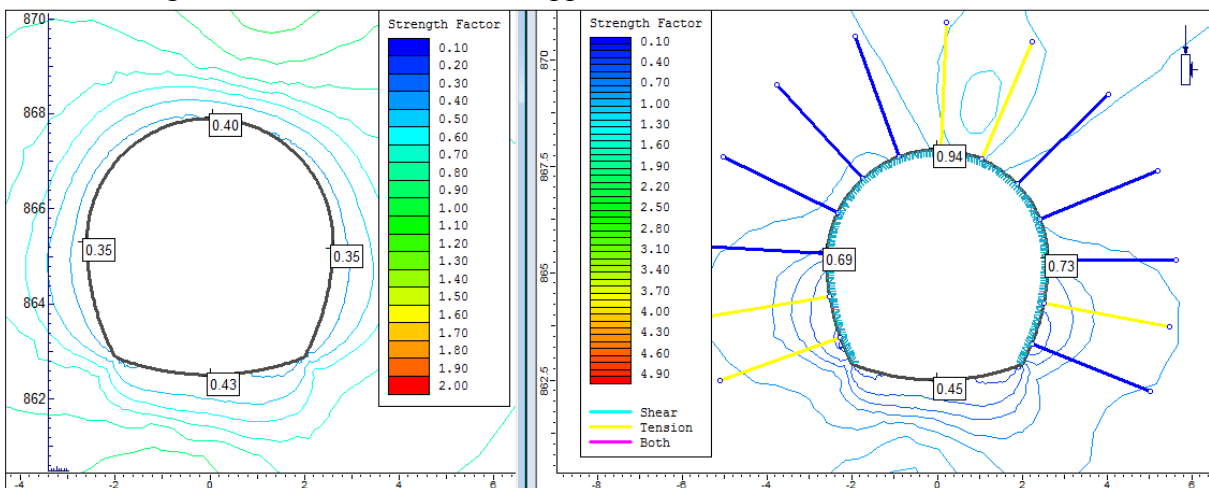
Figure D1.3: Model generation in tunnel section at Chainage 3+733

Appendix D2: Elastic analysis results at chainage 3+190

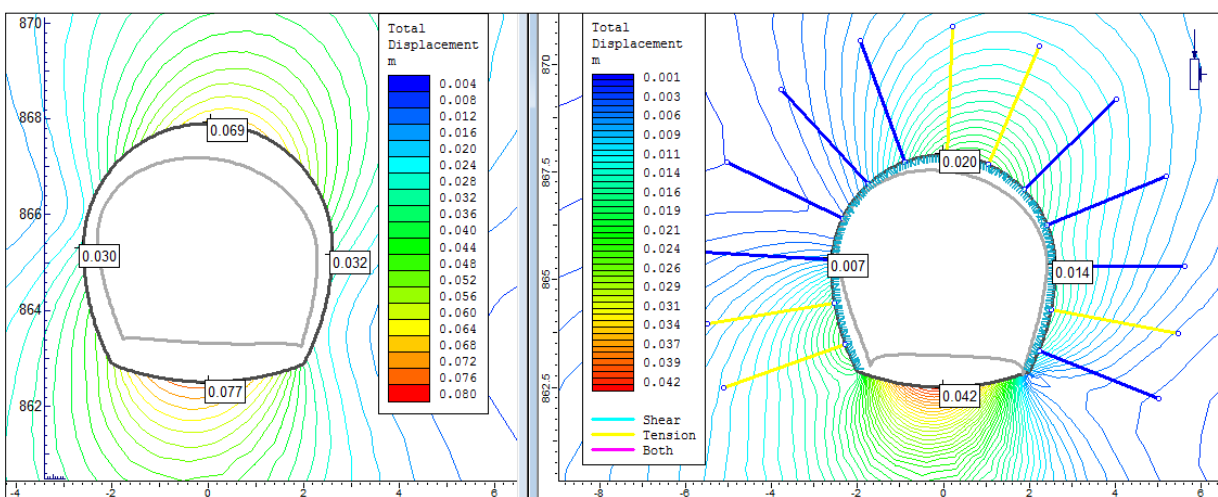
1. Major principle stress with and without support



2. Strength factor with and without support

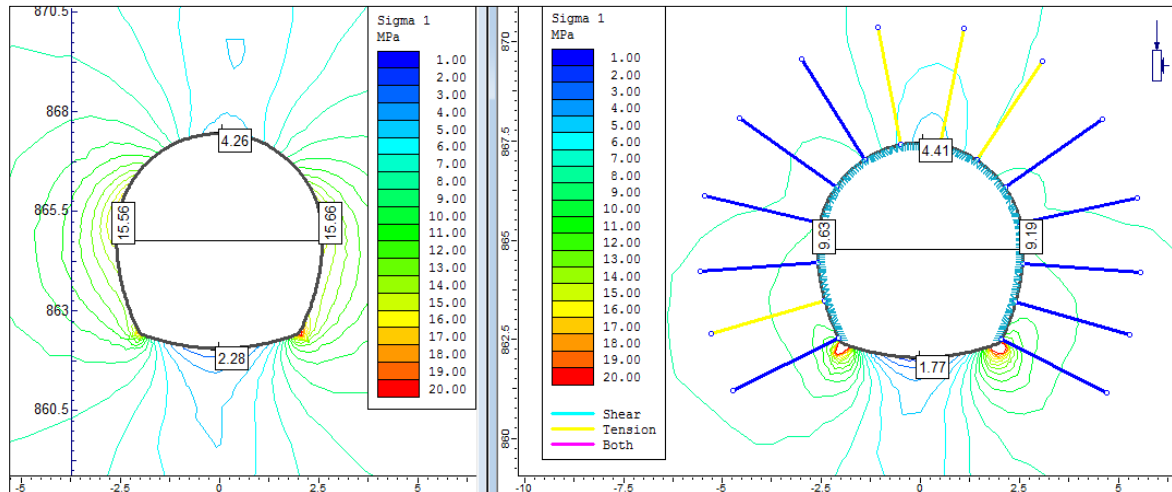


3. Total displacement with and without support

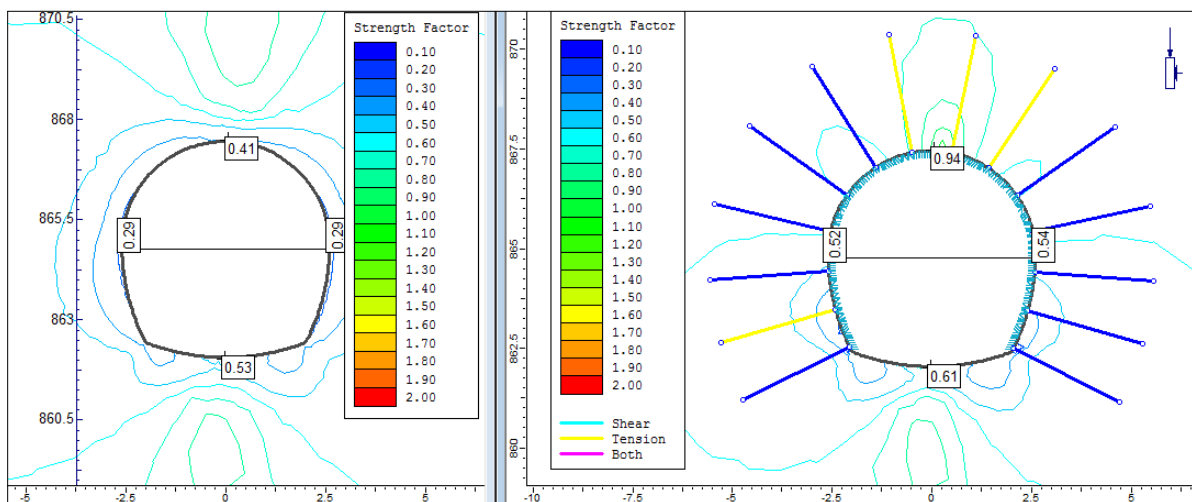


Appendix D3: Elastic analysis results at chainage 3+420

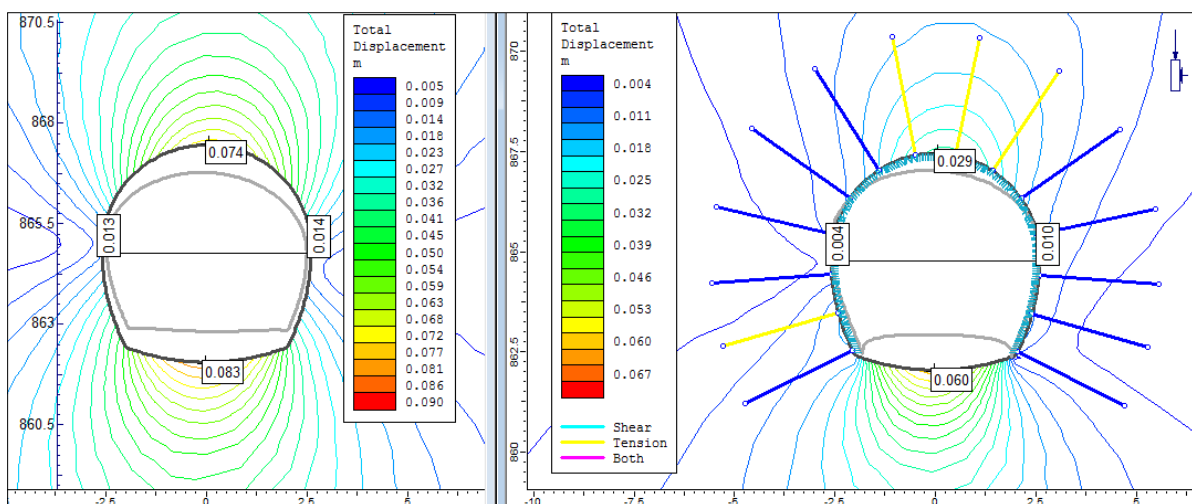
1. Major principle stress with and without support



2. Strength factor with and without support

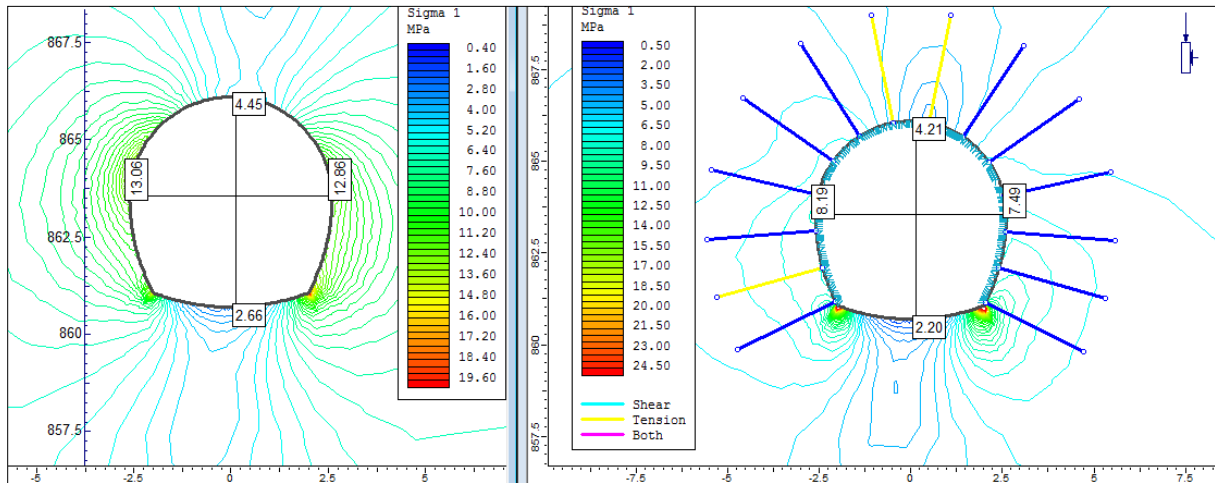


3. Total displacement with and without support

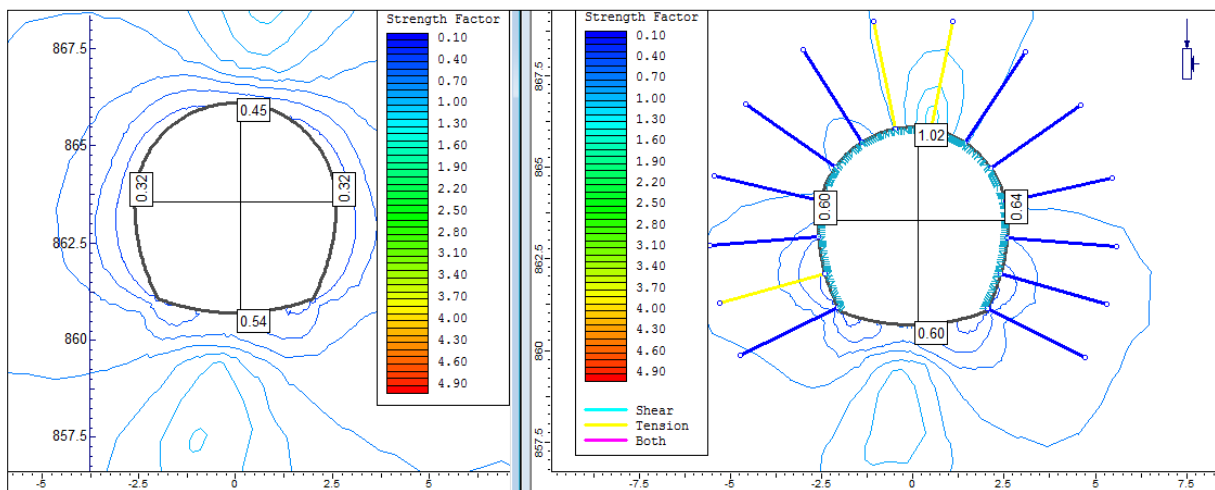


Appendix D4: Elastic analysis results at chainage 3+733

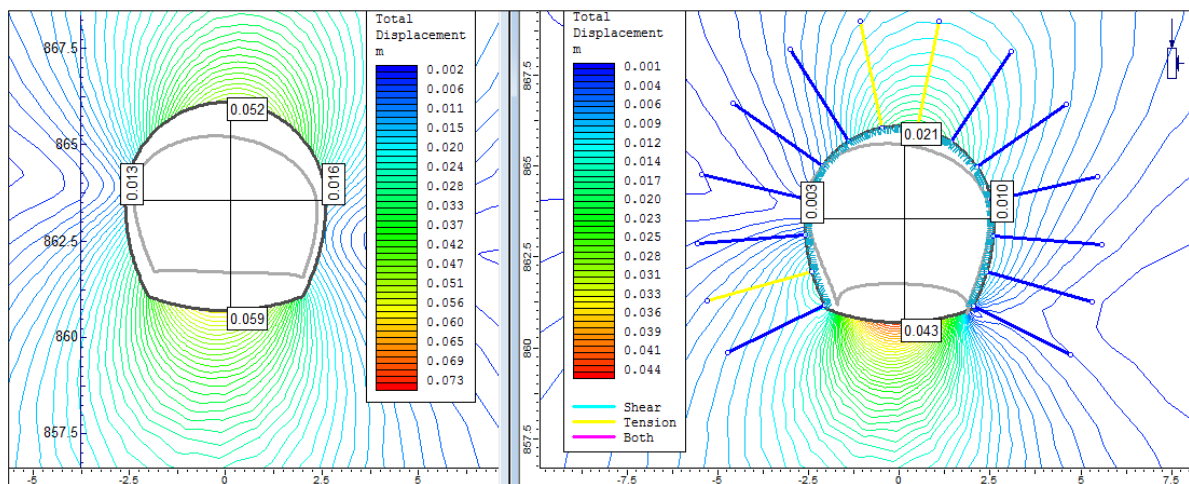
1. Major principle stress with and without support



2. Strength factor with and without support

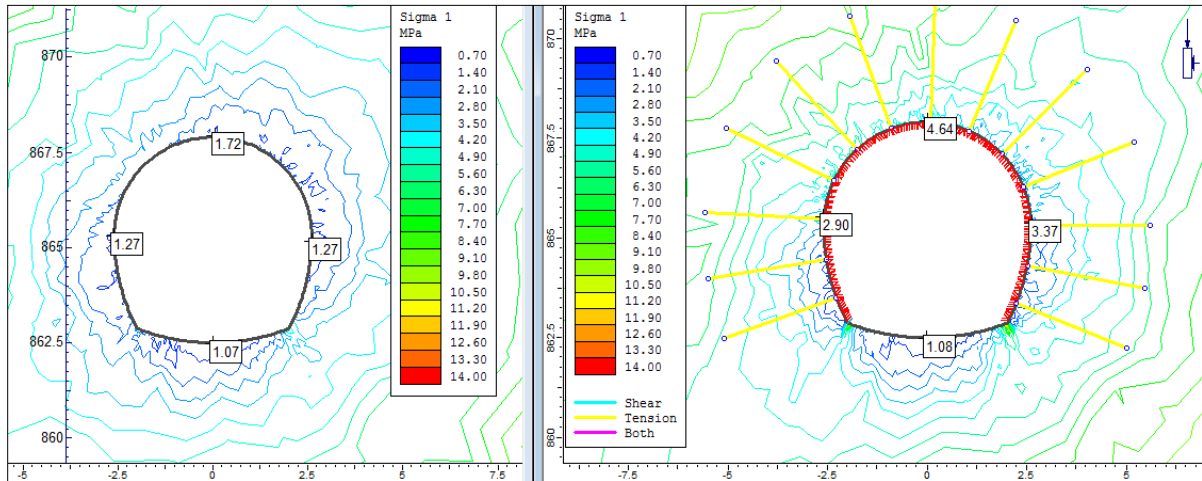


3. Total displacement with and without support

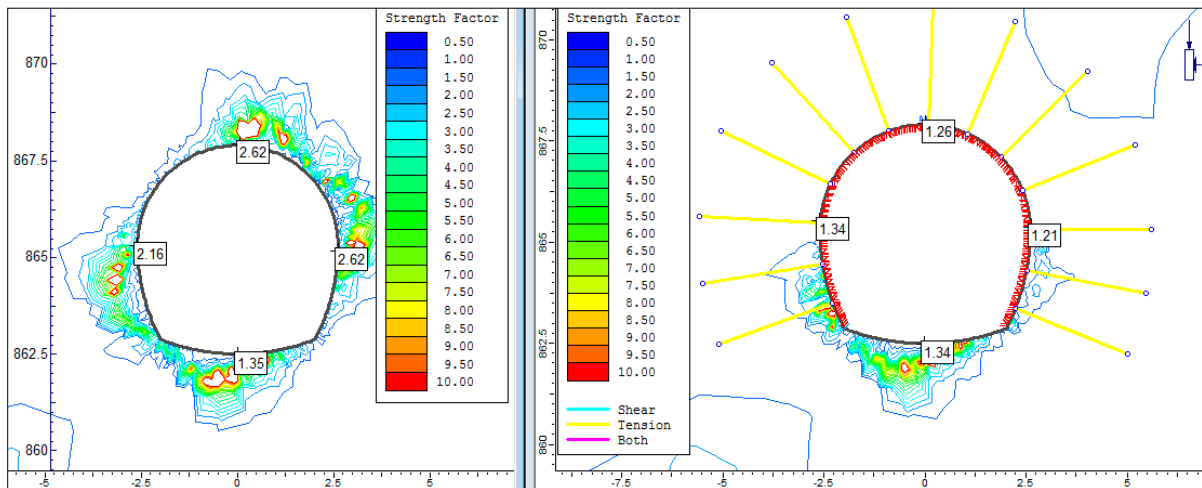


Appendix D5: Plastic analysis of tunnel section at chainage 3+190

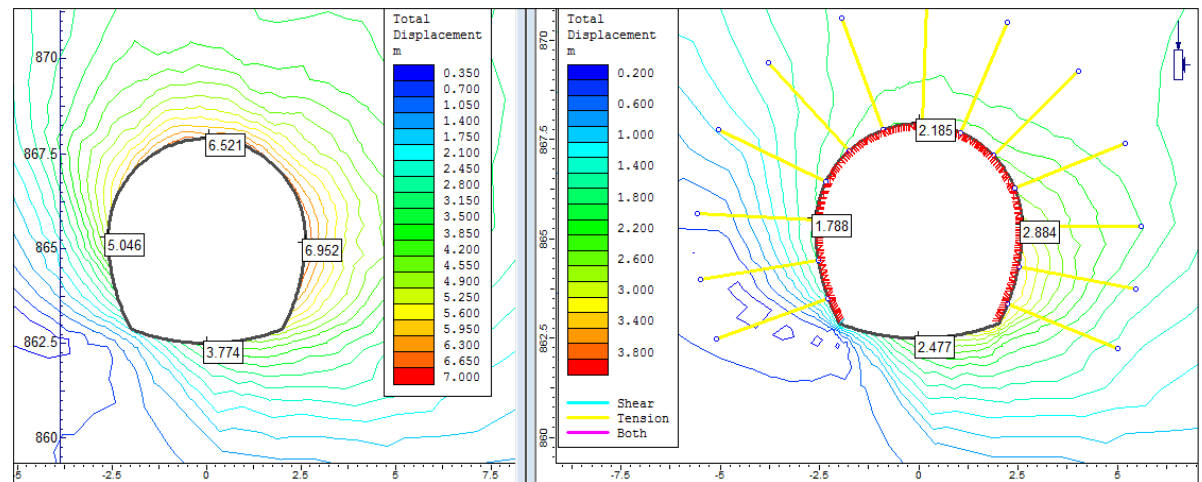
1. Major principle stress with and without support



2. Strength factor with and without support

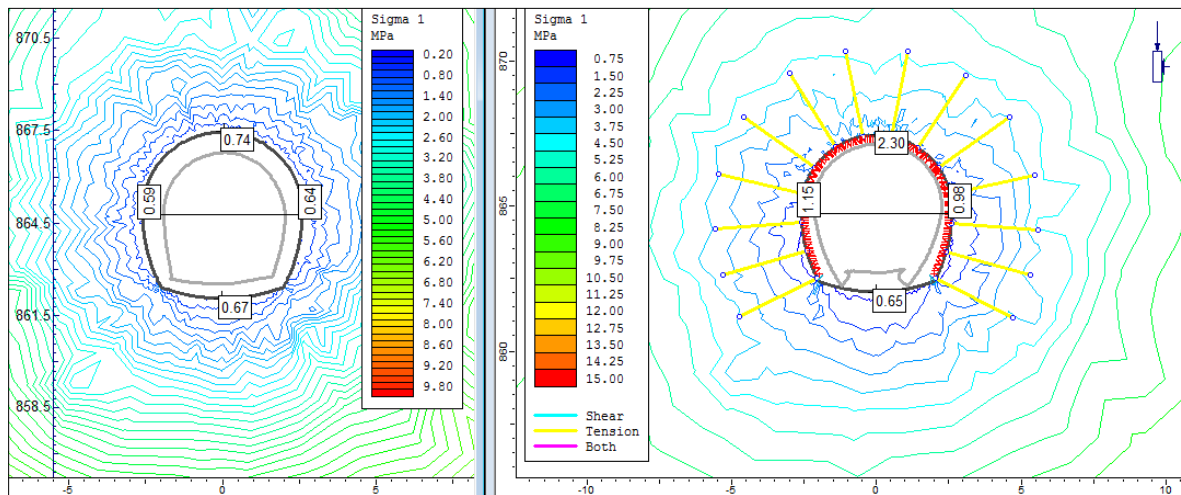


3. Total displacement with and without support

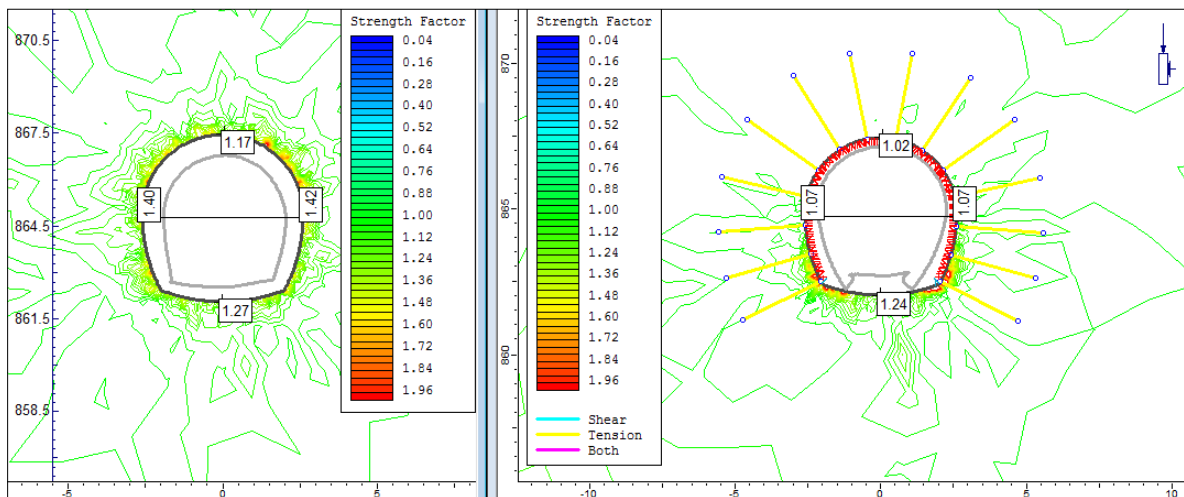


Appendix D6: Plastic analysis of tunnel section at chainage 3+420

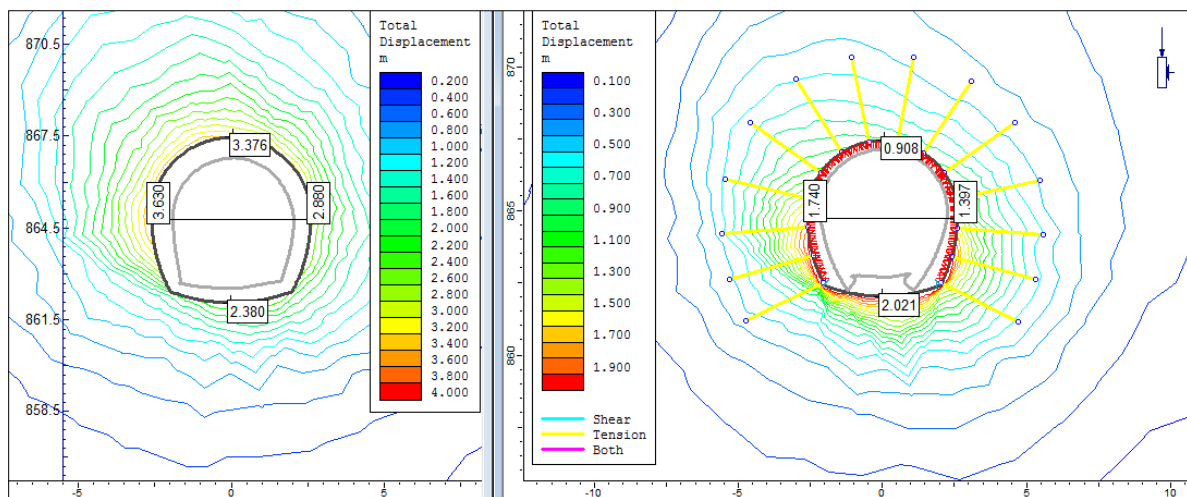
1. Major principle stress with and without support



2. Strength factor with and without support

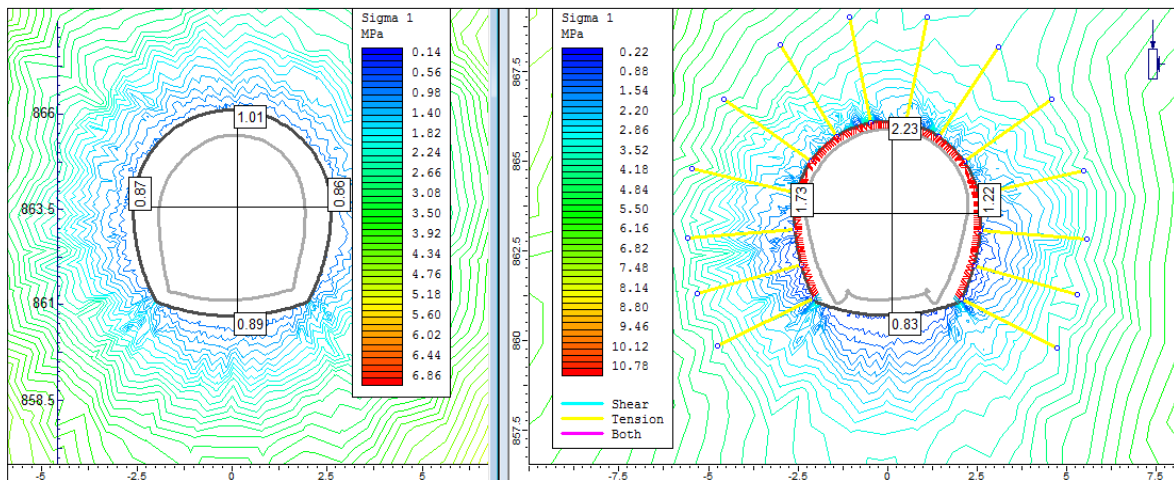


3. Total displacement with and without support

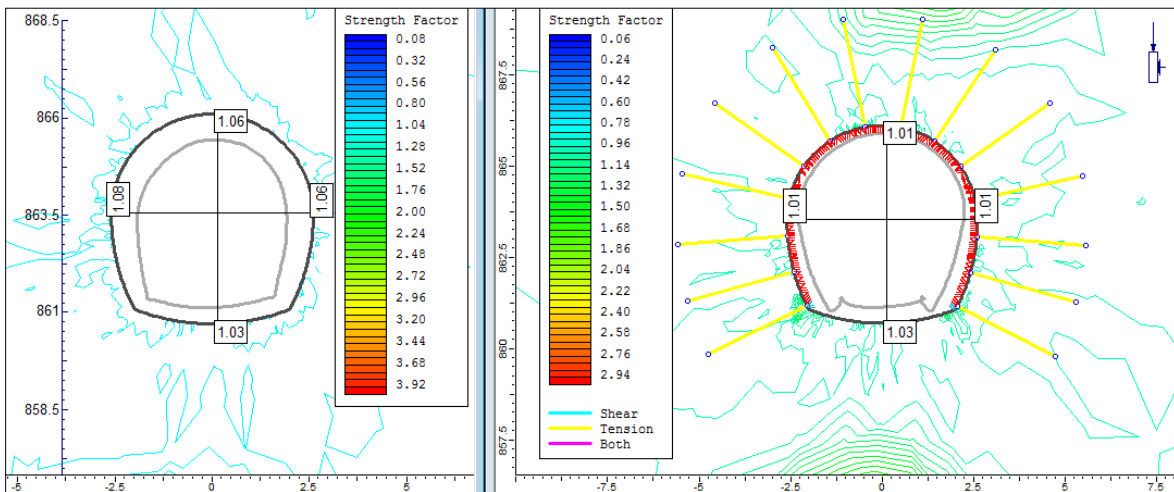


Appendix D7: Plastic analysis of tunnel section at chainage 3+733

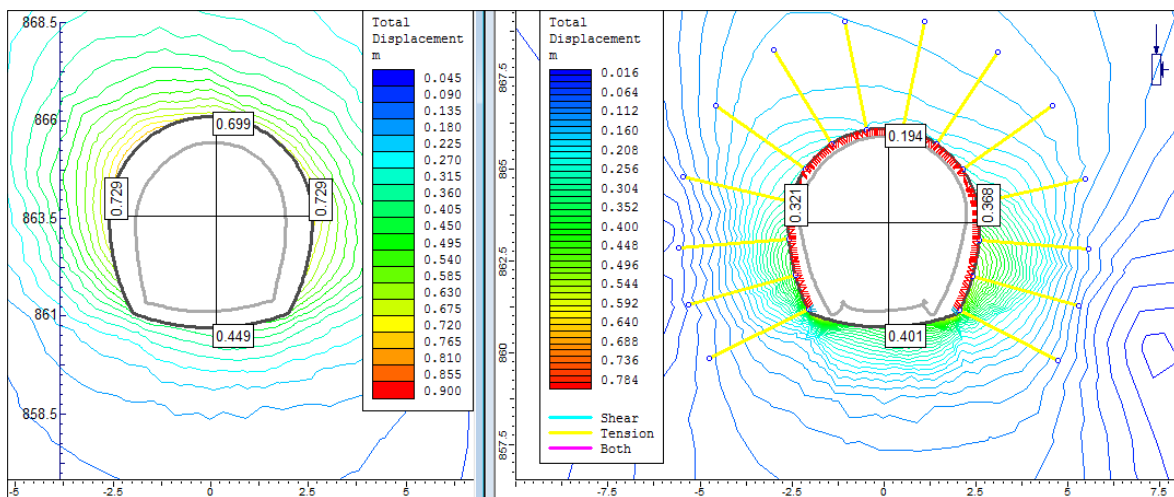
1. Major principle stress with and without support



2. Strength factor with and without support

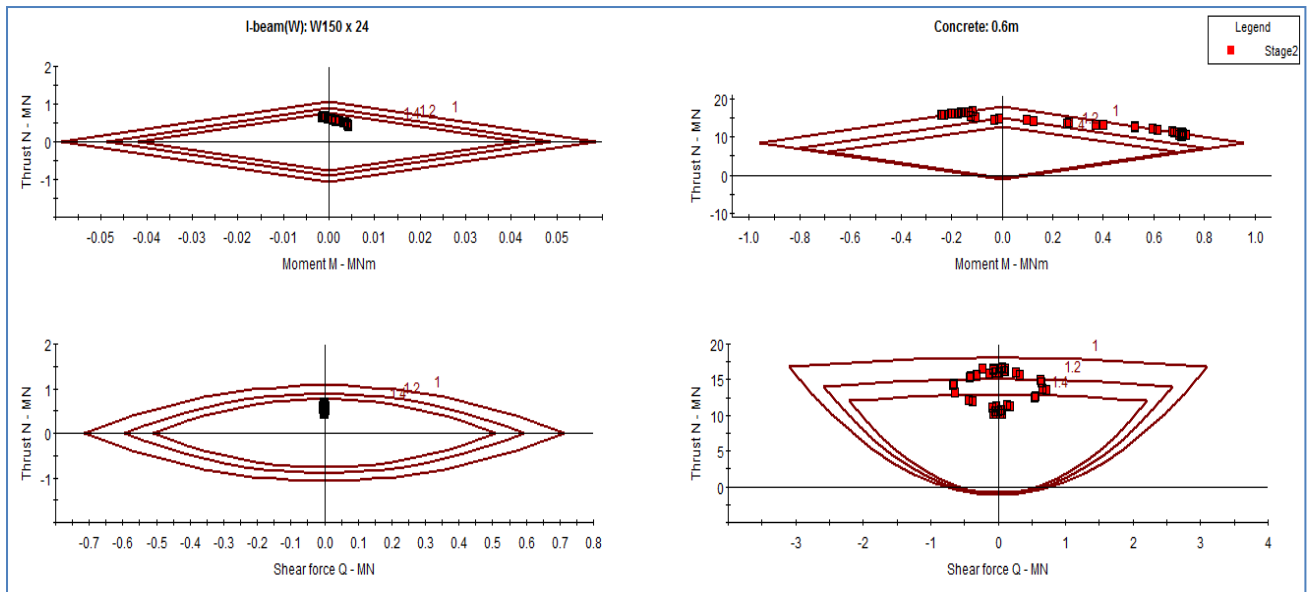


3. Total displacement with and without support

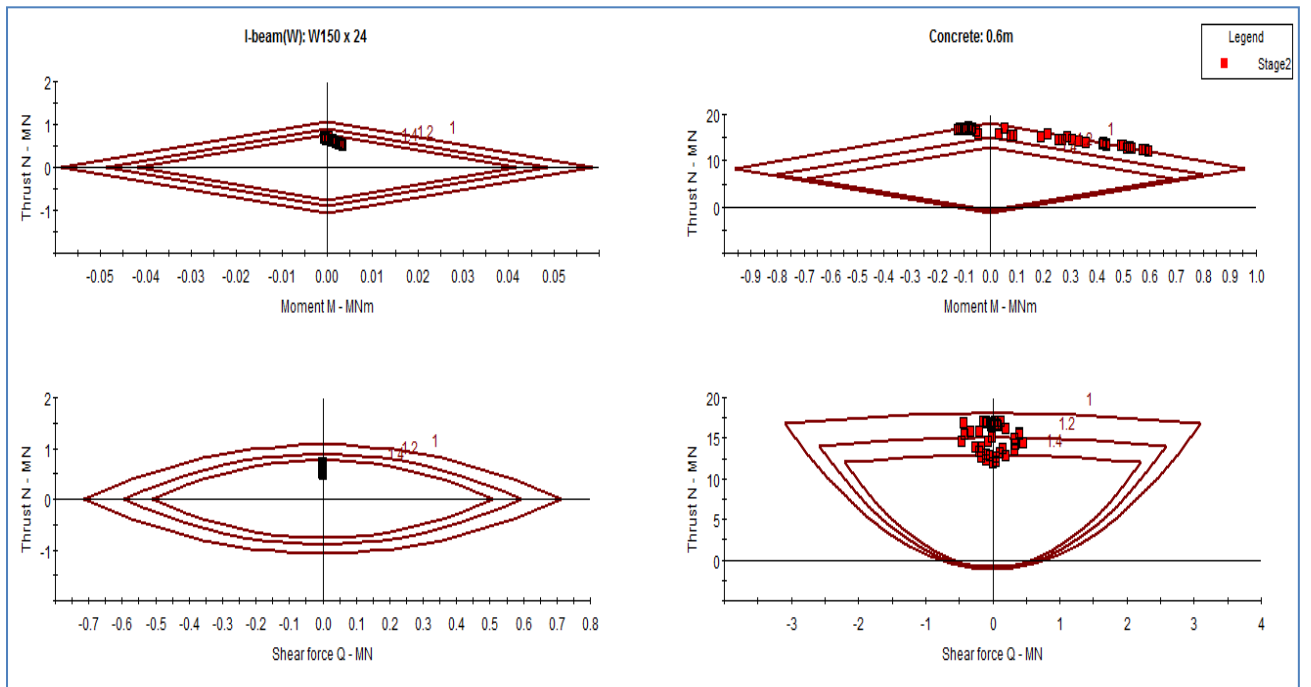


Appendix D8: Support capacity plots in case of circular section and lining (Steel set and shotcrete)

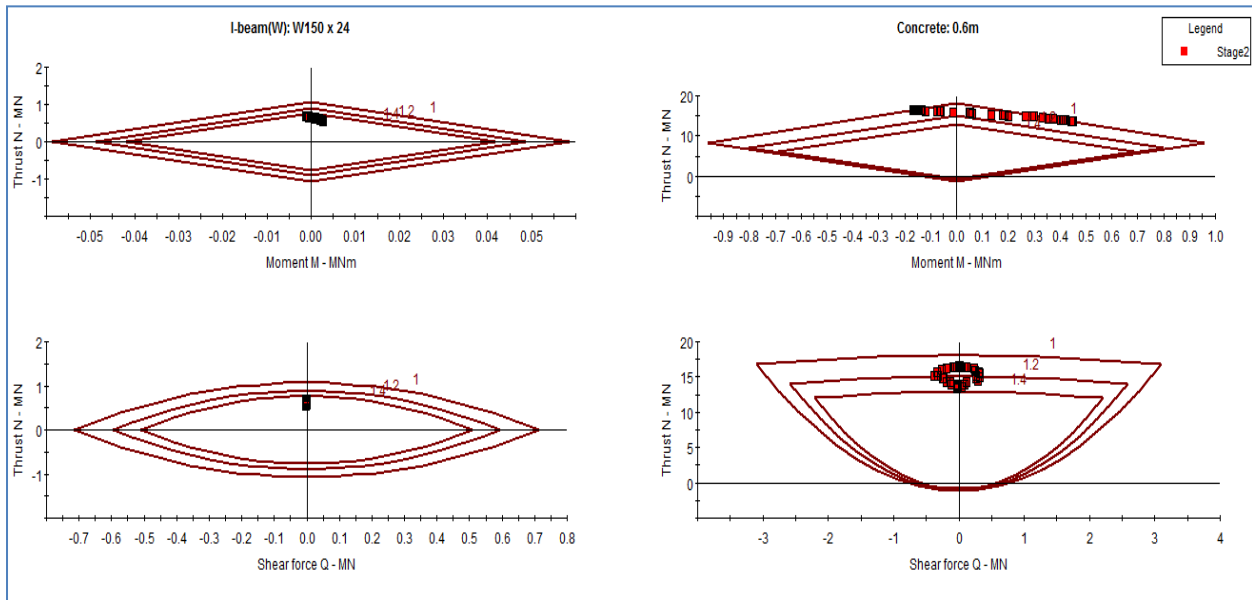
1. Tunnel section at chainage 3+190m



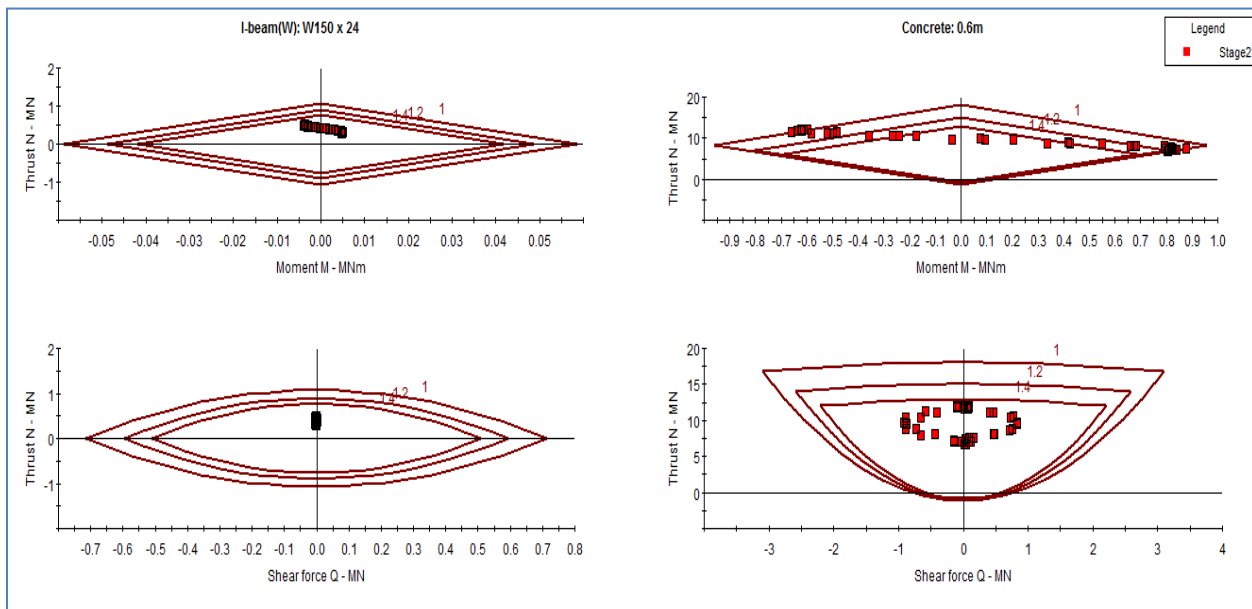
2. Tunnel section at chainage 3+404m



3. Tunnel section at chainage 3+420m



4. Tunnel section at chainage 3+733m



APPENDIX E: FORMAL LETTERS



Ref. no. HPDN-7

Date: 13.06.2012

To whom it may concern

Subject: Tunnel Data Collection for MSc Thesis Projects


This is to certify that Mr. Chhatra Bahadur Basnet, a Nepalese citizen and MSc fellow in Hydropower Development at the Faculty of Engineering Science and Technology - Norwegian University of Science and Technology (NTNU), is willing to carry out MSc Thesis in Rock Engineering and Tunnelling using the case project from his home country Nepal.

Mr. Basnet is visiting to Nepal on June 2012 to collect necessary geological, engineering geological data and information for his MSc Thesis Project. In this regards, I kindly request concern authorities / management / engineers / persons involved in the project to help him and give access and provide necessary data and information needed for his MSc Thesis work.

Your help will be a contribution in building highly skilled capabilities, which is a real need to Nepal and will be highly appreciated.

Sincerely yours,

Dr. Krishna Kanta Panthi
Associate Professor of Rock Engineering

 NTNU
Norges teknisk-naturvitenskapelige
universitet
Institutt for geologi og bergteknikk
7491 Trondheim

Postal Address:
Semsælunds Vei 1
7491, Trondheim, Norway

email:
krishna.panthi@ntnu.no
www.ntnu.no

Telephone:
+4773594824 (direct)
+4773594800
Fax: +47 73594814

Dr. Krishna Kanta Panthi
Associate Professor



NEPAL ELECTRICITY AUTHORITY

(Government of Nepal Undertaking)

Balanch, Darchula.
Phone/ Fax No. 994930022

Generation Construction CHAMELIYA HYDROELECTRIC PROJECT



Ref No. 069/70- 35

Date: July 25, 2012

Norwegian University of Science and Technology, (NTNU)
Norway

Ref: Data Collection for MSc Thesis Projects

Dear Sir,

This is to certify that **Mr. Chhatra Bahadur Basnet**, MSc student at NTNU, has been given access to the project data of Chameliya Hydropower Project according to the request made by NTNU. Mr. Basnet visited the site together with our Engineers and Geologists and has been acquainted with the project site. He was provided following project related data:

- Project Feasibility Study Report together with drawings
- Geological Assessment Report
- Laboratory Test of Rock Samples
- Photographs
- Other necessary drawings and data

We hope that Mr. Basnet will be able to come with fruitful conclusion through his thesis work on Rock Engineering focused on our Project.

Sincerely

.....
Gopal Babu Bhattarai
Project Director
Chameliya Hydropower Project